

Electronic Thesis and Dissertation Repository

11-17-2022 2:00 PM

Chromatin regulation by RB-interacting proteins in cellular immune functions

Seung June Kim, *The University of Western Ontario*

Supervisor: Dick, Frederick A., *The University of Western Ontario*

A thesis submitted in partial fulfillment of the requirements for the Doctor of Philosophy degree in Biochemistry

© Seung June Kim 2022

Follow this and additional works at: <https://ir.lib.uwo.ca/etd>



Part of the [Cell Biology Commons](#), [Genomics Commons](#), and the [Molecular Biology Commons](#)

Recommended Citation

Kim, Seung June, "Chromatin regulation by RB-interacting proteins in cellular immune functions" (2022). *Electronic Thesis and Dissertation Repository*. 8982.
<https://ir.lib.uwo.ca/etd/8982>

This Dissertation/Thesis is brought to you for free and open access by Scholarship@Western. It has been accepted for inclusion in Electronic Thesis and Dissertation Repository by an authorized administrator of Scholarship@Western. For more information, please contact wlsadmin@uwo.ca.

Abstract

The retinoblastoma protein (RB) is historically known for its function in cell cycle control. However, mice carrying targeted *Rb1* mutations have revealed that RB serves various non-cell cycle control roles. Notably, RB acts as a scaffold that recruits chromatin regulatory proteins, condensin II and enhancer of zeste homolog 2 (EZH2). These complexes protect the genome integrity through maintaining proper chromosome condensation, long range contacts, and transcriptionally repressive histone modification. This thesis explores the mechanistic links that regulate such RB-condensin II complex or that are leveraged upon pharmacological inhibition of the RB-EZH2 complex. First, I identified potential phosphorylation sites in the RB C-terminus (RBC) that may be downstream of T cell receptor (TCR) crosslinking in Jurkat leukemia T cells. I generated and validated phospho-specific antibodies that detect S838/T841 phosphorylation. Upon TCR crosslinking, S838/T841 phosphorylation was indeed detected. p38 mitogen activated protein kinase (MAPK), a known downstream target of TCR signaling, directly phosphorylated RB at S838/T841. Through Jurkat cells overexpressing a phospho-ablated mutant RB construct, I show that S838/T841 phosphorylation is required to dissociate condensin II from chromatin and facilitate chromosome decondensation. In the subsequent chapter, I investigated the consequence and mechanism of pharmacologically inhibiting EZH2. Upon EZH2 inhibition, splenic B cells specifically were eliminated *in vivo*, which was associated with increased transcription of repetitive elements. Using CRISPR-Cas9 to generate a novel mouse line with abrogated detection of repetitive element transcripts, named RIC mutant, I show that EZH2 inhibition signals inflammatory chemokine expression. This was mediated through reduced histone methylation by EZH2, followed by upregulation of repetitive elements and their detection by three cytosolic pattern recognition receptors (PRRs), RIG-I, MDA5 and cGAS. These PRRs were required to recruit pro-inflammatory immune cells to the spleen *in vivo* and eliminate B cells. Lastly, I show that RIG-I and cGAS are indispensable for activating anti-viral interferon gene expression in mouse melanoma cells upon EZH2 inhibition. Taken together, this work uncovers regulatory and molecular mechanisms that underlie a

biological function or targeted inhibition of chromatin regulatory proteins recruited by RB in immune cells.

Keywords

retinoblastoma protein, chromatin, condensin II, enhancer of zeste homolog 2, pattern recognition receptors, repetitive elements, viral mimicry

Summary for Lay Audience

The retinoblastoma protein (RB) was first discovered as a factor whose loss caused retinoblastoma in children. As such, it became known as a tumour suppressor. Subsequent molecular studies discovered that RB's tumour suppressive function comes from its ability to control cell cycle, a process where cells divide and proliferate. Indeed, uncontrolled cell cycle can cause cancer. Recently, various studies have found that RB has other roles outside of cell cycle control. RB acts as a scaffold for two proteins called condensin II and EZH2 to contact DNA. Condensin II and EZH2 are proteins that regulate chromatin—a higher order structure of DNA that is compacted and organized in three-dimension. This thesis investigates the mechanisms that govern RB-condensin II interaction, and the effect of inhibiting EZH2 function. First, I discovered that RB is modified at poorly characterized sites by phosphorylation, deposition of negatively charged atoms, upon stimulation that mimics T cell activation in Jurkat leukemia T cells. This activated a series of proteins to directly phosphorylate RB. This event caused both RB and condensin II to be dissociated from chromatin. Consistent with known condensin II function, its loss from chromatin caused chromatin to become less compact. Jurkat cells that express RB that cannot be phosphorylated were resistant to such consequences. Next, EZH2 inhibition eliminated B cells in the spleen, and caused repetitive DNA sequences to be copied into RNA. We created a novel mutant mouse line that is unable to detect such repetitive RNA to test whether it is linked to B cell death. Indeed, these mice did not activate inflammatory immune genes compared to control upon EZH2 inhibition. Importantly, EZH2 inhibition comparably blocked EZH2 function in both WT and mutant mice. The mutant mice were resistant to B cell death and infiltration of inflammatory immune cells in the spleen compared to control. Lastly, I report that detection of repetitive RNA is also important to activate anti-viral signaling upon EZH2 inhibition in cancer cells. Overall, this thesis uncovers a regulatory mechanism for RB-condensin II, and a molecular pathway activated upon inhibition of EZH2 in immune cells.

Co-Authorship Statement

All chapters were written by Seung Kim and edited by Dr. Fred Dick.

Dr. James MacDonald performed ELISA, *in vitro* kinase assay, RB immunoprecipitation, nuclear extract preparation and Western blotting shown in Figure 2.2 A, B, D and E.

Dr. Patti Kiser analyzed mouse histology shown in Figure 3.1A, B and 3.3F. Lindsay Drysdale performed zygote microinjection and transplant surgery to generate RIC mutant mosaic founders depicted in Figure 3.3A and 3.4A.

All other experiments in this thesis were performed by Seung Kim. Seung Kim and Dr. Fred Dick conceived all experiments.

Acknowledgments

I would like to thank my supervisor Fred for his mentorship over the years. My coming-of-age as a scientist began with Fred in the winter of my third year as an undergraduate student. His dedication to trainee development has kept me on track to go from a blank canvas to where I am today. He has been generous with his time, resources, and feedback that have allowed me to pursue ambitious goals and tackle them rigorously. His scientific pedagogy has made a lasting impression that I am fortunate to take with me.

I am also thankful to my committee members, Drs. DiMattia and DeKoter, for their insight. Their expertise in various aspects of my project helped me improve the quality of my work and challenged me to think critically.

The training environment would be incomplete without the support from past and present lab members. I did not pick up lab techniques by watching YouTube videos. Senior members have been patient with my learning curve. I hope I was able to return the favour to junior trainees. Many have had to put up with my impulse for drawing smile faces on nearly all solid surfaces in the lab. Coffee break chats and happy hours have kept the lab fun, and the science engaging.

I am grateful to various labs in the CRLP/VRL and the administrative staff for generously sharing and providing key pieces of equipment.

I wouldn't have been able to produce much of the data without consulting several staff scientists. Drs. Carter and Chadwick at Robarts helped me with sequencing and flow cytometry, respectively. Dr. DeKoter's lab generously shared their knowledge with splenic B cell isolation.

I am thankful to my family and friends for their material and moral support. My family has given me the freedom to pursue what I like doing. Trips and hangouts with my friends have helped me avoid burning out and kept me going for the long haul.

Dedication

In memory of my grandmother, Dr. Won-Ja Kang.

List of Abbreviations

3C: chromosome conformation capture	CNV: copy number variation
4C: circularized chromosome conformation capture	CRISPR: clustered regularly interspersed short palindromic repeats
ATRT: atypical teratoid/rhabdoid tumour	CT: chromosomal territories
bp: base pair	dCAP: <i>Drosophila</i> CAP
C-terminal: carboxy-terminal	DEAD: aspartate, glutamate, alanine, aspartate
CAC: colitis-associated cancer	DHFR: dihydrofolate reductase
CAP: chromosome associated protein	DLBCL: diffuse large B cell lymphoma
CBX: chromobox domain/protein	DNMT: DNA methyltransferase
CD: cluster of differentiation	DP: differentiation regulated transcription factor 1 polypeptide
Cas9: clustered regularly interspersed short palindromic repeats (CRISPR) associated protein 9	ds: double stranded
CDK: cyclin-dependent kinase	DSB: double strand break
cGAS: cyclic GMP-AMP synthase protein	DSS: dextran sodium sulphate
ChIP: chromatin immunoprecipitation	E: embryonic day
CIC: cancer initiating cell	E2F: E2 promoter binding factor
RIC: <i>Rigi, Ifih1, Cgas</i>	EBV: Epstein-Barr virus
	EED: embryonic ectoderm development

EGFR: epidermal growth factor receptor	H3K27me: histone 3 lysine 27 methylation
EOC: epithelial ovarian cancer	HAT: histone acetyltransferase
ERV: endogenous retrovirus	HAWK: HEAT repeat proteins associated with kleisins
ES: epithelioid sarcoma	HDAC: histone deacetylase
ESC: embryonic stem cell	HEAT: huntingtin, elongation factor 3, the PR65/A subunit of protein phosphatase 2A, TOR1
Ext: extract	HEK293T: human embryonic kidney 293 SV40 large T antigen cells
EZH2: enhancer of zeste homolog 2	HGSOC: high grade serous ovarian cancer
FL: follicular lymphoma	HR: homologous recombination
G1: Gap 1 phase of cell cycle	HSATII: human satellite II
G2: Gap 2 phase of cell cycle	HSV: human simplex virus
GAPDH: glyceraldehyde-3-phosphate dehydrogenase	IAP: intracisternal A-type particle
GC: germinal center	IBD: inflammatory bowel disease
gRNA: guide RNA	IC50: half maximal inhibitory concentration
GSEA: gene set enrichment analysis	ICB: immune checkpoint blockade
GST: glutathione S-transferase	IEC: intestinal epithelial cells
H&E: hematoxylin and eosin	
H2AK119ub: histone 2a lysine 119 ubiquitination	
H3K9me: histone 3 lysine 9 methylation	

IFN: interferon

Ifih1: interferon-induced helicase C domain-containing protein 1 gene

IgG: immunoglobulin G

IGV: integrated genome viewer

IL: interleukin

IP: immunoprecipitation

I.P.: intraperitoneal

IR: ionizing radiation

ISG: IFN-stimulated gene

kb: kilobase

kDa: kilodalton

KDM2B: lysine specific demethylase 2B

KO: knock-out

LINE: long interspersed nuclear element

LTR: long terminal repeat

LxCxE: leucine-any amino acid-cysteine-any amino acid-glutamate

M: mitosis

MACS: Model based analysis for ChIP-seq (peak calling software) OR magnetic-activated cell sorting

MAVS: mitochondrial anti-viral signaling protein

MBD: marked box domain

MDA5: melanoma differentiation-associated protein 5

MDSC: myeloid-derived suppressor cells

MEF: mouse embryonic fibroblast

N: haploid ploidy

N-terminal: amino terminal

NAHR: non-allelic homologous recombination

NCSLC: non-small cell lung cancer

NF- κ B: nuclear factor kappa beta

NGS: next generation sequencing

NHEJ: non-homologous end joining

p107: protein encoded by *RBL1*

p130: protein encoded by *RBL2*

PcG: polycomb group

PCGF: polycomb group ring finger protein

Ph: polyhomeotic protein

PHC: Ph homologous protein

PRC: polycomb repressive complex

PRR: pattern recognition receptor

PVA/CA: pervanadate/calyculin A

qRT: quantitative real-time

RAWUL: RING finger and WD40 ubiquitin-like

RB: retinoblastoma tumour suppressor protein

RBI: human RB gene

Rb1: mouse RB gene

Rb1^{ΔL}: mouse retinoblastoma

susceptibility gene containing I746A,

N750A and M754A substitutions

Rb1^{ΔS}: mouse retinoblastoma

susceptibility gene containing F832A substitution

RBBP4/7: retinoblastoma-binding protein 4/7

RBC: RB C-terminus

RBF1: *Drosophila* RB family homolog

RBL1: retinoblastoma like 1 gene

RBL2: retinoblastoma like 2 gene

RBLP: RB large pocket

RBN: RB N-terminus

RBR1: retinoblastoma related 1 protein

RIG-I: retinoic-acid inducible gene I protein

RING: really interesting new gene

RING1A/B: E3 ubiquitin-protein ligase RING1A/B

RLR: RIG-I-like receptor

RYBP: RING1 and YY1 binding protein

S: DNA synthesis phase

SAM: S-adenosyl methionine OR sterile alpha motif

seq: sequencing

SET: suppressor of variegation 3-9, enhancer of zeste, trithorax

Setdb1/2: SET domain bifurcated histone lysine methyltransferase 1/2

shRNA: short hairpin RNA

SINE: short interspersed nuclear element

siRNA: small interfering RNA

SMC: structural maintenance of
chromosomes

ss: single strand

STING: stimulator of IFN genes

Suv39h: suppressor of variegation 3-9
homolog

Suv420h: suppressor of variegation 4-20
homolog

SUZ12: suppressor of zeste 12 homolog

TAD: transactivation domain

TCR: T cell receptor

TNF: tumour necrosis factor

WGS: whole genome sequencing

WT: wild type

YAF2: YY1-associated protein 2

Table of Contents

Abstract.....	ii
Keywords	iv
Summary for Lay Audience.....	v
Co-Authorship Statement.....	vi
Acknowledgments.....	vii
Dedication	viii
List of Abbreviations	ix
Table of Contents.....	xiv
List of Figures	xix
List of Appendices	xxi
Chapter 1	1
1 Introduction	1
1.1 Retinoblastoma and the retinoblastoma protein (RB).....	1
1.2 The retinoblastoma protein regulates the cell cycle.....	2
1.3 The pocket domain and the RB pocket protein family	3
1.4 E2F transcription factors recruit RB family proteins to DNA	5
1.5 RB-E2F interaction is regulated by upstream cyclin-CDKs.....	6
1.6 RB C-terminal domain has a unique interaction with E2F1	9
1.7 The canonical versus non-canonical functions of RB.....	11
1.8 The non-canonical functions of RB may underlie sensitivity to chemotherapy and radiation upon RB loss	13
1.9 RB loss is associated with resistance to targeted molecular therapies.....	16
1.10 Targeted <i>Rb1</i> mutations have revealed non-canonical functions of the RB- E2F1 complex	18

1.11	The <i>Rb1^{AL}</i> mouse model reveals RB-E2F1 recruitment of condensin II to DNA	18
1.12	Condensin II is a SMC family protein complex	20
1.13	Condensins regulate chromosome dynamics in interphase nuclei.....	23
1.14	The <i>Rb1^{AS}</i> mouse model reveals RB-E2F1 recruitment of EZH2 to repetitive elements	24
1.15	PRC1 and PRC2 modify histone tails that compact chromatin and silence transcription	25
1.16	Epigenetic modifications silence repetitive elements	28
1.17	Various mechanisms enable repetitive elements to expand in the genome	29
1.18	Derepression of repetitive elements can be tumourigenic	29
1.19	Inhibition of transcriptionally repressive complexes derepresses repetitive elements and activates immune signaling in cancer cells	31
1.20	Rationale and objectives	32
1.21	References.....	35
Chapter 2.....		61
2	Phosphorylation of the RB C-terminus regulates condensin II release from chromatin.....	61
2.1	Abstract	61
2.2	Introduction.....	61
2.3	Materials and Methods.....	63
2.3.1	Antibodies	63
2.3.2	Cell culture and stimulation	64
2.3.3	Protein extract preparation	64
2.3.4	Immunoprecipitation.....	65
2.3.5	<i>In vitro</i> kinase assay	65
2.3.6	SDS-PAGE, Western blotting and Coomassie staining.....	66

2.3.7	Plasmids and lentiviral transduction	66
2.3.8	Chromatin sonication	67
2.3.9	Statistical analysis	67
2.4	Results	68
2.4.1	Detection of C-terminal RB phosphorylation on S838 and T841	68
2.4.2	Sequential activation of kinases in the TCR signaling pathway induces RB S838/T841 phosphorylation	73
2.4.3	RB S838/T841 phospho-acceptor mutants prevent condensin II unloading and chromatin decondensation	79
2.5	Discussion	85
2.6	References	87
Chapter 3	91
3	EZH2 inhibition stimulates viral mimicry causing immune destruction of splenic B cells	91
3.1	Abstract	91
3.2	Introduction	91
3.3	Materials and Methods	94
3.3.1	Data and code availability	94
3.3.2	Experimental model and subject details	94
3.3.3	Intraperitoneal injections	94
3.3.4	Cell culture	94
3.3.5	RNA extraction, qRT-PCR and sequencing	95
3.3.6	RNA sequencing analysis	96
3.3.7	ChIP sequencing	96
3.3.8	ChIP sequencing analysis	98
3.3.9	Flow cytometry	99

3.3.10	Protein extraction and pulldown assay	99
3.3.11	SDS-PAGE and Western blot	100
3.3.12	CRISPR-Cas9 generation of RIC mutant mice.....	100
3.3.13	Statistical analysis.....	101
3.4	Results.....	102
3.4.1	EZH2 inhibition upregulates repetitive elements specifically in B cells and causes cell death.....	102
3.4.2	Pattern recognition receptors are required for GSK343 induced B cell death in the spleen.....	107
3.4.3	EZH2 inhibition induces H3K27me3 loss at repetitive elements in B cells	113
3.4.4	Cytosolic PRRs are required for pro-inflammatory gene expression upon EZH2 inhibition	118
3.4.5	Cytosolic PRRs mediate an inflammatory response upon EZH2 inhibition.....	124
3.5	Discussion.....	130
3.6	References.....	133
Chapter 4.....		140
4	Both RIG-I and cGAS are required to upregulate interferon signaling upon EZH2 inhibition in B16 melanoma cells	140
4.1	Introduction.....	140
4.2	Materials and Methods.....	142
4.2.1	Cell culture and lentiviral transduction.....	142
4.2.2	RNA extraction and Quantitative real-time qPCR.....	142
4.2.3	RNA-seq analysis.....	143
4.2.4	Protein extraction, SDS-PAGE and Western blotting	143
4.3	Results.....	144

4.3.1	Generation of RIG-I KO, cGAS KO and RIG-I/cGAS double KO (DKO) cell lines.....	144
4.3.2	Both RIG-I and cGAS are indispensable to activate ISGs upon GSK343 treatment.	144
4.4	Discussion.....	151
4.5	References.....	152
Chapter 5	155
5	Discussion	155
5.1	Summary of findings.....	155
5.2	Diverse RB functions are regulated by phosphorylation	156
5.3	p38 MAPK-mediated RB phosphorylation in early development.....	157
5.4	Structural changes to the RB-E2F1 complex and its chromatin dissociation upon S838/T841 phosphorylation.....	158
5.5	The RIC mutant mouse model	159
5.6	Diverse consequences of pharmacological EZH2 inhibition.....	161
5.7	Implications for the use of EZH2 inhibitors in the clinic	164
5.8	Final summary	165
5.9	References.....	166
Appendices	174
Curriculum Vitae	185

List of Figures

Figure 1.1: Domain diagram of the pocket family proteins.....	4
Figure 1.2: Cell cycle control by RB.	7
Figure 1.3: Protein domains that mediate the general versus the specific RB-E2F interactions.....	10
Figure 1.4: The RB-E2F1 complex is required for non-canonical functions of RB beyond cell cycle control.	12
Figure 1.5: The relationship between <i>RBI</i> loss, response to chemotherapy and resistance to targeted therapies.	14
Figure 1.6: Structural maintenance of chromosomes (SMC) family proteins and condensin function in an interphase nucleus.	21
Figure 1.7: Mammalian homologs of the polycomb group (PcG) genes form the polycomb repressive complex 1 and 2 (PRC1/2).	26
Figure 2.1: Putative phosphorylation of the RB C-terminus.	69
Figure 2.2: Detection of phosphorylation of S838/T841 on RB.....	71
Figure 2.3 Phosphorylation of RB on S838/T841 is dependent on p38.	74
Figure 2.4: T cell receptor signaling causes RB S838/T841 phosphorylation.	77
Figure 2.5: Non-phosphorylatable S838A/T841A RB prevents CAP-H2 chromatin unloading upon T cell receptor crosslinking.....	80
Figure 2.6: RB S838/T841 phosphorylation regulates chromatin dynamics upon T cell receptor signaling.....	83

Figure 3.1: GSK343 induces inflammation and B cell death.	103
Figure 3.2: GSK343 upregulates repetitive element expression in splenic B cells.	105
Figure 3.3: <i>Rigi/Ifih1/Cgas</i> (RIC) triple mutant mice are resistant to GSK343 killing of B cells.	109
Figure 3.4: Strategy to generate and genotype RIC mutant mice.	111
Figure 3.5: Distribution and loss of H3K27me3 peaks globally or at repetitive elements.	114
Figure 3.6: GSK343 induces loss of H3K27me3 at repetitive elements in splenic B cells.	116
Figure 3.7: Cytosolic PRRs are required for GSK343 induced inflammatory signaling in B cells.	119
Figure 3.8: Changes in gene/repetitive element expression and H3K27me3 upon GSK343 treatment in RIC mutant splenic B cells.	121
Figure 3.9: Gating strategy and absolute cell counts of splenic immune cells.	126
Figure 3.10: Cytosolic PRRs mediate GSK343 induced inflammation <i>in vivo</i>	127
Figure 3.11: Model of EZH2 inhibition and activation of inflammation.	131
Figure 4.1: Generation of RIG-I/cGAS single or double KO B16-F10 melanoma cells and induction of ISGs upon GSK343 treatment.	145
Figure 4.2: RIG-I and/or cGAS deletion blocks B16-F10 cells from significantly upregulating IFN and innate immune genes and pathways upon GSK343 treatment. ...	148
Figure 4.3: Sterol biosynthetic process gene set is commonly upregulated upon GSK343 treatment regardless of RIG-I/cGAS expression.	150

List of Appendices

Appendix A: List of primers	174
Appendix B: List of reagents	176
Appendix C: PCR mixes and reactions.....	182
Appendix D: RIC mutant alleles.....	184
Appendix E: Off-target mutations in RIC mutant founder mice	184

Chapter 1

1 Introduction

1.1 Retinoblastoma and the retinoblastoma protein (RB)

The onset of the childhood cancer retinoblastoma was initially attributed to a dominant gene mutation that was inherited or sporadic (Neel and Falls, 1951; Schappert-Kimmijser et al., 1966; Smith and Sorsby, 1958). The notion of its dominant inheritance was supported by a high percentage of disease affection within several sibships (Griffith and Sorsby, 1944). Further studies of family pedigrees and retinoblastoma incidence suggested that such inherited dominant mutation displays incomplete penetrance. Later, statistical analysis of bilateral (both eyes) or unilateral (one eye) retinoblastoma that were either inherited or sporadic suggested that a minimum of two mutations would cause retinoblastoma (Knudson, 1971). In this study, the relationship between bilateral or unilateral retinoblastomas and their time of diagnosis supported the notion that two mutation events occurring at a constant rate were the genetic mechanism underlying retinoblastoma. This “two-hit hypothesis” posited that the first mutation can be either inherited or sporadic and the second mutation is sporadic. Affected children with inherited retinoblastoma are at higher risk of developing retinoblastoma because only one more mutation, or “hit”, is required, in contrast to non-hereditary retinoblastoma that requires two. The significance of the two requisite mutations was then interpreted as the loss of both alleles of a tumour suppressive gene and its complete loss of function leading to the malignancy (Comings, 1973).

Early observations of chromosome 13q14 deletion in retinoblastomas hinted that such tumour suppressive gene may be found at this “retinoblastoma locus” (Cavenee et al., 1983, 1985; Dryja et al., 1984; Francke and Kung, 1976; Godbout et al., 1983; Lele et al., 1963; Sparkes et al., 1980, 1983; Vogel, 1979; Yunis and Ramsay, 1978). It was also noted that loss of heterozygosity at this locus was associated with retinoblastoma, which is consistent with the two-hit hypothesis. Finally, a single gene was cloned from this locus, and confirmed to be deleted in retinoblastomas and osteosarcomas (Friend et al.,

1986; Lee et al., 1987). This gene became known as the retinoblastoma susceptibility gene (*RBI*).

1.2 The retinoblastoma protein regulates the cell cycle

Loss of *RBI* was initially only apparent in retinoblastomas and osteosarcomas, suggesting that the retinoblastoma protein (RB) may be a tissue-specific tumour suppressor. However, proteins coded by oncogenic viruses, called oncoproteins, were shown to bind to RB and inactivate it, and this process was required for cell transformation (DeCaprio et al., 1988; Dyson et al., 1989; Whyte et al., 1988, 1989). These oncoproteins included adenovirus E1A, simian virus 40 T antigen and human papilloma virus E7. This suggested that RB may play its role as a tumour suppressor in a broader context.

In addition, it was observed that loss of RB caused loss of control of cell proliferation, a “hallmark” feature of cancer (Bookstein et al., 1990; Hanahan and Weinberg, 2000; Huang et al., 1988; Takahashi et al., 1991). Rescuing RB function in cells with mutant RB reduced proliferation, colony formation and tumorigenicity *in vivo* (Huang et al., 1988). Early mechanistic insight into RB’s role as a tumour suppressor came from the observation that RB was phosphorylated in late G1, which suggested that it may play a role in cell cycle control, and was consistent with its loss and subsequent loss of proliferation control (DeCaprio et al., 1988).

The early mechanistic insight into RB-dependent cell cycle control was based on RB's interaction with differentiation-regulated transcription factor 1 (DRTF1), also known as the E2a-binding factor (E2F), named after its transcriptional activity at the adenovirus E2 promoter (Bandara and La Thangue, 1991; Chellappan et al., 1991; Chittenden et al., 1991; Kovesdi et al., 1987). E2F was shown to form a heterodimeric transcription factor with DRTF1-polypeptide 1 (DP1) (Girling et al., 1993). E2F/DP1 target genes were shown to contain an E2F-consensus motif in their promoters that were activated in an E2F-dependent manner in reporter assays (Boeuf et al., 1990; Kovesdi et al., 1987; Yee et al., 1987).

Furthermore, the first genes to be regulated by both cell cycle control and E2F-dependent transcription were discovered: *MYC* that promotes cell proliferation and dihydrofolate reductase that is involved in metabolism (Blake and Azizkhan, 1989; Hiebert et al., 1992; Thalmeier et al., 1989). These findings suggested that RB suppresses tumorigenesis through its inactivation of E2F transcription factors and their transcription of cell cycle genes, a process that can be deregulated by viral oncoproteins (Nevins, 1992).

1.3 The pocket domain and the RB pocket protein family

Based on sequence homology with RB and the ability to bind to viral oncoproteins, two proteins, p107 (*RBL1* gene) and p130 (*RBL2*), were additionally discovered (Cobrinik et al., 1993; Ewen et al., 1991; Hannon et al., 1993; Li et al., 1993; Mayol et al., 1993; Zhu et al., 1993) (Figure 1.1A, B). RB, p107 and p130 constitute the “pocket protein” family named after their common structure. They share a hydrophobic “pocket” made up of two cyclin-like folds, called A/B subdomains, separated by an unstructured linker (Chow and Dean, 1996). The subdomains fold together to form a globular “small pocket” domain (Gibson et al., 1994; Lee et al., 1998). The small pocket domain binds to viral oncoproteins and is sufficient to silence transcription (Chow and Dean, 1996; Chow et al., 1996; Hu et al., 1990; Kaelin et al., 1990; Sellers et al., 1995). More specifically, protein crystallography revealed that there is a binding cleft in the B subdomain known as the LxCxE binding site (Kaelin et al., 1990; Lee et al., 1998). This was named after the fact that viral oncoproteins binding here have such conserved motif. It has been described that this binding cleft is used by several chromatin and transcription regulators such as histone deacetylases, DNA methyltransferase 1 (DNMT1), histone methyltransferases and condensin II (Brehm et al., 1998; Longworth et al., 2008; Magnaghi-Jaulin et al., 1998; Nielsen et al., 2001; Robertson et al., 2000). The large pocket refers to the combination of the small pocket and a C-terminal domain in all three pocket proteins. This represents the minimal region to maintain negative growth control and interact with and inhibit E2F transcription factor (Hiebert et al., 1992; Qin et al., 1992).

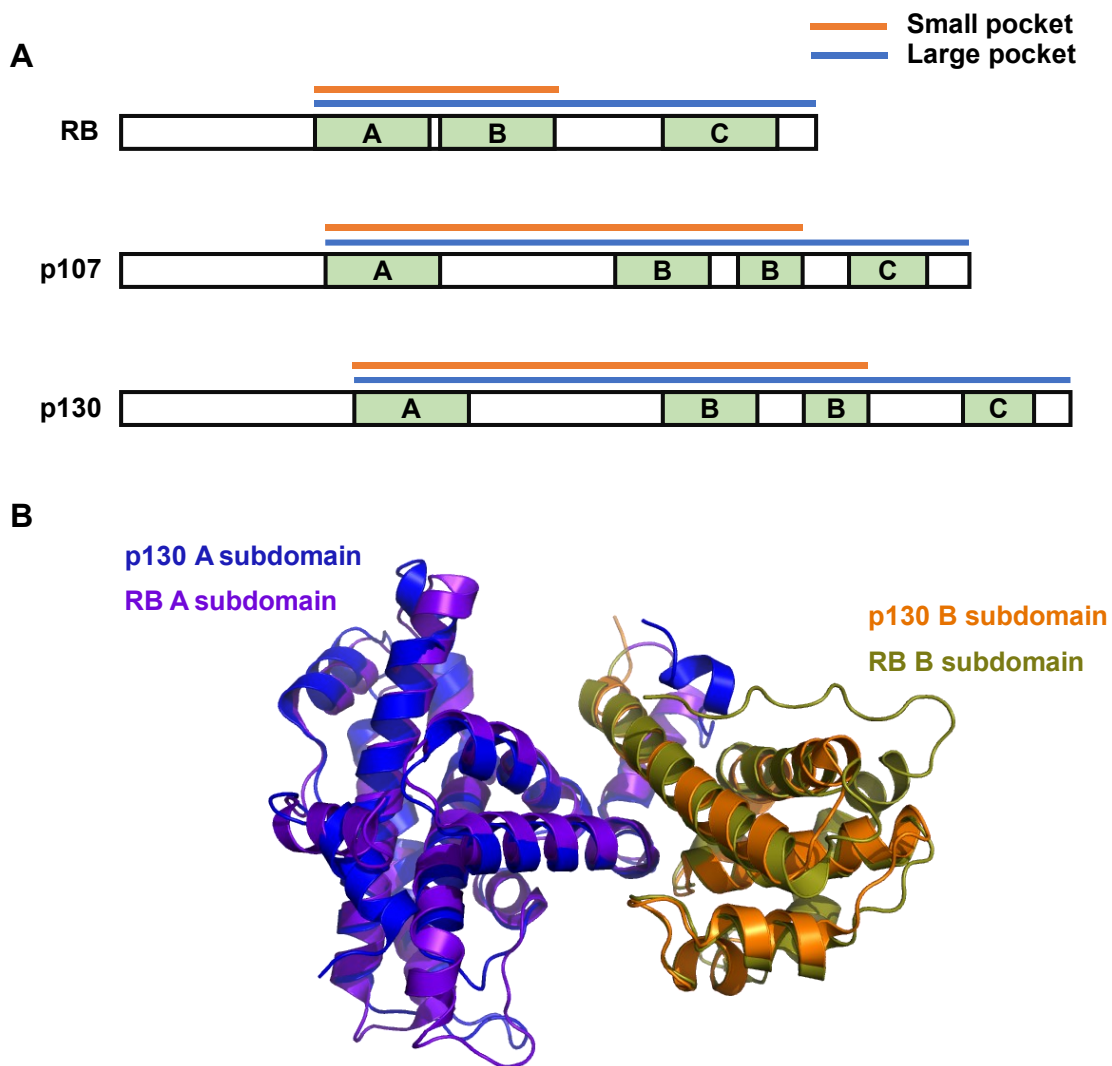


Figure 1.1: Domain diagram of the pocket family proteins.

(A) The three pocket proteins share A, B and C subdomains that construct the small and large pocket domain, indicated by horizontal lines above. (B) Superimposed small pocket domains of human p130 (PDB: 4YOZ) and RB (PDB: 1N4M).

1.4 E2F transcription factors recruit RB family proteins to DNA

Like the pocket protein family, there is a family of E2F transcription factors, and there are nuanced similarities and differences between their functions based on structure. There are nine E2F proteins encoded from eight *E2F* genes in mammals; alternate promoters yield E2F3a and E2F3b (Johnson and Degregori, 2006). All family members have a conserved DNA binding domain (Girling et al., 1993; Morgunova et al., 2015; Wu et al., 1995; Zheng et al., 1999). E2F1-6 share a conserved dimerization domain used to interact with DP family proteins. It follows that E2F7 and E2F8 do not bind to DP family proteins. Instead, they form homo/heterodimers with themselves (Morgunova et al., 2015). Each of DP family proteins, DP1, DP2/3 and DP4, prefers certain E2F interaction. Most importantly, DP1 heterodimerizes with E2F1, E2F2 and E2F3a to form “activator” E2Fs for their localization at promoters of genes related to cell cycle progression and DNA synthesis (DeGregori and Johnson, 2006). In contrast to the activators, E2F4-8 are classified as “repressor” E2Fs based on their role in cell cycle exit and differentiation (Chen et al., 2009). However, more recent studies suggest that this binary categorization appears to be an oversimplification as the “activator” E2Fs have been shown to repress as many as genes as they activate (Henley and Dick, 2012).

In regard to E2F interaction with the pocket proteins, E2F1-5 share a conserved transactivation domain (TAD) in their C-terminus required to activate transcription upon inactivation and loss of interaction with the pocket proteins (Dimova and Dyson, 2005). More specifically, this domain mediates the interaction between E2F1-4 and RB small pocket, and E2F4/5 and p107/p130 small pocket. Lacking the TAD, E2F6-8 do not interact with any pocket proteins (Dimova and Dyson, 2005; van den Heuvel and Dyson, 2008). Lastly, all pocket proteins rely on their interaction with E2Fs to bind DNA as they lack intrinsic DNA binding capacity.

1.5 RB-E2F interaction is regulated by upstream cyclin-CDKs.

A number of observations hinted that post-translational, not transcriptional, mechanism regulated RB activity (Dick and Rubin, 2013). First, RB is expressed in both dividing and non-dividing cells unlike p107 and p130, and its expression is relatively stable through the cell cycle (Buchkovich et al., 1989; Classon and Dyson, 2001). In contrast, p107 is a known E2F target whose expression is lower in quiescent cells and upregulated in S phase. p130 expression decreases through G1 and S phase and is more highly expressed in quiescent or differentiated cells (Xiao et al., 1996; Zhu et al., 1995). Furthermore, a family of serine/threonine kinases called cyclin-dependent kinases (CDKs) emerged as the likely upstream regulator of the RB-E2F interaction, its inactivation of E2F target gene transcription and proliferation, in line with the earlier observation that RB was heavily modified at the G1-S phase transition (Bremner et al., 1995; DeCaprio et al., 1989, 1992). This notion was based on finding CDK consensus sites dispersed throughout RB, and that RB-mediated cell cycle arrest could be overcome by overexpressing cyclins E or A (Bandara et al., 1991).

In early G1, hypophosphorylated RB binds and sequesters E2F transcription factor (Figure 1.2). Phosphorylation-mediated RB inactivation begins with extracellular signals such as mitogen growth factor signaling that leads to accumulation of D-type cyclins (D1, D2 and D3) (Donjerkovic and Scott, 2000). Cyclin D-CDK4/6 complex partially phosphorylates RB, at which point the cell is irreversibly committed to cell cycle entry (Hochegger et al., 2008). This induces E-type cyclins (E1 and E2) expression which bind to CDK2. Cyclin E-CDK2 complex further phosphorylates RB to its hyperphosphorylated form (Calbó et al., 2002). These complexes compete with PP1 phosphatase for a minimal binding site in the RB C-terminus (RBC) (Hirschi et al., 2010). RB hyperphosphorylation and its dissociation from E2F alleviates E2F to transcribe cell cycle genes (Burke et al., 2012).

Protein-protein interaction studies with truncated RB and E2F fragments with phosphomimetic substitutions at CDK phosphorylation sites revealed how CDK phosphorylation induces conformational changes to RB that disrupts its interaction with

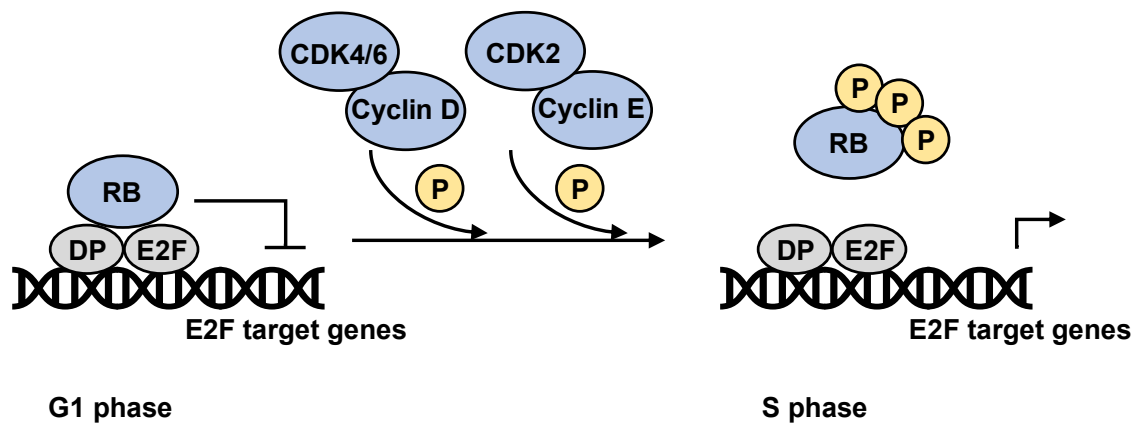


Figure 1.2: Cell cycle control by RB.

In early G1, the RB-E2F complex represses transcription of E2F target genes. Upon mitotic stimulation, cyclin-cyclin dependent kinase (CDK) complexes hyperphosphorylate RB, which dissociates RB from E2F transcription factors. This allows E2F target genes to be expressed and cells to enter S phase.

the E2F transactivation domain. S608/S612 phosphorylation in the linker between the A/B subdomain causes the linker to bind the pocket, which disrupts the subdomain from folding into the small pocket (Burke et al., 2010, 2012). Similarly, T356/T373 phosphorylation allows the RB N-terminus to fold onto the pocket domain. S788/S795 phosphorylation allows RBC to block the most upstream residues of the E2F transactivation domain from binding the pocket (Burke et al., 2014). Such inducible intramolecular interactions created by CDK phosphorylation have an additive effect that allosterically inhibits the E2F transactivation domain from binding the RB pocket.

On the other hand, there are mechanisms that resist RB hyperphosphorylation. For example, etoposide-induced DNA damage response facilitates K810 methylation of RB by Set7/9 methyltransferase (Carr et al., 2011). Crystal structures showed that this methylation sterically hinders with the active site of cyclin-CDK2, thereby diminishing overall RB phosphorylation at CDK-dependent sites. Functionally, expression of K810 methylation-ablated RB mutant promotes cell cycle arrest in a Set7/9-dependent manner. Furthermore, K873/874 acetylation by p300 histone acetyltransferase (HAT) blocks RB phosphorylation by cyclin E-CDK2 and blocks cell cycle progression (Chan et al., 2001a). Mechanistically, these post-translational modifications disrupt a conserved cyclin-CDK binding motif in RBC composed of basic residues (Adams et al., 1999). Furthermore, cyclin-CDK complexes that inactivate RB can themselves be inactivated by the inhibitors of CDK4 (INK4) and CDK-interacting protein/kinase inhibitory protein (Cip/Kip) families (Sherr and Roberts, 1999). INK4 family includes p16^{INK4a}, p15^{INK4b}, p18^{INK4c} and p19^{INK4d} (Chan et al., 1995; Guan et al., 1994; Hannon and Beach, 1994; Hirai et al., 1995; Serrano et al., 1993). Cip/Kip family includes p21^{Cip1}, p27^{Kip1} and p57^{Kip2} (Gu et al., 1993; Lee et al., 1995; Polyak et al., 1994a; Toyoshima and Hunter, 1994). These are aptly described as CDK inhibitors (CKIs). While INK4 proteins target the cyclin D-CDK4/6 complex, Cip/Kip proteins inhibit a wider range of cyclin D-, E- and A-CDK complexes. As mentioned above, mitogenic stimuli activates cyclin D accumulation and cyclin D-CDK complexes. Conversely, anti-mitogenic signals promote INK4 and Cip/Kip family protein activity (Polyak et al., 1994b; Reynisdóttir et al., 1995).

1.6 RB C-terminal domain has a unique interaction with E2F1

Further efforts to elucidate the interaction between RB and E2F with various mutant constructs provided insight into a second site in RBC downstream of the pocket domain that interact with E2F1 (Dick and Dyson, 2003) (Figure 1.3). For RB this was mapped to amino acid residues 825-860 (Julian et al., 2008). For E2F1, this was mapped to residues 1-374 and named the marked box domain (MBD) that was non-overlapping and distinct from the transactivation domain that interacts with the RB pocket. The MBD of E2F1 could be substituted into E2F3 to confer a gain-of-function interaction between E2F3 and RBC (Julian et al., 2008). Conversely, E2F1-RBC interaction was abrogated by substitution with E2F3's MBD. A valine at residue 276 in the MBD of E2F1 was shown to be crucial for maintaining its interaction with RBC. In addition, RB is the only pocket protein in the family that has such interaction with E2F1 (Cecchini and Dick, 2011). Based on the nature of such specificity, the interaction between E2F1-4 transactivation domain and the small pocket became known as the “general” interaction; that between RBC and E2F1 MBD became known as the “specific” interaction.

Owing to the structural difference between the two interaction schemes, the RB-E2F1 complex has distinct biochemical properties. Through the specific interaction, the RB-E2F1 complex is not disrupted by the adenoviral E1A (Seifried et al., 2008). This contrasts with E2F4 that can be competitively displaced by E1A as it can only rely on its interaction with the small pocket. As mentioned above, the small pocket houses the LxCxE binding cleft that viral oncoproteins bind to inactivate RB repression of E2F. In addition, the RB-E2F1 complex has a lower affinity for probes containing E2F consensus sequence, and fails to repress luciferase reporters controlled by E2F promoters (Dick and Dyson, 2003; Julian et al., 2008). Most strikingly, CDK phosphorylation of RB that leverages intramolecular electrostatic forces to disrupt the small pocket-TAD interaction does not affect the RB-E2F1 complex. This was demonstrated through endogenous RB immunoprecipitation (IP) experiments where E2F1 interacted with both hypo and hyperphosphorylated RB whereas E2F3 only interacted with hypophosphorylated RB

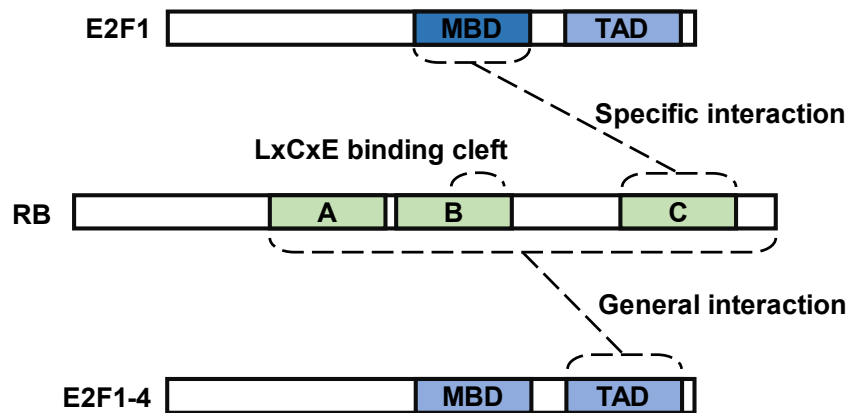


Figure 1.3: Protein domains that mediate the general versus the specific RB-E2F interactions.

The general interaction refers to RB large pocket-E2F transactivation domain (TAD) binding. The LxCxE binding cleft is located at the B subdomain of the pocket. E2F1 has a unique interaction among other E2Fs with the C-terminus of RB through its marked box domain (MBD).

(Cecchini and Dick, 2011). Such endogenous RB-E2F1 complex has been reported in independent studies (Calbó et al., 2002; Ianari et al., 2009; Wells et al., 2003).

In contrast to other E2Fs, E2F1 positively regulates transcription of pro-apoptotic genes and DNA repair (Irwin et al., 2000; Lin et al., 2001). As the RB-E2F1 complex bound by the specific interaction has a lower affinity to E2F consensus sequence and reduced transcriptional repression, the role of this complex in regulating a cell cycle-independent function such as apoptosis and DNA repair seemed plausible. Indeed, overexpression of RB mutant with abrogated general interaction with E2Fs was sufficient to inhibit E2F1-induced apoptosis (Dick and Dyson, 2003). A regulatory activity through the specific interaction is evident in another study that showed that the MBD of E2F1 is essential for inducing apoptosis based on chimeric E2F1 and E2F3 constructs (Hallstrom and Nevins, 2003). Furthermore, etoposide-induced DNA damage establishes a pool of RB-E2F1 complex that is required to promote transcription of the pro-apoptotic genes, *TP73* and *CASP7* (Carnevale et al., 2012). These observations suggest that the biochemically distinct RB-E2F1 complex may have many roles in cell cycle independent processes.

1.7 The canonical versus non-canonical functions of RB

The canonical model of RB function refers to RB-E2F mediated transcriptional control that is regulated by upstream cyclin-CDK complexes at G1-S checkpoint (Dick et al., 2018). Many lines of emerging data, however, suggests that there is a subset of RB that does not adhere to this scheme, which are collectively described as non-canonical functions of RB (Figure 1.4). Biochemically, many of these processes appear to rely on the RB-E2F1 complex mediated by the specific interaction. Lysine methylation that resists CDK-dependent RB phosphorylation and subsequent loss of E2F repression may also allow RB to conserve its non-canonical functions post G1-S checkpoint.

One of the distinguishing features of the non-canonical functions of RB is its genomic localization outside of E2F target promoters that contain a consensus DNA motif. For example, RB is recruited to sites of DNA double strand breaks (DSBs) to

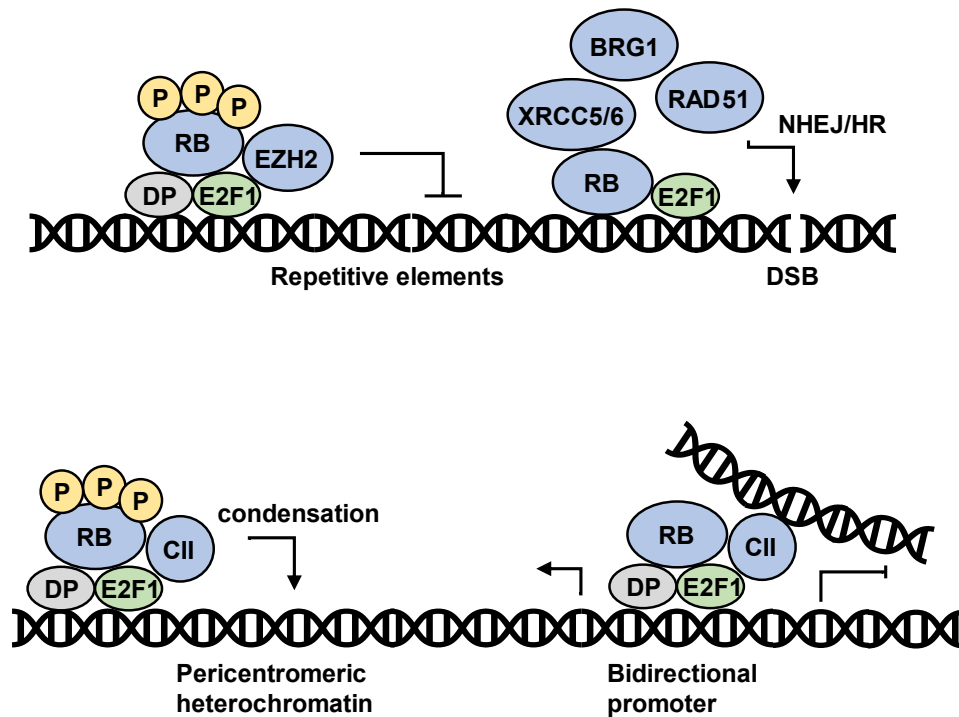


Figure 1.4: The RB-E2F1 complex is required for non-canonical functions of RB beyond cell cycle control.

The RB-E2F1 complex, mediated by the specific interaction, is resistant to cyclin-CDK phosphorylation and maintains their interaction. The RB-E2F1 complex has various functions unrelated to repression of E2F transcription factors. The complex recruits EZH2 to silence various repetitive elements through histone tail methylation. RB and E2F1 are required to assemble machinery involved in non-homologous end joining (NHEJ) and homologous recombination (HR) repair at DNA double strand breaks (DSBs). The LxCxE binding cleft in RB mediates condensin II (CII) recruitment to pericentromeric heterochromatin, which in turn facilitates chromosome condensation during mitosis. In an interphase nucleus, condensin II also regulates transcription at bidirectional promoters through maintaining long-range chromosome interactions.

facilitate repair processes via homologous recombination (HR) or nonhomologous end-joining (NHEJ) (Marshall et al., 2019; Vélez-Cruz et al., 2016). At DSBs induced by ionizing radiation (IR), RB and E2F1 cooperate with each other to recruit BRG1, which in turn facilitates DNA end resection and HR. RB N-terminus interaction with the core components of NHEJ machinery, XRCC5/6, mediates clearance of IR-induced DSB based on NHEJ-dependent GFP reporters and immunofluorescence staining (Cook et al., 2015). Similarly, loss of retinoblastoma-related 1 (RBR1), the RB homolog in *Arabidopsis*, results in a failure to recruit components of HR repair machinery, RAD51 and BRCA1, to DSBs induced by genotoxic drugs (Biedermann et al., 2017; Horvath et al., 2017). Furthermore, the RB-E2F1 complex recruits condensin II and enhancer of zeste homolog 2 (EZH2) to pericentromeric heterochromatin and repetitive elements, whose loss results in genome instability (Coschi et al., 2010, 2014; Ishak et al., 2016). Their discovery and function will be discussed in depth later.

1.8 The non-canonical functions of RB may underlie sensitivity to chemotherapy and radiation upon RB loss

The contribution of such non-canonical functions of RB to genome stability may explain the effect of RB loss on drug sensitivity (Figure 1.5A). The molecular profiling of 230 untreated lung adenocarcinoma samples established that the RB pathway, including RB itself, cyclin D, CDK4/6 and CDK inhibitor 2A gene (*CDKN2A*) that encodes upstream p16^{INK4a}, is commonly deregulated through somatic mutations and copy number variations (Collisson et al., 2014). Strikingly, loss of RB or its inactivation by hyperphosphorylation is associated with improved survival in patients treated with platinum chemotherapy for lung adenocarcinoma or its parent non-small cell lung cancer (NSCLC) (Cecchini et al., 2015; Zhao et al., 2012). Notably, RB expression was not associated with any change in proliferation, E2F target gene expression or E2F1-induced apoptosis (Cecchini et al., 2015). RB ablation in lung and other cancer cell lines also induced increased sensitivity to chemotherapy in culture and reduced viability *in vivo* (Marshall et al., 2019; Zagorski et al., 2007). Furthermore, these findings have been

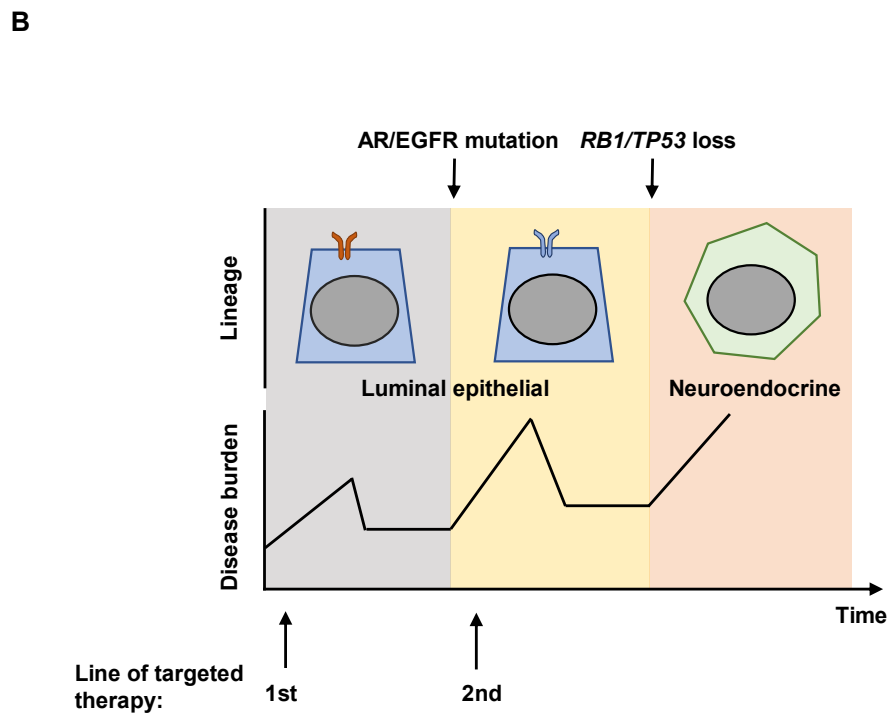
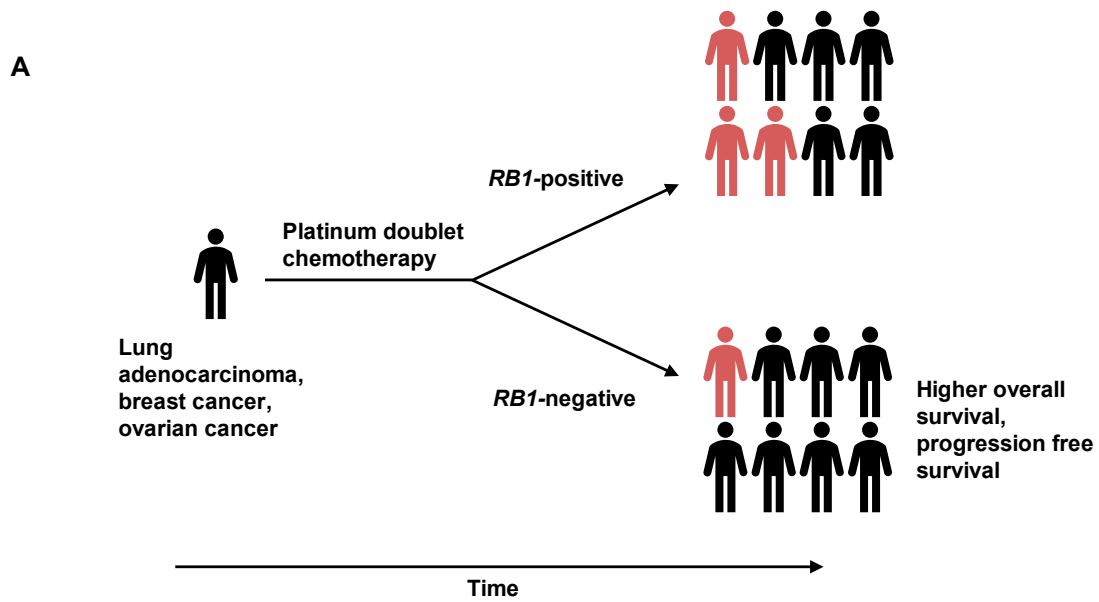


Figure 1.5: The relationship between *RB1* loss, response to chemotherapy and resistance to targeted therapies.

Figure 1.5: The relationship between *RB1* loss, response to chemotherapy and resistance to targeted therapies.

(A) Loss of RB is associated with better clinical outcomes in patients treated with chemotherapy for lung adenocarcinoma, breast, and ovarian cancer. (B) Loss of RB is associated with neuroendocrine transdifferentiation of initially luminal epithelial prostate cancer and lung adenocarcinoma. Through such process, cancer proliferation is no longer dependent on androgen receptor (AR) or epidermal growth factor receptor (EGFR) signaling, rendering existing therapeutics targeting such signaling pathways ineffective.

extended to breast and ovarian cancer (Kommos et al., 2007; Witkiewicz et al., 2012). Mutations in HR and DNA repair machinery proteins and RB loss were enriched in long progression free and long-term survivors among high grade serous ovarian cancer (HGSOC) patients (Garsed et al., 2018). Consistent with this, germline and somatic HR deficiency has been established to predict favourable response to chemotherapy in epithelial ovarian cancer (EOC) (Alsop et al., 2012; Bolton et al., 2012; Pennington et al., 2014).

The role of RB-dependent cell cycle arrest upon DNA damage induced by chemotherapy is not sufficient to account for the relationship between RB loss and improved sensitivity to chemotherapy (Knudsen et al., 2000). p53 inactivation would similarly abrogate DNA damage induced cell cycle arrest, as p53 is upstream of RB in this pathway (Sherr and McCormick, 2002). However, p53 status is not associated with better survival upon chemotherapy in NSCLC (Zagorski et al., 2007). Taken together, RB's status as a strong predictor for better responsiveness in various cancers is not easily reconciled simply based on the understanding of RB's canonical functions. However, RB's non-canonical role in maintaining genome integrity through recruiting HR and NHEJ machinery and chromatin remodeling or regulatory proteins such as condensin II and EZH2 can explain how loss of such function would sensitize cancer cells to chemotherapy and improve clinical outcome (Figure 1.4).

1.9 RB loss is associated with resistance to targeted molecular therapies.

Emerging evidence of resistance mechanisms to targeted molecular therapies also suggests that the canonical functions of RB only describes a facet of RB function (Dick et al., 2018) (Figure 1.5B). For example, prostate cancers rely on androgen receptor (AR) signaling for growth and survival. There have been iterations of anti-androgen therapy that blocks various aspects of AR signaling (Tran et al., 2009). Despite these efforts, original prostate adenocarcinoma cells can undergo histological transdifferentiation from luminal epithelial to a neuroendocrine appearance (Watson et al., 2015). This resistance mechanism can arise in response to the latest anti-androgens like enzalutamide,

completely bypassing AR signaling for growth and survival. RB loss is associated with such treatment acquired neuroendocrine prostate cancer in comparison to the original prostate adenocarcinoma (Abeshouse et al., 2015; Rickman et al., 2017). In human and mouse models, combined loss of p53, RB or PTEN is sufficient to induce lineage plasticity in prostate adenocarcinoma cells where a subpopulation gains neuroendocrine features and their lineage becomes heterogeneous (Ku et al., 2017; Mu et al., 2017). Again, RB loss did not significantly affect proliferation in these models (Ku et al., 2017).

RB loss has also been documented in resistance to epidermal growth factor receptor (EGFR) tyrosine kinase receptor inhibitors for treating lung adenocarcinoma. In a subset of patients, several somatic mutations in EGFR renders it a target for inhibitors such as gefitinib (Lynch et al., 2004). Like prostate cancer, the first line of resistance arose from additional EGFR mutations that reduced inhibitor binding and restored EGFR signaling (Kobayashi et al., 2005; Yun et al., 2007). Even against the third-generation inhibitors such as osimertinib that targets gefitinib-resistant mutant EGFR, the original adenocarcinoma cells can become resistant to EGFR inhibitors through neuroendocrine transformation at which point EGFR signaling is no longer necessary for uncontrolled proliferation (Ham et al., 2016; Kim et al., 2015; Piotrowska et al., 2015).

These examples suggest that RB loss promotes lineage plasticity as a resistance mechanism through a mechanism independent of its repression of E2F target genes and cell cycle entry. A plausible explanation is that RB loss derepresses repetitive elements and pluripotency factors such as OCT4 and SOX2 (Dick et al., 2018). Upregulation of satellite repeats, long interspersed nuclear element 1 (LINE-1) and nearby neuroendocrine-related genes has been reported in various epithelial cancers including prostate cancer (Ting et al., 2011). As mentioned above, the RB-E2F1 complex recruits EZH2 to silence satellite repeats, LINEs and more (Figure 1.4, Ishak et al., 2016). In addition, RB loss can induce expression of OCT4 and SOX2 among other embryonic stem cell genes in mouse embryonic fibroblasts (MEFs) (Liu et al., 2009). Mechanistically, RB is required to recruit HDAC and EZH2 to *Oct4* and *Sox2* regulatory elements to repress their expression through histone tail modifications (Kareta et al., 2015). This is consistent with SOX2 upregulation upon ablating both p53 and RB in a

human prostate cancer cell line (Mu et al., 2017). SOX2, in turn, promotes expression of neuroendocrine markers over luminal ones like AR, a process that can be reversed by blocking SOX2. The mounting evidence of the relationship between RB loss and neuroendocrine transdifferentiation as a resistance mechanism to targeted therapy in prostate and lung cancer supports the notion of non-canonical functions of RB outside of cell cycle control through E2F repression.

1.10 Targeted *Rb1* mutations have revealed non-canonical functions of the RB-E2F1 complex

Given the structure-function relationship of RB-E2F complexes, inducing targeted mutations in RB's various binding surfaces that specifically disrupt certain protein-protein interaction was a logical approach to dissect these non-canonical functions of RB. Notably, recent characterization of two mouse models harbouring mutant RB alleles, named *Rb1^{ΔL}* and *Rb1^{ΔS}*, has revealed that the RB-E2F1 complex recruits chromatin regulatory complexes to DNA in asynchronously dividing cells (Coschi et al., 2010, 2014; Isaac et al., 2006; Ishak et al., 2016; Marshall et al., 2020). I will next describe the two mouse models, the chromatin regulatory complexes, their functions, and implications for this thesis.

1.11 The *Rb1^{ΔL}* mouse model reveals RB-E2F1 recruitment of condensin II to DNA

The LxCxE binding cleft is conserved among the pocket proteins despite its susceptibility to inactivation by viral oncoproteins (Lee et al., 1998). This suggests that this binding site may be involved in processes other than E2F-repression mediated cell cycle control. Initially, the interaction between the LxCxE binding cleft and chromatin modifying proteins such as HDAC1/2, Suv39h1, DNMT1 and the SWI/SNF complex were merely thought to inhibit E2F target transcription and cell cycle progression (Brehm et al., 1998; Dunaief et al., 1994; Lai et al., 1999; Luo et al., 1998; Magnaghi-Jaulin et al., 1998; Nielsen et al., 2001; Robertson et al., 2000; Zhang et al., 2000). However, mice carrying the *Rb1^{ΔL}* (for LxCxE) allele, which consists of I746A, N750A and M754A substitutions, revealed a new function (Isaac et al., 2006). These substitutions render the

LxCxE binding cleft inactive for protein-protein interaction based on GST-tagged protein pulldown experiments. As expected, *Rb1^{ΔL}* MEFs maintain E2F and cell cycle regulation and become quiescent in serum-starved or confluent growth conditions. This is consistent with *in vitro* studies that showed cells expressing mutant RB with specific loss of the LxCxE binding cleft can repress promoters containing E2F consensus motif, and briefly maintain cell cycle arrest (Chan et al., 2001b; Chen and Wang, 2000; Dahiya et al., 2000; Dick et al., 2000).

Mitotic defects in MEFs were the most apparent loss of function in *Rb1^{ΔL}* mice (Coschi et al., 2010; Isaac et al., 2006). Compared to WT, the mutant MEFs displayed hypocondensed chromatin at metaphase that were slower to align. Sister chromatids also lagged during separation, leading to prolonged anaphase. Centromere fusions and chromosome missegregation were also observed through immunofluorescence microscopy. Likely because of these defects, proliferating *Rb1^{ΔL}* MEFs had more proportion of cells with aneuploidy indicated by >4N DNA content.

Such phenotype combined with existing literature suggested that abrogated recruitment of condensin II by RB was the molecular determinant. Condensin II maintains chromosome condensation in prometaphase and structure during mitosis, especially at centromeres (Hagstrom et al., 2002; Ribeiro et al., 2009; Yong-Gonzalez et al., 2007). It was first reported in *Drosophila* that RBF1 (RB homolog) interacts with dCAP-D3 subunit of condensin II to maintain chromatin structure through the LxCxE binding cleft. This finding was also extended to human cells (Longworth et al., 2008). In *Rb1^{ΔL}* MEFs, condensin II was the only structural maintenance of chromosomes (SMC) family protein complex whose chromatin binding was reduced (Coschi et al., 2010). Furthermore, shRNA-mediated knockdown of CAP-D3 subunit recapitulated chromosome condensation and separation defects seen in *Rb1^{ΔL}* MEFs. Chromatin immunoprecipitation (ChIP) experiments revealed that an RB-E2F1-condensin II complex localizes to pericentromeric heterochromatin (Coschi et al., 2014). Its absence induces DSBs at this region in S phase. This is consistent with centromere fusions seen in *Rb1^{ΔL}* MEFs during metaphase. Furthermore, decreased condensin II recruitment to pericentromeric heterochromatin and aberrant DNA replication and mitotic chromosome

segregation were evident upon loss of one *Rb1* allele, which indicates that this non-cell cycle function of RB is haploinsufficient. Lastly, the cooperation between RB and E2F1 is crucial for the chromatin localization of this complex (Coschi et al., 2014). In *E2f1*^{-/-} MEFs, CAP-D3 subunit of condensin II loses recruitment to pericentromeric heterochromatin. Likewise, E2F1 recruitment to this region requires RB expression. These observations have established that the RB-E2F1 complex recruits condensin II to pericentromeric heterochromatin in early mitosis to ensure proper chromosome condensation.

More recent data also found that the RB-E2F1 complex recruits condensin II through the LxCxE binding cleft to bidirectional promoters and regulates their transcription (Marshall et al., 2020). In *Rb1*^{ΔL} MEFs, one of the two genes controlled by a bidirectional promoter is often transcriptionally deregulated. Chromosome conformation capture (3C) and circularized 3C (4C) assays showed that *Rb1*^{ΔL} MEFs have similar short range chromosome interactions, but deregulated long-range contacts compared to wild type (WT). For example, *Usp5/Cdca3* bidirectional promoter interaction with *Hoxa10* was seen less frequently in *Rb1*^{ΔL} MEFs compared to WT. Such deregulation may underpin the loss of transcriptional insulation of bidirectional promoters. Importantly, inducing aneuploidy and delayed mitotic progression in WT MEFs did not recapitulate the dichotomous transcriptional deregulation at bidirectional promoters. This suggests that abrogated condensin II function in mitosis in *Rb1*^{ΔL} MEFs is not responsible for deregulated gene expression, even though a similar relationship has been observed in fission yeast (Hocquet et al., 2018).

1.12 Condensin II is a SMC family protein complex

The structural maintenance of chromosomes (SMC) family of proteins consists of condensin I, condensin II, cohesin and the SMC5/6 complex (Hirano, 2012; Losada and Hirano, 2005) (Figure 1.6A-B). These complexes have a core component made up with a heterodimer between two SMC proteins. In eukaryotes, SMC1 and 3 form cohesin, and SMC2 and 4 form both condensin I and II (SMC5 and 6 for the SMC5/6 complex). These SMC subunits are evolutionarily conserved in all three phyla of life and share a ‘hinge’

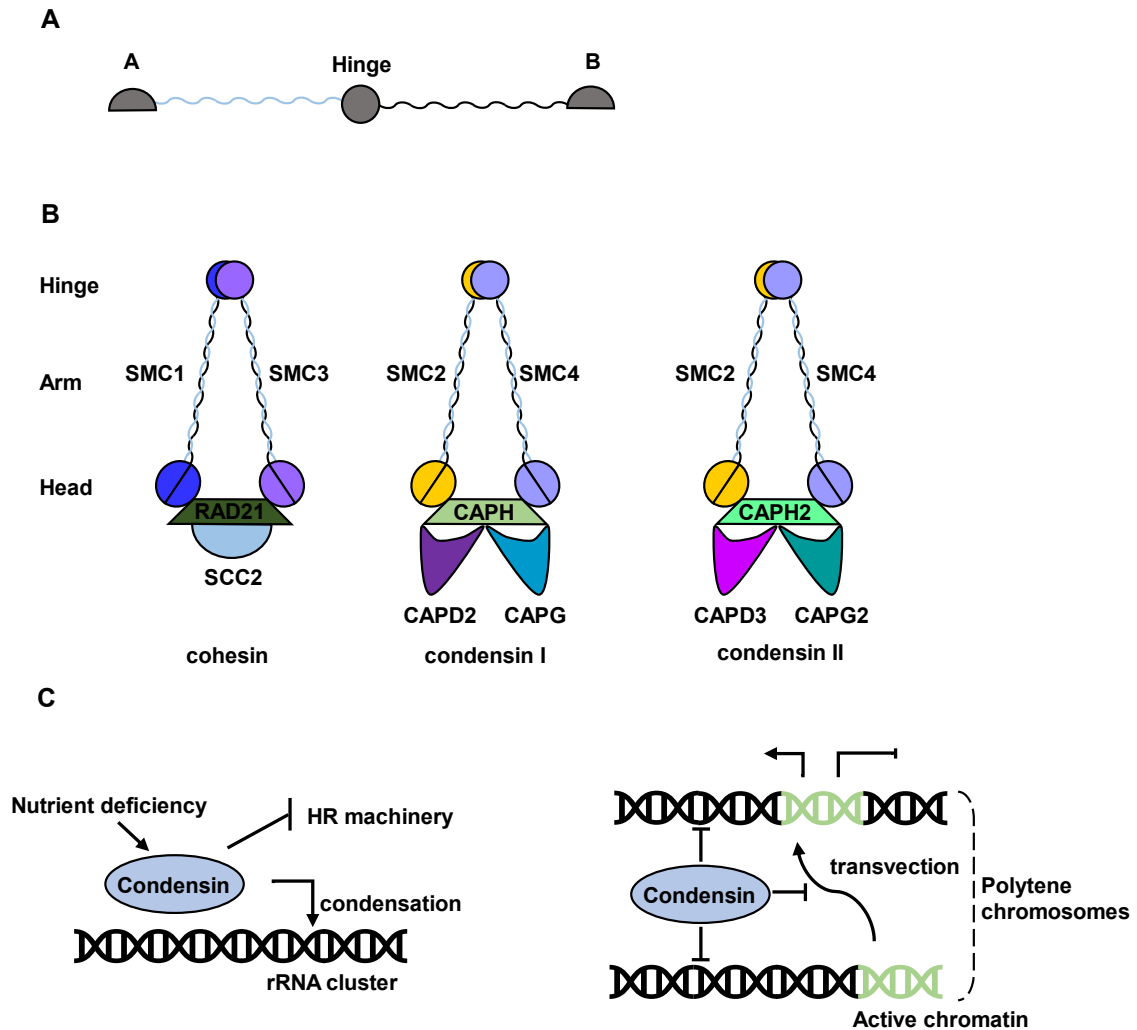


Figure 1.6: Structural maintenance of chromosomes (SMC) family proteins and condensin function in an interphase nucleus.

(A) An SMC protein diagram that depicts two subdomains (A and B) that form the head domain, and the hinge in the middle. (B) Subunit composition of cohesin, condensin I and condensin II. The hinge domains of the SMC heterodimers separate the two head domains connected to the hinges by the coiled-coil arms. RAD21 and SCC2 are cohesin's non-SMC subunits. Condensin I contains the kleisin CAP-H and HAWK proteins CAP-D2 and CAP-G. Condensin II contains the kleisin CAP-H2 and HAWK proteins CAP-D3 and CAP-G2. C. Upon nutrient deficiency, condensins block homologous recombination and condense rRNA gene cluster to protect its integrity (left). Condensins block association between polytene chromosomes and consequently transvection, where transcription is affected by *trans*-acting regulatory elements.

domain in the middle that allows the protein to fold in half (Cobbe and Heck, 2004). Based on electron microscopy and protein crystallography, SMC1/3 dimer hinge of cohesin forms a ring shape whereas SMC2/4 dimer hinge of condensins is rod-shaped (Anderson et al., 2002). The hinge-hinge interaction accounts for most of SMC protein dimerization (Haering et al., 2002; Hirano, 2002; Kurze et al., 2011). The N- and C-terminus form the head domain which is connected to the hinge by a 50-nm long antiparallel coiled coil arm (Melby et al., 1998). The head domain has ATPase activity that regulates the interaction between two head domains of an SMC dimer. The head mediates interaction with a kleisin family protein at its N and C-terminus: CAP-H and CAP-H2 for condensin I and II, respectively). These kleisin proteins recruit two additional subunits known as HEAT repeat proteins associated with kleisins (HAWK) proteins: CAP-D2 and CAP-G, CAP-D3 and CAP-G2 for condensin I and II, respectively. Cohesin consists of the kleisin protein RAD21 and HAWK protein SCC2 (Losada and Hirano, 2005).

In general, cohesin and condensin act to resolve sister chromatids and facilitate chromosome condensation, respectively. During DNA replication, cohesin maintains cohesion between sister chromatids by forming various ring-like structures around DNA (Gruber et al., 2003; Losada et al., 2002; Nasmyth, 2011). Into prophase and metaphase, a majority of cohesin is targeted for dissociation from chromatin, leaving a small pool at pericentromeric heterochromatin protected by the shugoshin protein (Clift et al., 2009; Giménez-Abián et al., 2004; Marston et al., 2004; Sumara et al., 2002). The mitotic spindle pulls against such chromatin-cohesin complex to align chromosomes at the metaphase plate. In the meantime, condensin II associates with chromosomes more stably to facilitate chromosome condensation (Gerlich et al., 2006). This is aided by condensin I that gains access to chromatin upon nuclear envelope breakdown in prometaphase. This temporal difference is due to the fact that condensin I is mostly cytoplasmic whereas condensin II is mostly nuclear throughout interphase (Gerlich et al., 2006; Hirota et al., 2004; Ono et al., 2004). Functionally, condensin I is involved in lateral compaction while condensin II supports axial shortening of chromosomes (Green et al., 2012; Shintomi and Hirano, 2011). At the start of anaphase, shugoshin degradation and RAD21 cleavage

open the ring structure and release cohesin from chromatin, allowing sister chromatids to be separated to opposite ends of daughter cells (Hauf et al., 2001; Uhlmann et al., 1999). Subsequently, condensin I is unloaded and exported out of the nucleus and condensin II partially loses affinity to DNA (Jeppsson et al., 2014).

1.13 Condensins regulate chromosome dynamics in interphase nuclei

Condensins perform additional roles outside of mitosis (Figure 1.6C). For example, in *Saccharomyces cerevisiae*, condensin is recruited to ribosomal RNA (rRNA) genes that are clustered together in tandem on chromosome XII (Petes, 1979). Upon nutrient starvation, condensin facilitates condensation of rRNA genes and blocks HR machinery (Tsang et al., 2007). This protects rRNA genes from aberrant recombination that can affect rRNA copy number and stability. In addition, condensin II promotes dissociation of polytene chromosomes, which are paired homologous chromosomes in polyploid cells, in *Drosophila* ovarian nurse cells undergoing oogenesis (Apte and Meller, 2012; Dej and Spradling, 1999; Hartl et al., 2008). Their dissociation also negatively regulates transvection, where transcription is controlled by *trans*-acting DNA regulatory elements between homologous chromosomes. Condensin II subunits dCAP-H2, dCAP-D3 and SMC2 have been identified as factors that antagonize such homologous chromosome pairing in a high-throughput screen (Joyce et al., 2012). More specifically, *Drosophila* Hi-C data showed that condensin II is required to block interaction between active chromatin (Rowley et al., 2019). Following the disruption of homology-paired chromosomal interaction in the fifth endocycle of oogenesis, condensin II also facilitates formation of chromosomal territories (CTs) (Bauer et al., 2012). These CTs were marked by axial chromosome compaction, and diffusion of pericentromeric and centeromeric regions throughout the nucleus. In contrast, condensin II subunit CAP-H2 mutant cells exhibited a Rab1 conformation, where such regions are clustered together at a single pole, which indicates that their chromosomes could not be reorganized. Lastly, highly condensed chromatin of naive peripheral T cells is required for quiescence and resistance to cytokine-mediated activation (Rawlings et al., 2011). Their chromatin condensation may be mediated by condensin II as a mutant allele of the kleisin subunit

CAP-H2 disrupts chromatin condensation in developing thymocytes, and results in cell death (Gosling et al., 2007; Rawlings et al., 2011). Overall, these examples demonstrate that condensin complexes are key factors that regulate chromatin dynamics in an interphase nucleus.

1.14 The *Rb1^{ΔS}* mouse model reveals RB-E2F1 recruitment of EZH2 to repetitive elements

Based on early work that showed the specific interaction between RB and E2F1, another mouse model carrying the *Rb1^{ΔS}* allele was created (Cecchini and Dick, 2011; Dick and Dyson, 2003; Ishak et al., 2016). F832A substitution rendered the specific interaction inactive. Like *Rb1^{ΔL}* mice, this loss of function did not affect the expression of RB, p107 or p130, or cell cycle control and repression of E2F target genes compared to WT (Ishak et al., 2016). This is consistent with GST pulldown experiments that showed *RB^{ΔS}* maintains interaction with E2F1's TAD through its pocket domain, but unable to bind E2F1's MBD. CHIP-seq for RB in both arrested and proliferating MEFs showed that RB is broadly recruited to various repetitive elements in intergenic and intronic regions of the genome. Strikingly, this recruitment was abrogated in *Rb1^{ΔS}* MEFs to a level comparable to *Rb1^{-/-}* MEFs. The functional role of RB at repetitive elements became evident through microarray data that showed upregulation of repetitive elements in *Rb1^{ΔS}* MEFs. Mechanistically, RB recruits enhancer of zeste homolog 2 (EZH2), the catalytic subunit of the polycomb repressive complex 2 (PRC2) to repetitive elements to silence their transcription (Ishak et al., 2016). *Rb1^{ΔS}* mutation abrogated this recruitment and induces loss of the repressive histone mark, H3K27me3, deposited by EZH2. Like the RB-E2F1-condensin II complex, this RB-EZH2 complex is dependent on E2F1 as RB localization at repetitive elements was diminished in *E2f1^{-/-}* MEFs. Lastly, *Rb1^{ΔS}* mice succumbed to spontaneous lymphomas, particularly in the spleen, which is consistent with decreased H3K27me3 at repetitive elements and their upregulated transcription in splenocytes (Ishak et al., 2016).

1.15 PRC1 and PRC2 modify histone tails that compact chromatin and silence transcription

EZH2 is one of many mammalian homologs of *Drosophila* polycomb group (PcG) proteins. These genes were identified as *trans*-acting factors that suppress expression of homeotic (*Hox*) genes that establish segmental identity along the anterior-posterior axis (Lewis, 1978). Adult male flies with mutant PcG genes develop aberrant comb-like structures on their legs (Lewis, 1947). In mammals, these proteins assemble two complexes, polycomb repressive complex 1 and 2 (PRC1/2) (Figure 1.7). These complexes have different structures and catalytic activities, but ultimately support transcriptional repression (Cao et al., 2002, 2005; Kirmizis et al., 2004; Wang et al., 2004a).

PRC2 is comprised of four core subunits that form a four-lobed structure: EZH2 (or EZH1), suppressor of zeste 12 homolog (SUZ12), embryonic ectoderm development (EED) and retinoblastoma-binding protein 4/7 (RBBP4/7) (Cao and Zhang, 2004a; Cao et al., 2002; Kuzmichev et al., 2002; Montgomery et al., 2005; Pasini et al., 2004). The catalytic activity occurs in a lobe formed by the C-terminus of EZH2 that contains a cysteine-rich region (CXC) and the SET domain, which is highly conserved among other lysine methyltransferases. A series of hydrophobic residues provides a channel for the aliphatic chain of the lysine substrate. The cofactor S-adenosyl methionine (SAM) binds to a region further downstream where it is positioned close to the target lysine. However, EZH2 alone has no catalytic activity; SUZ12 and EED are required to prevent EZH2 from autoinhibition where its C-terminal domain allosterically blocks the active site (Antonyamy et al., 2013; Cao and Zhang, 2004b; Wu et al., 2013). The C-terminal domain of EED can bind H3K27me₃, which allosterically activates the catalytic activity of PRC2 (Margueron et al., 2009). In addition to the core subunits, a set of accessory subunits defines two subcomplexes of PRC2, without which the core complex cannot be recruited to chromatin (Choi et al., 2017; Healy et al., 2019; Højfeldt et al., 2019; Holoch and Margueron, 2017; van Mierlo et al., 2019; Youmans et al., 2018).

A heterodimer of RING1A or RING1B and one of the six polycomb group ring finger (PCGF1-6) proteins forms the core PRC1 (Chittock et al., 2017). Their C-terminal

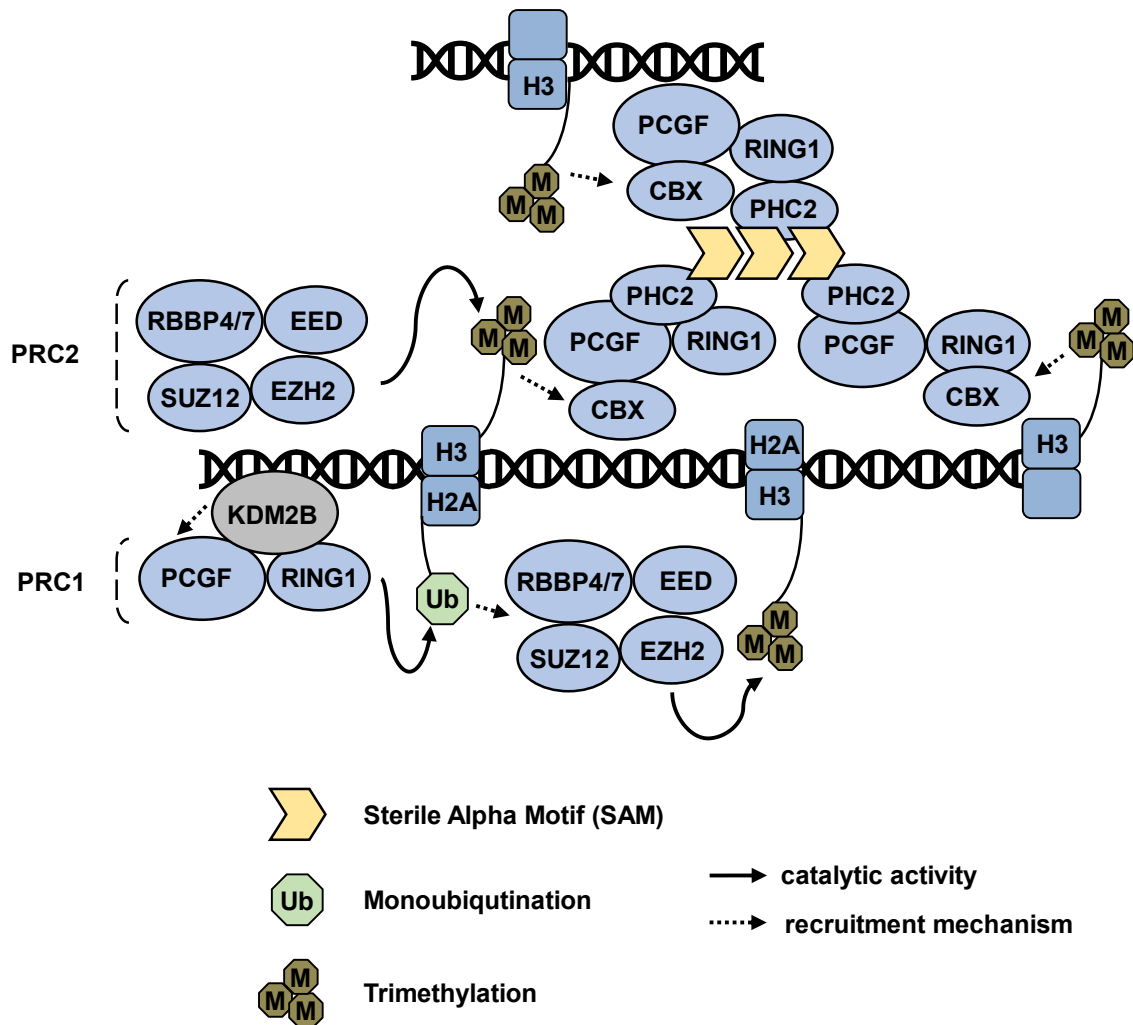


Figure 1.7: Mammalian homologs of the polycomb group (PcG) genes form the polycomb repressive complex 1 and 2 (PRC1/2).

PRC2 consists of four core subunits: SUZ12, EZH2, EED and RBBP4/7. PRC2 catalyzes histone 3 lysine 27 methylation. PRC1 consists of two core subunits, RING1A/B and one of six PCGF proteins, and catalyzes histone 2a lysine 119 ubiquitination. Such histone tail modifications often cooperate with each other, depending on PRC1 subunit composition.

ring finger and WD40 ubiquitin-like (RAWUL) domains dictate interaction with other subunits. RING1 RAWUL recruits either a chromobox (CBX) protein or RYBP (or its homolog YAF2). PCGF2 and 4 are mutually exclusive with RYBP/YAF2, while the other four are mutually exclusive with CBX proteins. A Polyhomeotic (Ph) homologous protein (PHC) that has a sterile alpha motif (SAM) is associated with CBX-PRC1. Such PRC1 subtypes achieve transcriptional repression through SAM oligomerization instead of H2AK119ub (Blackledge et al., 2014, Isono et al., 2013, Robinson et al., 2012, Tsuboi et al., 2018). Interestingly, each of the six PCGF proteins is associated with distinct genomic localization of their parent PRC1 and functional processes regulated by their target genes (Gao et al., 2012). The RING proteins are ubiquitin E3 ligases that catalyze histone 2A lysine 119 ubiquitination (H2AK119ub). This process follows a cascade of E1, E2 and E3 ligases that carries ubiquitin through various covalent bonds that are created then broken, which ultimately arrives at the ϵ -amino group of the target lysine (Pickart, 2001).

The role of H2AK119ub appears to be context dependent. Early electron microscopy data showed that loose “beads-on-a-string” nucleosomal arrays did not require histone tails to be compacted in the presence of PRC1 *in vitro* (Francis et al., 2004). In addition, catalytically inactive RING1B mutant is sufficient to compact *Hox* genes and repress their expression in embryonic stem cells (ESCs) (Eskeland et al., 2010). However, catalytically active RING1A/B is required to repress differentiation markers and maintain ESC identity (Endoh et al., 2012). Furthermore, H2AK119ub and H3K27me3 have been shown to cooperate with each other. Earlier studies showed that PRC1 and PRC2 function in a hierarchical manner where CBX protein-containing PRC1 recognizes PRC2-deposited H3K27me3 (Cao et al., 2002; Wang et al., 2004b). This is consistent with co-localization of PRC1 and PRC2 at PcG targets in *Drosophila* and mice (Boyer et al., 2006; Ku et al., 2008; Schwartz et al., 2006). In addition, RING1B deletion does not affect H3K27me3 in ESCs (Endoh et al., 2012). However, this model has been recently challenged as RYBP-PRC1 that lacks a chromodomain motif is recruited to certain PcG targets and deposits H2AK119ub despite H3K27me3 depletion (Tavares et al., 2012). Furthermore, the hierarchical model, where H3K27me precedes H2AK119ub

deposition, is controversial as co-depletion of RING1A and RING1B and subsequent loss of H2AK119ub lead to loss of global H3K27me3 (Blackledge et al., 2014). This study also identified a PCGF1-PRC1 complex that is recruited *de novo* to non-methylated DNA through a histone demethylase KDM2B, which precedes PRC2 binding and H3K27me3. Notably, this PRC1 subtype has H2AK119ub catalytic activity in contrast to CBX-associated PRC1. Conversely, recognition of H2AK119ub by PRC2 requires accessory subunits JARID2 and AEBP2 (Kalb et al., 2014). Overall, these findings show that the interplay between PRC1 and PRC2 activity is complex and varies based on PRC1 subunit composition.

1.16 Epigenetic modifications silence repetitive elements

Along with PRC1 and PRC2, other histone tail modifications and DNA methylation reduce DNA accessibility for transcriptional machinery. For example, Suv39h1 and Setdb1 deposits histone 3 lysine 9 trimethylation (H3K9me3) at pericentromeric and telomeric repeats, and intracisternal A-type particle (IAP) long terminal repeat (LTR) in MEFs and mESCs (Martens et al., 2005). Setdb1 also catalyzes H3K9me3 at LINEs and ERVs in developing mouse embryos (Bulut-Karslioglu et al., 2014; Karimi et al., 2011; Liu et al., 2014; Matsui et al., 2010; Sharif et al., 2016). Although these reports did not find a strong link between SINEs and Suv39h1, expression of a primate-specific SINE, called Alu, was increased upon inhibition of SUV39H1 in HeLa cells (Kondo and Issa, 2003). Suv420h proteins also catalyze histone 4 lysine 20 di/trimethylation (H4K20me2/3) at centromeric, pericentromeric and telomeric repeats (Jorgensen et al., 2013).

Furthermore, DNA methylation of cytosines also silences various repetitive elements. In mammals, DNMT1 maintains DNA methylation following DNA replication where the daughter copy passively loses DNA methylation (Moore et al., 2013). On the other hand, Dnmt3a/b methylates DNA *de novo* during embryogenesis. Deletion of Dnmt1 induces loss of DNA methylation at IAP and centromeric repeats in mESCs (Li et al., 1992; Walsh et al., 1998). In line with this, mice carrying a hypomorphic *Dnmt1* allele exhibit global DNA hypomethylation and succumb to thymic lymphoma, in which somatic retrotransposition of IAP often drives tumorigenesis (Howard et al., 2008).

Another study found that both Dnmt1 and Dnmt3a/b are required to maintain DNA methylation at LINES in mESCs (Liang et al., 2002). These examples demonstrate the breadth of various mechanisms that silence repetitive elements.

1.17 Various mechanisms enable repetitive elements to expand in the genome

The most abundant repetitive element by copy number and coverage are retrotransposons, which are a class of mobile elements (Lander et al., 2001). They are first copied into an RNA intermediate, reverse transcribed to cDNA, then inserted into new genomic locations. For example, long interspersed nuclear elements (LINEs) are autonomous retrotransposons as they have coding capacity for reverse transcriptase and an RNA-binding protein that facilitates their insertion (Kazazian and Moran, 1998; Levin and Moran, 2011). Other retrotransposons such as short interspersed nuclear elements (SINEs) are non-autonomous as they lack coding capacity, and thus are dependent on protein machinery coded by other LINEs (Dewannieux et al., 2003). The third class of retrotransposons consists of endogenous retroviruses (ERVs) which are remnants of ancient retroviral infections that have been largely mutated over time and are unlikely to form new infectious virions (Deininger et al., 2003). However, their transcripts have been detected in normal human tissues (Seifarth et al., 2005). Lastly, tandem repeats that account for the remainder of repetitive DNA are mainly found at telomeric ends, and centromeres and pericentromeres to make up satellite DNA (Blackburn and Szostak, 1984). Tandem repeats are classically known to be propagated through strand slippage error during replication, but recent evidence suggests that satellite DNA at pericentromeres can expand through an RNA intermediate and subsequent reverse transcription and integration (Bersani et al., 2015; Levinson and Gutman, 1987; Tachida and Iizuka, 1992).

1.18 Derepression of repetitive elements can be tumourigenic

The mobility of repetitive elements in the host genome through various mechanisms may be deleterious to the host as somatic retrotransposon insertions into

genic regions can deregulate mRNA expression and function. Indeed, germline and somatic retrotransposon insertions have been implicated with several diseases, including cancer. A comprehensive computational analysis of whole genome sequencing (WGS) from nearly 3000 normal tissue and tumour pairs across thirty-eight tumour types revealed over 19 000 somatic LINE-1 retrotransposition events in lung squamous, head and neck, colorectal and endometrial cancers (Rodriguez-Martin et al., 2020). Several similar high-throughput sequencing studies have also found LINE-1 retrotransposition associated with tumourigenesis (Criscione et al., 2014; Lee et al., 2012; Shukla et al., 2013; Solyom et al., 2012). Furthermore, clonal expansion of LINE-1 has been observed in a progression of esophageal adenocarcinoma from a premalignant or normal state, suggesting a causative role for retrotransposon insertion in tumourigenesis (Doucet-O'Hare et al., 2015; Ewing et al., 2015). Like retrotransposons, RNA-intermediate based expansion of pericentromeric satellite repeats has been linked to cancer. Somatic gain of human satellite II (HSAT II) copy number was correlated with some tumours compared to corresponding germline samples, and inhibition of HSAT II reverse transcription resulted in decreased tumour size in a mouse xenograft model (Bersani et al., 2015). Thus, the mobility of retrotransposons and certain satellite repeats can promote tumourigenesis.

There are also mobility-independent mechanisms that can be deleterious. LINE and SINE elements can drive aberrant non-allelic homologous recombination (NAHR) as recent computational and chromosomal microarray analysis have linked ERVs and LINEs to copy number variations (CNVs) via NAHR in patients (Campbell et al., 2014; Startek et al., 2015). In addition, exaptation of ERVs' long terminal repeats (LTRs) has been reported to seed driver mutations of several human cancers. LTRs have promoters, enhancers, and splice donor sites that may cause ectopic gene expression or generate truncated/chimeric protein (Babaian and Mager, 2016). For example, a LTR2 promoter driven transcript of fatty acid binding protein (FABP7) gene was found in a subset of diffuse large B cell lymphomas (DLBCL), and DLBCL cell line proliferation and growth in vitro were dependent on its expression (Lock et al., 2014). Furthermore, oncogene upregulation from epigenetically reactivated repetitive elements has been found across 15 different cancer types with varying prevalence (Jang et al., 2019). For example, DNA

demethylation of the AluJb SINE allows its promoter to drive LIN28B expression, a known oncogene, that promotes proliferation and migration of lung cancer cells. Overall, lack of repetitive element silencing can seed tumourigenesis.

1.19 Inhibition of transcriptionally repressive complexes derepresses repetitive elements and activates immune signaling in cancer cells

However, the consequences of repetitive element expression are ambivalent depending on the context. An emerging body of literature describes a curious relationship between repetitive elements and immune activation, now known as a kind of viral mimicry. For example, induction of dsRNA produced from ERVs upon DNMT inhibition using a pharmacological inhibitor resulted in reduced proliferation and activation of type I interferon (IFN) in colorectal cancer initiating cells (CICs) and ovarian cancer cells (Liu et al., 2018; Roulois et al., 2015). Furthermore, EZH2 drug inhibition suppressed ocular herpes simplex virus (HSV) infection and upregulated immune cell recruitment *in vivo* (Arbuckle et al., 2017). This is important because progressive removal of H3K27me3 on HSV genome has been reported to coincide with HSV gene expression, so one would expect EZH2 inhibition to promote viral propagation (Lee et al., 2016). Likewise, EZH2 inhibition in prostate cancer cells induced dsRNA accumulation and interferon stimulated genes (ISGs) and promoted anti-tumour adaptive immune function *in vivo* (Morel et al., 2021). Clinically, high expression of DNMT inhibition-induced viral defense genes was correlated with better prognosis for epithelial ovarian cancer patients (Chiappinelli et al., 2015). These observations suggest that an acute derepression of repetitive elements can promote an anti-tumour response, at least in certain contexts.

Taken together, an important distinction between anti-tumour versus pro-tumour outcomes of upregulated and derepressed repetitive elements is that the former is acutely induced by pharmacological inhibitors, which signals anti-viral and anti-tumour response through innate nucleic-acid binding pattern recognition receptors (PRRs). Their function is to detect viral DNA/RNA and signal a pro-inflammatory, anti-viral, cytotoxic response. Retinoic acid inducible gene I (RIG-I)-like receptors (RLRs), RIG-I and melanoma differentiation-associated protein 5 (MDA5), recognize viral RNA in the cytoplasm,

undergo conformational changes that allow interaction with their downstream adaptor, mitochondrial anti-viral signalling protein (MAVS), and lead to expression of type I IFN (Goubau et al., 2013; Hartmann, 2017; Kato et al., 2006; Schmidt et al., 2012; Wu and Hur, 2015; Yoneyama et al., 2004). These interferons then induce expression of hundreds of interferon-stimulated genes (ISGs) and the pro-inflammatory interferon, IFN- γ , that create an inflammatory, anti-viral environment. The MDA5-MAVS axis has been shown to antagonize proliferation of colorectal CICs *in vivo* as shRNA mediated knock-down of MDA5 or MAVS abrogated the effect of DNMT inhibition (Roulois et al., 2015). Furthermore, Cyclic-GMP-AMP synthase (cGAS) has been reported to be crucial for type I interferon response against DNA and ssRNA viruses (Goubau et al., 2013; Sun et al., 2013). cGAS produces cyclic GMP-AMP upon DNA binding, which then acts as a second messenger to activate stimulator of IFN genes (STING) (Wu et al., 2013b). Activation of STING induces its relocalization in the endoplasmic reticulum, subsequent phosphorylation, and production of type I interferons (Ishikawa and Barber, 2008; Ishikawa et al., 2009). For example, anti-tumour activity against prostate cancer cells upon EZH2 inhibition was found to be mechanistically dependent on STING activation (Morel et al., 2021).

1.20 Rationale and objectives

Elucidation of RB function began with its role as a tumour suppressor based on its cell cycle control through E2F transcription factor repression. However, clinical observations and targeted RB mutant mice in parallel have shown that it has non-canonical roles, especially as a scaffold for chromatin regulatory complexes. Specifically, the RB-E2F1 complex recruits condensin II and EZH2 to various genomic locations that include bidirectional promoters, pericentromeric and other repetitive elements to control gene expression through long range chromosome contact, condense chromatin, and silence repetitive elements.

Despite the known consequences of condensin II loss in various model systems and its inferred functions, a molecular mechanism that regulates RB-E2F1 recruitment of condensin II to chromatin is poorly characterized. Indeed, the *Rb1^{AL}* or *Rb1^{AS}* alleles were generated based on minimal binding regions required for interaction and supporting

crystal structures, not some post-translationally inducible modification (Isaac et al., 2006; Ishak et al., 2016; Julian et al., 2008). Ironically, this represents a gap in our knowledge in contrast with our understanding of RB phosphorylation that inactivates RB repression of E2Fs and cell cycle progression, and RB methylation that counters cyclin-CDK dependent RB phosphorylation. Furthermore, the *Rbl^{4S}* mice have revealed that EZH2 recruited by the RB-E2F1 complex may play a special role in splenocytes given their susceptibility to spontaneous splenic lymphomas. Also considering that repetitive elements are upregulated in splenocytes upon loss of RB-E2F1 interaction, EZH2 recruitment and loss of H3K27me₃, this hints that EZH2 inhibition may induce viral mimicry in normal immune cells, a notion that has not yet been tested. Therefore, the overall aim of this thesis is to characterize the mechanisms that either control or act downstream of chromatin regulatory complexes recruited by the RB-E2F1 complex.

In chapter 2, we hypothesized that non-CDK phosphorylation of the RB C-terminus regulates chromatin localization of RB. Based on existing phosphoproteomic data, we noted that S838/T841 phosphorylation is inducible upon T cell receptor (TCR) crosslinking in Jurkat leukemia T cells. We generated novel phosphospecific antibodies that can detect S838/T841 phosphorylation of RB upon activation of Jurkat cells. Next, we tested whether p38 MAPK, a known downstream target of TCR activation, can phosphorylate RB on S838/T841 using a selective p38 inhibitor. Next, we fractionated chromatin to assess RB, E2F1 and condensin II localization. To establish a mechanistic connection between RB S838/T841 phosphorylation and the recruitment of these proteins, we generated Jurkat cells stably expressing an RB construct with alanine substitutions at S838/T841 and demonstrated resistance to unloading. Lastly, we tested the impact of condensin II unloading from chromatin upon RB phosphorylation on chromatin compaction.

In chapter 3, a new mouse model with inactivated cytosolic PRRs, called RIC, was generated by CRISPR-Cas9 to disrupt the detection of repetitive elements and subsequent signaling upon EZH2 inhibition. We hypothesized that cytosolic PRRs mechanistically link EZH2 inhibition with anti-viral signaling and immune activation. We administered a small molecule EZH2 inhibitor via intraperitoneal injections (I.P.) to

WT mice to characterize its effect on the spleen. Through RNA-seq, we quantified the breadth and magnitude of derepression of repetitive elements in splenic B cells. To corroborate their upregulation, ChIP-seq was performed to test whether H3K27me3 was reduced at repetitive elements to allow for their expression. To find functional pathways that are disrupted in RIC mutant compared to WT in response to EZH2 inhibition, RNA-seq data was analyzed through GSEA. Finally, we compared the immune composition of the spleen to test whether EZH2 inhibition can activate an immune response *in vivo* in a cytosolic PRR-dependent manner.

In chapter 4, we hypothesized that the cytosolic PRRs mediate anti-viral signaling in B16-F10 melanoma cells in response to EZH2 inhibition. We established RIG-I KO, cGAS KO and RIG-I/cGAS double KO cells with a lentiviral CRISPR-Cas9 system. Again, we performed RNA-seq and GSEA to quantify upregulation of repetitive elements and to find functional pathways that are abrogated by loss of the cytosolic PRRs.

1.21 References

- Abeshouse, A., Ahn, J., Akbani, R., Ally, A., Amin, S., Andry, C.D., Annala, M., Aprikian, A., Armenia, J., Arora, A., et al. (2015). The Molecular Taxonomy of Primary Prostate Cancer. *Cell* *163*, 1011–1025. <https://doi.org/10.1016/j.cell.2015.10.025>.
- Adams, P.D., Li, X., Sellers, W.R., Baker, K.B., Leng, X., Harper, J.W., Taya, Y., and Kaelin, W.G. (1999). Retinoblastoma Protein Contains a C-terminal Motif That Targets It for Phosphorylation by Cyclin-cdk Complexes. *Mol Cell Biol* *19*, 1068–1080. <https://doi.org/10.1128/MCB.19.2.1068>.
- Alsop, K., Fereday, S., Meldrum, C., deFazio, A., Emmanuel, C., George, J., Dobrovic, A., Birrer, M.J., Webb, P.M., Stewart, C., et al. (2012). BRCA Mutation Frequency and Patterns of Treatment Response in BRCA Mutation–Positive Women With Ovarian Cancer: A Report From the Australian Ovarian Cancer Study Group. *J Clin Oncol* *30*, 2654–2663. <https://doi.org/10.1200/JCO.2011.39.8545>.
- Anderson, D.E., Losada, A., Erickson, H.P., and Hirano, T. (2002). Condensin and cohesin display different arm conformations with characteristic hinge angles. *Journal of Cell Biology* *156*, 419–424. <https://doi.org/10.1083/jcb.200111002>.
- Antonyamy, S., Condon, B., Druzina, Z., Bonanno, J.B., Gheyi, T., Zhang, F., MacEwan, I., Zhang, A., Ashok, S., Rodgers, L., et al. (2013). Structural context of disease-associated mutations and putative mechanism of autoinhibition revealed by X-ray crystallographic analysis of the EZH2-SET domain. *PLoS One* *8*, e84147. <https://doi.org/10.1371/journal.pone.0084147>.
- Apte, M.S., and Meller, V.H. (2012). Homologue Pairing in Flies and Mammals: Gene Regulation When Two Are Involved. *Genet Res Int* *2012*, 430587. <https://doi.org/10.1155/2012/430587>.
- Arbuckle, J.H., Gardina, P.J., Gordon, D.N., Hickman, H.D., Yewdell, J.W., Pierson, T.C., Myers, T.G., and Kristie, T.M. (2017). Inhibitors of the Histone Methyltransferases EZH2/1 Induce a Potent Antiviral State and Suppress Infection by Diverse Viral Pathogens. *MBio* *8*, e01141-17. <https://doi.org/10.1128/mBio.01141-17>.
- Babaian, A., and Mager, D.L. (2016). Endogenous retroviral promoter exaptation in human cancer. *Mob DNA* *7*, 24. <https://doi.org/10.1186/s13100-016-0080-x>.
- Bandara, L.R., and La Thangue, N.B. (1991). Adenovirus E1a prevents the retinoblastoma gene product from complexing with a cellular transcription factor. *Nature* *351*, 494–497. <https://doi.org/10.1038/351494a0>.
- Bandara, L.R., Adamczewski, J.P., Hunt, T., and La Thangue, N.B. (1991). Cyclin A and the retinoblastoma gene product complex with a common transcription factor. *Nature* *352*, 249–251. <https://doi.org/10.1038/352249a0>.

Bauer, C.R., Hartl, T.A., and Bosco, G. (2012). Condensin II Promotes the Formation of Chromosome Territories by Inducing Axial Compaction of Polyploid Interphase Chromosomes. *PLOS Genetics* 8, e1002873. <https://doi.org/10.1371/journal.pgen.1002873>.

Bersani, F., Lee, E., Kharchenko, P.V., Xu, A.W., Liu, M., Xega, K., MacKenzie, O.C., Brannigan, B.W., Wittner, B.S., Jung, H., et al. (2015). Pericentromeric satellite repeat expansions through RNA-derived DNA intermediates in cancer. *PNAS* 112, 15148–15153. <https://doi.org/10.1073/pnas.1518008112>.

Biedermann, S., Harashima, H., Chen, P., Heese, M., Bouyer, D., Sofroni, K., and Schnittger, A. (2017). The retinoblastoma homolog RBR 1 mediates localization of the repair protein RAD 51 to DNA lesions in *Arabidopsis*. *EMBO J* 36, 1279–1297. <https://doi.org/10.15252/embj.201694571>.

Blackburn, E.H., and Szostak, J.W. (1984). THE MOLECULAR STRUCTURE OF CENTROMERES AND TELOMERES. *Annu. Rev. Biochem.* 53, 163–194. <https://doi.org/10.1146/annurev.bi.53.070184.001115>.

Blackledge, N.P., Farcas, A.M., Kondo, T., King, H.W., McGouran, J.F., Hanssen, L.L.P., Ito, S., Cooper, S., Kondo, K., Koseki, Y., et al. (2014). Variant PRC1 Complex-Dependent H2A Ubiquitylation Drives PRC2 Recruitment and Polycomb Domain Formation. *Cell* 157, 1445–1459. <https://doi.org/10.1016/j.cell.2014.05.004>.

Blake, M.C., and Azizkhan, J.C. (1989). Transcription factor E2F is required for efficient expression of the hamster dihydrofolate reductase gene in vitro and in vivo. *Mol Cell Biol* 9, 4994–5002. <https://doi.org/10.1128/mcb.9.11.4994-5002.1989>.

Boeuf, H., Reimund, B., Jansen-Durr, P., and Kédinger, C. (1990). Differential activation of the E2F transcription factor by the adenovirus E1a and E1V products in F9 cells. *Proc Natl Acad Sci U S A* 87, 1782–1786. <https://doi.org/10.1073/pnas.87.5.1782>.

Bolton, K.L., Chenevix-Trench, G., Goh, C., Sadetzki, S., Ramus, S.J., Karlan, B.Y., Lambrechts, D., Despierre, E., Barrowdale, D., McGuffog, L., et al. (2012). Association Between BRCA1 and BRCA2 Mutations and Survival in Women With Invasive Epithelial Ovarian Cancer. *JAMA* 307, 382–389. <https://doi.org/10.1001/jama.2012.20>.

Bookstein, R., Rio, P., Madreperla, S.A., Hong, F., Allred, C., Grizzle, W.E., and Lee, W.H. (1990). Promoter deletion and loss of retinoblastoma gene expression in human prostate carcinoma. *Proc Natl Acad Sci U S A* 87, 7762–7766. <https://doi.org/10.1073/pnas.87.19.7762>.

Boyer, L.A., Plath, K., Zeitlinger, J., Brambrink, T., Medeiros, L.A., Lee, T.I., Levine, S.S., Wernig, M., Tajonar, A., Ray, M.K., et al. (2006). Polycomb complexes repress developmental regulators in murine embryonic stem cells. *Nature* 441, 349–353. <https://doi.org/10.1038/nature04733>.

- Brehm, A., Miska, E.A., McCance, D.J., Reid, J.L., Bannister, A.J., and Kouzarides, T. (1998). Retinoblastoma protein recruits histone deacetylase to repress transcription. *Nature* 391, 597–601. <https://doi.org/10.1038/35404>.
- Bremner, R., Cohen, B.L., Sopta, M., Hamel, P.A., Ingles, C.J., Gallie, B.L., and Phillips, R.A. (1995). Direct transcriptional repression by pRB and its reversal by specific cyclins. *Mol Cell Biol* 15, 3256–3265. <https://doi.org/10.1128/MCB.15.6.3256>.
- Buchkovich, K., Duffy, L.A., and Harlow, E. (1989). The retinoblastoma protein is phosphorylated during specific phases of the cell cycle. *Cell* 58, 1097–1105. [https://doi.org/10.1016/0092-8674\(89\)90508-4](https://doi.org/10.1016/0092-8674(89)90508-4).
- Bulut-Karslioglu, A., De La Rosa-Velázquez, I.A., Ramirez, F., Barenboim, M., Onishi-Seebacher, M., Arand, J., Galán, C., Winter, G.E., Engist, B., Gerle, B., et al. (2014). Suv39h-Dependent H3K9me3 Marks Intact Retrotransposons and Silences LINE Elements in Mouse Embryonic Stem Cells. *Molecular Cell* 55, 277–290. <https://doi.org/10.1016/j.molcel.2014.05.029>.
- Burke, J.R., Deshong, A.J., Pelton, J.G., and Rubin, S.M. (2010). Phosphorylation-induced conformational changes in the retinoblastoma protein inhibit E2F transactivation domain binding. *J Biol Chem* 285, 16286–16293. <https://doi.org/10.1074/jbc.M110.108167>.
- Burke, J.R., Hura, G.L., and Rubin, S.M. (2012). Structures of inactive retinoblastoma protein reveal multiple mechanisms for cell cycle control. *Genes Dev* 26, 1156–1166. <https://doi.org/10.1101/gad.189837.112>.
- Burke, J.R., Liban, T.J., Restrepo, T., Lee, H.-W., and Rubin, S.M. (2014). Multiple mechanisms for E2F binding inhibition by phosphorylation of the retinoblastoma protein C-terminal domain. *J Mol Biol* 426, 245–255. <https://doi.org/10.1016/j.jmb.2013.09.031>.
- Calbó, J., Parreño, M., Sotillo, E., Yong, T., Mazo, A., Garriga, J., and Graña, X. (2002). G1 Cyclin/Cyclin-dependent Kinase-coordinated Phosphorylation of Endogenous Pocket Proteins Differentially Regulates Their Interactions with E2F4 and E2F1 and Gene Expression. *J. Biol. Chem.* 277, 50263–50274. <https://doi.org/10.1074/jbc.M209181200>.
- Campbell, I.M., Gambin, T., Dittwald, P., Beck, C.R., Shuvarikov, A., Hixson, P., Patel, A., Gambin, A., Shaw, C.A., Rosenfeld, J.A., et al. (2014). Human endogenous retroviral elements promote genome instability via non-allelic homologous recombination. *BMC Biol* 12, 74. <https://doi.org/10.1186/s12915-014-0074-4>.
- Cao, R., and Zhang, Y. (2004a). The functions of E(Z)/EZH2-mediated methylation of lysine 27 in histone H3. *Curr Opin Genet Dev* 14, 155–164. <https://doi.org/10.1016/j.gde.2004.02.001>.
- Cao, R., and Zhang, Y. (2004b). SUZ12 is required for both the histone methyltransferase activity and the silencing function of the EED-EZH2 complex. *Mol Cell* 15, 57–67. <https://doi.org/10.1016/j.molcel.2004.06.020>.

- Cao, R., Wang, L., Wang, H., Xia, L., Erdjument-Bromage, H., Tempst, P., Jones, R.S., and Zhang, Y. (2002). Role of Histone H3 Lysine 27 Methylation in Polycomb-Group Silencing. *Science* 298, 1039–1043. <https://doi.org/10.1126/science.1076997>.
- Cao, R., Tsukada, Y.-I., and Zhang, Y. (2005). Role of Bmi-1 and Ring1A in H2A ubiquitylation and Hox gene silencing. *Mol Cell* 20, 845–854. <https://doi.org/10.1016/j.molcel.2005.12.002>.
- Carnevale, J., Palander, O., Seifried, L.A., and Dick, F.A. (2012). DNA Damage Signals through Differentially Modified E2F1 Molecules To Induce Apoptosis. *Molecular and Cellular Biology* 32, 900–912. <https://doi.org/10.1128/MCB.06286-11>.
- Carr, S.M., Munro, S., Kessler, B., Oppermann, U., and La Thangue, N.B. (2011). Interplay between lysine methylation and Cdk phosphorylation in growth control by the retinoblastoma protein: Methylation and phosphorylation interplay on pRb. *The EMBO Journal* 30, 317–327. <https://doi.org/10.1038/emboj.2010.311>.
- Cavenee, W.K., Dryja, T.P., Phillips, R.A., Benedict, W.F., Godbout, R., Gallie, B.L., Murphree, A.L., Strong, L.C., and White, R.L. (1983). Expression of recessive alleles by chromosomal mechanisms in retinoblastoma. *Nature* 305, 779–784. <https://doi.org/10.1038/305779a0>.
- Cavenee, W.K., Hansen, M.F., Nordenskjold, M., Kock, E., Maumenee, I., Squire, J.A., Phillips, R.A., and Gallie, B.L. (1985). Genetic origin of mutations predisposing to retinoblastoma. *Science* 228, 501–503. <https://doi.org/10.1126/science.3983638>.
- Cecchini, M.J., and Dick, F.A. (2011). The biochemical basis of CDK phosphorylation-independent regulation of E2F1 by the retinoblastoma protein. *Biochem. J.* 434, 297–308. <https://doi.org/10.1042/BJ20101210>.
- Cecchini, M.J., Ishak, C.A., Passos, D.T., Warner, A., Palma, D.A., Howlett, C.J., Driman, D.K., and Dick, F.A. (2015). Loss of the retinoblastoma tumor suppressor correlates with improved outcome in patients with lung adenocarcinoma treated with surgery and chemotherapy. *Human Pathology* 46, 1922–1934. <https://doi.org/10.1016/j.humpath.2015.08.010>.
- Chan, F.K., Zhang, J., Cheng, L., Shapiro, D.N., and Winoto, A. (1995). Identification of human and mouse p19, a novel CDK4 and CDK6 inhibitor with homology to p16ink4. *Mol Cell Biol* 15, 2682–2688. <https://doi.org/10.1128/MCB.15.5.2682>.
- Chan, H.M., Krstic-Demonacos, M., Smith, L., Demonacos, C., and Thangue, N.B.L. (2001a). Acetylation control of the retinoblastoma tumour-suppressor protein. *Nat Cell Biol* 3, 667–674. <https://doi.org/10.1038/35083062>.
- Chan, H.M., Smith, L., and La Thangue, N.B. (2001b). Role of LXCXE motif-dependent interactions in the activity of the retinoblastoma protein. *Oncogene* 20, 6152–6163. <https://doi.org/10.1038/sj.onc.1204793>.

- Chellappan, S.P., Hiebert, S., Mudryj, M., Horowitz, J.M., and Nevins, J.R. (1991). The E2F transcription factor is a cellular target for the RB protein. *Cell* 65, 1053–1061. [10.1016/0092-8674\(91\)90557-f](https://doi.org/10.1016/0092-8674(91)90557-f).
- Chen, T.-T., and Wang, J.Y.J. (2000). Establishment of Irreversible Growth Arrest in Myogenic Differentiation Requires the RB LXCXE-Binding Function. *Mol Cell Biol* 20, 5571–5580. <https://doi.org/10.1128/MCB.20.15.5571-5580.2000>.
- Chen, H.-Z., Tsai, S.-Y., and Leone, G. (2009). Emerging roles of E2Fs in cancer: an exit from cell cycle control. *Nat Rev Cancer* 9, 785–797. <https://doi.org/10.1038/nrc2696>.
- Chiappinelli, K.B., Strissel, P.L., Desrichard, A., Li, H., Henke, C., Akman, B., Hein, A., Rote, N.S., Cope, L.M., Snyder, A., et al. (2015). Inhibiting DNA Methylation Causes an Interferon Response in Cancer via dsRNA Including Endogenous Retroviruses. *Cell* 162, 974–986. <https://doi.org/10.1016/j.cell.2015.07.011>.
- Chittenden, T., Livingston, D.M., and Kaelin, W.G. (1991). The T/E1A-binding domain of the retinoblastoma product can interact selectively with a sequence-specific DNA-binding protein. *Cell* 65, 1073–1082. [https://doi.org/10.1016/0092-8674\(91\)90559-h](https://doi.org/10.1016/0092-8674(91)90559-h).
- Chittock, E.C., Latwiel, S., Miller, T.C.R., and Müller, C.W. (2017). Molecular architecture of polycomb repressive complexes. *Biochem Soc Trans* 45, 193–205. <https://doi.org/10.1042/BST20160173>.
- Choi, J., Bachmann, A.L., Tauscher, K., Benda, C., Fierz, B., and Müller, J. (2017). DNA binding by PHF1 prolongs PRC2 residence time on chromatin and thereby promotes H3K27 methylation. *Nat Struct Mol Biol* 24, 1039–1047. <https://doi.org/10.1038/nsmb.3488>.
- Chow, K.N., and Dean, D.C. (1996). Domains A and B in the Rb pocket interact to form a transcriptional repressor motif. *Mol Cell Biol* 16, 4862–4868. <https://doi.org/10.1128/MCB.16.9.4862>.
- Chow, K.N., Starostik, P., and Dean, D.C. (1996). The Rb family contains a conserved cyclin-dependent-kinase-regulated transcriptional repressor motif. *Mol Cell Biol* 16, 7173–7181. <https://doi.org/10.1128/MCB.16.12.7173>.
- Classon, M., and Dyson, N. (2001). p107 and p130: versatile proteins with interesting pockets. *Exp Cell Res* 264, 135–147. <https://doi.org/10.1006/excr.2000.5135>.
- Clift, D., Bizzari, F., and Marston, A.L. (2009). Shugoshin prevents cohesin cleavage by PP2A(Cdc55)-dependent inhibition of separase. *Genes Dev* 23, 766–780. <https://doi.org/10.1101/gad.507509>.
- Cobbe, N., and Heck, M.M.S. (2004). The evolution of SMC proteins: phylogenetic analysis and structural implications. *Mol Biol Evol* 21, 332–347. <https://doi.org/10.1093/molbev/msh023>.

- Cobrinik, D., Whyte, P., Peeper, D.S., Jacks, T., and Weinberg, R.A. (1993). Cell cycle-specific association of E2F with the p130 E1A-binding protein. *Genes Dev.* *7*, 2392–2404. <https://doi.org/10.1101/gad.7.12a.2392>.
- Collisson, E.A., Campbell, J.D., Brooks, A.N., Berger, A.H., Lee, W., Chmielecki, J., Beer, D.G., Cope, L., Creighton, C.J., Danilova, L., et al. (2014). Comprehensive molecular profiling of lung adenocarcinoma. *Nature* *511*, 543–550. <https://doi.org/10.1038/nature13385>.
- Comings, D.E. (1973). A general theory of carcinogenesis. *Proc Natl Acad Sci U S A* *70*, 3324–3328. <https://doi.org/10.1073/pnas.70.12.3324>.
- Cook, R., Zoumpoulidou, G., Luczynski, M.T., Rieger, S., Moquet, J., Spanswick, V.J., Hartley, J.A., Rothkamm, K., Huang, P.H., and Mittnacht, S. (2015). Direct Involvement of Retinoblastoma Family Proteins in DNA Repair by Non-homologous End-Joining. *Cell Reports* *10*, 2006–2018. <https://doi.org/10.1016/j.celrep.2015.02.059>.
- Coschi, C.H., Martens, A.L., Ritchie, K., Francis, S.M., Chakrabarti, S., Berube, N.G., and Dick, F.A. (2010). Mitotic chromosome condensation mediated by the retinoblastoma protein is tumor-suppressive. *Genes Dev.* *24*, 1351–1363. <https://doi.org/10.1101/gad.1917610>.
- Coschi, C.H., Ishak, C.A., Gallo, D., Marshall, A., Talluri, S., Wang, J., Cecchini, M.J., Martens, A.L., Percy, V., Welch, I., et al. (2014). Haploinsufficiency of an RB-E2F1-Condensin II Complex Leads to Aberrant Replication and Aneuploidy. *Cancer Discovery* *4*, 840–853. <https://doi.org/10.1158/2159-8290.CD-14-0215>.
- Criscione, S.W., Zhang, Y., Thompson, W., Sedivy, J.M., and Neretti, N. (2014). Transcriptional landscape of repetitive elements in normal and cancer human cells. *BMC Genomics* *15*, 583. <https://doi.org/10.1186/1471-2164-15-583>.
- Dahiya, A., Gavin, M.R., Luo, R.X., and Dean, D.C. (2000). Role of the LXCXE Binding Site in Rb Function. *Mol Cell Biol* *20*, 6799–6805. <https://doi.org/10.1128/MCB.20.18.6799-6805.2000>.
- DeCaprio, J.A., Ludlow, J.W., Figge, J., Shew, J.-Y., Huang, C.-M., Lee, W.-H., Marsilio, E., Paucha, E., and Livingston, D.M. (1988). SV40 large tumor antigen forms a specific complex with the product of the retinoblastoma susceptibility gene. *Cell* *54*, 275–283. [https://doi.org/10.1016/0092-8674\(88\)90559-4](https://doi.org/10.1016/0092-8674(88)90559-4).
- DeCaprio, J.A., Ludlow, J.W., Lynch, D., Furukawa, Y., Griffin, J., Piwnicka-Worms, H., Huang, C.M., and Livingston, D.M. (1989). The product of the retinoblastoma susceptibility gene has properties of a cell cycle regulatory element. *Cell* *58*, 1085–1095. [https://doi.org/10.1016/0092-8674\(89\)90507-2](https://doi.org/10.1016/0092-8674(89)90507-2).
- DeCaprio, J.A., Furukawa, Y., Ajchenbaum, F., Griffin, J.D., and Livingston, D.M. (1992). The retinoblastoma-susceptibility gene product becomes phosphorylated in

multiple stages during cell cycle entry and progression. *Proc Natl Acad Sci U S A* *89*, 1795–1798. <https://doi.org/10.1073/pnas.89.5.1795>.

DeGregori, J., and Johnson, D.G. (2006). Distinct and Overlapping Roles for E2F Family Members in Transcription, Proliferation and Apoptosis. *Curr Mol Med* *6*, 739–748. <https://doi.org/10.2174/1566524010606070739>.

Deininger, P.L., Moran, J.V., Batzer, M.A., and Kazazian, H.H. (2003). Mobile elements and mammalian genome evolution. *Curr Opin Genet Dev* *13*, 651–658. <https://doi.org/10.1016/j.gde.2003.10.013>.

Dej, K.J., and Spradling, A.C. (1999). The endocycle controls nurse cell polytene chromosome structure during *Drosophila* oogenesis. *Development* *126*, 293–303. <https://doi.org/10.1242/dev.126.2.293>.

Dewannieux, M., Esnault, C., and Heidmann, T. (2003). LINE-mediated retrotransposition of marked Alu sequences. *Nat Genet* *35*, 41–48. <https://doi.org/10.1038/ng1223>.

Dick, F.A., and Dyson, N. (2003). pRB Contains an E2F1-Specific Binding Domain that Allows E2F1-Induced Apoptosis to Be Regulated Separately from Other E2F Activities. *Molecular Cell* *12*, 639–649. [https://doi.org/10.1016/S1097-2765\(03\)00344-7](https://doi.org/10.1016/S1097-2765(03)00344-7).

Dick, F.A., and Rubin, S.M. (2013). Molecular mechanisms underlying RB protein function. *Nat Rev Mol Cell Biol* *14*, 297–306. <https://doi.org/10.1038/nrm3567>.

Dick, F.A., Sailhamer, E., and Dyson, N.J. (2000). Mutagenesis of the pRB Pocket Reveals that Cell Cycle Arrest Functions Are Separable from Binding to Viral Oncoproteins. *Mol Cell Biol* *20*, 3715–3727. <https://doi.org/10.1128/MCB.20.10.3715-3727.2000>.

Dick, F.A., Goodrich, D.W., Sage, J., and Dyson, N.J. (2018). Non-canonical functions of the RB protein in cancer. *Nat Rev Cancer* *18*, 442–451. <https://doi.org/10.1038/s41568-018-0008-5>.

Dimova, D.K., and Dyson, N.J. (2005). The E2F transcriptional network: old acquaintances with new faces. *Oncogene* *24*, 2810–2826. <https://doi.org/10.1038/sj.onc.1208612>.

Donjerkovic, D., and Scott, D.W. (2000). Regulation of the G1 phase of the mammalian cell cycle. *Cell Res* *10*, 1–16. <https://doi.org/10.1038/sj.cr.7290031>.

Doucet-O'Hare, T.T., Rodić, N., Sharma, R., Darbari, I., Abril, G., Choi, J.A., Ahn, J.Y., Cheng, Y., Anders, R.A., Burns, K.H., et al. (2015). LINE-1 expression and retrotransposition in Barrett's esophagus and esophageal carcinoma. *PNAS* *112*, E4894–E4900. <https://doi.org/10.1073/pnas.1502474112>.

Dryja, T.P., Cavenee, W., White, R., Rapaport, J.M., Petersen, R., Albert, D.M., and Bruns, G.A. (1984). Homozygosity of chromosome 13 in retinoblastoma. *N Engl J Med* 310, 550–553. <https://doi.org/10.1056/NEJM198403013100902>.

Dunaief, J.L., Strober, B.E., Guha, S., Khavari, P.A., Ålin, K., Luban, J., Begemann, M., Crabtree, G.R., and Goff, S.P. (1994). The retinoblastoma protein and BRG1 form a complex and cooperate to induce cell cycle arrest. *Cell* 79, 119–130. [https://doi.org/10.1016/0092-8674\(94\)90405-7](https://doi.org/10.1016/0092-8674(94)90405-7).

Dyson, N., Buchkovich, K., Whyte, P., and Harlow, E. (1989). The cellular 107K protein that binds to adenovirus E1A also associates with the large T antigens of SV40 and JC virus. *Cell* 58, 249–255. [https://doi.org/10.1016/0092-8674\(89\)90839-8](https://doi.org/10.1016/0092-8674(89)90839-8).

Endoh, M., Endo, T.A., Endoh, T., Isono, K., Sharif, J., Ohara, O., Toyoda, T., Ito, T., Eskeland, R., Bickmore, W.A., et al. (2012). Histone H2A Mono-Ubiquitination Is a Crucial Step to Mediate PRC1-Dependent Repression of Developmental Genes to Maintain ES Cell Identity. *PLOS Genetics* 8, e1002774. <https://doi.org/10.1371/journal.pgen.1002774>.

Eskeland, R., Leeb, M., Grimes, G.R., Kress, C., Boyle, S., Sproul, D., Gilbert, N., Fan, Y., Skoultchi, A.I., Wutz, A., et al. (2010). Ring1B Compacts Chromatin Structure and Represses Gene Expression Independent of Histone Ubiquitination. *Molecular Cell* 38, 452–464. <https://doi.org/10.1016/j.molcel.2010.02.032>.

Ewen, M.E., Xing, Y.G., Lawrence, J.B., and Livingston, D.M. (1991). Molecular cloning, chromosomal mapping, and expression of the cDNA for p107, a retinoblastoma gene product-related protein. *Cell* 66, 1155–1164. [https://doi.org/10.1016/0092-8674\(91\)90038-z](https://doi.org/10.1016/0092-8674(91)90038-z).

Ewing, A.D., Gacita, A., Wood, L.D., Ma, F., Xing, D., Kim, M.-S., Manda, S.S., Abril, G., Pereira, G., Makohon-Moore, A., et al. (2015). Widespread somatic L1 retrotransposition occurs early during gastrointestinal cancer evolution. *Genome Res* 25, 1536–1545. <https://doi.org/10.1101/gr.196238.115>.

Francis, N.J., Kingston, R.E., and Woodcock, C.L. (2004). Chromatin compaction by a polycomb group protein complex. *Science* 306, 1574–1577. <https://doi.org/10.1126/science.1100576>.

Francke, U., and Kung, F. (1976). Sporadic bilateral retinoblastoma and 13q-chromosomal deletion. *Med Pediatr Oncol* 2, 379–385. <https://doi.org/10.1002/mpo.2950020404>.

Friend, S.H., Bernards, R., Rogelj, S., Weinberg, R.A., Rapaport, J.M., Albert, D.M., and Dryja, T.P. (1986). A human DNA segment with properties of the gene that predisposes to retinoblastoma and osteosarcoma. *Nature* 323, 643–646. <https://doi.org/10.1038/323643a0>.

- Gao, Z., Zhang, J., Bonasio, R., Strino, F., Sawai, A., Parisi, F., Kluger, Y., and Reinberg, D. (2012). PCGF Homologs, CBX Proteins, and RYBP Define Functionally Distinct PRC1 Family Complexes. *Molecular Cell* 45, 344–356. <https://doi.org/10.1016/j.molcel.2012.01.002>.
- Garsed, D.W., Alsop, K., Fereday, S., Emmanuel, C., Kennedy, C.J., Etemadmoghadam, D., Gao, B., GebSKI, V., Garès, V., Christie, E.L., et al. (2018). Homologous Recombination DNA Repair Pathway Disruption and Retinoblastoma Protein Loss Are Associated with Exceptional Survival in High-Grade Serous Ovarian Cancer. *Clinical Cancer Research* 24, 569–580. <https://doi.org/10.1158/1078-0432.CCR-17-1621>.
- Gerlich, D., Hirota, T., Koch, B., Peters, J.-M., and Ellenberg, J. (2006). Condensin I Stabilizes Chromosomes Mechanically through a Dynamic Interaction in Live Cells. *Current Biology* 16, 333–344. <https://doi.org/10.1016/j.cub.2005.12.040>.
- Gibson, T.J., Thompson, J.D., Blocker, A., and Kouzarides, T. (1994). Evidence for a protein domain superfamily shared by the cyclins, TFIIB and RB/p107. *Nucleic Acids Res* 22, 946–952. <https://doi.org/10.1093/nar/22.6.946>.
- Giménez-Abián, J.F., Sumara, I., Hirota, T., Hauf, S., Gerlich, D., de la Torre, C., Ellenberg, J., and Peters, J.-M. (2004). Regulation of sister chromatid cohesion between chromosome arms. *Curr Biol* 14, 1187–1193. <https://doi.org/10.1016/j.cub.2004.06.052>.
- Girling, R., Partridge, J.F., Bandara, L.R., Burden, N., Totty, N.F., Hsuan, J.J., and La Thangue, N.B. (1993). A new component of the transcription factor DRTF1/E2F. *Nature* 362, 83–87. <https://doi.org/10.1038/362083a0>.
- Godbout, R., Dryja, T.P., Squire, J., Gallie, B.L., and Phillips, R.A. (1983). Somatic inactivation of genes on chromosome 13 is a common event in retinoblastoma. *Nature* 304, 451–453. <https://doi.org/10.1038/304451a0>.
- Gosling, K.M., Makaroff, L.E., Theodoratos, A., Kim, Y.-H., Whittle, B., Rui, L., Wu, H., Hong, N.A., Kennedy, G.C., Fritz, J.-A., et al. (2007). A mutation in a chromosome condensin II subunit, kleisin beta, specifically disrupts T cell development. *Proceedings of the National Academy of Sciences* 104, 12445–12450. <https://doi.org/10.1073/pnas.0704870104>.
- Goubau, D., Deddouche, S., and Reis e Sousa, C. (2013). Cytosolic sensing of viruses. *Immunity* 38, 855–869. <https://doi.org/10.1016/j.immuni.2013.05.007>.
- Green, L.C., Kalitsis, P., Chang, T.M., Cipetic, M., Kim, J.H., Marshall, O., Turnbull, L., Whitchurch, C.B., Vagnarelli, P., Samejima, K., et al. (2012). Contrasting roles of condensin I and II in mitotic chromosome formation. *Journal of Cell Science* jcs.097790. <https://doi.org/10.1242/jcs.097790>.
- Griffith, A.D., and Sorsby, A. (1944). THE GENETICS OF RETINOBLASTOMA. *Br J Ophthalmol* 28, 279–293. <https://doi.org/10.1136/bjo.28.6.279>.

- Gruber, S., Haering, C.H., and Nasmyth, K. (2003). Chromosomal cohesin forms a ring. *Cell* *112*, 765–777. [https://doi.org/10.1016/s0092-8674\(03\)00162-4](https://doi.org/10.1016/s0092-8674(03)00162-4).
- Gu, Y., Turck, C.W., and Morgan, D.O. (1993). Inhibition of CDK2 activity in vivo by an associated 20K regulatory subunit. *Nature* *366*, 707–710. <https://doi.org/10.1038/366707a0>.
- Guan, K.L., Jenkins, C.W., Li, Y., Nichols, M.A., Wu, X., O’Keefe, C.L., Matera, A.G., and Xiong, Y. (1994). Growth suppression by p18, a p16INK4/MTS1- and p14INK4B/MTS2-related CDK6 inhibitor, correlates with wild-type pRb function. *Genes Dev* *8*, 2939–2952. <https://doi.org/10.1101/gad.8.24.2939>.
- Haering, C.H., Löwe, J., Hochwagen, A., and Nasmyth, K. (2002). Molecular architecture of SMC proteins and the yeast cohesin complex. *Mol Cell* *9*, 773–788. [https://doi.org/10.1016/s1097-2765\(02\)00515-4](https://doi.org/10.1016/s1097-2765(02)00515-4).
- Hagstrom, K.A., Holmes, V.F., Cozzarelli, N.R., and Meyer, B.J. (2002). *C. elegans* condensin promotes mitotic chromosome architecture, centromere organization, and sister chromatid segregation during mitosis and meiosis. *Genes Dev* *16*, 729–742. <https://doi.org/10.1101/gad.968302>.
- Hallstrom, T.C., and Nevins, J.R. (2003). Specificity in the activation and control of transcription factor E2F-dependent apoptosis. *Proc. Natl. Acad. Sci. U.S.A.* *100*, 10848–10853. <https://doi.org/10.1073/pnas.1831408100>.
- Ham, J.S., Kim, S., Kim, H.K., Byeon, S., Sun, J.-M., Lee, S., Ahn, J.S., Park, K., Choi, Y.-L., Han, J., et al. (2016). Two Cases of Small Cell Lung Cancer Transformation from EGFR Mutant Adenocarcinoma During AZD9291 Treatment. *Journal of Thoracic Oncology* *11*, e1–e4. <https://doi.org/10.1016/j.jtho.2015.09.013>.
- Hanahan, D., and Weinberg, R.A. (2000). The hallmarks of cancer. *Cell* *100*, 57–70. [https://doi.org/10.1016/s0092-8674\(00\)81683-9](https://doi.org/10.1016/s0092-8674(00)81683-9).
- Hannon, G.J., and Beach, D. (1994). p15INK4B is a potential effector of TGF-beta-induced cell cycle arrest. *Nature* *371*, 257–261. <https://doi.org/10.1038/371257a0>.
- Hannon, G.J., Demetrick, D., and Beach, D. (1993). Isolation of the Rb-related p130 through its interaction with CDK2 and cyclins. *Genes Dev* *7*, 2378–2391. <https://doi.org/10.1101/gad.7.12a.2378>.
- Hartl, T.A., Smith, H.F., and Bosco, G. (2008). Chromosome Alignment and Transvection Are Antagonized by Condensin II. *Science* *322*, 1384–1387. <https://doi.org/10.1126/science.1164216>.
- Hartmann, G. (2017). Nucleic Acid Immunity. *Adv Immunol* *133*, 121–169. <https://doi.org/10.1016/bs.ai.2016.11.001>.

- Hauf, S., Waizenegger, I.C., and Peters, J.M. (2001). Cohesin cleavage by separase required for anaphase and cytokinesis in human cells. *Science* 293, 1320–1323. <https://doi.org/10.1126/science.1061376>.
- Healy, E., Mucha, M., Glancy, E., Fitzpatrick, D.J., Conway, E., Neikes, H.K., Monger, C., Van Mierlo, G., Baltissen, M.P., Koseki, Y., et al. (2019). PRC2.1 and PRC2.2 Synergize to Coordinate H3K27 Trimethylation. *Mol Cell* 76, 437–452.e6. <https://doi.org/10.1016/j.molcel.2019.08.012>.
- Henley, S.A., and Dick, F.A. (2012). The retinoblastoma family of proteins and their regulatory functions in the mammalian cell division cycle. *Cell Div* 7, 10. <https://doi.org/10.1186/1747-1028-7-10>.
- van den Heuvel, S., and Dyson, N.J. (2008). Conserved functions of the pRB and E2F families. *Nat Rev Mol Cell Biol* 9, 713–724. <https://doi.org/10.1038/nrm2469>.
- Hiebert, S.W., Chellappan, S.P., Horowitz, J.M., and Nevins, J.R. (1992). The interaction of RB with E2F coincides with an inhibition of the transcriptional activity of E2F. *Genes & Development* 6, 177–185. <https://doi.org/10.1101/gad.6.2.177>.
- Hirai, H., Roussel, M.F., Kato, J.Y., Ashmun, R.A., and Sherr, C.J. (1995). Novel INK4 proteins, p19 and p18, are specific inhibitors of the cyclin D-dependent kinases CDK4 and CDK6. *Mol Cell Biol* 15, 2672–2681. <https://doi.org/10.1128/mcb.15.5.2672>.
- Hirano, M. (2002). Hinge-mediated dimerization of SMC protein is essential for its dynamic interaction with DNA. *The EMBO Journal* 21, 5733–5744. <https://doi.org/10.1093/emboj/cdf575>.
- Hirano, T. (2012). Condensins: universal organizers of chromosomes with diverse functions. *Genes Dev.* 26, 1659–1678. <https://doi.org/10.1101/gad.194746.112>.
- Hirota, T., Gerlich, D., Koch, B., Ellenberg, J., and Peters, J.-M. (2004). Distinct functions of condensin I and II in mitotic chromosome assembly. *J Cell Sci* 117, 6435–6445. <https://doi.org/10.1242/jcs.01604>.
- Hirschi, A., Cecchini, M., Steinhardt, R.C., Schamber, M.R., Dick, F.A., and Rubin, S.M. (2010). An overlapping kinase and phosphatase docking site regulates activity of the retinoblastoma protein. *Nat Struct Mol Biol* 17, 1051–1057. <https://doi.org/10.1038/nsmb.1868>.
- Hochegger, H., Takeda, S., and Hunt, T. (2008). Cyclin-dependent kinases and cell-cycle transitions: does one fit all? *Nat Rev Mol Cell Biol* 9, 910–916. <https://doi.org/10.1038/nrm2510>.
- Hocquet, C., Robellet, X., Modolo, L., Sun, X.-M., Burny, C., Cuylen-Haering, S., Toselli, E., Clauder-Münster, S., Steinmetz, L., Haering, C.H., et al. (2018). Condensin controls cellular RNA levels through the accurate segregation of chromosomes instead of directly regulating transcription. *ELife* 7, e38517. <https://doi.org/10.7554/eLife.38517>.

- Højfeldt, J.W., Hedehus, L., Laugesen, A., Tatar, T., Wiehle, L., and Helin, K. (2019). Non-core Subunits of the PRC2 Complex Are Collectively Required for Its Target-Site Specificity. *Mol Cell* 76, 423-436.e3. <https://doi.org/10.1016/j.molcel.2019.07.031>.
- Holoch, D., and Margueron, R. (2017). Mechanisms Regulating PRC2 Recruitment and Enzymatic Activity. *Trends Biochem Sci* 42, 531–542. <https://doi.org/10.1016/j.tibs.2017.04.003>.
- Horvath, B.M., Kourova, H., Nagy, S., Nemeth, E., Magyar, Z., Papdi, C., Ahmad, Z., Sanchez-Perez, G.F., Perilli, S., Blilou, I., et al. (2017). *Arabidopsis* RETINOBLASTOMA RELATED directly regulates DNA damage responses through functions beyond cell cycle control. *EMBO J* 36, 1261–1278. <https://doi.org/10.15252/embj.201694561>.
- Howard, G., Eiges, R., Gaudet, F., Jaenisch, R., and Eden, A. (2008). Activation and transposition of endogenous retroviral elements in hypomethylation induced tumors in mice. *Oncogene* 27, 404–408. <https://doi.org/10.1038/sj.onc.1210631>.
- Hu, Q.J., Dyson, N., and Harlow, E. (1990). The regions of the retinoblastoma protein needed for binding to adenovirus E1A or SV40 large T antigen are common sites for mutations. *EMBO J* 9, 1147–1155. <https://doi.org/10.1002/j.1460-2075.1990.tb08221.x>.
- Huang, H.J., Yee, J.K., Shew, J.Y., Chen, P.L., Bookstein, R., Friedmann, T., Lee, E.Y., and Lee, W.H. (1988). Suppression of the neoplastic phenotype by replacement of the RB gene in human cancer cells. *Science* 242, 1563–1566. <https://doi.org/10.1126/science.3201247>.
- Ianari, A., Natale, T., Calo, E., Ferretti, E., Alesse, E., Screpanti, I., Haigis, K., Gulino, A., and Lees, J.A. (2009). Proapoptotic Function of the Retinoblastoma Tumor Suppressor Protein. *Cancer Cell* 15, 184–194. <https://doi.org/10.1016/j.ccr.2009.01.026>.
- Irwin, M., Marin, M.C., Phillips, A.C., Seelan, R.S., Smith, D.I., Liu, W., Flores, E.R., Tsai, K.Y., Jacks, T., Vousden, K.H., et al. (2000). Role for the p53 homologue p73 in E2F-1-induced apoptosis. *Nature* 407, 645–648. <https://doi.org/10.1038/35036614>.
- Isaac, C.E., Francis, S.M., Martens, A.L., Julian, L.M., Seifried, L.A., Erdmann, N., Binné, U.K., Harrington, L., Sicinski, P., Bérubé, N.G., et al. (2006). The Retinoblastoma Protein Regulates Pericentric Heterochromatin. *Mol Cell Biol* 26, 3659–3671. <https://doi.org/10.1128/MCB.26.9.3659-3671.2006>.
- Ishak, C.A., Marshall, A.E., Passos, D.T., White, C.R., Kim, S.J., Cecchini, M.J., Ferwati, S., MacDonald, W.A., Howlett, C.J., Welch, I.D., et al. (2016). An RB-EZH2 Complex Mediates Silencing of Repetitive DNA Sequences. *Mol Cell* 64, 1074–1087. <https://doi.org/10.1016/j.molcel.2016.10.021>.
- Ishikawa, H., and Barber, G.N. (2008). STING is an endoplasmic reticulum adaptor that facilitates innate immune signalling. *Nature* 455, 674–678. <https://doi.org/10.1038/nature07317>.

- Ishikawa, H., Ma, Z., and Barber, G.N. (2009). STING regulates intracellular DNA-mediated, type I interferon-dependent innate immunity. *Nature* *461*, 788–792. <https://doi.org/10.1038/nature08476>.
- Isono, K., Endo, T.A., Ku, M., Yamada, D., Suzuki, R., Sharif, J., Ishikura, T., Toyoda, T., Bernstein, B.E., and Koseki, H. (2013). SAM Domain Polymerization Links Subnuclear Clustering of PRC1 to Gene Silencing. *Developmental Cell* *26*, 565–577. [10.1016/j.devcel.2013.08.016](https://doi.org/10.1016/j.devcel.2013.08.016).
- Jang, H.S., Shah, N.M., Du, A.Y., Dailey, Z.Z., Pehrsson, E.C., Godoy, P.M., Zhang, D., Li, D., Xing, X., Kim, S., et al. (2019). Transposable elements drive widespread expression of oncogenes in human cancers. *Nat Genet* *51*, 611–617. <https://doi.org/10.1038/s41588-019-0373-3>.
- Jeppsson, K., Kanno, T., Shirahige, K., and Sjögren, C. (2014). The maintenance of chromosome structure: positioning and functioning of SMC complexes. *Nat Rev Mol Cell Biol* *15*, 601–614. <https://doi.org/10.1038/nrm3857>.
- Johnson, D.G., and Degregori, J. (2006). Putting the Oncogenic and Tumor Suppressive Activities of E2F into Context. *Curr Mol Med* *6*, 731–738. <https://doi.org/10.2174/1566524010606070731>.
- Jorgensen, S., Schotta, G., and Sorensen, C.S. (2013). Histone H4 Lysine 20 methylation: key player in epigenetic regulation of genomic integrity. *Nucleic Acids Research* *41*, 2797–2806. <https://doi.org/10.1093/nar/gkt012>.
- Joyce, E.F., Williams, B.R., Xie, T., and Wu, C. (2012). Identification of Genes That Promote or Antagonize Somatic Homolog Pairing Using a High-Throughput FISH-Based Screen. *PLOS Genetics* *8*, e1002667. <https://doi.org/10.1371/journal.pgen.1002667>.
- Julian, L.M., Palander, O., Seifried, L.A., Foster, J.E.G., and Dick, F.A. (2008). Characterization of an E2F1-specific binding domain in pRB and its implications for apoptotic regulation. *Oncogene* *27*, 1572–1579. <https://doi.org/10.1038/sj.onc.1210803>.
- Kaelin, W.G., Ewen, M.E., and Livingston, D.M. (1990). Definition of the minimal simian virus 40 large T antigen- and adenovirus E1A-binding domain in the retinoblastoma gene product. *Mol Cell Biol* *10*, 3761–3769. <https://doi.org/10.1128/mcb.10.7.3761-3769.1990>.
- Kalb, R., Latwiel, S., Baymaz, H.I., Jansen, P.W.T.C., Müller, C.W., Vermeulen, M., and Müller, J. (2014). Histone H2A monoubiquitination promotes histone H3 methylation in Polycomb repression. *Nat Struct Mol Biol* *21*, 569–571. [10.1038/nsmb.2833](https://doi.org/10.1038/nsmb.2833).
- Kareta, M.S., Gorges, L.L., Hafeez, S., Benayoun, B.A., Marro, S., Zmoos, A.-F., Cecchini, M.J., Spacek, D., Batista, L.F.Z., O'Brien, M., et al. (2015). Inhibition of Pluripotency Networks by the Rb Tumor Suppressor Restricts Reprogramming and Tumorigenesis. *Cell Stem Cell* *16*, 39–50. <https://doi.org/10.1016/j.stem.2014.10.019>.

Karimi, M.M., Goyal, P., Maksakova, I.A., Bilenky, M., Leung, D., Tang, J.X., Shinkai, Y., Mager, D.L., Jones, S., Hirst, M., et al. (2011). DNA Methylation and SETDB1/H3K9me3 Regulate Predominantly Distinct Sets of Genes, Retroelements, and Chimeric Transcripts in mESCs. *Cell Stem Cell* 8, 676–687. <https://doi.org/10.1016/j.stem.2011.04.004>.

Kato, H., Takeuchi, O., Sato, S., Yoneyama, M., Yamamoto, M., Matsui, K., Uematsu, S., Jung, A., Kawai, T., Ishii, K.J., et al. (2006). Differential roles of MDA5 and RIG-I helicases in the recognition of RNA viruses. *Nature* 441, 101–105. <https://doi.org/10.1038/nature04734>.

Kazazian, H.H., and Moran, J.V. (1998). The impact of L1 retrotransposons on the human genome. *Nat. Genet* 19, 19–24. <https://doi.org/10.1038/ng0598-19>.

Kim, T.M., Song, A., Kim, D.-W., Kim, S., Ahn, Y.-O., Keam, B., Jeon, Y.K., Lee, S.-H., Chung, D.H., and Heo, D.S. (2015). Mechanisms of Acquired Resistance to AZD9291: A Mutation-Selective, Irreversible EGFR Inhibitor. *Journal of Thoracic Oncology* 10, 1736–1744. <https://doi.org/10.1097/JTO.0000000000000688>.

Kirmizis, A., Bartley, S.M., Kuzmichev, A., Margueron, R., Reinberg, D., Green, R., and Farnham, P.J. (2004). Silencing of human polycomb target genes is associated with methylation of histone H3 Lys 27. *Genes Dev* 18, 1592–1605. <https://doi.org/10.1101/gad.1200204>.

Knudsen, K.E., Booth, D., Naderi, S., Sever-Chroneos, Z., Fribourg, A.F., Hunton, I.C., Feramisco, J.R., Wang, J.Y.J., and Knudsen, E.S. (2000). RB-Dependent S-Phase Response to DNA Damage. *Mol Cell Biol* 20, 7751–7763. <https://doi.org/10.1128/MCB.20.20.7751-7763.2000>.

Knudson, A.G. (1971). Mutation and Cancer: Statistical Study of Retinoblastoma. *Proceedings of the National Academy of Sciences* 68, 820–823. <https://doi.org/10.1073/pnas.68.4.820>.

Kobayashi, S., Boggon, T.J., Dayaram, T., Jänne, P.A., Kocher, O., Meyerson, M., Johnson, B.E., Eck, M.J., Tenen, D.G., and Halmos, B. (2005). EGFR Mutation and Resistance of Non-Small-Cell Lung Cancer to Gefitinib. *N Engl J Med* 352, 786–792. <https://doi.org/10.1056/NEJMoa044238>.

Kommoss, S., du Bois, A., Ridder, R., Trunk, M.J., Schmidt, D., Pfisterer, J., and Kommoss, F. (2007). Independent prognostic significance of cell cycle regulator proteins p16INK4a and pRb in advanced-stage ovarian carcinoma including optimally debulked patients: a translational research subprotocol of a randomised study of the Arbeitsgemeinschaft Gynaekologische Onkologie Ovarian Cancer Study Group. *Br J Cancer* 96, 306–313. <https://doi.org/10.1038/sj.bjc.6603531>.

Kondo, Y., and Issa, J.-P.J. (2003). Enrichment for Histone H3 Lysine 9 Methylation at Alu Repeats in Human Cells. *J. Biol. Chem* 278, 27658–27662. <https://doi.org/10.1074/jbc.M304072200>.

- Kovesdi, I., Reichel, R., and Nevins, J.R. (1987). Role of an adenovirus E2 promoter binding factor in E1A-mediated coordinate gene control. *Proc Natl Acad Sci U S A* *84*, 2180–2184. <https://doi.org/10.1073/pnas.84.8.2180>.
- Ku, M., Koche, R.P., Rheinbay, E., Mendenhall, E.M., Endoh, M., Mikkelsen, T.S., Presser, A., Nusbaum, C., Xie, X., Chi, A.S., et al. (2008). Genomewide Analysis of PRC1 and PRC2 Occupancy Identifies Two Classes of Bivalent Domains. *PLOS Genetics* *4*, e1000242. <https://doi.org/10.1371/journal.pgen.1000242>.
- Ku, S.Y., Rosario, S., Wang, Y., Mu, P., Seshadri, M., Goodrich, Z.W., Goodrich, M.M., Labbé, D.P., Gomez, E.C., Wang, J., et al. (2017). *Rbl* and *Trp53* cooperate to suppress prostate cancer lineage plasticity, metastasis, and antiandrogen resistance. *Science* *355*, 78–83. <https://doi.org/10.1126/science.aah4199>.
- Kurze, A., Michie, K.A., Dixon, S.E., Mishra, A., Itoh, T., Khalid, S., Strmecki, L., Shirahige, K., Haering, C.H., Löwe, J., et al. (2011). A positively charged channel within the Smc1/Smc3 hinge required for sister chromatid cohesion: Positively charged hinge channel required for cohesion. *The EMBO Journal* *30*, 364–378. <https://doi.org/10.1038/emboj.2010.315>.
- Kuzmichev, A., Nishioka, K., Erdjument-Bromage, H., Tempst, P., and Reinberg, D. (2002). Histone methyltransferase activity associated with a human multiprotein complex containing the Enhancer of Zeste protein. *Genes Dev* *16*, 2893–2905. <https://doi.org/10.1101/gad.1035902>.
- Lai, A., Lee, J.M., Yang, W.-M., DeCaprio, J.A., Kaelin, W.G., Seto, E., and Branton, P.E. (1999). RBP1 Recruits Both Histone Deacetylase-Dependent and -Independent Repression Activities to Retinoblastoma Family Proteins. *Mol Cell Biol* *19*, 6632–6641. <https://doi.org/10.1128/MCB.19.10.6632>.
- Lander, E.S., Linton, L.M., Birren, B., Nusbaum, C., Zody, M.C., Baldwin, J., Devon, K., Dewar, K., Doyle, M., FitzHugh, W., et al. (2001). Initial sequencing and analysis of the human genome. *Nature* *409*, 860–921. <https://doi.org/10.1038/35057062>.
- Lee, E., Iskow, R., Yang, L., Gokcumen, O., Haseley, P., Luquette, L.J., Lohr, J.G., Harris, C.C., Ding, L., Wilson, R.K., et al. (2012). Landscape of somatic retrotransposition in human cancers. *Science* *337*, 967–971. <https://doi.org/10.1126/science.1222077>.
- Lee, J.O., Russo, A.A., and Pavletich, N.P. (1998). Structure of the retinoblastoma tumour-suppressor pocket domain bound to a peptide from HPV E7. *Nature* *391*, 859–865. <https://doi.org/10.1038/36038>.
- Lee, J.S., Raja, P., and Knipe, D.M. (2016). Herpesviral ICP0 Protein Promotes Two Waves of Heterochromatin Removal on an Early Viral Promoter during Lytic Infection. *mBio* *7*, e02007-15. [10.1128/mBio.02007-15](https://doi.org/10.1128/mBio.02007-15).

- Lee, M.H., Reynisdóttir, I., and Massagué, J. (1995). Cloning of p57KIP2, a cyclin-dependent kinase inhibitor with unique domain structure and tissue distribution. *Genes Dev.* 9, 639–649. <https://doi.org/10.1101/gad.9.6.639>.
- Lee, W.H., Shew, J.Y., Hong, F.D., Sery, T.W., Donoso, L.A., Young, L.J., Bookstein, R., and Lee, E.Y. (1987). The retinoblastoma susceptibility gene encodes a nuclear phosphoprotein associated with DNA binding activity. *Nature* 329, 642–645. <https://doi.org/10.1038/329642a0>.
- Lele, K.P., Penrose, L.S., and Stallard, H.B. (1963). CHROMOSOME DELETION IN A CASE OF RETINOBLASTOMA. *Ann Hum Genet* 27, 171–174. <https://doi.org/10.1111/j.1469-1809.1963.tb00209.x>.
- Levin, H.L., and Moran, J.V. (2011). Dynamic interactions between transposable elements and their hosts. *Nat. Rev. Genet* 12, 615–627. <https://doi.org/10.1038/nrg3030>.
- Levinson, G., and Gutman, G.A. (1987). Slipped-strand mispairing: a major mechanism for DNA sequence evolution. *Mol Biol Evol* 4, 203–221. <https://doi.org/10.1093/oxfordjournals.molbev.a040442>.
- Lewis, E.B. (1978). A gene complex controlling segmentation in *Drosophila*. *Nature* 276, 565–570. <https://doi.org/10.1038/276565a0>.
- Lewis, P.H. (1947). New mutants report. *Drosophila Information Service* 21, 69. .
- Li, E., Bestor, T.H., and Jaenisch, R. (1992). Targeted mutation of the DNA methyltransferase gene results in embryonic lethality. *Cell* 69, 915–926. [https://doi.org/10.1016/0092-8674\(92\)90611-F](https://doi.org/10.1016/0092-8674(92)90611-F).
- Li, Y., Graham, C., Lacy, S., Duncan, A.M., and Whyte, P. (1993). The adenovirus E1A-associated 130-kD protein is encoded by a member of the retinoblastoma gene family and physically interacts with cyclins A and E. *Genes Dev* 7, 2366–2377. <https://doi.org/10.1101/gad.7.12a.2366>.
- Liang, G., Chan, M.F., Tomigahara, Y., Tsai, Y.C., Gonzales, F.A., Li, E., Laird, P.W., and Jones, P.A. (2002). Cooperativity between DNA Methyltransferases in the Maintenance Methylation of Repetitive Elements. *Molecular and Cellular Biology*. 10.1128/MCB.22.2.480-491.2002.
- Lin, W.C., Lin, F.T., and Nevins, J.R. (2001). Selective induction of E2F1 in response to DNA damage, mediated by ATM-dependent phosphorylation. *Genes Dev* 15, 1833–1844. .
- Liu, M., Thomas, S.L., DeWitt, A.K., Zhou, W., Madaj, Z.B., Ohtani, H., Baylin, S.B., Liang, G., and Jones, P.A. (2018). Dual Inhibition of DNA and Histone Methyltransferases Increases Viral Mimicry in Ovarian Cancer Cells. *Cancer Res* 78, 5754–5766. <https://doi.org/10.1158/0008-5472.CAN-17-3953>.

- Liu, S., Brind'Amour, J., Karimi, M.M., Shirane, K., Bogutz, A., Lefebvre, L., Sasaki, H., Shinkai, Y., and Lorincz, M.C. (2014). Setdb1 is required for germline development and silencing of H3K9me3-marked endogenous retroviruses in primordial germ cells. *Genes Dev.* 28, 2041–2055. <https://doi.org/10.1101/gad.244848.114>.
- Liu, Y., Clem, B., Zuba-Surma, E.K., El-Naggar, S., Telang, S., Jenson, A.B., Wang, Y., Shao, H., Ratajczak, M.Z., Chesney, J., et al. (2009). Mouse Fibroblasts Lacking RB1 Function Form Spheres and Undergo Reprogramming to a Cancer Stem Cell Phenotype. *Cell Stem Cell* 4, 336–347. <https://doi.org/10.1016/j.stem.2009.02.015>.
- Lock, F.E., Rebollo, R., Miceli-Royer, K., Gagnier, L., Kuah, S., Babaian, A., Sistiaga-Poveda, M., Lai, C.B., Nemirovsky, O., Serrano, I., et al. (2014). Distinct isoform of FABP7 revealed by screening for retroelement-activated genes in diffuse large B-cell lymphoma. *Proc Natl Acad Sci U S A* 111, E3534-3543. <https://doi.org/10.1073/pnas.1405507111>.
- Longworth, M.S., Herr, A., Ji, J.-Y., and Dyson, N.J. (2008). RBF1 promotes chromatin condensation through a conserved interaction with the Condensin II protein dCAP-D3. *Genes & Development* 22, 1011–1024. <https://doi.org/10.1101/gad.1631508>.
- Losada, A., and Hirano, T. (2005). Dynamic molecular linkers of the genome: the first decade of SMC proteins. *Genes Dev.* 19, 1269–1287. <https://doi.org/10.1101/gad.1320505>.
- Losada, A., Hirano, M., and Hirano, T. (2002). Cohesin release is required for sister chromatid resolution, but not for condensin-mediated compaction, at the onset of mitosis. *Genes Dev* 16, 3004–3016. <https://doi.org/10.1101/gad.249202>.
- Luo, R.X., Postigo, A.A., and Dean, D.C. (1998). Rb Interacts with Histone Deacetylase to Repress Transcription. *Cell* 92, 463–473. [https://doi.org/10.1016/S0092-8674\(00\)80940-X](https://doi.org/10.1016/S0092-8674(00)80940-X).
- Lynch, T.J., Bell, D.W., Sordella, R., Gurubhagavatula, S., Okimoto, R.A., Brannigan, B.W., Harris, P.L., Haserlat, S.M., Supko, J.G., Haluska, F.G., et al. (2004). Activating Mutations in the Epidermal Growth Factor Receptor Underlying Responsiveness of Non-Small-Cell Lung Cancer to Gefitinib. *N Engl J Med* 350, 2129–2139. <https://doi.org/10.1056/NEJMoa040938>.
- Magnaghi-Jaulin, L., Groisman, R., Naguibneva, I., Robin, P., Lorain, S., Le Villain, J.P., Troalen, F., Trouche, D., and Harel-Bellan, A. (1998). Retinoblastoma protein represses transcription by recruiting a histone deacetylase. *Nature* 391, 601–605. <https://doi.org/10.1038/35410>.
- Margueron, R., Justin, N., Ohno, K., Sharpe, M.L., Son, J., Drury, W.J., Voigt, P., Martin, S.R., Taylor, W.R., De Marco, V., et al. (2009). Role of the polycomb protein EED in the propagation of repressive histone marks. *Nature* 461, 762–767. <https://doi.org/10.1038/nature08398>.

- Marshall, A.E., Roes, M.V., Passos, D.T., DeWeerd, M.C., Chaikovsky, A.C., Sage, J., Howlett, C.J., and Dick, F.A. (2019). *RB1* Deletion in Retinoblastoma Protein Pathway-Disrupted Cells Results in DNA Damage and Cancer Progression. *Mol Cell Biol* 39, e00105-19. <https://doi.org/10.1128/MCB.00105-19>.
- Marshall, A.E., Ishak, C.A., and Dick, F.A. (2020). An RB-Condensin II Complex Mediates Long-Range Chromosome Interactions and Influences Expression at Divergently Paired Genes. *Mol Cell Biol* 40, e00452-19. <https://doi.org/10.1128/MCB.00452-19>.
- Marston, A.L., Tham, W.-H., Shah, H., and Amon, A. (2004). A genome-wide screen identifies genes required for centromeric cohesion. *Science* 303, 1367–1370. <https://doi.org/10.1126/science.1094220>.
- Martens, J.H.A., O’Sullivan, R.J., Braunschweig, U., Opravil, S., Radolf, M., Steinlein, P., and Jenuwein, T. (2005). The profile of repeat-associated histone lysine methylation states in the mouse epigenome. *EMBO J* 24, 800–812. [10.1038/sj.emboj.7600545](https://doi.org/10.1038/sj.emboj.7600545).
- Matsui, T., Leung, D., Miyashita, H., Maksakova, I.A., Miyachi, H., Kimura, H., Tachibana, M., Lorincz, M.C., and Shinkai, Y. (2010). Proviral silencing in embryonic stem cells requires the histone methyltransferase ESET. *Nature* 464, 927–931. <https://doi.org/10.1038/nature08858>.
- Mayol, X., Graña, X., Baldi, A., Sang, N., Hu, Q., and Giordano, A. (1993). Cloning of a new member of the retinoblastoma gene family (pRb2) which binds to the E1A transforming domain. *Oncogene* 8, 2561–2566. .
- Melby, T.E., Ciampaglio, C.N., Briscoe, G., and Erickson, H.P. (1998). The Symmetrical Structure of Structural Maintenance of Chromosomes (SMC) and MukB Proteins: Long, Antiparallel Coiled Coils, Folded at a Flexible Hinge. *Journal of Cell Biology* 142, 1595–1604. <https://doi.org/10.1083/jcb.142.6.1595>.
- van Mierlo, G., Veenstra, G.J.C., Vermeulen, M., and Marks, H. (2019). The Complexity of PRC2 Subcomplexes. *Trends Cell Biol* 29, 660–671. <https://doi.org/10.1016/j.tcb.2019.05.004>.
- Montgomery, N.D., Yee, D., Chen, A., Kalantry, S., Chamberlain, S.J., Otte, A.P., and Magnuson, T. (2005). The murine polycomb group protein Eed is required for global histone H3 lysine-27 methylation. *Curr Biol* 15, 942–947. <https://doi.org/10.1016/j.cub.2005.04.051>.
- Moore, L.D., Le, T., and Fan, G. (2013). DNA Methylation and Its Basic Function. *Neuropsychopharmacol* 38, 23–38. <https://doi.org/10.1038/npp.2012.112>.
- Morel, K.L., Sheahan, A.V., Burkhart, D.L., Baca, S.C., Boufaied, N., Liu, Y., Qiu, X., Cañadas, I., Roehle, K., Heckler, M., et al. (2021). EZH2 inhibition activates a dsRNA-STING-interferon stress axis that potentiates response to PD-1 checkpoint blockade in prostate cancer. *Nat Cancer* 2, 444–456. <https://doi.org/10.1038/s43018-021-00185-w>.

- Morgunova, E., Yin, Y., Jolma, A., Dave, K., Schmierer, B., Popov, A., Eremina, N., Nilsson, L., and Taipale, J. (2015). Structural insights into the DNA-binding specificity of E2F family transcription factors. *Nat Commun* 6, 10050. <https://doi.org/10.1038/ncomms10050>.
- Mu, P., Zhang, Z., Benelli, M., Karthaus, W.R., Hoover, E., Chen, C.-C., Wongvipat, J., Ku, S.-Y., Gao, D., Cao, Z., et al. (2017). *SOX2* promotes lineage plasticity and antiandrogen resistance in *TP53* - and *RBI* -deficient prostate cancer. *Science* 355, 84–88. <https://doi.org/10.1126/science.aah4307>.
- Nasmyth, K. (2011). Cohesin: a catenase with separate entry and exit gates? *Nat Cell Biol* 13, 1170–1177. <https://doi.org/10.1038/ncb2349>.
- Neel, J.V., and Falls, H.F. (1951). The Rate of Mutation of the Gene Responsible for Retinoblastoma in Man. *Science* 114, 419–422. .
- Nevins, J.R. (1992). E2F: a link between the Rb tumor suppressor protein and viral oncoproteins. *Science* 258, 424–429. <https://doi.org/10.1126/science.1411535>.
- Nielsen, S.J., Schneider, R., Bauer, U.M., Bannister, A.J., Morrison, A., O’Carroll, D., Firestein, R., Cleary, M., Jenuwein, T., Herrera, R.E., et al. (2001). Rb targets histone H3 methylation and HP1 to promoters. *Nature* 412, 561–565. <https://doi.org/10.1038/35087620>.
- Ono, T., Fang, Y., Spector, D.L., and Hirano, T. (2004). Spatial and temporal regulation of Condensins I and II in mitotic chromosome assembly in human cells. *Mol Biol Cell* 15, 3296–3308. <https://doi.org/10.1091/mbc.e04-03-0242>.
- Pasini, D., Bracken, A.P., Jensen, M.R., Denchi, E.L., and Helin, K. (2004). Suz12 is essential for mouse development and for EZH2 histone methyltransferase activity. *EMBO J* 23, 4061–4071. <https://doi.org/10.1038/sj.emboj.7600402>.
- Pennington, K.P., Walsh, T., Harrell, M.I., Lee, M.K., Pennil, C.C., Rendi, M.H., Thornton, A., Norquist, B.M., Casadei, S., Nord, A.S., et al. (2014). Germline and Somatic Mutations in Homologous Recombination Genes Predict Platinum Response and Survival in Ovarian, Fallopian Tube, and Peritoneal Carcinomas. *Clinical Cancer Research* 20, 764–775. <https://doi.org/10.1158/1078-0432.CCR-13-2287>.
- Petes, T.D. (1979). Yeast ribosomal DNA genes are located on chromosome XII. *Proc Natl Acad Sci U S A* 76, 410–414. <https://doi.org/10.1073/pnas.76.1.410>.
- Pickart, C.M. (2001). Mechanisms Underlying Ubiquitination. *Annu. Rev. Biochem.* 70, 503–533. <https://doi.org/10.1146/annurev.biochem.70.1.503>.
- Piotrowska, Z., Niederst, M.J., Karlovich, C.A., Wakelee, H.A., Neal, J.W., Mino-Kenudson, M., Fulton, L., Hata, A.N., Lockerman, E.L., Kalsy, A., et al. (2015). Heterogeneity Underlies the Emergence of EGFRT790 Wild-Type Clones Following

Treatment of T790M-Positive Cancers with a Third-Generation EGFR Inhibitor. *Cancer Discovery* 5, 713–722. <https://doi.org/10.1158/2159-8290.CD-15-0399>.

Polyak, K., Kato, J.Y., Solomon, M.J., Sherr, C.J., Massague, J., Roberts, J.M., and Koff, A. (1994a). p27Kip1, a cyclin-Cdk inhibitor, links transforming growth factor-beta and contact inhibition to cell cycle arrest. *Genes Dev* 8, 9–22. <https://doi.org/10.1101/gad.8.1.9>.

Polyak, K., Lee, M.H., Erdjument-Bromage, H., Koff, A., Roberts, J.M., Tempst, P., and Massagué, J. (1994b). Cloning of p27Kip1, a cyclin-dependent kinase inhibitor and a potential mediator of extracellular antimitogenic signals. *Cell* 78, 59–66. [https://doi.org/10.1016/0092-8674\(94\)90572-x](https://doi.org/10.1016/0092-8674(94)90572-x).

Qin, X.Q., Chittenden, T., Livingston, D.M., and Kaelin, W.G. (1992). Identification of a growth suppression domain within the retinoblastoma gene product. *Genes Dev.* 6, 953–964. <https://doi.org/10.1101/gad.6.6.953>.

Rawlings, J.S., Gatzka, M., Thomas, P.G., and Ihle, J.N. (2011). Chromatin condensation via the condensin II complex is required for peripheral T-cell quiescence. *EMBO J.* 30, 263–276. <https://doi.org/10.1038/emboj.2010.314>.

Reynisdóttir, I., Polyak, K., Iavarone, A., and Massagué, J. (1995). Kip/Cip and Ink4 Cdk inhibitors cooperate to induce cell cycle arrest in response to TGF-beta. *Genes Dev* 9, 1831–1845. <https://doi.org/10.1101/gad.9.15.1831>.

Ribeiro, S.A., Gatlin, J.C., Dong, Y., Joglekar, A., Cameron, L., Hudson, D.F., Farr, C.J., McEwen, B.F., Salmon, E.D., Earnshaw, W.C., et al. (2009). Condensin Regulates the Stiffness of Vertebrate Centromeres. *MBoC* 20, 2371–2380. <https://doi.org/10.1091/mbc.e08-11-1127>.

Rickman, D.S., Beltran, H., Demichelis, F., and Rubin, M.A. (2017). Biology and evolution of poorly differentiated neuroendocrine tumors. *Nat Med* 23, 664–673. <https://doi.org/10.1038/nm.4341>.

Robertson, K.D., Ait-Si-Ali, S., Yokochi, T., Wade, P.A., Jones, P.L., and Wolffe, A.P. (2000). DNMT1 forms a complex with Rb, E2F1 and HDAC1 and represses transcription from E2F-responsive promoters. *Nat Genet* 25, 338–342. <https://doi.org/10.1038/77124>.

Robinson, A.K., Leal, B.Z., Chadwell, L.V., Wang, R., Ilangovan, U., Kaur, Y., Junco, S.E., Schirf, V., Osmulski, P.A., Gaczynska, M., et al. (2012). The growth-suppressive function of the polycomb group protein polyhomeotic is mediated by polymerization of its sterile alpha motif (SAM) domain. *J Biol Chem* 287, 8702–8713. [10.1074/jbc.M111.336115](https://doi.org/10.1074/jbc.M111.336115).

Rodriguez-Martin, B., Alvarez, E.G., Baez-Ortega, A., Zamora, J., Supek, F., Demeulemeester, J., Santamarina, M., Ju, Y.S., Temes, J., Garcia-Souto, D., et al. (2020). Pan-cancer analysis of whole genomes identifies driver rearrangements promoted by LINE-1 retrotransposition. *Nature Genetics* 52, 306–319. [10.1038/s41588-019-0562-0](https://doi.org/10.1038/s41588-019-0562-0).

- Roulois, D., Loo Yau, H., Singhania, R., Wang, Y., Danesh, A., Shen, S.Y., Han, H., Liang, G., Jones, P.A., Pugh, T.J., et al. (2015). DNA-Demethylating Agents Target Colorectal Cancer Cells by Inducing Viral Mimicry by Endogenous Transcripts. *Cell* 162, 961–973. <https://doi.org/10.1016/j.cell.2015.07.056>.
- Rowley, M.J., Lyu, X., Rana, V., Ando-Kuri, M., Karns, R., Bosco, G., and Corces, V.G. (2019). Condensin II Counteracts Cohesin and RNA Polymerase II in the Establishment of 3D Chromatin Organization. *Cell Reports* 26, 2890-2903.e3. <https://doi.org/10.1016/j.celrep.2019.01.116>.
- Schappert-Kimmijser, J., Hemmes, G.D., and Nijland, R. (1966). The heredity of retinoblastoma. *Ophthalmologica* 151, 197–213. <https://doi.org/10.1159/000304891>.
- Schmidt, A., Rothenfusser, S., and Hopfner, K.-P. (2012). Sensing of viral nucleic acids by RIG-I: From translocation to translation. *Eur. J. Cell Biol* 91, 78–85. <https://doi.org/10.1016/j.ejcb.2011.01.015>.
- Schwartz, Y.B., Kahn, T.G., Nix, D.A., Li, X.-Y., Bourgon, R., Biggin, M., and Pirrotta, V. (2006). Genome-wide analysis of Polycomb targets in *Drosophila melanogaster*. *Nat Genet* 38, 700–705. <https://doi.org/10.1038/ng1817>.
- Seifarth, W., Frank, O., Zeilfelder, U., Spiess, B., Greenwood, A.D., Hehlmann, R., and Leib-Mösch, C. (2005). Comprehensive Analysis of Human Endogenous Retrovirus Transcriptional Activity in Human Tissues with a Retrovirus-Specific Microarray. *J Virol* 79, 341–352. <https://doi.org/10.1128/JVI.79.1.341-352.2005>.
- Seifried, L.A., Talluri, S., Cecchini, M., Julian, L.M., Mymryk, J.S., and Dick, F.A. (2008). pRB-E2F1 Complexes Are Resistant to Adenovirus E1A-Mediated Disruption. *J Virol* 82, 4511–4520. <https://doi.org/10.1128/JVI.02713-07>.
- Sellers, W.R., Rodgers, J.W., and Kaelin, W.G. (1995). A potent transrepression domain in the retinoblastoma protein induces a cell cycle arrest when bound to E2F sites. *Proc Natl Acad Sci U S A* 92, 11544–11548. <https://doi.org/10.1073/pnas.92.25.11544>.
- Serrano, M., Hannon, G.J., and Beach, D. (1993). A new regulatory motif in cell-cycle control causing specific inhibition of cyclin D/CDK4. *Nature* 366, 704–707. <https://doi.org/10.1038/366704a0>.
- Sharif, J., Endo, T.A., Nakayama, M., Karimi, M.M., Shimada, M., Katsuyama, K., Goyal, P., Brind'Amour, J., Sun, M.-A., Sun, Z., et al. (2016). Activation of Endogenous Retroviruses in *Dnmt1* $-/-$ ESCs Involves Disruption of SETDB1-Mediated Repression by NP95 Binding to Hemimethylated DNA. *Cell Stem Cell* 19, 81–94. <https://doi.org/10.1016/j.stem.2016.03.013>.
- Sherr, C.J., and McCormick, F. (2002). The RB and p53 pathways in cancer. *Cancer Cell* 2, 103–112. [https://doi.org/10.1016/S1535-6108\(02\)00102-2](https://doi.org/10.1016/S1535-6108(02)00102-2).

Sherr, C.J., and Roberts, J.M. (1999). CDK inhibitors: positive and negative regulators of G1-phase progression. *Genes Dev.* *13*, 1501–1512. .

Shintomi, K., and Hirano, T. (2011). The relative ratio of condensin I to II determines chromosome shapes. *Genes Dev.* *25*, 1464–1469. <https://doi.org/10.1101/gad.2060311>.

Shukla, R., Upton, K.R., Muñoz-Lopez, M., Gerhardt, D.J., Fisher, M.E., Nguyen, T., Brennan, P.M., Baillie, J.K., Collino, A., Ghisletti, S., et al. (2013). Endogenous retrotransposition activates oncogenic pathways in hepatocellular carcinoma. *Cell* *153*, 101–111. <https://doi.org/10.1016/j.cell.2013.02.032>.

Smith, S.M., and Sorsby, A. (1958). Retinoblastoma: some genetic aspects. *Ann Hum Genet* *23*, 50–58. <https://doi.org/10.1111/j.1469-1809.1958.tb01441.x>.

Solyom, S., Ewing, A.D., Rahrman, E.P., Doucet, T., Nelson, H.H., Burns, M.B., Harris, R.S., Sigmon, D.F., Casella, A., Erlanger, B., et al. (2012). Extensive somatic L1 retrotransposition in colorectal tumors. *Genome Res* *22*, 2328–2338. <https://doi.org/10.1101/gr.145235.112>.

Sparkes, R.S., Sparkes, M.C., Wilson, M.G., Towner, J.W., Benedict, W., Murphree, A.L., and Yunis, J.J. (1980). Regional assignment of genes for human esterase D and retinoblastoma to chromosome band 13q14. *Science* *208*, 1042–1044. <https://doi.org/10.1126/science.7375916>.

Sparkes, R.S., Murphree, A.L., Lingua, R.W., Sparkes, M.C., Field, L.L., Funderburk, S.J., and Benedict, W.F. (1983). Gene for hereditary retinoblastoma assigned to human chromosome 13 by linkage to esterase D. *Science* *219*, 971–973. <https://doi.org/10.1126/science.6823558>.

Startek, M., Szafranski, P., Gambin, T., Campbell, I.M., Hixson, P., Shaw, C.A., Stankiewicz, P., and Gambin, A. (2015). Genome-wide analyses of LINE–LINE-mediated nonallelic homologous recombination. *Nucleic Acids Research* *43*, 2188–2198. <https://doi.org/10.1093/nar/gku1394>.

Sumara, I., Vorlaufer, E., Stukenberg, P.T., Kelm, O., Redemann, N., Nigg, E.A., and Peters, J.-M. (2002). The dissociation of cohesin from chromosomes in prophase is regulated by Polo-like kinase. *Mol Cell* *9*, 515–525. [https://doi.org/10.1016/s1097-2765\(02\)00473-2](https://doi.org/10.1016/s1097-2765(02)00473-2).

Sun, L., Wu, J., Du, F., Chen, X., and Chen, Z.J. (2013). Cyclic GMP-AMP synthase is a cytosolic DNA sensor that activates the type I interferon pathway. *Science* *339*, 786–791. <https://doi.org/10.1126/science.1232458>.

Tachida, H., and Iizuka, M. (1992). Persistence of repeated sequences that evolve by replication slippage. *Genetics* *131*, 471–478. <https://doi.org/10.1093/genetics/131.2.471>.

Takahashi, R., Hashimoto, T., Xu, H.J., Hu, S.X., Matsui, T., Miki, T., Bigo-Marshall, H., Aaronson, S.A., and Benedict, W.F. (1991). The retinoblastoma gene functions as a

growth and tumor suppressor in human bladder carcinoma cells. *Proc Natl Acad Sci U S A* 88, 5257–5261. <https://doi.org/10.1073/pnas.88.12.5257>.

Tavares, L., Dimitrova, E., Oxley, D., Webster, J., Poot, R., Demmers, J., Bezstarosti, K., Taylor, S., Ura, H., Koide, H., et al. (2012). RYBP-PRC1 Complexes Mediate H2A Ubiquitylation at Polycomb Target Sites Independently of PRC2 and H3K27me3. *Cell* 148, 664–678. <https://doi.org/10.1016/j.cell.2011.12.029>.

Thalmeier, K., Synovzik, H., Mertz, R., Winnacker, E.L., and Lipp, M. (1989). Nuclear factor E2F mediates basic transcription and trans-activation by E1a of the human MYC promoter. *Genes Dev* 3, 527–536. <https://doi.org/10.1101/gad.3.4.527>.

Ting, D.T., Lipson, D., Paul, S., Brannigan, B.W., Akhavanfard, S., Coffman, E.J., Contino, G., Deshpande, V., Iafrate, A.J., Letovsky, S., et al. (2011). Aberrant Overexpression of Satellite Repeats in Pancreatic and Other Epithelial Cancers. *Science* 331, 593–596. <https://doi.org/10.1126/science.1200801>.

Toyoshima, H., and Hunter, T. (1994). p27, a novel inhibitor of G1 cyclin-Cdk protein kinase activity, is related to p21. *Cell* 78, 67–74. [https://doi.org/10.1016/0092-8674\(94\)90573-8](https://doi.org/10.1016/0092-8674(94)90573-8).

Tran, C., Ouk, S., Clegg, N.J., Chen, Y., Watson, P.A., Arora, V., Wongvipat, J., Smith-Jones, P.M., Yoo, D., Kwon, A., et al. (2009). Development of a Second-Generation Antiandrogen for Treatment of Advanced Prostate Cancer. *Science* 324, 787–790. <https://doi.org/10.1126/science.1168175>.

Tsang, C.K., Li, H., and Zheng, X.S. (2007). Nutrient starvation promotes condensin loading to maintain rDNA stability. *EMBO J* 26, 448–458. <https://doi.org/10.1038/sj.emboj.7601488>.

Tsuboi, M., Kishi, Y., Yokozeki, W., Koseki, H., Hirabayashi, Y., and Gotoh, Y. (2018). Ubiquitination-Independent Repression of PRC1 Targets during Neuronal Fate Restriction in the Developing Mouse Neocortex. *Developmental Cell* 47, 758–772.e5. [10.1016/j.devcel.2018.11.018](https://doi.org/10.1016/j.devcel.2018.11.018).

Uhlmann, F., Lottspeich, F., and Nasmyth, K. (1999). Sister-chromatid separation at anaphase onset is promoted by cleavage of the cohesin subunit Scc1. *Nature* 400, 37–42. <https://doi.org/10.1038/21831>.

Vélez-Cruz, R., Manickavinayaham, S., Biswas, A.K., Clary, R.W., Premkumar, T., Cole, F., and Johnson, D.G. (2016). RB localizes to DNA double-strand breaks and promotes DNA end resection and homologous recombination through the recruitment of BRG1. *Genes Dev.* 30, 2500–2512. <https://doi.org/10.1101/gad.288282.116>.

Vogel, F. (1979). Genetics of retinoblastoma. *Hum Genet* 52, 1–54. <https://doi.org/10.1007/BF00284597>.

- Walsh, C.P., Chaillet, J.R., and Bestor, T.H. (1998). Transcription of IAP endogenous retroviruses is constrained by cytosine methylation. *Nat Genet* 20, 116–117. <https://doi.org/10.1038/2413>.
- Wang, H., Wang, L., Erdjument-Bromage, H., Vidal, M., Tempst, P., Jones, R.S., and Zhang, Y. (2004a). Role of histone H2A ubiquitination in Polycomb silencing. *Nature* 431, 873–878. <https://doi.org/10.1038/nature02985>.
- Wang, L., Brown, J.L., Cao, R., Zhang, Y., Kassis, J.A., and Jones, R.S. (2004b). Hierarchical recruitment of polycomb group silencing complexes. *Mol Cell* 14, 637–646. <https://doi.org/10.1016/j.molcel.2004.05.009>.
- Watson, P.A., Arora, V.K., and Sawyers, C.L. (2015). Emerging mechanisms of resistance to androgen receptor inhibitors in prostate cancer. *Nat Rev Cancer* 15, 701–711. <https://doi.org/10.1038/nrc4016>.
- Wells, J., Yan, P.S., Cechvala, M., Huang, T., and Farnham, P.J. (2003). Identification of novel pRb binding sites using CpG microarrays suggests that E2F recruits pRb to specific genomic sites during S phase. *Oncogene* 22, 1445–1460. <https://doi.org/10.1038/sj.onc.1206264>.
- Whyte, P., Buchkovich, K.J., Horowitz, J.M., Friend, S.H., Raybuck, M., Weinberg, R.A., and Harlow, E. (1988). Association between an oncogene and an anti-oncogene: the adenovirus E1A proteins bind to the retinoblastoma gene product. *Nature* 334, 124–129. <https://doi.org/10.1038/334124a0>.
- Whyte, P., Williamson, N.M., and Harlow, E. (1989). Cellular targets for transformation by the adenovirus E1A proteins. *Cell* 56, 67–75. [https://doi.org/10.1016/0092-8674\(89\)90984-7](https://doi.org/10.1016/0092-8674(89)90984-7).
- Witkiewicz, A.K., Ertel, A., McFalls, J., Valsecchi, M.E., Schwartz, G., and Knudsen, E.S. (2012). RB-Pathway Disruption Is Associated with Improved Response to Neoadjuvant Chemotherapy in Breast Cancer. *Clin Cancer Res* 18, 5110–5122. <https://doi.org/10.1158/1078-0432.CCR-12-0903>.
- Wu, B., and Hur, S. (2015). How RIG-I like receptors activate MAVS. *Curr Opin Virol* 12, 91–98. <https://doi.org/10.1016/j.coviro.2015.04.004>.
- Wu, C.L., Zukerberg, L.R., Ngwu, C., Harlow, E., and Lees, J.A. (1995). In vivo association of E2F and DP family proteins. *Mol Cell Biol* 15, 2536–2546. <https://doi.org/10.1128/MCB.15.5.2536>.
- Wu, H., Zeng, H., Dong, A., Li, F., He, H., Senisterra, G., Seitova, A., Duan, S., Brown, P.J., Vedadi, M., et al. (2013a). Structure of the catalytic domain of EZH2 reveals conformational plasticity in cofactor and substrate binding sites and explains oncogenic mutations. *PLoS One* 8, e83737. <https://doi.org/10.1371/journal.pone.0083737>.

- Wu, J., Sun, L., Chen, X., Du, F., Shi, H., Chen, C., and Chen, Z.J. (2013b). Cyclic GMP-AMP is an endogenous second messenger in innate immune signaling by cytosolic DNA. *Science* 339, 826–830. <https://doi.org/10.1126/science.1229963>.
- Xiao, Z.X., Ginsberg, D., Ewen, M., and Livingston, D.M. (1996). Regulation of the retinoblastoma protein-related protein p107 by G1 cyclin-associated kinases. *Proc Natl Acad Sci U S A* 93, 4633–4637. <https://doi.org/10.1073/pnas.93.10.4633>.
- Yee, A.S., Reichel, R., Kovcsdi, I., and Nevins, J.R. (1987). Promoter interaction of the E1A-inducible factor E2F and its potential role in the formation of a multi-component complex. *EMBO J* 6, 2061–2068. <https://doi.org/10.1002/j.1460-2075.1987.tb02471.x>.
- Yoneyama, M., Kikuchi, M., Natsukawa, T., Shinobu, N., Imaizumi, T., Miyagishi, M., Taira, K., Akira, S., and Fujita, T. (2004). The RNA helicase RIG-I has an essential function in double-stranded RNA-induced innate antiviral responses. *Nat Immunol* 5, 730–737. <https://doi.org/10.1038/ni1087>.
- Yong-Gonzalez, V., Wang, B.-D., Butylin, P., Ouspenski, I., and Strunnikov, A. (2007). Condensin function at centromere chromatin facilitates proper kinetochore tension and ensures correct mitotic segregation of sister chromatids: Condensin and centromere. *Genes to Cells* 12, 1075–1090. <https://doi.org/10.1111/j.1365-2443.2007.01109.x>.
- Youmans, D.T., Schmidt, J.C., and Cech, T.R. (2018). Live-cell imaging reveals the dynamics of PRC2 and recruitment to chromatin by SUZ12-associated subunits. *Genes Dev* 32, 794–805. <https://doi.org/10.1101/gad.311936.118>.
- Yun, C.-H., Boggon, T.J., Li, Y., Woo, M.S., Greulich, H., Meyerson, M., and Eck, M.J. (2007). Structures of Lung Cancer-Derived EGFR Mutants and Inhibitor Complexes: Mechanism of Activation and Insights into Differential Inhibitor Sensitivity. *Cancer Cell* 11, 217–227. <https://doi.org/10.1016/j.ccr.2006.12.017>.
- Yunis, J.J., and Ramsay, N. (1978). Retinoblastoma and subband deletion of chromosome 13. *Am J Dis Child* 132, 161–163. <https://doi.org/10.1001/archpedi.1978.02120270059012>.
- Zagorski, W.A., Knudsen, E.S., and Reed, M.F. (2007). Retinoblastoma Deficiency Increases Chemosensitivity in Lung Cancer. *Cancer Research* 67, 8264–8273. <https://doi.org/10.1158/0008-5472.CAN-06-4753>.
- Zhang, H.S., Gavin, M., Dahiya, A., Postigo, A.A., Ma, D., Luo, R.X., Harbour, J.W., and Dean, D.C. (2000). Exit from G1 and S Phase of the Cell Cycle Is Regulated by Repressor Complexes Containing HDAC-Rb-hSWI/SNF and Rb-hSWI/SNF. *Cell* 101, 79–89. [https://doi.org/10.1016/S0092-8674\(00\)80625-X](https://doi.org/10.1016/S0092-8674(00)80625-X).
- Zhao, W., Huang, C.C., Otterson, G.A., Leon, M.E., Tang, Y., Shilo, K., and Villalona, M.A. (2012). Altered p16INK4 and RB1 Expressions Are Associated with Poor Prognosis in Patients with Nonsmall Cell Lung Cancer. *Journal of Oncology* 2012, 1–7. <https://doi.org/10.1155/2012/957437>.

Zheng, N., Fraenkel, E., Pabo, C.O., and Pavletich, N.P. (1999). Structural basis of DNA recognition by the heterodimeric cell cycle transcription factor E2F-DP. *Genes Dev* 13, 666–674. <https://doi.org/10.1101/gad.13.6.666>.

Zhu, L., van den Heuvel, S., Helin, K., Fattaey, A., Ewen, M., Livingston, D., Dyson, N., and Harlow, E. (1993). Inhibition of cell proliferation by p107, a relative of the retinoblastoma protein. *Genes Dev* 7, 1111–1125. <https://doi.org/10.1101/gad.7.7a.1111>.

Zhu, L., Zhu, L., Xie, E., and Chang, L.S. (1995). Differential roles of two tandem E2F sites in repression of the human p107 promoter by retinoblastoma and p107 proteins. *Mol Cell Biol* 15, 3552–3562. <https://doi.org/10.1128/MCB.15.7.3552>.

Chapter 2

2 Phosphorylation of the RB C-terminus regulates condensin II release from chromatin

2.1 Abstract

The retinoblastoma tumour suppressor protein (RB) plays an important role in biological processes such as cell cycle control, DNA damage repair, epigenetic regulation, and genome stability. The canonical model of RB regulation is that cyclin-CDKs phosphorylate, and render RB inactive in late G1/S, promoting entry into S phase. Recently, mono-phosphorylated RB species were described to have distinct cell-cycle independent functions, suggesting that a phosphorylation code dictates diversity of RB function. However, a biologically relevant, functional role of RB phosphorylation at non-CDK sites has remained elusive. Here, we investigated S838/T841 dual phosphorylation, its upstream stimulus, and downstream functional output. We found that mimicking T cell receptor activation in Jurkat leukemia cells induced sequential activation of downstream kinases including p38 MAPK, and RB S838/T841 phosphorylation. This signaling pathway disrupts RB and condensin II interaction with chromatin. Using cells expressing a WT or S838A/T841A mutant RB fragment, we present evidence that deficiency for this phosphorylation event prevents condensin II release from chromatin.

2.2 Introduction

The retinoblastoma tumour suppressor protein (RB) is well-characterized for its role in regulating entry into the cell cycle, and this is its canonical function. In G1, RB is bound to E2F transcription factors, repressing their ability to express cell cycle target genes (Chellappan et al., 1991; Weinberg, 1995). Upon growth stimulation, cyclin D accumulates and binds to cyclin-dependent-kinases 4/6 (CDK4/6). Cyclin D-CDK4/6 complexes phosphorylate RB, partially relieving E2F repression (Lundberg and Weinberg, 1998). This leads to expression of cyclin E, and cyclin E-bound CDK2 hyperphosphorylates RB. Hyperphosphorylated RB is thought to be inactivated, and free

E2F transcription factors drive gene expression required for subsequent cell cycle progression (DeGregori et al., 1997; Dyson, 1998; Mittnacht, 1998).

This model, however, represents only one facet of RB function, and CDK-independent roles are emerging. These non-canonical functions are ascribed to a pool of chromatin-bound RB that localize to various parts of the genome. For example, RB is required for recruiting DNA repair machinery for non-homologous end joining (NHEJ) and homology-directed repair (HR) pathways at double strand breaks (DSBs) (Cook et al., 2015; Vélez-Cruz et al., 2016). In addition, RB recruits epigenetic writers to repetitive elements that deposit repressive histone marks (Ishak et al., 2016; Manning et al., 2014). Heterochromatinization of repetitive elements may be required to silence their transcription to avoid an autoimmune response, and maintain chromosome stability (Chiappinelli et al., 2015; Manning et al., 2014; Rajshekar et al., 2018; Roulois et al., 2015). In particular, RB-dependent maintenance of histone 4 lysine 20 tri-methylation (H4K20me3) at pericentromeric repeats is required for proper chromatid segregation in anaphase (Manning et al., 2014). Furthermore, disrupting RB interaction with structural maintenance of chromatin containing complexes such as condensin II at pericentromeric repeats results in mitotic errors, replication defects and aneuploidy (Coschi et al., 2014; Longworth et al., 2008). Therefore, existing literature suggests that there is a pool of RB that is resistant to CDK inactivation and binds chromatin to carry out cell cycle-independent functions.

Mechanistically, post-translational modifications regulate RB's diverse functions (MacDonald and Dick, 2012). Notably, phosphorylation of RB can regulate its cell cycle-independent functions. For example, CDK4/6 phosphorylation of RB at S249/T252 allows RB to bind and inactivate the NF κ B family protein p65 and its immune-suppressive transcriptional program in prostate cancer cells (Jin et al., 2019). In addition, stress-induced p38 mitogen activated protein kinase (MAPK) activation phosphorylates RB at S249/T252 to negate inactivation by CDKs and prevent cell cycle entry (Gubern et al., 2016). Furthermore, mono-phosphorylation of RB at its thirteen CDK phosphorylation sites confer ability to activate distinct transcriptional programs beyond cell cycle genes such as inflammatory response and mitochondrial oxidative

phosphorylation (Sanidas et al., 2019). However, these studies have primarily focused on phosphorylation at CDK consensus sites, and RB phosphorylation at non-CDK sites and their functional outcomes are not fully characterized. Upon apoptotic stimulation, p38 MAPK, but not CDKs, phosphorylate RB at non-CDK sites, and activates E2F1 transcription in a reporter assay (Nath et al., 2003). Specific non-CDK phosphorylation sites, and their relevance to cellular function remain to be elucidated.

Here, we characterize RB phosphorylation on S838 and T841 (S838/T841) as a mechanistic link between T cell receptor (TCR) activation and chromatin decondensation in Jurkat T cells. Prompted by existing phospho-proteomic data, we generated an antibody specific to phosphorylation at S838/T841. We show that p38 MAPK is an upstream kinase that induces RB phosphorylation at these sites upon stimulus that mimics TCR activation in culture. Finally, we demonstrate that inability to phosphorylate these sites leads to defective condensin II release from chromatin.

2.3 Materials and Methods

2.3.1 Antibodies

Anti-RB pS838/pT841 antibody was produced in rabbits by Covance (Pennsylvania, USA). The peptide immunogen corresponded to the sequence 834-SIGE(pS)FG(pT)SEKF-845 of pRB. Peptides were immobilized using the Sulfo-link coupling reagent (Thermo Fisher) following the manufacturer's recommendations. The phospho-specific antibody was purified using standard procedures by passing serum first over the nonphosphorylated peptide column and secondly over the phosphorylated-peptide column to remove any antibodies recognizing the nonphosphorylated species. Anti-RB pS838/pT841 antibody was used in primary antibody solution at 0.5 mg/ml for Western blotting. Anti-MAPKAPK-2 pT334 (27B7), p38 pT180/pY182 (9211), total p38 (9212), α -tubulin (11H10), and RB pS807/pS811 (9308) antibodies were obtained from Cell Signaling Technology. Anti-HA antibody (3F10) was from Sigma. Anti-RB monoclonal antibody (G3-245) was from BD Pharmingen, RB rabbit polyclonal antibodies and E2F1 antibody (C-20) were from Santa Cruz, CAP-H2 antibody (A302-275A) was from Bethyl Laboratories. Anti-rabbit or anti-mouse IgG goat antibody

conjugated to HRP was from GE Healthcare. For TCR activation studies, anti-CD3 ϵ (OKT3) and CD28 (CD28.2) antibodies were from BioLegend, and light chain-specific goat anti-mouse IgG (115-005-174) was from Jackson ImmunoResearch Labs. Details are included in Appendix B.

2.3.2 Cell culture and stimulation

Suspension Jurkat cells were grown in DMEM enriched with 10% v/v FBS, L-glutamine, penicillin and streptomycin at 37 °C in 5% CO₂. For SB203580 inhibitor pre-treatment, Jurkat cells (10⁷) were suspended in 5 mL enriched DMEM and SB203580 (Cell Signaling Technology) was added from 10 mM stock to a final concentration of 10 μ M. Equal volume of DMSO was added to control samples. The cells were then incubated at 37 °C for 2 hours until treatment with pervanadate and calyculin (PVA/CA). Cells were centrifuged at 300 \times g for 5 min at 4 °C and washed twice with PBS. After the last wash the pellet was resuspended in 5 mL enriched DMEM and PVA/CA were added to a final concentration of 100 and 0.1 μ M, respectively. Control samples received equal volumes of PBS and DMSO vehicles, respectively. Both groups were incubated at 37 °C for 20 min. TCR activation was achieved as previously described with modifications (Dephoure et al., 2008). Jurkat cells (5 \times 10⁶) were resuspended in 1 mL enriched media and treated with 5 μ g/mL anti-CD3 ϵ and CD28 antibodies, and 30 μ g/mL goat anti-mouse IgG to crosslink the primary antibodies. The cells were then incubated for indicated times at 37 °C after which they were harvested.

2.3.3 Protein extract preparation

All of the following lysis buffers were supplemented with 250 μ M Na₃VO₄, 5 mM NaF, 1 mM PMSF, 5 μ g/L aprotinin and leupeptin immediately before use. For whole cell extract (WCE), cells were washed twice with cold PBS and resuspended in lysis buffer containing 25 mM Tris-Cl pH 7.5, 100 mM NaCl, 5% (v/v) glycerol, and 1% (v/v) NP-40 and incubated on ice for 10 min. Insoluble material was cleared by centrifugation at 12 000 \times g at 4 °C for 10 min. For nuclear extract (NE), cells were washed twice with cold PBS, resuspended in hypotonic lysis buffer containing 10 mM Tris-Cl pH 7.5, 10 mM KCl, 3 mM MgCl₂, 1 mM EDTA and 0.05% (v/v) NP-40, and

incubated on ice for 5 min. Nuclei were isolated by centrifuging the suspension at $1300 \times g$ at $4^\circ C$ for 5 min. The pelleted nuclei were washed twice in the same buffer. The nuclei were lysed in buffer containing 20 mM Tris-Cl pH 7.5, 420 mM NaCl, 1.5 mM $MgCl_2$, 0.2 mM EDTA, 25% (v/v) glycerol, 0.1% (v/v) NP-40 and incubated on ice for 10 min. Insoluble material was cleared by centrifugation at $12\,000 \times g$ at $4^\circ C$ for 10 min. For chromatin fractionation, PBS washed cells were incubated for 10 min on ice in buffer containing 10 mM Tris-Cl pH 8.0, 10 mM KCl, 1.5 mM $MgCl_2$, 0.34 M sucrose, 10% (v/v) glycerol and 0.1% (v/v) Triton X-100 to lyse outer membrane. Nuclei were isolated by centrifuging the suspension at $1300 \times g$ at $4^\circ C$ for 5 min. The pelleted nuclei were washed twice in the same buffer without Triton X-100. The nuclei were lysed in buffer containing 3 mM EDTA and 0.2 mM EGTA for 30 min on ice with occasional mixing. Nucleoplasmic fraction was removed by centrifuging the lysate at $4000 \times g$ at $4^\circ C$ for 5 min. Remaining chromatin fraction was solubilized with DNaseI treatment at $37^\circ C$ for 10 min in buffer containing 10 mM Tris-Cl, 2.5 mM $MgCl_2$, 0.5 mM $CaCl_2$. Protein concentration was quantified by Bradford assay following standard procedures.

2.3.4 Immunoprecipitation

Antibodies to RB or pp38 T180/Y182 were diluted 1:50 in whole cell extract containing 1 to 2 mg total protein. The lysates were incubated at $4^\circ C$ overnight with gentle agitation. 50 μL Dynabeads Protein G (Thermo Fisher) was added and incubated at $4^\circ C$ for 2 hours with gentle agitation. A magnet was used to immobilize the beads and to discard the supernatant.

2.3.5 *In vitro* kinase assay

Immunoprecipitated pp38 T180/Y182-Dynabeads complexes were used in kinase assays similar to previous reports. The complexes were resuspended in 50 μL kinase buffer containing 25 mM Tris-Cl pH 7.5, 5 mM β -glycerophosphate, 10 mM $MgCl_2$, 0.25 mM Na_3VO_4 and 5 mM NaF. Each of the time points consisted of a 40 μL reaction containing 5 μL of immunoprecipitated kinase, 10 μg of GST-RBC, 1 mM ATP, and 50 μM SB203580 (where indicated) in kinase buffer. GST fusion proteins were expressed in *E. coli* BL21 (DE3) and purified with Glutathione Sepharose 4B (Sigma) following the

manufacturer's recommendation. The reactions were prepared on ice then transferred to 37 °C to start the assay. After the given incubation times, the immunoprecipitated proteins were immobilized with a magnet and the remaining supernatant was saved.

2.3.6 SDS-PAGE, Western blotting and Coomassie staining

Protein extracts, supernatants and immunoprecipitated beads were diluted in SDS-PAGE sample buffer to a final concentration of 62.5 mM Tris-Cl pH 6.8, 10% glycerol, 2% SDS, 72.5 mM β -mercaptoethanol, and 0.005% bromophenol blue. SDS-PAGE was performed following standard procedures. After gel electrophoresis, proteins were transferred to PVDF membrane and incubated with primary antibodies diluted in 5% milk or BSA in TBS-T over night at 4 °C with gentle agitation. Membranes were washed five times in tris buffered saline-Tween 20 (TBS-T) for 5 min and incubated with horseradish peroxidase (HRP)-conjugated goat secondary antibody for one hour at room temperature. Membranes were washed again, incubated in SuperSignal WestDura (Thermo Fisher) for 5 min protected from light and developed on a ChemiDoc (Bio-rad). For Coomassie staining, gels were washed three times in water, and incubated in GelCode Blue (Thermo Fisher) over night at room temperature with gentle agitation. Stained gels were washed again twice in water. Bands were imaged on a ChemiDoc.

2.3.7 Plasmids and lentiviral transduction

Briefly, pSicoR-Ef1a-mCh-Puro (Addgene #31845) was double-digested with AfeI and SmaI to replace mCherry coding sequence with that of RBLP with matching sticky ends in-frame. S838A/T841A substituted plasmid was made with QuikChange Site-directed mutagenesis kit (Agilent), following manufacturer's recommendations and mutagenic primers (Appendix A). HEK293T cells at 70% confluency on 10-cm plates were transfected with 12 μ g expression vector, 9 μ g pMD2.G (Addgene #12259) and 3 μ g psPAX2 (Addgene #12260) using Lipofectamine 3000 (Life Technologies) following manufacturer's recommendations. Two days later, the cell media was harvested and passed through a 0.45 μ m filter. Jurkat cells (10^6) were transduced with the filtrate containing 8 μ g/mL polybrene. Transduced Jurkat cells were maintained in 0.3 μ g/mL puromycin.

2.3.8 Chromatin sonication

Jurkat cells were washed twice in PBS and fixed in 1% formaldehyde/PBS for 10 min at room temperature with gentle agitation. Fixation was quenched with 0.125 M glycine for 5 min at room temperature. Cells were washed twice in cold PBS and incubated for 10 min on ice in buffer containing 10 mM HEPES pH 6.5, 10 mM EDTA, 0.5 mM EGTA and 0.25% Triton X-100. Nuclei were isolated by centrifuging the suspension at $600 \times g$ at 4 °C for 5 min. The pelleted nuclei were lysed and washed twice in buffer containing 10 mM HEPES pH 6.5, 10 mM EDTA, 0.5 mM EGTA and 200 mM NaCl. Chromatin isolated from three million cells was resuspended in 300 μ L of buffer containing 50 mM Tris-Cl pH 8.0, 1 mM EDTA, 0.5 % Triton X-100 and 1% SDS, and aliquoted into 1.5 mL microtubes (Diagenode). All of the above lysis buffers were supplemented with 250 μ M Na_3VO_4 , 5 mM NaF, 1 mM PMSF, 5 μ g/mL aprotinin and leupeptin immediately before use. Chromatin was sonicated in Bioruptor Pico (Diagenode) at 4 °C with one to four cycles. Each cycle consisted of 15 seconds ON and 30 seconds OFF. After sonication, chromatin-protein complexes were reverse-crosslinked by adding NaCl to a final concentration of 200 mM to each sample and incubating overnight at 65 °C. RNA and protein were removed by RNase A and proteinase K digestion, respectively. DNA was isolated by phenol-chloroform extraction and ethanol precipitation and analyzed on 3% agarose gels. DNA was stained with ethidium bromide and visualized on Chemi Doc. High molecular weight DNA bands were quantified as a percentage of the total lane intensity with lower threshold cut-off at 100 bp using Image Lab 5.2.

2.3.9 Statistical analysis

All statistical analyses were performed on Prism 8. CAP-H2 chromatin loading relative to SMC1 in untransduced cells was compared using Student's t-test. That of HA-RBLP WT or AA expressing cells was compared using two-way ANOVA and Sidak's multiple comparisons test. For sonicated chromatin densitometry, the mean of triplicate values was compared between treatment conditions, or cell lines, as indicated by two-way ANOVA. Sidak's multiple comparison test was used.

2.4 Results

2.4.1 Detection of C-terminal RB phosphorylation on S838 and T841

Multiple residues located throughout RB are phosphorylated, and the functional roles of CDK sites have been extensively characterized. Many of these modifications serve to inactivate its canonical function of negatively regulating cell cycle entry through E2F transcription factor binding. Interestingly, RB mono-phosphorylation of CDK sites has been shown to activate specific molecular functions of RB that may extend beyond cell cycle control (Sanidas et al., 2019). We sought to identify RB phosphorylation at new sites and determining their roles in RB regulation.

Figure 2.1A depicts the open reading frame of RB, its known CDK phosphorylation sites (top) and potential phospho-acceptor residues that are uncharacterized (bottom). We focused on RB C-terminus (RBC) as it forms a strand-loop-helix, and any phosphorylation within this region is likely to disrupt protein-protein interactions, leading to a novel functional outcome (Rubin et al., 2005). To identify candidate phosphorylation sites for our investigation, we curated predicted phosphorylation events within tryptic fragments corresponding to RBC from available phospho-proteomic data in different cells or tissues upon various treatments (Figure 2.1B) (Dephoure et al., 2008; Hoffert et al., 2006; Hornbeck et al., 2012; Huttlin et al., 2010; Kettenbach et al., 2011; Mayya et al., 2009; Mertins et al., 2013; Sharma et al., 2014; Zhou et al., 2013). A positive prediction for each serine or threonine residue is shaded in blue.

The phospho-proteomic data reveal various combinations of serine and threonine residues within RBC are readily phosphorylated, supporting the idea that the RB phosphorylation “code” is yet incomplete. There is significant variability between the data sets on which exact sites are phosphorylated. This may indicate that complex, differential phosphorylation events occur in RBC depending on the cell type and stimulus, or that whole cell proteomics cannot accurately discern between neighbouring

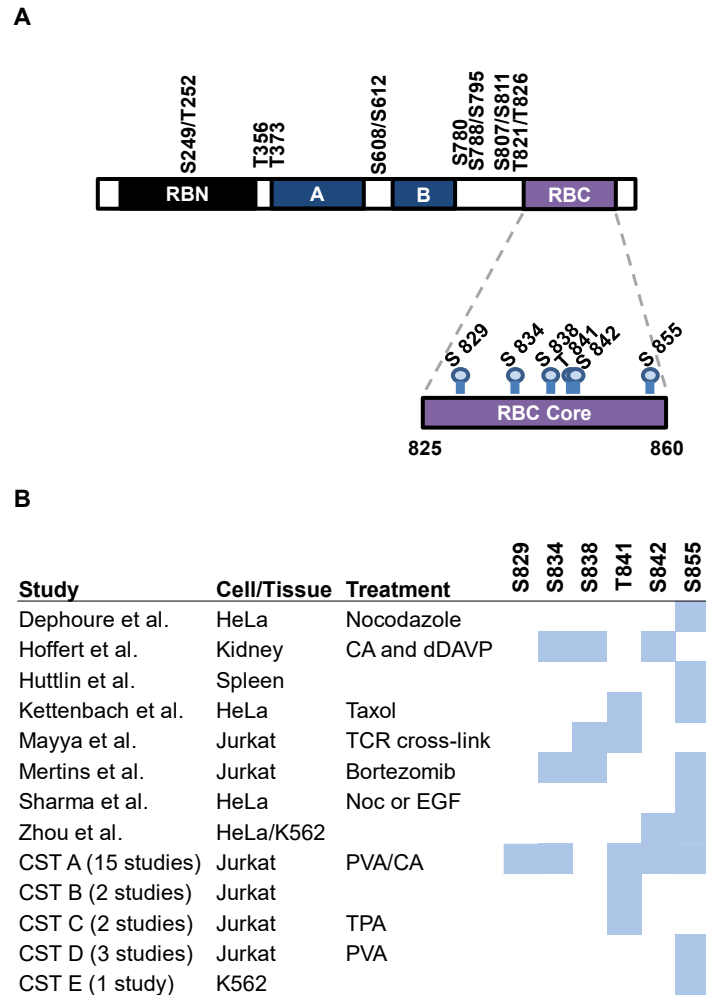


Figure 2.1: Putative phosphorylation of the RB C-terminus.

(A) The open reading frame for RB is shown depicting known CDK phosphorylation sites (top), and uncharacterized, non-CDK phosphorylation sites in RBC (bottom). RB N-terminal domain (RBN), A and B halves of the pocket domain, and RB C-terminal domain (RBC) are shown. (B) Chart displaying potential phosphorylation sites in the amino acid 825-860 region of the RB C-terminus. Putative phosphorylation sites identified in publicly available phosphoproteomic studies are shaded in blue and the relevant data sources are indicated. CST – Cell Signaling Technologies data set.

phosphorylation events. While all of these potential modifications can be found in untreated cells, we focused on S838 and T841 phosphorylation because it is inducible upon TCR activation, a relevant signaling pathway in Jurkat leukemic T cells.

In order to study S838 and T841 phosphorylation on RB further, we sought to generate a specific antibody for these modifications. We generated rabbit anti serum against an RB derived peptide corresponding to amino acids 834-845, phosphorylated on S838 and T841. An ELISA was performed to confirm the specificity of our antibodies following purification from the anti-serum. We found that anti-RB pS838/pT841 antibodies had a 10-fold higher affinity for the S838/T841 phosphorylated RB peptide than its unphosphorylated counterpart (Figure 2.2A). Next, we sought to find evidence for RB phosphorylation on S838/T841 in vitro as predicted by phospho-proteomic data. We incubated glutathione S-transferase-tagged RBC (GST-RBC) with whole cell extract (Ext) from Jurkat cells treated with phosphatase inhibitors pervanadate and calyculin A (PVA/CA) to globally activate kinases that may phosphorylate RB. We found a time-dependent increase in RB S838/T841 phosphorylation in the presence of ATP (Figure 2.2B). To account for the possibility that our antibody cross-reacts with other phosphorylation events in RBC (amino acids 792-928), we repeated the experiment with GST-RBC where S838 and T841 were substituted to alanine either together or as single mutants. This reveals that this antibody requires either S838 or T841 phosphorylation, but not both (Figure 2.2C). For this reason, we describe the antibodies and detected phosphorylation events throughout this paper as pS838/pT841 because phosphorylation of either site alone, or both in combination, is possible. With the specificity of our antibody established, we determined if endogenous RB is phosphorylated on S838/T841. We treated Jurkat cells with PVA/CA to activate kinases and RB phosphorylation, prepared nuclear extracts (NE) and immunoblotted with our antibody. RB phosphorylation on S838/T841 was increased upon PVA/CA treatment, but it was also evident that our antibody cross-reacted with approximately six or seven proteins other than RB (Figure 2.2D). To ensure we were certain of RB's identity, we repeated the cell treatment and immunoprecipitated total RB from Jurkat NE and

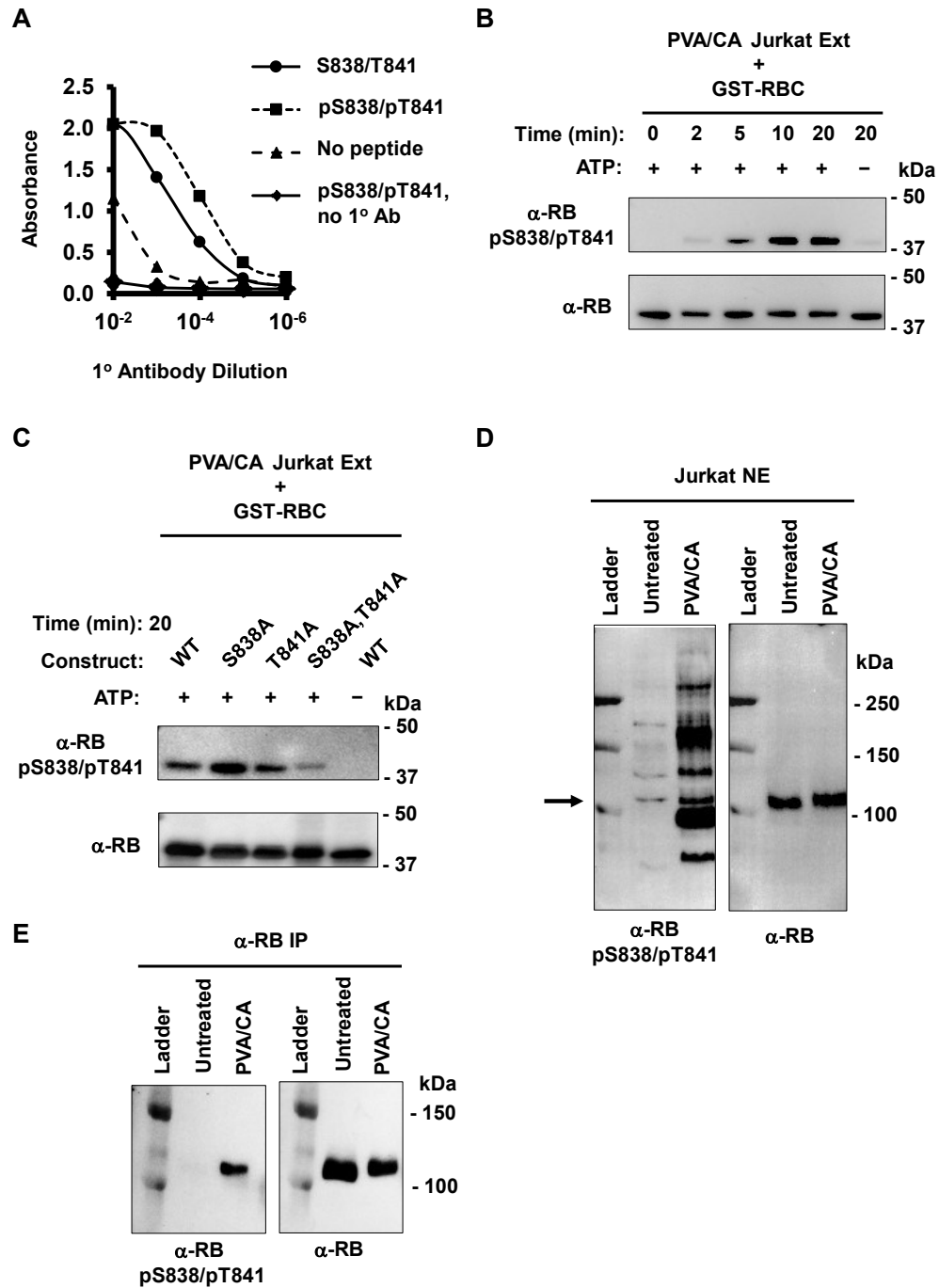


Figure 2.2: Detection of phosphorylation of S838/T841 on RB.

Figure 2.2: Detection of phosphorylation of S838/T841 on RB.

(A) Rabbit anti-serum was generated by immunizing animals with a peptide phosphorylated at S838 and T841. Phosphorylation-specific antibodies were purified and an ELISA was performed to determine their specificity. Phosphorylated or unphosphorylated peptides were adhered to microplate wells and incubated with anti-RB pS838/pT841 antibodies. Control wells contained either no peptide or no antibody. Antibody binding was measured colorimetrically and graphed. **(B)** A GST-tagged RBC fragment (aa 792-928) was incubated with PVA/CA treated Jurkat whole cell extract for the indicated times, and omission of ATP was used as a negative control. Phosphorylation status was determined by immunoblotting with the anti-RB pS838/pT841, and blotting with anti-RB antibodies was used as a loading control. **(C)** WT or mutant GST-RBC proteins were incubated with PVA/CA treated Jurkat extracts with or without ATP for 20 min. Phosphorylation status was measured as in B. **(D)** S838/T841 phosphorylation of endogenous RB was detected by western blotting with anti-RB pS838/pT841 antibodies in PVA/CA treated Jurkat nuclear extracts (NE). This membrane was stripped and reprobed for RB and the arrow indicates the corresponding RB band. **(E)** Jurkat cells were treated with PVA/CA, and RB was immunoprecipitated from NE with an α -RB antibody-coupled to Protein G Dynabeads. Phosphorylation status of S838/T841 was determined by western blotting.

performed an immunoblot with anti-RB pS838/pT841 antibodies. Once again, we confirmed that RB phosphorylation on S838/T841 was induced upon PVA/CA treatment (Figure 2.2E). In all subsequent experiments, we first immunoprecipitated RB then probed with the antibody to assess S838/T841 phosphorylation.

These data demonstrate that our antibody is highly specific for phosphorylation within RBC, namely on S838/T841. Although it cross-reacts with a small number of nuclear proteins, first enriching for RB by immunoprecipitation is a robust and specific means of detecting phosphorylation of these sites. More importantly, we have shown the first line of evidence that S838/T841 phosphorylation is a bona fide RB post-translational modification that has not yet been studied functionally.

2.4.2 Sequential activation of kinases in the TCR signaling pathway induces RB S838/T841 phosphorylation

As a first step to understanding the functional role for RB S838/T841 phosphorylation, we sought to identify the kinase that was responsible for this modification. p38 MAPK has been shown to phosphorylate RB even when CDK sites are mutated (Nath et al., 2003). Therefore, we pre-treated Jurkat cells with a p38 inhibitor, SB203580, then stimulated phosphorylation with PVA/CA. We found that SB203580 pre-treatment strongly reduced RB S838/T841 phosphorylation despite PVA/CA treatment (Figure 2.3A). As a positive control for p38 inhibition, we also measured phosphorylation of a known p38 target, MAPKAPK-2, and found that phosphorylation of its activation loop at T334 was also reduced. Next, we determined if immunoprecipitated p38 can phosphorylate RB at S838/T841 in vitro. We first isolated p38 by immunoprecipitating the active form with anti-p38 pT180/pY182 phosphorylation specific antibodies. It was then incubated with GST-RBC in the presence or absence of its inhibitor. p38 phosphorylation of RB increased over time, and its inhibitor largely abrogated this effect (Figure 2.3B).

These experiments strongly suggest that RB phosphorylation at S838/T841 is dependent on p38. PVA/CA treatment indiscriminately activates kinases, yet selective inhibition of p38 was sufficient to reduce RB phosphorylation to background level.

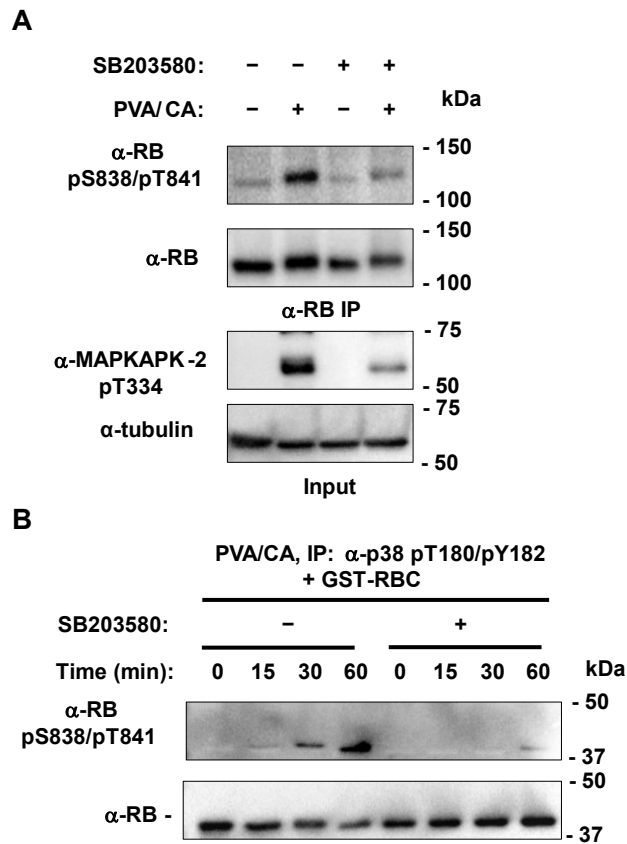


Figure 2.3 Phosphorylation of RB on S838/T841 is dependent on p38.

(A) Jurkat cells were treated with PVA/CA with or without 10 μ M SB203580, a p38 inhibitor. RB was immunoprecipitated from lysates with an α -RB antibody bound to Protein G Dynabeads, and phosphorylation of S838/T841 was detected by immunoblotting. As a positive control for p38 inhibition, phosphorylation of a known p38 phosphorylation target, T334 on MAPKAPK-2, was detected by western blotting. (B) Jurkat cells were treated with PVA/CA, and active p38 was immunoprecipitated from whole cell lysates with α -p38 pT180/pY182 antibodies bound to Protein G Dynabeads. Immunoprecipitated p38 was resuspended in kinase buffer containing GST-RBC, with or without 50 μ M SB203580 for the indicated amount of time. Phosphorylation of S838/T841 and GST-RBC was detected by western blotting as indicated.

Furthermore, partially purified, active p38 was necessary and sufficient to induce RB phosphorylation *in vitro* suggesting it may do so directly.

PVA/CA treatment has served as a way to easily and efficiently induce phosphorylation of RB. However, this treatment activates many pathways and hence does not offer insight into specific stimuli that induce RB S838/T841 phosphorylation under physiological conditions. Since p38 is a downstream target of T cell receptor (TCR) signaling, and Jurkat cells are leukemic T cells, we hypothesized that TCR activation phosphorylates RB through p38. We mimicked TCR activation by treating cells with an antibody cocktail that physically aggregates TCR and its co-stimulatory receptor together, as previously reported (Smith-Garvin et al., 2009; Trickett and Kwan, 2003). We then detected phosphorylation-dependent activation of proteins in the signaling pathway by immunoblotting. We observed rapid activation of ZAP70 within the first five minutes of antibody crosslinking, and peak activation of p38 soon after at 15 minutes (Figure 2.4A). TCR activation reproducibly induced p38 activation within the first 30 minutes (Figure 2.4B). At 30 minutes we immunoprecipitated RB and found strong S838/T841 phosphorylation (Figure 2.4C). In addition, TCR activation did not induce additional phosphorylation of neighbouring CDK phosphorylation sites, S807 and S811 consistent with these cells already being in a proliferative state. S838/T841 phosphorylated RB also retained its interaction with E2F1 and E2F2 as they were comparably co-immunoprecipitated relative to untreated cells. The shift in E2F2 migration upon TCR activation is consistent with previous proteomic data that report S117/S123 phosphorylation in Jurkat cells upon PVA/CA or TCR activation (Hornbeck et al., 2012; Mayya et al., 2009).

These experiments implicate TCR activation as a relevant mechanism that induces RB S838/T841 phosphorylation and suggests that RB S838/T841 phosphorylation may regulate its non-canonical functions. Our antibody cocktail treatment appears to closely mimic TCR activation as both ZAP70 and p38 were activated sequentially in the anticipated order. A slight temporal delay in peak phosphorylation of ZAP70, p38 and ultimately RB also suggests that this signaling cascade is biologically relevant to TCR

activation. Furthermore, because S838/T841 phosphorylation in response to TCR signaling is unlinked to CDK phosphorylation its function is unlikely to be related to cell cycle entry or control of E2F-dependent transcription.

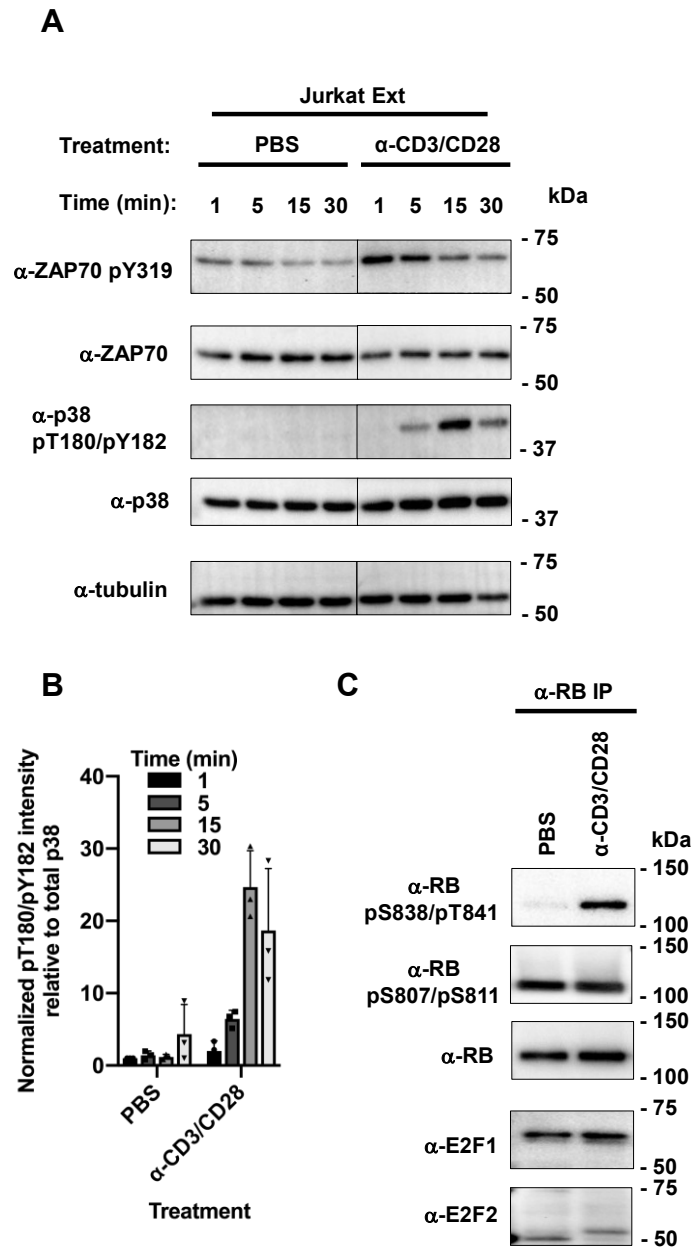


Figure 2.4: T cell receptor signaling causes RB S838/T841 phosphorylation.

Figure 2.4: T cell receptor signaling causes RB S838/T841 phosphorylation.

(A) Jurkat cells were treated with PBS, or anti-CD3, anti-CD28, and a secondary antibody to cross link T cell receptors for the indicated time points. Each time point was quenched by washing cells with cold PBS and immediately lysed to generate whole cell extracts. Abundance of phosphorylated species relative to total ZAP70 and p38 was determined with immunoblotting as a read-out. Relevant lanes from a single whole image were spliced together at the vertical line in the center for each blot. (B) Jurkat cells were treated as in A for 30 minutes. RB was immunoprecipitated from whole cell extracts with α -RB antibodies bound to Protein G Dynabeads. RB phosphorylation on S838/T841 and S807/S811 was determined by blotting, and co-immunoprecipitating E2Fs were detected similarly.

2.4.3 RB S838/T841 phospho-acceptor mutants prevent condensin II unloading and chromatin decondensation

The majority of previously described RB function stems from its ability to occupy chromatin. For example, RB protects genome integrity during mitosis by recruiting the condensin II complex to pericentromeric heterochromatin (Coschi et al., 2014). In addition, the condensin II complex has a role in developing T cells. The *nessy* mutant allele of CAP-H2, one of the subunits of the complex, results in defective condensation of T cell chromatin and development (Gosling et al., 2007; Rawlings et al., 2011). Since RB is phosphorylated under conditions that mimic TCR signaling, and is known to recruit condensin II to chromatin, we hypothesized that RB S838/T841 phosphorylation may regulate RB-condensin II interactions on chromatin in T cells.

In order to compare chromatin occupancy upon TCR crosslinking, we first sought to establish that this stimulus did not affect total expression of the proteins of interest. Indeed, we confirmed that expression of CAP-H2, RB, E2F1 and SMC1, a cohesin subunit, was not changed in whole cell extracts (Figure 2.5A, left). However, TCR crosslinking for 30 minutes induced release of RB, E2F1, and CAP-H2, but not SMC1 from chromatin (Figure 2.5A, right). Using densitometric analysis of these experiments we found that TCR crosslinking released 40% of CAP-H2 from chromatin (Figure 2.5B). To examine the precise role of S838/T841 phosphorylation in this process, we created a phospho-acceptor mutation in RB with a S838A/T841A double alanine substitution. To stably express this mutant in cells, we generated lentiviral vectors coding for HA-tagged large pocket fragment of RB (RBLP, amino acids 379-928). Jurkat cells were transduced with lentiviruses expressing either the WT RBLP (RBLP-WT) or S838A/T841A (RBLP-AA) construct (Figure 2.5C). We confirmed equivalent expression of both constructs by immunoblotting for the HA-tag (Figure 2.5D). We cross-linked TCRs as before and investigated CAP-H2 and SMC1 chromatin levels (Figure 2.5E). This revealed that RBLP-AA expressing cells retained similar levels of chromatin-bound CAP-H2 as unstimulated cells and that RBLP-WT expressing cells released CAP-H2 similarly to untransduced Jurkat cells (Figure 2.5E). We normalized CAP-H2 release to SMC1 bound

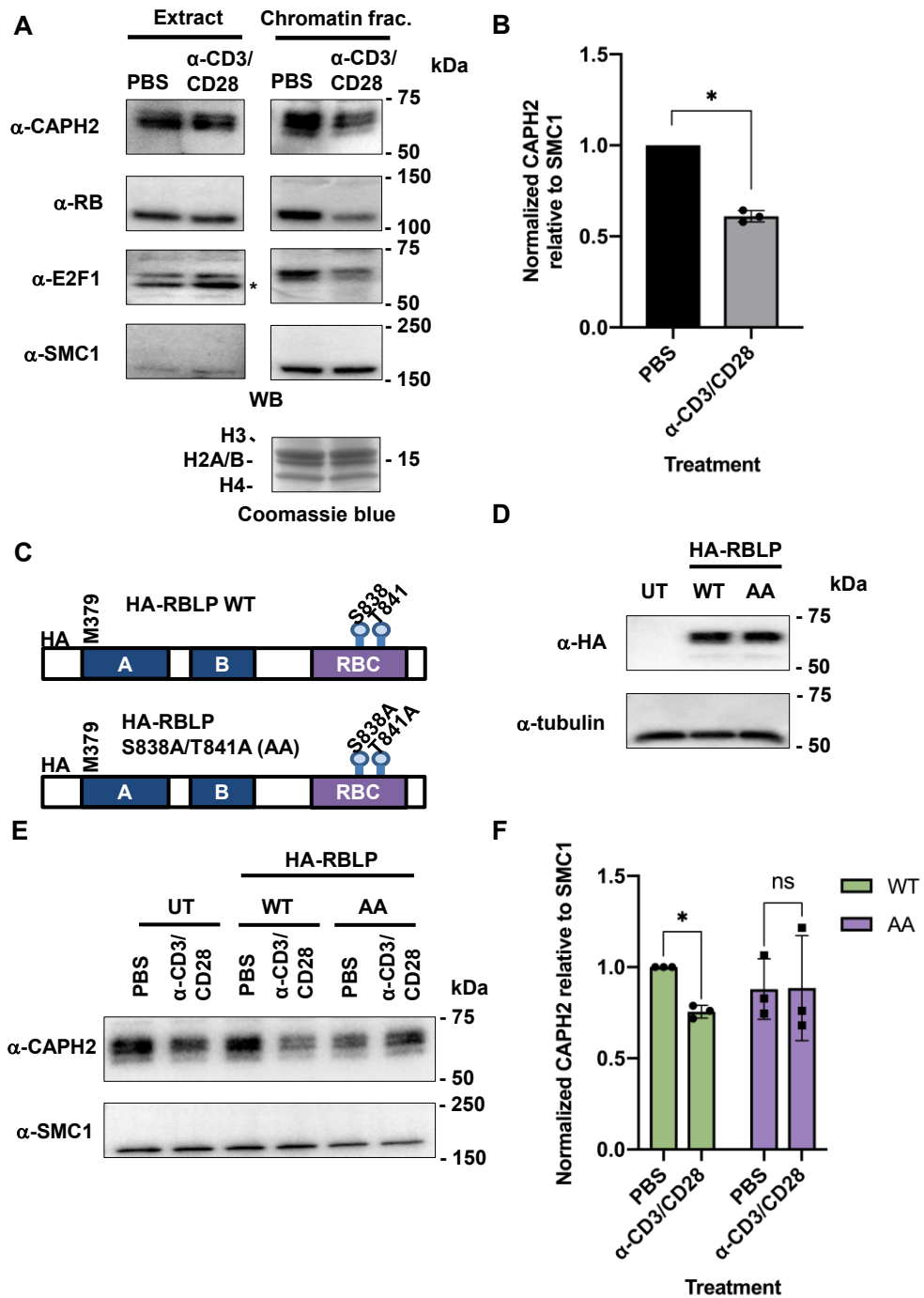


Figure 2.5: Non-phosphorylatable S838A/T841A RB prevents CAP-H2 chromatin unloading upon T cell receptor crosslinking.

Figure 2.5: Non-phosphorylatable S838A/T841A RB prevents CAP-H2 chromatin unloading upon T cell receptor crosslinking.

(A) Jurkat cells were treated as indicated for 30 minutes, whole cell extracts and chromatin fractions were prepared, and expression levels of the indicated proteins were detected by western blotting. Histone levels serve as loading control and were detected by Coomassie Blue staining. * indicates non-specific band. (B) Relative levels of CAP-H2 in chromatin fractions was normalized to SMC1 and compared between treated and untreated conditions (n=3, * P < 0.05, Student's t-test). (C) The open reading frame for WT and mutant RBLP constructs (aa 379-928) are shown depicting their relevant coding regions and HA tags. The mutant construct labelled RBLP AA carries double alanine substitutions at S838 and T841. (D) Lentiviruses were used to transduce RBLP and the AA mutant construct into Jurkat cells. Expression of exogenous RBLP was detected by western blotting for HA. Tubulin blots serve as loading controls. (E) Jurkat cells expressing either WT or RBLP, or untransduced controls (UT) were subjected to TCR crosslinking for 30 minutes. Chromatin fractions were prepared, and levels of the indicated proteins were detected by western blotting. (F) Levels of chromatin associated CAP-H2 was normalized to SMC1 and compared between PBS and TCR crosslinked conditions (n=3, * P < 0.05, Two-way ANOVA and Sidak's multiple comparisons test).

chromatin levels to quantitate the inhibition of CAP-H2 release by RBLP-AA (Figure 2.5F). These experiments confirm that the inability to phosphorylate RB at S838/T841 dominantly blocks condensin II release from chromatin.

Next, we sought to describe a biochemical consequence of defective CAP-H2 unloading. To assess changes in chromatin structure upon TCR-crosslinking, we used sensitivity to sonication-induced chromatin shearing as a read-out for chromatin compaction as previously reported (Figure 2.6A) (Rawlings et al., 2011). Untreated or TCR crosslinked cells were fixed to immobilize DNA-protein contacts and fractionated to obtain total chromatin. Isolated chromatin was sheared by a range of sonication cycles, and the presence of high molecular weight DNA fragments was detected by agarose gel electrophoresis and ethidium bromide staining. In line with Figure 2.5A, TCR crosslinking decreased the amount of high molecular weight DNA remaining after the same number of sonication cycles compared to control cells that were untreated (Figure 2.6B-C). We repeated this TCR crosslinking experiment using cells that express RBLP-WT or the -AA mutant. This revealed that chromatin isolated from RBLP-AA expressing cells was sheared less effectively compared to that from RBLP-WT expressing cells (Figure 2.6D-E). This suggests that the RB S838A/T841A mutant disrupts TCR crosslink-mediated chromatin decondensation and suggests that the phosphorylation of RB on these sites plays a key role in chromatin decondensation by releasing RB and condensin II from chromatin.

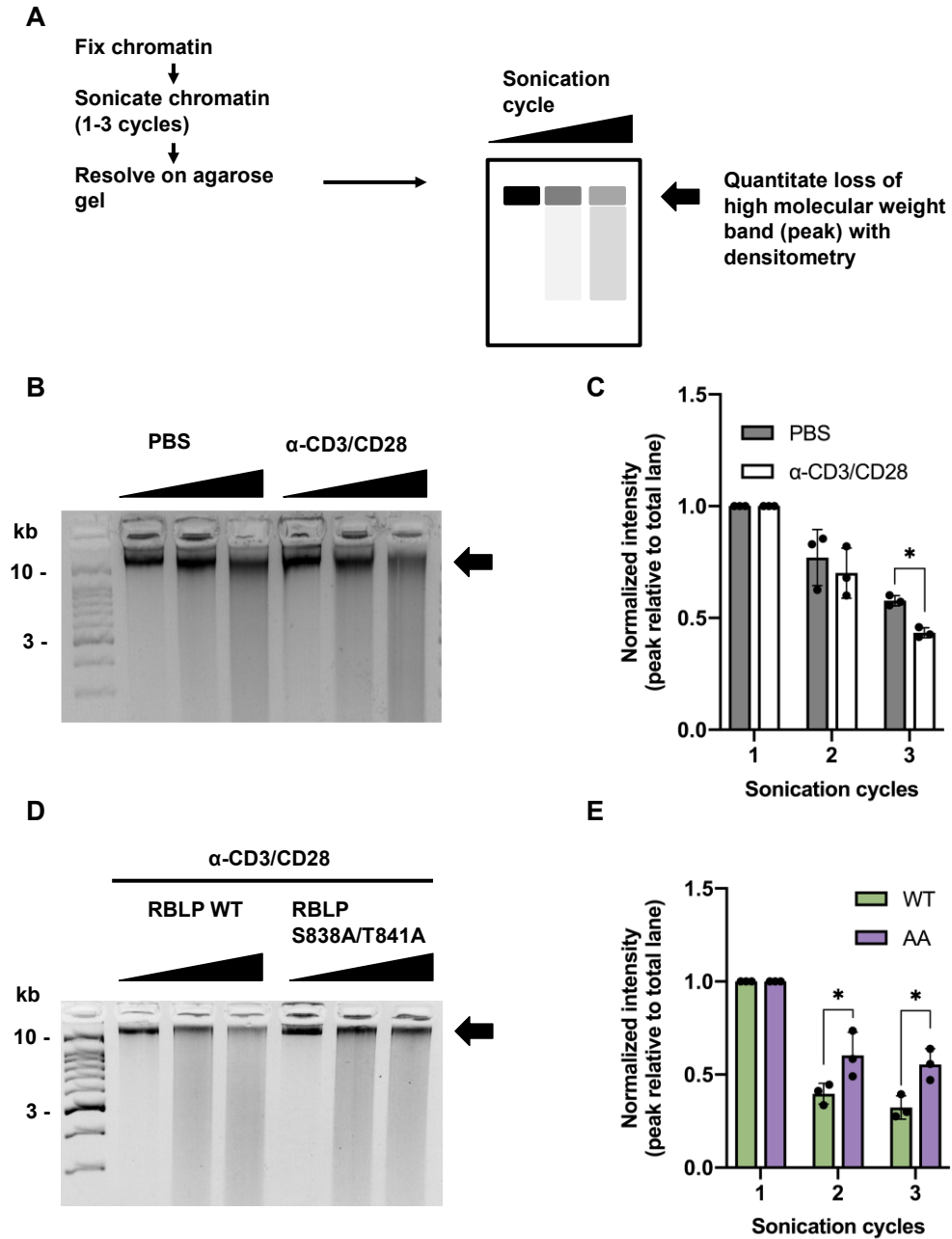


Figure 2.6: RB S838/T841 phosphorylation regulates chromatin dynamics upon T cell receptor signaling.

Figure 2.6: RB S838/T841 phosphorylation regulates chromatin dynamics upon T cell receptor signaling.

(A) Jurkat cells were stimulated by T cell receptor crosslinking as indicated. Cells were fixed and lysed to obtain chromatin fractions. Chromatin was sonicated for one to three cycles. Protein-DNA crosslinks were reversed, and DNA was purified, and analyzed on a 3% agarose gel. DNA was stained with ethidium bromide and visualized on a Chemi Doc. The high molecular weight DNA band indicated by the arrow was quantified on Image Lab and intensity is expressed as a percentage of the total lane normalized within in each group. (B) Untransduced Jurkat cells were PBS or TCR crosslinked as described in A. Chromatin fragmentation is shown. (C) Percent high molecular weight DNA quantities were averaged and graphed ($n = 3$, * indicates $P < 0.05$, two-way ANOVA with Sidak's multiple comparisons test). (D) Lentiviral transduced Jurkat cells were stimulated by T cell receptor crosslinking, fixed, and lysed to obtain chromatin fractions. Chromatin was sonicated for increasing number of cycles and analyzed as in A. (E) The high molecular weight band indicated by the arrow was quantified, averaged and graphed, ($n = 3$, * indicates $P < 0.05$, Two-way ANOVA with Sidak's multiple comparisons test).

2.5 Discussion

In this report, we characterized a functional role for non-CDK phosphorylation of RB. By curating existing phospho-proteomic data, we generated and validated S838/T841 phospho-specific antibodies. With this tool, we showed that p38 MAPK is an upstream kinase that can direct RB phosphorylation, and that TCR crosslinking induces a signaling cascade that ultimately phosphorylates RB in Jurkat cells on these sites. To probe its mechanistic role, we generated cell lines that stably express phospho-acceptor mutant RB. Finally, our data demonstrates that when RB is unable to be phosphorylated at S838/T841, TCR signaling is unable to release condensin II from chromatin. This conclusion is consistent with previous work that describes RB-condensin II chromatin interactions and T cell development, and contributes to our understanding of an emerging RB phosphorylation code.

TCR crosslinking induced marked loss of chromatin bound CAP-H2, but not SMC1, suggesting large scale, yet selective reorganization of chromatin architecture. Importantly, expression of RBLP-AA was sufficient to disrupt TCR crosslinking induced CAP-H2 release. The selective nature of RB regulation of condensin II in Jurkat T cells agrees with the previous characterization of the *nessy* mutant CAP-H2 allele that is responsible for defective T cell differentiation. Recently published work may inform future studies on specific consequences of the release of CAP-H2 in this model. CAP-H2 and transcription factor IIIC (TFIIIC) localize to histone clusters in mouse embryonic stem cells, and serve to maintain topologically-associated-domains that regulates transcription (Yuen et al., 2017). In addition, RB-condensin II complexes can regulate transcription at bi-directional promoters, and maintain long-range chromosomal interactions. ChIP-sequencing (ChIP-Seq) for condensin II and TFIIIC components upon TCR crosslinking may inform site-specific loss of interaction, and the mechanistic role of RB can be delineated with a phospho-acceptor RB mutant. For increased sensitivity, gene editing technologies should be adopted to mutate endogenous RB, or deplete endogenous RB with an inducible system as previously reported. ChIP-seq data should be interpreted together with high-throughput chromosome conformation capture (3C) such as 4C-seq to fully characterize functional consequences.

We speculate that RB phosphorylation at S838/T841 may be a key step in naive T cell activation. Previous work has demonstrated that chromatin condensation orchestrated by condensin II is required to avoid cell death in developing thymocytes (Rawlings et al., 2011). Once mature, these cells become quiescent. Upon TCR activation through cognate antigen binding and co-stimulation, re-entry into cell cycle is coupled with chromatin decondensation and nuclear expansion in naïve T cells. Loss of CAP-H2 chromatin occupancy upon TCR crosslinking in Jurkat T cells is in line with such macromolecular changes during T cell activation. Furthermore, TCR crosslinking with CD3/CD28 antibodies specifically induced RB phosphorylation at S838/T841, but not at its CDK sites. RB interaction with E2F transcription factors was also unaffected. These data suggest that S838/T841 phosphorylation is functionally distinct from canonical cell-cycle control by RB that may also be cell type specific. Future work with peripheral T cells *ex vivo* is warranted to support this model.

Ultimately, our work adds a layer of complexity to phosphorylation dependent regulation of RB function. The canonical model of cell cycle control by RB has been binary; cyclin-CDK driven RB hyperphosphorylation renders RB's negative regulation of E2F transcription factors inactive. Recently, however, various mono-phosphorylated RB species at one of its CDK sites have been shown to regulate cell-cycle independent transcription programs. We showed that cell-cycle independent TCR crosslinking induces a signaling cascade via p38 that can ultimately phosphorylate RB at S838/T841. Future work is warranted to characterize the relevance and functional roles of S838/T841 phosphorylation in other physiological circumstances.

2.6 References

- Chellappan, S.P., Hiebert, S., Mudryj, M., Horowitz, J.M., and Nevins, J.R. (1991). The E2F transcription factor is a cellular target for the RB protein. *Cell* *65*, 1053–1061. .
- Chiappinelli, K.B., Strissel, P.L., Desrichard, A., Li, H., Henke, C., Akman, B., Hein, A., Rote, N.S., Cope, L.M., Snyder, A., et al. (2015). Inhibiting DNA Methylation Causes an Interferon Response in Cancer via dsRNA Including Endogenous Retroviruses. *Cell* *162*, 974–986. <https://doi.org/10.1016/j.cell.2015.07.011>.
- Cook, R., Zoumpoulidou, G., Luczynski, M.T., Rieger, S., Moquet, J., Spanswick, V.J., Hartley, J.A., Rothkamm, K., Huang, P.H., and Mittnacht, S. (2015). Direct Involvement of Retinoblastoma Family Proteins in DNA Repair by Non-homologous End-Joining. *Cell Reports* *10*, 2006–2018. <https://doi.org/10.1016/j.celrep.2015.02.059>.
- Coschi, C.H., Ishak, C.A., Gallo, D., Marshall, A., Talluri, S., Wang, J., Cecchini, M.J., Martens, A.L., Percy, V., Welch, I., et al. (2014). Haploinsufficiency of an RB-E2F1-Condensin II Complex Leads to Aberrant Replication and Aneuploidy. *Cancer Discovery* *4*, 840–853. <https://doi.org/10.1158/2159-8290.CD-14-0215>.
- DeGregori, J., Leone, G., Miron, A., Jakoi, L., and Nevins, J.R. (1997). Distinct roles for E2F proteins in cell growth control and apoptosis. *Proceedings of the National Academy of Sciences of the United States of America* *94*, 7245–7250. <https://doi.org/10.1073/pnas.94.14.7245>.
- Dephoure, N., Zhou, C., Villen, J., Beausoleil, S.A., Bakalarski, C.E., Elledge, S.J., and Gygi, S.P. (2008). A quantitative atlas of mitotic phosphorylation. *Proceedings of the National Academy of Sciences* *105*, 10762–10767. <https://doi.org/10.1073/pnas.0805139105>.
- Dyson, N. (1998). The regulation of E2F by pRB-family proteins. *Genes & Development* *12*, 2245–2262. <https://doi.org/10.1101/gad.12.15.2245>.
- Gosling, K.M., Makaroff, L.E., Theodoratos, A., Kim, Y.-H., Whittle, B., Rui, L., Wu, H., Hong, N.A., Kennedy, G.C., Fritz, J.-A., et al. (2007). A mutation in a chromosome condensin II subunit, kleisin beta, specifically disrupts T cell development. *Proceedings of the National Academy of Sciences* *104*, 12445–12450. <https://doi.org/10.1073/pnas.0704870104>.
- Gubern, A., Joaquin, M., Marquès, M., Maseres, P., Garcia-Garcia, J., Amat, R., González-Nuñez, D., Oliva, B., Real, F.X., de Nadal, E., et al. (2016). The N-Terminal Phosphorylation of RB by p38 Bypasses Its Inactivation by CDKs and Prevents Proliferation in Cancer Cells. *Molecular Cell* *64*, 25–36. <https://doi.org/10.1016/j.molcel.2016.08.015>.
- Hoffert, J.D., Pisitkun, T., Wang, G., Shen, R.-F., and Knepper, M.A. (2006). Quantitative phosphoproteomics of vasopressin-sensitive renal cells: regulation of

- aquaporin-2 phosphorylation at two sites. *Proceedings of the National Academy of Sciences of the United States of America* *103*, 7159–7164. <https://doi.org/10.1073/pnas.0600895103>.
- Hornbeck, P.V., Kornhauser, J.M., Tkachev, S., Zhang, B., Skrzypek, E., Murray, B., Latham, V., and Sullivan, M. (2012). PhosphoSitePlus: a comprehensive resource for investigating the structure and function of experimentally determined post-translational modifications in man and mouse. *Nucleic Acids Research* *40*, D261–270. <https://doi.org/10.1093/nar/gkr1122>.
- Huttlin, E.L., Jedrychowski, M.P., Elias, J.E., Goswami, T., Rad, R., Beausoleil, S.A., Villén, J., Haas, W., Sowa, M.E., and Gygi, S.P. (2010). A tissue-specific atlas of mouse protein phosphorylation and expression. *Cell* *143*, 1174–1189. <https://doi.org/10.1016/j.cell.2010.12.001>.
- Ishak, C.A., Marshall, A.E., Passos, D.T., White, C.R., Kim, S.J., Cecchini, M.J., Ferwati, S., MacDonald, W.A., Howlett, C.J., Welch, I.D., et al. (2016). An RB-EZH2 Complex Mediates Silencing of Repetitive DNA Sequences. *Molecular Cell* *64*, 1074–1087. <https://doi.org/10.1016/j.molcel.2016.10.021>.
- Jin, X., Ding, D., Yan, Y., Li, H., Wang, B., Ma, L., Ye, Z., Ma, T., Wu, Q., Rodrigues, D.N., et al. (2019). Phosphorylated RB Promotes Cancer Immunity by Inhibiting NF- κ B Activation and PD-L1 Expression. *Molecular Cell* *73*, 22–35.e6. <https://doi.org/10.1016/j.molcel.2018.10.034>.
- Kettenbach, A.N., Schweppe, D.K., Faherty, B.K., Pechenick, D., Pletnev, A.A., and Gerber, S.A. (2011). Quantitative phosphoproteomics identifies substrates and functional modules of Aurora and Polo-like kinase activities in mitotic cells. *Science Signaling* *4*, rs5. <https://doi.org/10.1126/scisignal.2001497>.
- Longworth, M.S., Herr, A., Ji, J.-Y., and Dyson, N.J. (2008). RBF1 promotes chromatin condensation through a conserved interaction with the Condensin II protein dCAP-D3. *Genes & Development* *22*, 1011–1024. <https://doi.org/10.1101/gad.1631508>.
- Lundberg, A.S., and Weinberg, R.A. (1998). Functional inactivation of the retinoblastoma protein requires sequential modification by at least two distinct cyclin-cdk complexes. *Molecular and Cellular Biology* *18*, 753–761. <https://doi.org/10.1128/mcb.18.2.753>.
- MacDonald, J.I., and Dick, F.A. (2012). Posttranslational Modifications of the Retinoblastoma Tumor Suppressor Protein as Determinants of Function. *Genes & Cancer* *3*, 619–633. <https://doi.org/10.1177/1947601912473305>.
- Manning, A.L., Yazinski, S.A., Nicolay, B., Bryll, A., Zou, L., and Dyson, N.J. (2014). Suppression of Genome Instability in pRB-Deficient Cells by Enhancement of Chromosome Cohesion. *Molecular Cell* *53*, 993–1004. <https://doi.org/10.1016/j.molcel.2014.01.032>.

- Mayya, V., Lundgren, D.H., Hwang, S.-I., Rezaul, K., Wu, L., Eng, J.K., Rodionov, V., and Han, D.K. (2009). Quantitative Phosphoproteomic Analysis of T Cell Receptor Signaling Reveals System-Wide Modulation of Protein-Protein Interactions. *Science Signaling* 2, ra46–ra46. <https://doi.org/10.1126/scisignal.2000007>.
- Mertins, P., Qiao, J.W., Patel, J., Udeshi, N.D., Clauser, K.R., Mani, D.R., Burgess, M.W., Gillette, M.A., Jaffe, J.D., and Carr, S.A. (2013). Integrated proteomic analysis of post-translational modifications by serial enrichment. *Nature Methods* 10, 634–637. <https://doi.org/10.1038/nmeth.2518>.
- Mittnacht, S. (1998). Control of pRB phosphorylation. *Current Opinion in Genetics & Development* 8, 21–27. [https://doi.org/10.1016/s0959-437x\(98\)80057-9](https://doi.org/10.1016/s0959-437x(98)80057-9).
- Nath, N., Wang, S., Betts, V., Knudsen, E., and Chellappan, S. (2003). Apoptotic and mitogenic stimuli inactivate Rb by differential utilization of p38 and cyclin-dependent kinases. *Oncogene* 22, 5986–5994. <https://doi.org/10.1038/sj.onc.1206843>.
- Rajshekar, S., Yao, J., Arnold, P.K., Payne, S.G., Zhang, Y., Bowman, T.V., Schmitz, R.J., Edwards, J.R., and Goll, M. (2018). Pericentromeric hypomethylation elicits an interferon response in an animal model of ICF syndrome. *eLife* 7. <https://doi.org/10.7554/eLife.39658>.
- Rawlings, J.S., Gatzka, M., Thomas, P.G., and Ihle, J.N. (2011). Chromatin condensation via the condensin II complex is required for peripheral T cell quiescence. *The EMBO Journal* 30, 263–276. <https://doi.org/10.1038/emboj.2010.314>.
- Roulois, D., Loo Yau, H., Singhania, R., Wang, Y., Danesh, A., Shen, S.Y., Han, H., Liang, G., Jones, P.A., Pugh, T.J., et al. (2015). DNA-Demethylating Agents Target Colorectal Cancer Cells by Inducing Viral Mimicry by Endogenous Transcripts. *Cell* 162, 961–973. <https://doi.org/10.1016/j.cell.2015.07.056>.
- Rubin, S.M., Gall, A.-L., Zheng, N., and Pavletich, N.P. (2005). Structure of the Rb C-terminal domain bound to E2F1-DP1: a mechanism for phosphorylation-induced E2F release. *Cell* 123, 1093–1106. <https://doi.org/10.1016/j.cell.2005.09.044>.
- Sanidas, I., Morris, R., Fella, K.A., Rumde, P.H., Boukhali, M., Tai, E.C., Ting, D.T., Lawrence, M.S., Haas, W., and Dyson, N.J. (2019). A Code of Mono-phosphorylation Modulates the Function of RB. *Molecular Cell* 73, 985-1000.e6. <https://doi.org/10.1016/j.molcel.2019.01.004>.
- Sharma, K., D'Souza, R.C.J., Tyanova, S., Schaab, C., Wiśniewski, J.R., Cox, J., and Mann, M. (2014). Ultradeep Human Phosphoproteome Reveals a Distinct Regulatory Nature of Tyr and Ser/Thr-Based Signaling. *Cell Reports* 8, 1583–1594. <https://doi.org/10.1016/j.celrep.2014.07.036>.
- Smith-Garvin, J.E., Koretzky, G.A., and Jordan, M.S. (2009). T Cell Activation. *Annual Review of Immunology* 27, 591–619. <https://doi.org/10.1146/annurev.immunol.021908.132706>.

Trickett, A., and Kwan, Y.L. (2003). T cell stimulation and expansion using anti-CD3/CD28 beads. *Journal of Immunological Methods* 275, 251–255. [https://doi.org/10.1016/S0022-1759\(03\)00010-3](https://doi.org/10.1016/S0022-1759(03)00010-3).

Vélez-Cruz, R., Manickavinayaham, S., Biswas, A.K., Clary, R.W., Premkumar, T., Cole, F., and Johnson, D.G. (2016). RB localizes to DNA double-strand breaks and promotes DNA end resection and homologous recombination through the recruitment of BRG1. *Genes & Development* 30, 2500–2512. <https://doi.org/10.1101/gad.288282.116>.

Weinberg, R.A. (1995). The retinoblastoma protein and cell cycle control. *Cell* 81, 323–330. .

Yuen, K.C., Slaughter, B.D., and Gerton, J.L. (2017). Condensin II is anchored by TFIIIC and H3K4me3 in the mammalian genome and supports the expression of active dense gene clusters. *Science Advances* 3, e1700191. <https://doi.org/10.1126/sciadv.1700191>.

Zhou, H., Di Palma, S., Preisinger, C., Peng, M., Polat, A.N., Heck, A.J.R., and Mohammed, S. (2013). Toward a Comprehensive Characterization of a Human Cancer Cell Phosphoproteome. *Journal of Proteome Research* 12, 260–271. <https://doi.org/10.1021/pr300630k>.

Chapter 3

3 EZH2 inhibition stimulates viral mimicry causing immune destruction of splenic B cells

3.1 Abstract

EZH2 is a histone methyltransferase that deposits H3K27me_{2/3} in repressive heterochromatin during development and it is misregulated in tumorigenesis. Pharmacologic inhibition of repressive epigenetic writers can induce viral mimicry in cancer cells, where upregulated repetitive elements are detected by cytosolic pattern recognition receptors (PRRs) to activate inflammatory signaling. Here we demonstrate that systemic administration of EZH2 inhibitors stimulates inflammation and immune self-recognition of resting splenic B cells. We generated a novel cytosolic PRR loss-of-function mouse model called RIC with mutations in *Rigi*, *Ifih1* (MDA5), and *Cgas*. In both WT and RIC mutant B cells, EZH2 inhibition induced loss of H3K27me₃ at repetitive elements and upregulated their expression. However, expression of inflammatory chemokines in B cells was interrupted by the RIC mutations. Furthermore, infiltration of cytotoxic T cells and neutrophils into the spleen in response to EZH2 inhibition was blocked in RIC mutants preserving viability of B cells. This study demonstrates a pharmacologically induced mechanism of inflammation that causes self-recognition and B cell death.

3.2 Introduction

Enhancer of zeste homolog 2 (EZH2) is the catalytic subunit of the Polycomb Repressive Complex 2 (PRC2) that deposits di- and tri-methylation of histone 3 at lysine 27 (H3K27me_{2/3}) (Cao et al., 2002; Kuzmichev et al., 2002; Margueron et al., 2008). These are repressive histone modifications that cooperate with histone 2a lysine 119 ubiquitination (H2AK119ub) to silence transcription and compact chromatin (Dellino et al., 2004; Eskeland et al., 2010; Francis et al., 2004; Ku et al., 2008; Leeb et al., 2010; Müller et al., 2002; Tamburri et al., 2020; Wang et al., 2004). The latter modification is catalyzed by the Polycomb Repressive Complex 1 (PRC1), and the two PRCs were originally described in *Drosophila* as repressors of homeotic genes that dictate

segmentation along the anterior-posterior axis (Schuettengruber et al., 2007). In mammals, the catalytic activity of EZH2 in PRC2 facilitates roles in cell fate determination (Yin et al., 2015), stem cell renewal (Collinson et al., 2016), and tumorigenesis (Souroullas et al., 2016). For example, EZH2 is required for B cell differentiation in the bone marrow during hematopoiesis (Su et al., 2003), and germinal centre (GC) formation (Béguelin et al., 2017). Furthermore, EZH2 overexpression and gain-of-function mutations have been identified in different cancer types and are especially prominent in B cell lymphomas (Béguelin et al., 2020; Kleer et al., 2003; Varambally et al., 2002; Velichutina et al., 2010; Wassef et al., 2015; Zhao et al., 2019). Mechanistically, somatic mutations at EZH2Y641 render it dominantly active, increasing H3K27me3 globally, and repressing cell cycle control genes such as CDKN2A (Yap et al., 2011). This has prompted the development of EZH2 inhibitors that are currently in clinical trials (McCabe et al., 2012; Morschhauser et al., 2020).

Such role in gene regulation represents only one facet of EZH2 activity. Indeed, repetitive sequences that make up the majority of mammalian genomes harbour H3K27me3 and other repressive epigenetic modifications (Bulut-Karslioglu et al., 2014; Day et al., 2010; Ishak et al., 2016; Karimi et al., 2011; Kondo and Issa, 2003; Koning et al., 2011; Liu et al., 2014; Martens et al., 2005). These modifications repress transcription of repetitive elements and limit mobility in the host genome. Loss of epigenetic modifications like H3K27me3 results in their upregulation. While a subset of repetitive elements has been exapted to serve the host cell, their derepression and subsequent upregulation have been linked to tumorigenesis (Babaian and Mager, 2016; Desai et al., 2017; Doucet-O'Hare et al., 2015; Ewing et al., 2015; Howard et al., 2008; Lamprecht et al., 2010; Levin and Moran, 2011; Lock et al., 2014; Rodriguez-Martin et al., 2020). Overall, the impact of EZH2 in mediating repression of repetitive elements in normal mammalian physiology is relatively unexplored.

Pharmacologically induced upregulation of repetitive elements by inhibiting repressive epigenetic writers has been shown to elicit anti-tumor responses (Chiappinelli et al., 2015; Liu et al., 2018; Morel et al., 2021; Roulois et al., 2015, Sheng et al., 2018). Tumour cells treated with small molecule inhibitors against DNA methyltransferases

(DNMTs) or EZH2 derepress the transcription of repetitive elements (Chiappinelli et al., 2015; Liu et al., 2018; Morel et al., 2021; Roulois et al., 2015). These transcripts form secondary structures that are detected by nucleic-acid sensing pattern recognition receptors (PRRs) such as RIG-I, MDA5, and cGAS. In general, PRRs are a part of the innate immune surveillance that detects molecular patterns associated with infectious agents such as bacteria and viruses, and signals downstream to either neutralize the threat or further activate the adaptive immune system (Goubau et al., 2013; Schmidt et al., 2012). This phenomenon has been described as ‘viral mimicry’, as upregulation of repetitive elements and subsequent activation of PRRs mimics a viral infection. While viral mimicry has been demonstrated in cancer cells as a therapeutic paradigm, it is unclear if normal untransformed cells possess the capacity for a similar response.

Interestingly, mice with defective EZH2 recruitment to repetitive elements caused by a mutation in the retinoblastoma tumour suppressor protein (pRB) succumb to lymphomas that often arise in the spleen and lymph nodes (Ishak et al., 2016). To investigate the significance of EZH2 regulation of genomic repeats, we utilized pharmacological inhibition of EZH2 to investigate its effects in resting splenic B cells. Short term EZH2 inhibition with GSK343 induced expression of repetitive elements and is accompanied by inflammation and death of B cells. To investigate if this effect is dependent on viral mimicry, we generated triple mutant *Rigi*, *Ifih1* (MDA5), and *Cgas* mutant mice (referred to as RIC mutant) to block detection by pattern recognition receptors. In both WT and RIC mutant B cells, GSK343 induced loss of H3K27me3 at repetitive elements and increased repeat expression. Unlike WT, the RIC mutant mice failed to upregulate pro-inflammatory cytokine signaling and chemokine genes in their B cells. This prevented infiltration of neutrophils and cytotoxic T cells into their spleens and preserved B cell viability. This study reveals that acute EZH2 inhibition in B cells causes a viral mimicry dependent, autoinflammatory phenotype that targets these cells.

3.3 Materials and Methods

3.3.1 Data and code availability

All high-throughput sequencing data have been deposited at GEO and are publicly available as of the date of publication. The accession number is listed in the key resources table. RNA-seq data of EBV infected human lymphoblastoid B cells was obtained from GEO under GSE125974 (Wang et al., 2019). Original Western blot images have been deposited at Mendeley and are publicly available as of the date of publication. This paper does not report original code. Any additional information required to reanalyze the data reported in this paper is available from the lead contact upon request.

3.3.2 Experimental model and subject details

C57BL/6NCrl (Charles River, #027) and RIC triple mutant mice (described below) were housed and monitored according to institutional animal use guidelines (protocol number 2020-039). Mice were given access to standard chow and water ad libitum and exposed to 12 h light/dark cycles in a pathogen-free exclusion facility. For I.P. injections and splenic B cell isolation, littermates 6-8 week old mice of both sexes were randomly assigned to experimental groups within each genotype.

3.3.3 Intraperitoneal injections

For GSK343 treatment, 6-8 week old mice were I.P injected with either 100 mg/kg GSK343 (Tocris, #6128) in 20 % (w/v) Captisol (Captisol, San Diego), pH 4.5 (with 1N acetic acid) or vehicle daily for two or five days. Mice were sacrificed, and the spleen and bone marrow were harvested for analysis. For poly(I:C) (Millipore-Sigma, #P1530) treatment, 6-8 week old male or female WT and RIC mutant mice were I.P injected with either 100 µg poly(I:C) or PBS. The next day, the mice were sacrificed, and the spleen was harvested for analysis.

3.3.4 Cell culture

For splenocyte culture, spleens were harvested from untreated WT and RIC mutant mice, gently homogenized with a syringe plunger and passed through a 40 µm mesh filter (Fisher Scientific, #08-771-1). Filtered cells were centrifuged at 300 x g for

10 min at 4 °C. The cell pellet was resuspended in ACK lysis buffer (150 mM NH₄Cl, 10 mM KHCO₃, 0.1 mM EDTA, pH 7.2) for 4 min at RT to lyse erythrocytes. Remaining splenic lymphocytes were washed twice with FACS buffer (5% BSA, 2 mM EDTA in PBS) and incubated in RPMI-1640 (Wisent) supplemented with 10% (v/v) FBS, 55 μM 2-ME, 2 mM L-glutamine, penicillin and streptomycin at 37 °C in 5% CO₂.

To isolate splenic B cells and non-B cells, washed splenic lymphocytes (5 x 10⁷) were resuspended in 450 μL FACS buffer and stained with 50 μL CD43 microbeads (Miltenyi Biotec, #130-049-801) on ice for 30 min. Cells were washed once, resuspended in 500 μL FACS buffer and passed through an LD column in a VarioMACS separator (Miltenyi Biotec, #130-042-901, #130-090-282) as per manufacturer's recommendation. CD43 microbead-labelled non-B cells were eluted from the column by applying the plunger. Purified B cells in the flow-through were incubated in RPMI-1640 supplemented as above plus 2 ng/mL IL-4 and BAFF (BioLegend, #574302, #591202) at 37 °C in 5% CO₂.

Cell viability was measured by trypan blue exclusion assay and quantified by Countess II (ThermoFisher).

3.3.5 RNA extraction, qRT-PCR and sequencing

Splenocytes or splenic B cells (5 x 10⁶ cells/mL) were treated with either DMSO or 0.5 μM GSK343 for 48 h. RNA was harvested using Monarch Total RNA miniprep kit (NEB, #T2010) and residual genomic DNA was digested by treating 1 μg total RNA with 1 U DNaseI (ThermoFisher, #18068015) for 15 min at RT. DNaseI was then inactivated by adding EDTA and incubating at 65 °C for 10 min. For qRT-PCR, RNA was then reverse-transcribed into cDNA with iScript Supermix (Biorad, #1708840) and diluted five-fold with H₂O. PCR was performed with iQ SYBR Green Supermix (Biorad, #1708882) on a CFX96 (Biorad). All primer sequences are described in Appendix A (Cecchini et al., 2014; Muotri et al., 2005; Stetson and Medzhitov, 2006). For sequencing, DNaseI-treated RNA was purified with Monarch RNA cleanup kit (NEB, #T2040). rRNA depletion and library preparation were performed with VAHTS total RNA-seq library prep kit (GeneBio, #NR603-01). Libraries were pooled and sequenced

on NextSeq 500 at the London Regional Genomics Center with a high output 75 cycle kit to yield single-end 75-bp reads.

3.3.6 RNA sequencing analysis

Demultiplexed FASTQ files were downloaded from BaseSpace. RepEnrich2 and featureCounts were used to quantify repetitive element expression (Criscione et al., 2014; Liao et al., 2014; Teissandier et al., 2019). Briefly, bowtie2/2.4.2 (Langmead and Salzberg, 2012) was used to map reads to mm10 with default settings. Resulting sam files were converted to bam files with samtools/1.12 (Li et al., 2009). RepeatMasker track for mm10 was filtered to remove simple repeats, then used to build a pseudogenome with RepEnrich2 subcommands. Fractional count tables were imported to RStudio running r/3.6.3. Alternatively, STAR/2.5.2b (Dobin et al., 2013) and featureCounts were used with recommended settings (Teissandier et al., 2019) with the filtered RepeatMasker track to generate count tables. For gene expression quantification, reads were mapped to mm10 genome with STAR/2.7.8a and resulting sam files were converted to sorted, indexed bam files with samtools/1.12. HTSeq/0.11.0 (Anders et al., 2015) was used to assign mapped reads to GENCODE mouse M22 comprehensive gene annotation (Frankish et al., 2019).

To identify differentially expressed repetitive elements or genes, edgeR/3.28.1 (Robinson et al., 2010) was used. Volcano plots, heatmaps and Venn diagrams were generated with EnhancedVolcano, heatmap.2 and VennDiagram (Chen and Boutros, 2011). GSEA was performed as recommended (Subramanian et al., 2005).

3.3.7 ChIP sequencing

Wild type and RIC mutant splenic B cells (5×10^6 cells/mL, 7.5×10^6 cells total) were treated with either DMSO or $0.5 \mu\text{M}$ GSK343 for 48 h. Cells were washed with PBS and resuspended in 1 mL 1% (v/v) formaldehyde in PBS to fix chromatin-protein complexes. After 5 min, the reaction was quenched by adding glycine to a final concentration of 0.125 M. Fixed cells were washed twice with PBS and incubated on ice for 10 min in lysis buffer 1 (10 mM HEPES pH 6.5, 10 mM EDTA, 0.5 mM EGTA, 0.25% Triton X-100). The suspension was centrifuged at $600 \times g$ for 5 min at 4°C to

isolate the nuclei. They were washed twice in wash buffer (10 mM HEPES pH 6.5, 1 mM EDTA, 0.5 mM EGTA, 200 mM NaCl) and resuspended in lysis buffer 2 (50 mM Tris pH 8.0, 1 mM EDTA, 0.5% Triton X-100, 1% SDS) to 7.5×10^6 cell/200 μ L in sonication tubes. Chromatin was sonicated to 100-600 bp fragments by four cycles of 30 s ON and OFF in Bioruptor Pico (Diagenode, #B01060010). Debris was cleared by centrifugation at 16 000 x g for 30 min at 4 °C. Then, chromatin was pre-cleared with 30 μ L Dynabeads Protein G (ThermoFisher, #10004D) by gentle end-to-end mixing at 4 °C for 2 h. Pre-cleared chromatin was diluted ten-fold in dilution buffer (50 mM Tris pH 8.0, 1 mM EDTA, 150 mM NaCl, 0.1% Triton X-100) and 5% (by volume) was saved as input until later. H3K27me3 antibody (4 μ g, Millipore-Sigma, #07-449) was added to pre-cleared chromatin (30 μ g) and mixed end-to-end at 4 °C overnight. The next day, antibody-chromatin complexes were captured by adding 50 μ L Dynabeads Protein G and gentle end-to-end mixing at 4 °C for 2 h. They were washed once with low salt buffer (20 mM Tris pH 8.0, 2 mM EDTA, 150 mM NaCl, 1% Triton X-100, 0.1% SDS), once with high salt buffer (20 mM Tris pH 8.0, 2 mM EDTA, 500 mM NaCl, 1% Triton X-100, 0.1% SDS), once with LiCl wash buffer (10 mM Tris pH 8.0, 1 mM EDTA, 0.25 M LiCl, 1% NP-40, 1% sodium deoxycholate) and twice with TE buffer (10 mM Tris pH 8.0, 1 mM EDTA). For each wash, the immunoprecipitated complexes were mixed end-to-end at 4 °C for 5 min. Antibody-chromatin complexes were eluted from Dynabeads by incubating in elution buffer (0.1 M NaHCO₃, 1% SDS) at 65 °C and vortexing. To the elution (ChIP) and input (saved earlier), NaCl was added to a final concentration of 200 mM to reverse crosslinked protein-DNA complexes and incubated overnight at 65 °C. The next day, the suspension was mixed with RNaseA and proteinase K to digest RNA and proteins, respectively, and incubated at 45 °C. Finally, ChIP and input chromatin were purified with Monarch PCR/DNA cleanup kit (NEB, #T1030) and eluted with H₂O. The following protease inhibitors were added immediately before use to all of the above buffers: 250 μ M Na₃VO₄, 1 mM NaF, 0.1 mM PMSF, 5 μ g/mL aprotinin and leupeptin. DNA yield was quantified with Qubit fluorometer (ThermoFisher). Following the manufacturer's recommendation, input (25 ng) or ChIP (0.5 ng) DNA were used to perform end repair, adaptor ligation and PCR amplification with NEBNext Ultra II DNA library prep kit and Multiplex Oligos (NEB, #E7645, #E7600). AmpureXP beads

(Beckman Coulter, #A63880) were used at 0.9–1.0x reaction volumes for size selection. Input or ChIP samples were amplified by ten or fifteen PCR cycles, respectively, which yielded ~600 ng DNA. Libraries were pooled and sequenced on NextSeq 500 at the London Regional Genomics Center with a high output 75 cycle kit to yield paired-end 38-bp read pairs.

3.3.8 ChIP sequencing analysis

Demultiplexed FASTQ files were downloaded from BaseSpace. First, ENCODE blacklist regions (Amemiya et al., 2019) were filtered out from subsequent analysis. Reads were mapped to mm10 genome with bowtie2/2.4.2 with `--sensitive-local` setting. Samtools/1.12 was used with `-f 0x2` option to keep concordantly mapped read pairs. Those read pairs were converted to sorted, indexed bam files. Biological duplicates were pooled together and MACS2/2.2.7.1 (Zhang et al., 2008) was used to call broad peaks, outputting broadPeak files (`-f BAMPE -g mm --broad --broad-cutoff 0.05`). A subcommand of deepTools/3.5.1 (Ramírez et al., 2016), `bamCoverage`, was used to generate reads-per-genomic-content (RPGC) normalized signal track (bw files) for all sequenced libraries. `plotEnrichment` (`--variableScales --ignoreDuplicates`), `computeMatrix` (`scale-regions --missingDataAsZero --skipZeros -b 1000 -a 1000`), `plotHeatmap` (`--colorMap 'inferno'`) and `plotProfile` commands (deepTools/3.5.1) were used to make barplots, heatmaps and profiles. Bedtools/2.30.0 (Quinlan and Hall, 2010) was used to find peaks or number of peaks that intersected with RepeatMasker features, or were unique or common between treatment conditions or genotypes. ChIPseeker (Yu et al., 2015) was used to annotate peaks based on known genomic features. To show read mapping (colour-coded by strand) in Figure 3.5B., samtools/1.12 was used with `-f 0x40` option to split read pairs into two bam files. A bam file of one of the read mates (a ChIP sample of DMSO-treated WT B cells) was imported to IGV/2.11.1 (Robinson et al., 2011) to show mapped reads at two loci. To show H3K27me3 signal enrichment at indicated loci (RPGC), bw files of biological replicates were merged together with `bigWigMerge` and `bedGraphToBigWig` (Kent et al., 2010). Merged signal track and broadPeak files were visualized on IGV/2.11.1. Peaks with a score less than 20 were filtered out.

3.3.9 Flow cytometry

Total splenocytes or bone marrow cells were isolated as described above. 2×10^6 cells were resuspended in PBS with ZombieNIR (1:500, BioLegend, #423105) and incubated on ice for 30 min to stain dead cells. Then, they were washed with FACS buffer and resuspended in pre-staining mix containing 50 μ L Brilliant Stain Buffer (BD Biosciences, #563794), 5 μ L TruStain monocyte blocker (BioLegend, #426102), 1 μ L TruStain FcX plus (BioLegend, #156603) and 27.4 μ L FACS buffer. Splenocytes were stained with the following antibody cocktail: anti-CD45.2 BV421 (BioLegend, #109831), anti-CD19 BV510 (BioLegend, #115545), anti-Ly6C BV605 (BioLegend, #128035), anti-CD11b FITC (BioLegend, #101206), anti-CD3 ϵ PerCP/Cy5.5 (BioLegend, #100327), anti-CD8 α PE (BioLegend, #100707) and anti-Ly6G APC (BioLegend, #127613). Bone marrow cells were stained with a similar panel but with the following substitution: anti-CD43 PerCP/Cy5.5 (BioLegend, #143219) and anti-CD45R PE (BioLegend, #103207). Stained cells were kept on ice for 30 min, then washed with FACS buffer. Cells were fixed in 100 μ L fixation buffer (BD Biosciences, #554655) on ice for 20 min. They were washed and resuspended in 500 μ L FACS buffer and 100 μ L Precision counting beads (BioLegend, #424902). Flow cytometry was performed on LSR II (BD Biosciences) at the London Regional Flow Cytometry Facility and analyzed with FlowJo/10.8.1. AbC total antibody compensation beads and ArC amine reactive compensation beads (ThermoFisher, #A10497, #A10628) were used to generate compensation matrices in FACSDiva (BD Biosciences). Gating strategy is described in Figure 3.9A.

3.3.10 Protein extraction and pulldown assay

Erythrocyte-lysed splenocytes were lysed in RIPA buffer (50 mM Tris pH 7.4, 150 mM NaCl, 1% NP-40, 0.5% sodium deoxycholate, 0.1% SDS, supplemented with protease inhibitors as above) on ice for 10 min. Chromatin fractions were prepared by lysing cells sequentially in buffer A (10 mM Tris pH 8.0, 10 mM KCl, 1.5 mM MgCl₂, 0.34 M sucrose, 10% (v/v) glycerol, 0.1% Triton-X, supplemented with protease inhibitors as above), then in buffer B (3 mM EDTA, 0.2 mM EGTA, supplemented with protease inhibitors as above) with occasional mixing. Cytoplasmic and nucleoplasmic

fractions were discarded by centrifugation, and resulting chromatin was digested with DNaseI in digestion buffer (20 mM Tris pH 7.5, 10 mM MgCl₂).

For cGAS pulldown assay, erythrocyte-lysed splenocytes were lysed in non-ionic buffer (25 mM HEPES, 100 mM NaCl, 1 mM EDTA, 10% (v/v) glycerol, 1% Triton X-100, supplemented with protease inhibitors as above) on ice for 10 min. Debris was cleared by centrifugation at 16 000 x g for 30 min at 4 °C. Bradford assays were used to quantify protein concentration. For the pulldown assay, 500 µg of extract was mixed with 400 pmol of 5' biotinylated ISD45 dsDNA and gently mixed end-to-end overnight at 4 °C. The next day, 20 µL streptavidin Dynabeads (ThermoFisher, #11205D) were added and gently mixed for 2 h at 4 °C. Pulldown complexes were washed once with non-ionic lysis buffer and once with non-ionic lysis buffer supplemented with 300 mM NaCl.

3.3.11 SDS-PAGE and Western blot

RIPA extracts or pulldown samples were denatured by adding Laemmli buffer to 1x and boiling at 95 °C for 5 min. SDS-PAGE was performed following standard procedures. Samples were transferred to PVDF membrane using TransBlot Turbo (Biorad) and blocked in 5% skim milk in TBST for 1 h at RT. Membranes were incubated overnight at 4 °C with gentle shaking with the following primary antibodies: α -tubulin (CST, #2125, 1:5000), cGAS (CST, #31659, 1:1000), MDA5 (CST, #5321, 1:1000), RIG-I (Santa Cruz, #376845, 1:1000). The next day, membranes were washed five times with TBST and incubated with the following secondary antibodies for 1 h at RT with gentle shaking: m-IgG Fc BP-HRP (Santa Cruz, #525409, 1:500) or AffiniPure goat anti-rabbit IgG-HRP (JIR, #111-035-144, 1:5000-10000). After five washes with TBST, membranes were incubated in SuperSignal WestDura (ThermoFisher, #34075) and visualized on a ChemiDoc (Biorad). Coomassie staining was performed with GelCode Blue (ThermoFisher, #24590).

3.3.12 CRISPR-Cas9 generation of RIC mutant mice

In vitro production of gRNAs and one-cell embryo injection were all performed as previously described (Wang et al., 2013). C57BL/6Crl mice were used as embryo donors, surrogate females and stud males. For restriction fragment length polymorphism

assays, each of the three target loci was PCR amplified from tail DNA with Phire Animal Tissue Direct PCR kit (ThermoFisher, #F140WH). These products were either left undigested or restriction digested with the indicated enzymes and resolved on an agarose gel and EtBr stained. PCR reactions were also cloned into a plasmid and Sanger sequencing was performed to find the exact deletions in all mutant alleles present in the colony (Appendix D). In addition, potential off-target sites were predicted in silico (Cradick et al., 2014) and the two highest ranked intergenic and intragenic loci were genotyped through PCR amplification and sequencing (Appendix E).

3.3.13 Statistical analysis

All statistical analyses were performed with Prism 9. All relevant details are described in the figure legends.

3.4 Results

3.4.1 EZH2 inhibition upregulates repetitive elements specifically in B cells and causes cell death

Constitutive loss of EZH2-mediated repression of repetitive elements in immune cells caused by mutations in *Rb1* leads to their sporadic expression and lymphomagenesis (Ishak et al., 2016). To determine the effect of acute inhibition of EZH2 in resting splenocytes, 6-8 week old mice were injected with vehicle or GSK343 for two or five days and spleens were harvested for histology or flow cytometry (Figure 3.1A-B, Figure 3.2A). Following two treatments of GSK343, tingible body macrophages were evident within follicles suggesting B cell death and engulfment (Figure 3.1A, left). We confirmed B cell apoptosis in the follicles upon GSK343 treatment through cleaved caspase 3 staining (Figure 3.1A, right). Flow cytometry of splenocytes revealed a quantitative loss of CD-19⁺ B cells in GSK343 treated spleens and an increase in CD11b⁺Gr-1⁺ myeloid cells at the same time point (Figure 3.2B). Following five days of GSK343 treatment we performed H&E staining as well as IHC staining for CD68, a marker of monocytes/macrophages. This revealed that GSK343 treatment extensively reduced follicular regions of spleens and the smaller follicles that remained included notable acellular regions (Figure 3.1B). CD68 staining in vehicle treated controls was largely restricted to red pulp while GSK343 induced infiltration of these cells into the follicles (Figure 3.1C). Overall, these results show that a targeted inhibition of EZH2 disrupts splenic follicles and this effect is associated with the death of B cells and the arrival of neutrophils and macrophages.

Both drug-mediated inhibition of EZH2 and loss of EZH2 chromatin recruitment have been shown to derepress repetitive element expression (Ishak et al., 2016; Morel et al., 2021). Thus, we determined whether GSK343 treatment causes derepression of repetitive elements as a potential source of inflammatory stimulation. To achieve maximum inhibition of EZH2 with GSK343, without compromising viability during experiments, we determined the dose response curves to GSK343 of cultured splenocytes and magnetic-activated cell sorting (MACS) isolated B cells (Figure 3.2C). We found

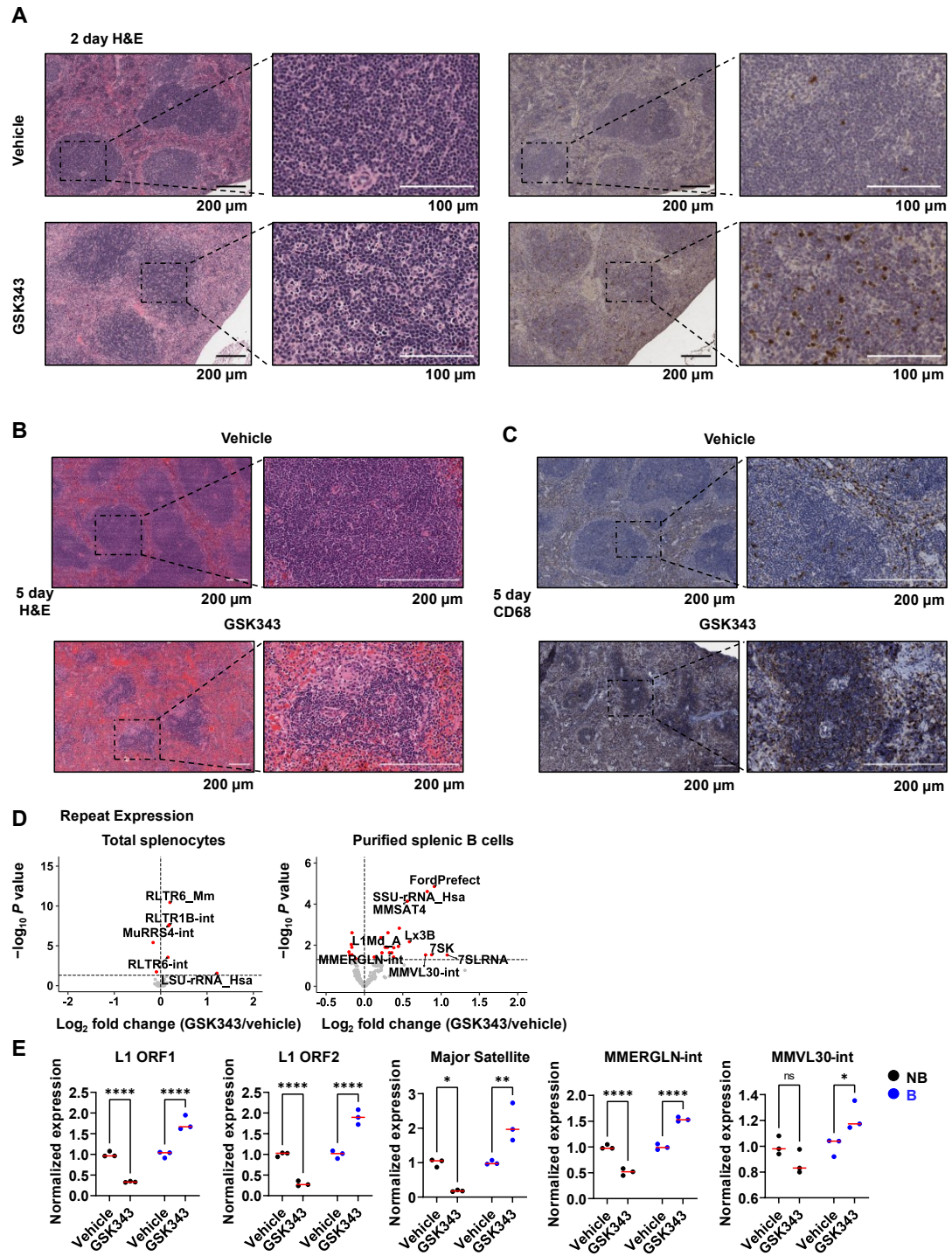


Figure 3.1: GSK343 induces inflammation and B cell death.

Figure 3.1: GSK343 induces inflammation and B cell death.

(A) Left: H&E staining of spleens following two days of vehicle or 100 mg/kg GSK343. White arrows indicate tingible body macrophages. Right: IHC staining for cleaved caspase 3. (B) H&E staining of spleens following 5 days of vehicle or 100 mg/kg GSK343. (C) CD68 staining of the spleen upon five daily I.P. injections of either vehicle or 100 mg/kg GSK343. (D) Volcano plot depicting up- or downregulated repetitive elements in total splenocytes (left) or purified splenic B cells (right) treated with either DMSO or 0.5 μ M GSK343 for 48 h in culture. (E) qRT-PCR of indicated repetitive elements in splenic B cells (blue) or non-B cells (NB, black) treated with either DMSO or 0.5 μ M GSK343 for 48h. Expression is shown as a ratio relative to the average of three DMSO-treated controls. * $p < 0.05$, ** $p < 0.005$, **** $p < 0.0001$ by two-way ANOVA with Sidak's multiple test correction.

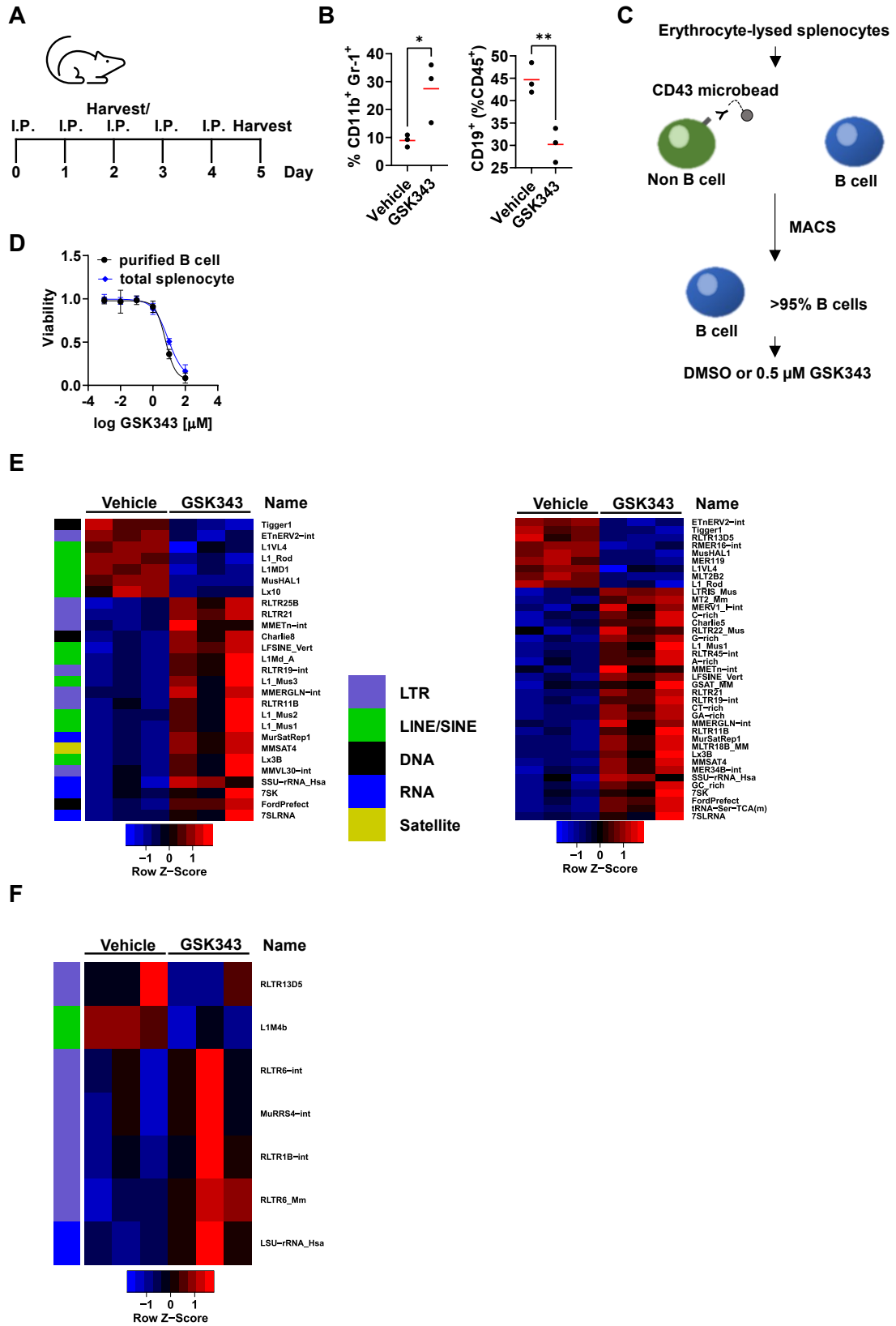


Figure 3.2: GSK343 upregulates repetitive element expression in splenic B cells.

Figure 3.2: GSK343 upregulates repetitive element expression in splenic B cells.

(A) Schematic illustrating I.P. injection schedule for 2 and 5 day experiments. (B) Percent of CD19⁺ or CD11b⁺ Gr-1⁺ cells in the spleen following two days of vehicle or 100 mg/kg GSK343 based on flow cytometry. (C) Schematic describing magnetic-assisted cell sorting (MACS) to purify splenic B cells. (D) Dose response curves of WT splenocytes and splenic B cells treated with indicated concentrations of GSK343 for 48 h. Viability was quantified by trypan blue exclusion assay. (E-F) Heatmap of differential repetitive element expression from purified B cells (E) or total splenocytes (F) treated with either DMSO or 0.5 μ M GSK343 for 48 h. Expression is shown as a Z-score of the mean of each row. RepEnrich2 pipeline is shown on the left, and featureCounts pipeline is shown in the right for (E).

that 0.5 μ M was the highest dose that did not affect viability in these 48 hour experiments and this was used for all subsequent experiments with cultured cells (Figure 3.2D).

RNA was extracted and sequenced from cultured total splenocytes or splenic B cells treated with either DMSO or 0.5 μ M GSK343 for 48 h in paired biological triplicates. RNA-seq data was analyzed with two established analysis pipelines (Criscione et al., 2014; Liao et al., 2014; Teissandier et al., 2019) to quantify expression of repetitive elements annotated in RepeatMasker (Karolchik et al., 2004). This experiment revealed that B cells upregulated numerous repetitive elements including LINE/SINEs, LTR containing ERVs, satellites, and DNA transposons (Figure 3.1D right, 3.2E). In contrast to purified B cells, total splenocytes did not robustly upregulate such variety of repetitive elements despite of comparable sensitivity to GSK343, suggesting that B cells are especially amenable to GSK343 induced misexpression of repeats (Figure 3.1D left, 3.2F). We also directly compared expression of various repetitive elements upon GSK343 treatment between purified splenic B cells and non-B (NB) cells (Figure 3.1E). Splenic lymphocytes were treated with DMSO or GSK343 in culture as previously, then subjected to MACS separation of B cells and NB cells. While NB cells downregulated expression of repetitive elements, purified B cells significantly upregulated their expression upon GSK343, which is consistent with the disruption of splenic follicles and B cell death *in vivo*, and RNA-seq data (Figure 3.1A-D).

Taken together, these data show that purified splenic B cells upregulate transcription of repetitive elements upon EZH2 inhibition at lower doses than induce cell death. In the context of systemic GSK343 treatment, EZH2 inhibition is associated with the disruption of splenic follicles, B cell death, and infiltration of monocytes and macrophages. One interpretation of these experiments is that EZH2 inhibition may stimulate an inflammatory response through misexpressed repeats in B cells.

3.4.2 Pattern recognition receptors are required for GSK343 induced B cell death in the spleen

Ectopic expression of repetitive elements and subsequent inflammatory signaling are described as a state of viral mimicry (Chen et al., 2021; Ishak and De Carvalho,

2020). Transcripts from repetitive elements form secondary structures that mimic those of viral replication and transcription. Cytosolic nucleic acid sensing pattern recognition receptors (PRRs) such as RIG-I, MDA5 and cGAS bind to dsRNA/DNA to activate a signaling cascade that upregulates inflammatory gene expression. Notably, others have shown that these cytosolic PRRs are mechanistically indispensable for DNMT or EZH2 inhibition-induced anti-tumour immune responses. We hypothesized that activation of pattern recognition receptors in splenic B cells underpin the inflammatory response following EZH2 inhibition with GSK343.

We created a loss of function mouse model in which PRR genes are disrupted. Briefly, three gRNAs, each targeting a coding exon for one of *Rigi*, *Ifih1* (MDA5), and *Cgas* were microinjected with a Cas9 expressing mRNA into single-cell zygotes to simultaneously mutate all three genes and disrupt their coding capacity (Wang et al., 2013) (Figure 3.3A). The resulting founder pups are potentially mosaic and were bred together to create biallelic F1 mutants that were characterized for their mutant alleles (Figure 3.4A-C). Mutant alleles were identified using a restriction fragment length polymorphism assay to identify indels in the three genes in F1 mice. Each gRNA cut site overlaps a restriction enzyme recognition site such that mutations disrupt restriction digestion (Figure 3.4B). We utilized this strategy to genotype animals and it confirmed these mice carried either homozygous or heterozygous mutant alleles for the three genes simultaneously (Figure 3.4C). All mutant alleles in our triple mutant colony were sequenced to characterize how they disrupt their respective gene (Appendix D). Lastly, we sought to identify any off-target mutations created by the gRNAs in the F1 mice that we bred for experiments. We sequenced the two highest ranked coding and non-coding, in silico predicted (Cradick et al., 2014), off-target loci per gRNA (six in total) in the three F1 mice. Out of 36 possible alleles, we only found two, one-bp deletions in non-coding regions (Appendix E) confirming high fidelity of targeting by this strategy. All triple mutant *Rigi*, *Ifih1*, and *Cgas* mice (henceforth called RIC mutant) used in this study are descendants from these three F1 animals and were compared against C57BL/6NCrl controls.

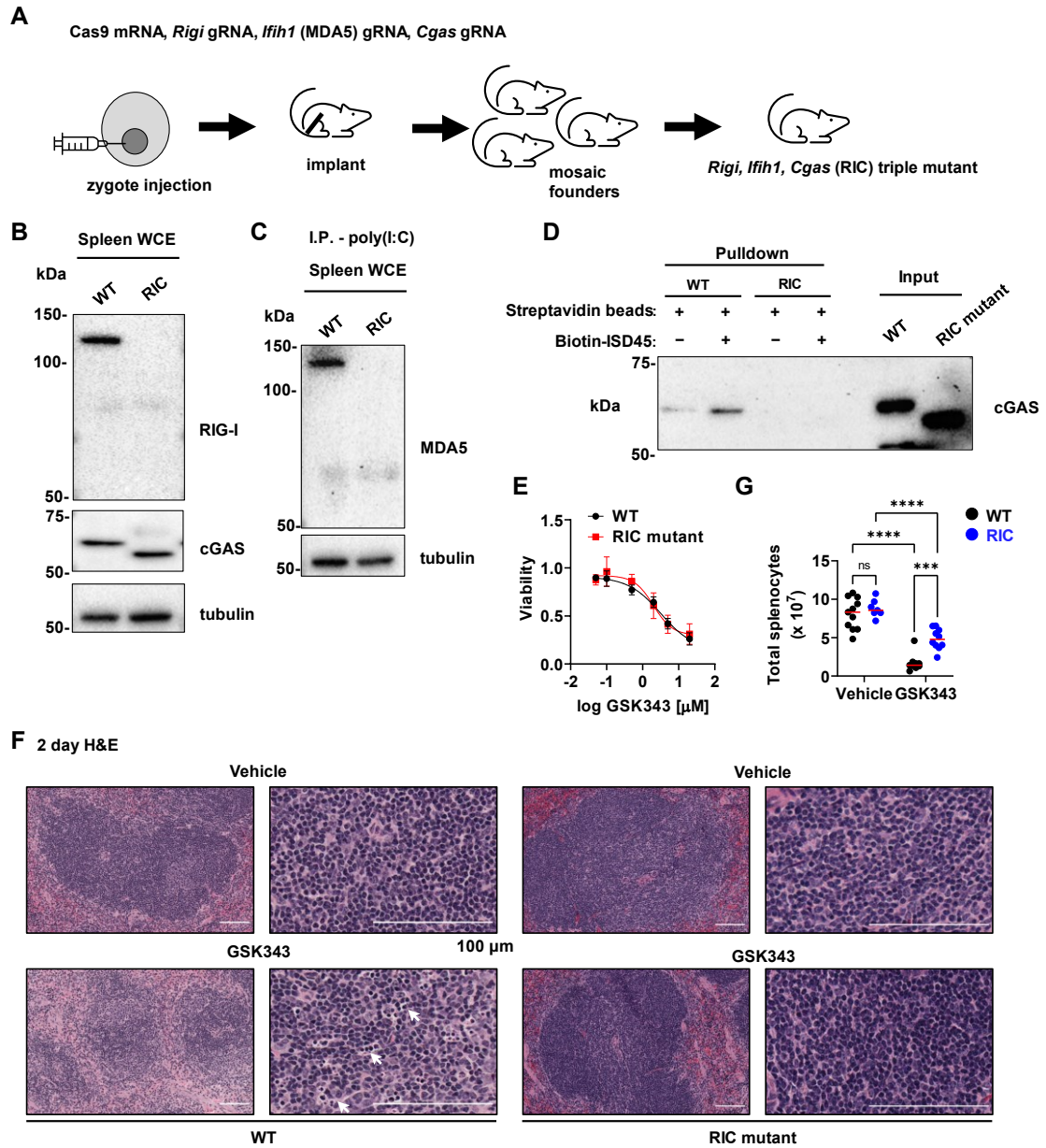


Figure 3.3: *Rigi/Ifih1/Cgas* (RIC) triple mutant mice are resistant to GSK343 killing of B cells.

Figure 3.3: *Rigi/Ifih1/Cgas*(RIC) triple mutant mice are resistant to GSK343 killing of B cells.

(A) Schematic highlighting the key steps of generating RIC triple mutant mice. gRNAs and Cas9 mRNA are microinjected into zygotes and transplanted into a surrogate female. Resulting mosaic founders are bred together to generate bona fide triple mutant mice. (B) Western blots of RIG-I and cGAS from whole cell extracts of WT and RIC mutant splenocytes. (C) Western blots of MDA5 from whole cell extracts of WT and RIC mutant splenocytes harvested from mice I.P. injected with poly(I:C). (D) Western blots of cGAS pulldown with biotinylated ISD45 probe and streptavidin beads from whole cell extracts of WT and RIC mutant splenocytes. (E) Dose response curves of WT and RIC mutant splenic B cells to GSK343. Viability was quantified by trypan blue exclusion assay. (F) H&E staining of the spleens following 2 days of vehicle or 100 mg/kg GSK343 in WT (top) or RIC mutant mice (bottom). White arrows indicate tingible body macrophages. (G) WT and RIC mutant mice were I.P. injected with either vehicle or 100 mg/kg/day GSK343 for two days. Spleens were harvested and live erythrocyte-lysed splenic lymphocytes were quantified by trypan blue exclusion assay. (n=7-10). Horizontal bars represent the mean. * $p < 0.05$, ** $p < 0.01$, *** $p < 0.001$, **** $p < 0.0001$ by Two-way ANOVA with Tukey's multiple test correction.

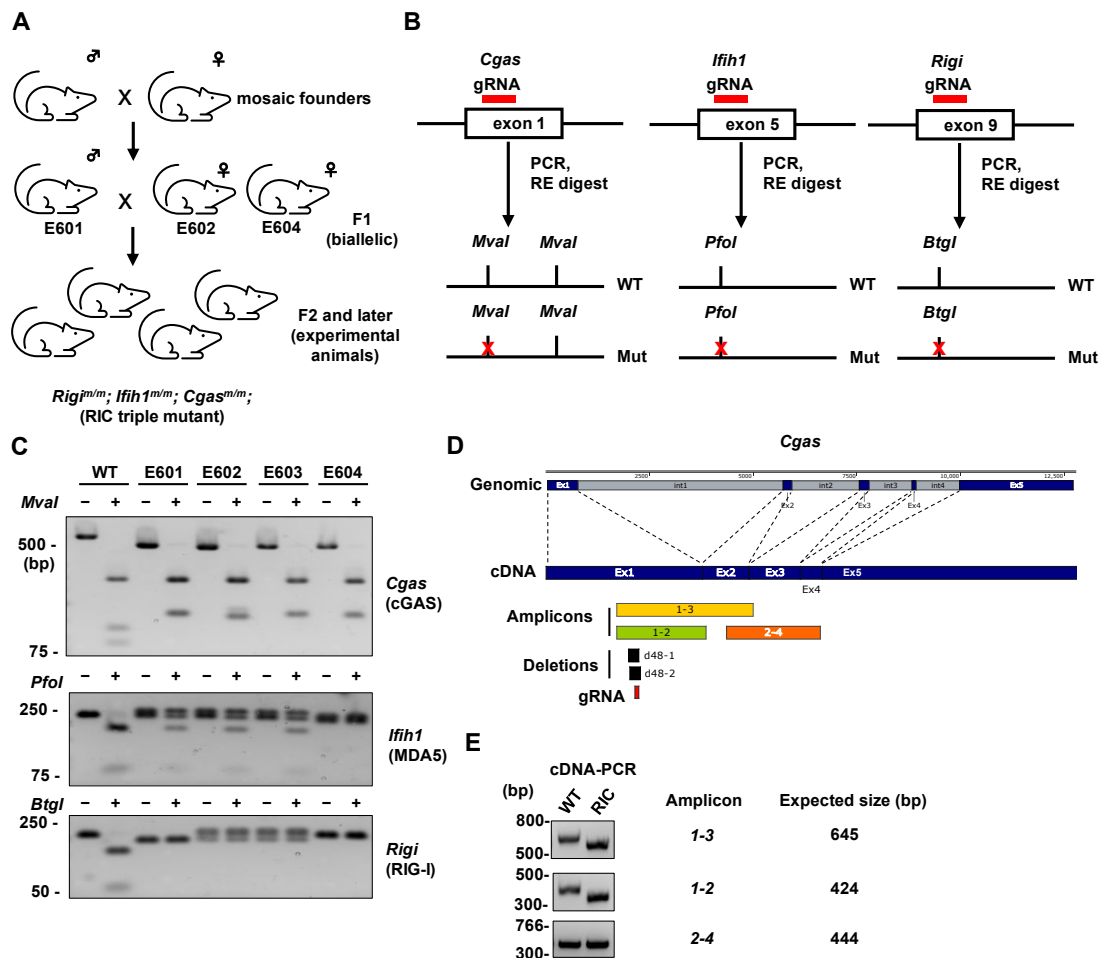


Figure 3.4: Strategy to generate and genotype RIC mutant mice.

(A) Schematic of to create non-mosaic F1 mutant mice (E601, E602 and E604) that were used to generate experimental RIC mutant animals. (B) Restriction fragment length polymorphism (RFLP) assays to distinguish between WT and mutant alleles for each targeted gene. Upon CRISPR-Cas9 mediated DSB and non-homologous end joining, indicated restriction digest sites are disrupted. gRNA-targeted loci are PCR amplified and restriction digested. Resulting fragments are resolved by agarose gel electrophoresis. (C) EtBr stained gels showing RFLP between WT and F1 mutants. Tail DNA was used to PCR amplify target exons of each gene, followed by digestion with the indicated restriction enzymes. (D) The structure of *Cgas* genome and mRNA as well as PCR amplicons and gRNA recognition site used to map deletions. (E) EtBr stained gels showing *Cgas* cDNA amplicons of WT and RIC mutant B cells as described in (D).

We characterized expression from these mutant alleles by western blotting. We found that RIC mutant splenocytes completely lost RIG-I and MDA5 expression (Figure 3.3B & C), confirming that *Rigi* and *Ifih1* mutations are null alleles. The truncated cGAS detected by western blotting (Figure 3.3B) agrees with the 48-bp deletions found in two distinct *Cgas* alleles (Figure 3.4D & E). These N-terminal, in frame deletions, encode functionally inactive cGAS as it fails to bind a known dsDNA target, ISD45, in a streptavidin-biotin pulldown assay (Hansen et al., 2014) (Figure 3.3D). Furthermore, streptavidin alone has been shown to bind and activate cGAS, and truncated cGAS has also lost this interaction (Zhang et al., 2020) (Figure 3.3D).

To understand the role of PRR sensing in the response to EZH2 inhibition, RIC mutant B cells were isolated from spleens and treated with GSK343. This revealed a similar dose response to GSK343 as WT (Figure 3.3E), indicating that the cell intrinsic response to GSK343 is unaffected by the RIC mutations. Systemic treatment of RIC mutant mice with GSK343 was performed and spleens were examined after two days of treatment. Necrosis and infiltration of tingible body macrophages were less prominent in RIC mutant follicles (Figure 3.3F). In addition, we compared the number of live splenocytes upon two-day GSK343 treatment in WT and RIC mutant mice (Figure 3.3G). As expected, we found no significant difference in total splenocytes at baseline. GSK343 treatment significantly reduced total splenocyte count by six-fold in WT, but only 1.5-fold in RIC mutants. These observations suggest that the functional loss of the cytosolic PRRs in the RIC mutant largely abrogates the cell death phenotype in spleens of GSK343 treated mice.

Through CRISPR-Cas9, we generated triple mutant RIC mice that are deficient for PRR function. The functional loss of the cytosolic PRRs did not affect purified B cell sensitivity to GSK343 in culture, but did inhibit B cell death in spleens of GSK343 treated mice. This suggests that PRR function is required for inflammation and B cell death in response to EZH2 inhibition.

3.4.3 EZH2 inhibition induces H3K27me3 loss at repetitive elements in B cells

We investigated the effect of EZH2 inhibition with GSK343 at the chromatin level in isolated WT and RIC mutant B cells. We performed ChIP-seq of H3K27me3 in DMSO or GSK343 treated cells in biological duplicates. We obtained high quality sequencing libraries from input controls and H3K27me3 associated fragments (Figure 3.5A & B), we then identified H3K27me3 peaks using MACS2 and quantified read fragment enrichment at those peaks. As expected, most high-scoring peaks found in vehicle treated samples were shared by WT and RIC mutants (Fig 3.5C). This confirms that the baseline EZH2 locations of H3K27me3 deposition is independent of functional expression of the cytosolic PRRs. We then compared loss of H3K27me3 upon GSK343 treatment with their respective vehicle treated genotype controls. Figure 3.6A depicts normalized read fragment enrichment where each row represents a scaled peak length with 1 kb flanking each end. The sum of the rows represents all the peaks identified in vehicle-treated, control ChIP samples for each genotype (WT and RIC mutant). At these baseline H3K27me3 peaks, GSK343 decreased enrichment in both WT and RIC mutants (5th and 6th vs. 7th and 8th columns). Next, we sought to determine with which genomic features H3K27me3 peaks are associated. We annotated the peaks found in each ChIP sample (pooling biological replicates together) based on their proximity to known genes. Upon GSK343 treatment, we observed a similar change in the distribution of peak annotations (Figure 3.6B). Notably, the absolute fold decrease in peak count was the greatest in intronic and intergenic regions for both WT and RIC mutant upon GSK343 treatment (Figure 3.6C). The pattern of absolute fold decrease was also comparable between the two genotypes. Intronic and intergenic regions contain repetitive elements and H3K27me3 is decreased the most in these categories. The absolute number of repetitive elements that intersect with peaks was decreased upon GSK343 treatment and this effect was also similar between genotypes (Figure 3.6D). In addition, we confirmed that H3K27me3 signal enrichment at peaks intersecting with repetitive elements was decreased upon GSK343 treatment in both genotypes (Figure 3.6E-F, 3.5D).

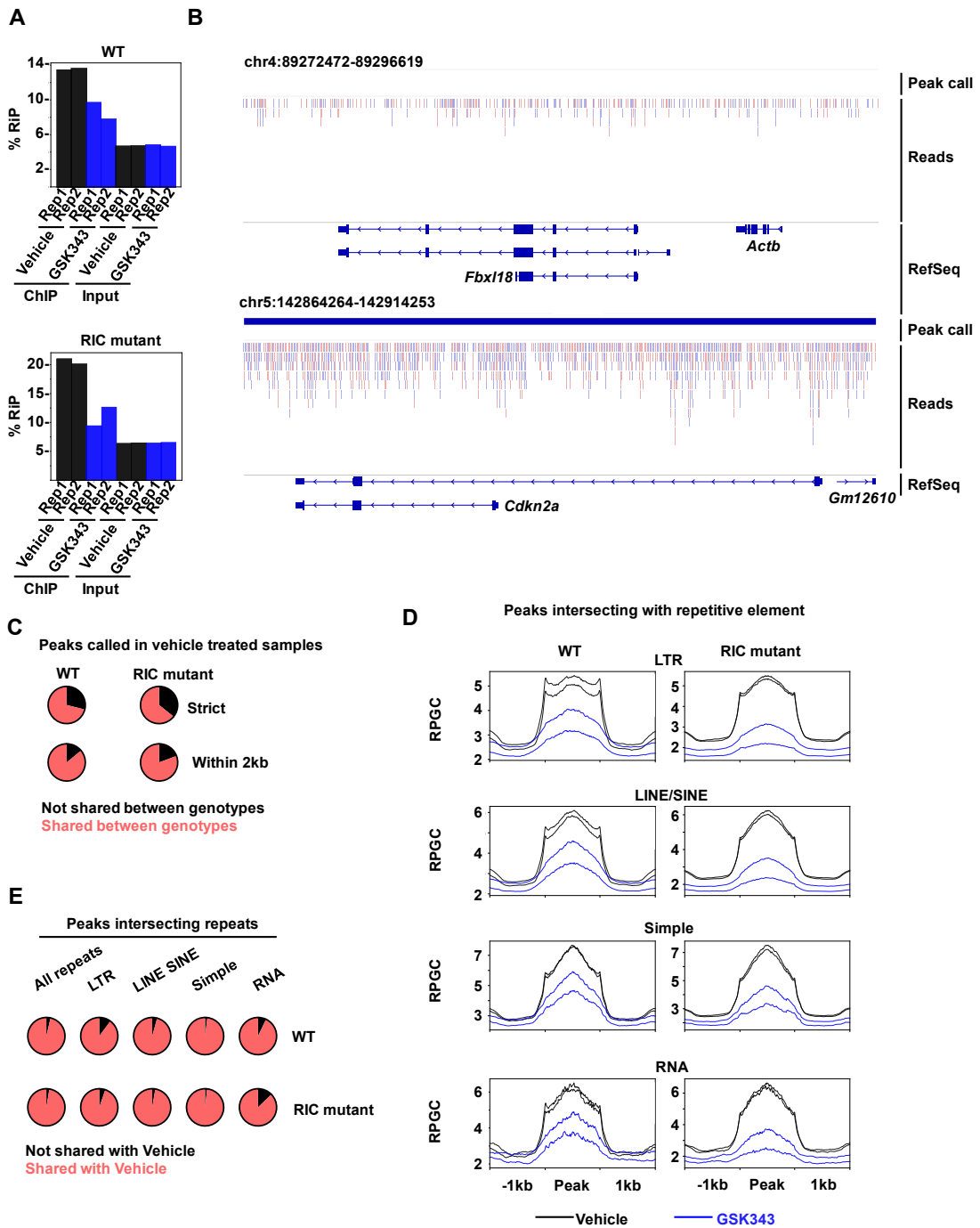


Figure 3.5: Distribution and loss of H3K27me3 peaks globally or at repetitive elements.

Figure 3.5: Distribution and loss of H3K27me3 peaks globally or at repetitive elements.

(A) % reads in peaks (RiP) of all sequenced libraries. (B) Genome track view showing read alignment color-coded by alignment strand at one negative (top) and one positive (bottom) control locus. (C) Proportions of total peaks called in DMSO treated samples that are either not shared or shared between genotypes (top). Proportions of peaks called in DMSO treated samples that are either not shared or shared within 2 kb of each other between genotypes (bottom). (D) Enrichment profiles of H3K27me3 ChIP-seq reads at peaks called in DMSO or GSK343 treated samples intersecting with indicated repetitive elements. Each box shows the average profile of scaled repetitive elements with 1 kb flanking each end. Biological duplicates for each treatment condition are shown as separate curves. (E) Proportions of total peaks intersecting with indicated repetitive elements called in GSK343 treated samples that are either shared or not shared with DMSO treated samples.

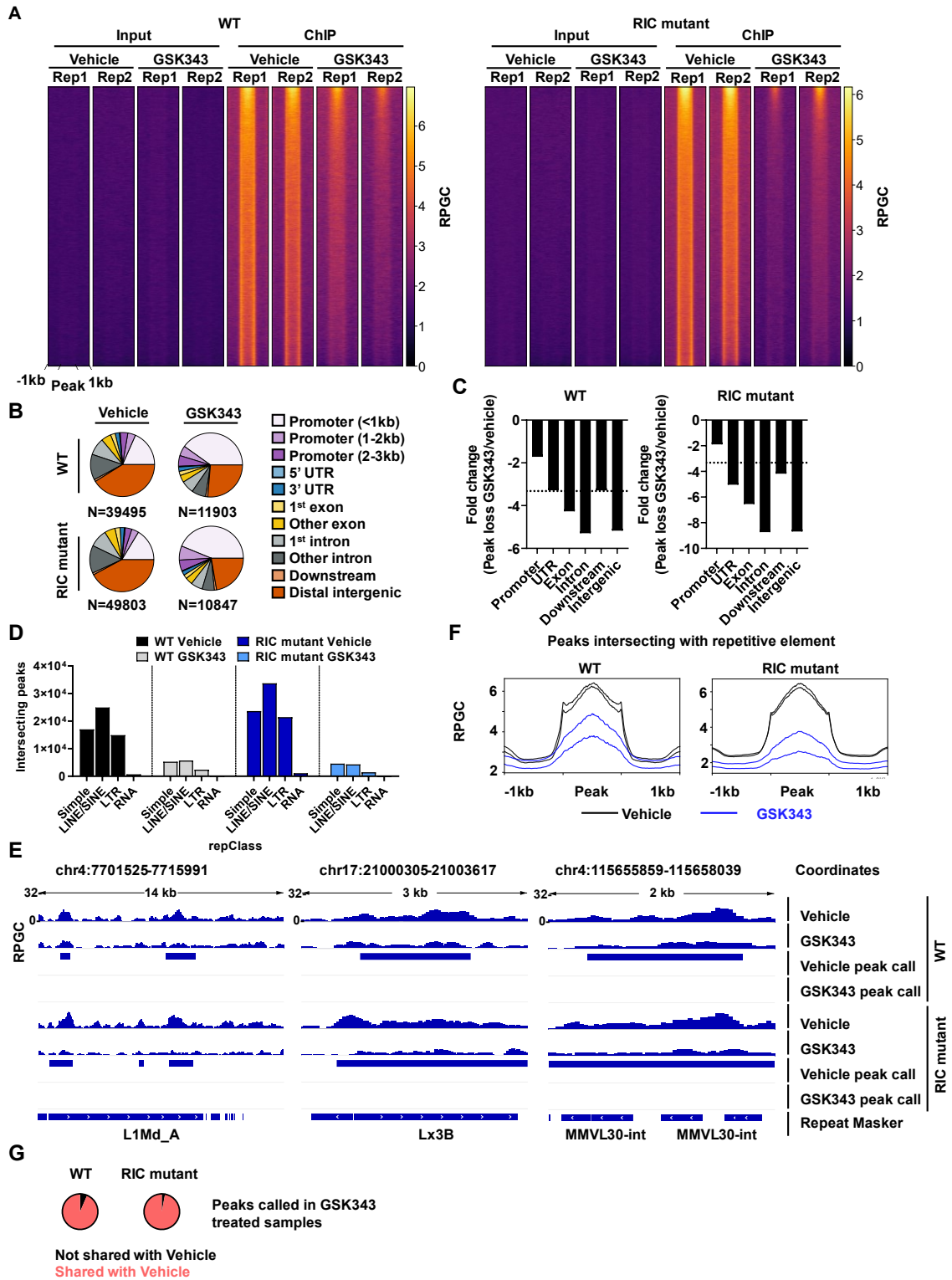


Figure 3.6: GSK343 induces loss of H3K27me3 at repetitive elements in splenic B cells.

Figure 3.6: GSK343 induces loss of H3K27me3 at repetitive elements in splenic B cells.

(A) Heatmap of input and H3K27me3 ChIP-seq read enrichment at all peaks called in DMSO treated samples. Splenic B cells were treated with either DMSO or 0.5 μ M GSK343 for 48h. Enrichment was quantified as reads per genomic content (RPGC). Each row represents a scaled DMSO peak location with 1 kb flanking each end. Rows are sorted by decreasing enrichment. (B) Distribution of peaks amongst the indicated genomic features in each sample. (C) Fold-change of the number of called peaks annotated with indicated genomic features. Horizontal dotted lines indicate overall fold change. (D) Number of repetitive elements in each indicated repClass that intersect with called peaks in each sample condition shown. (E) Three genome track views showing normalized coverage (RPGC) of H3K27me3 signal track for indicated sample conditions at repetitive elements. Horizontal bars indicate either peak calls or repetitive element annotations. (F) Enrichment profiles of H3K27me3 ChIP-seq reads at peaks called in DMSO or GSK343 treated samples intersecting with repetitive elements. Each box shows the average profile of scaled repetitive elements with 1 kb flanking each end. Biological duplicates for each treatment condition are shown as separate curves. (G) Proportions of total peaks called in GSK343 treated samples that are either shared or not shared with DMSO treated samples.

Finally, we tested whether H3K27me3 peaks in GSK343 treated samples were also found in DMSO treated samples. Discordance could occur if H3K27me3 peaks in GSK343 treated samples potentially represent *de novo* methylation, as opposed to baseline peaks that persisted after EZH2 inhibition. Peaks called in GSK343 treated samples were largely common with those of DMSO treated samples (Figure 3.6G, 3.5E), and this is observed across a range of repeat element types. This confirms that pharmacological inhibition of EZH2 with GSK343 decreases H3K27me3 deposition at baseline loci, but does not cause dispersion or migration of heterochromatin islands containing H3K27me3.

To summarize, we have shown that GSK343 decreases H3K27me3, particularly at repetitive elements in both WT and RIC mutant B cells. This confirms that inactivation of cytosolic PRRs has no bearing on H3K27me3 containing heterochromatin or the effect of EZH2 inhibition on H3K27me3 reduction.

3.4.4 Cytosolic PRRs are required for pro-inflammatory gene expression upon EZH2 inhibition

Since GSK343 induces comparable loss of H3K27me3 in both WT and RIC mutant B cells, we next investigated its effects on the transcriptome. WT and RIC mutant B cells were treated with DMSO or GSK343 as before, RNA was extracted, and we performed RNA-seq to identify differentially expressed repetitive elements and genes, and significantly enriched gene sets. Consistent with similar effects by GSK343 on H3K27me3 between WT and RIC mutant mice, upregulation of many of the same repeats also took place in RIC mutants (Figure 3.7A, 3.84A-B). Next, we observed that a few genes such as *Ahr*, *Cebpa* and *Scin* stood out as the top upregulated genes upon GSK343 treatment compared to vehicle in both WT and RIC mutant splenic B cells (Figure 3.7B, 3.8C). We asked if upregulation of these genes were associated with corresponding loss of H3K27me3 that would enable their upregulation. Indeed, we observed loss of H3K27me3 signal at these genes as evidenced by peak loss or diminished signal intensity in both WT and RIC mutants (Figure 3.7C, 3.8D). This is in line with our expectation for EZH2 inhibition and its effect on genes silenced by H3K27me3.

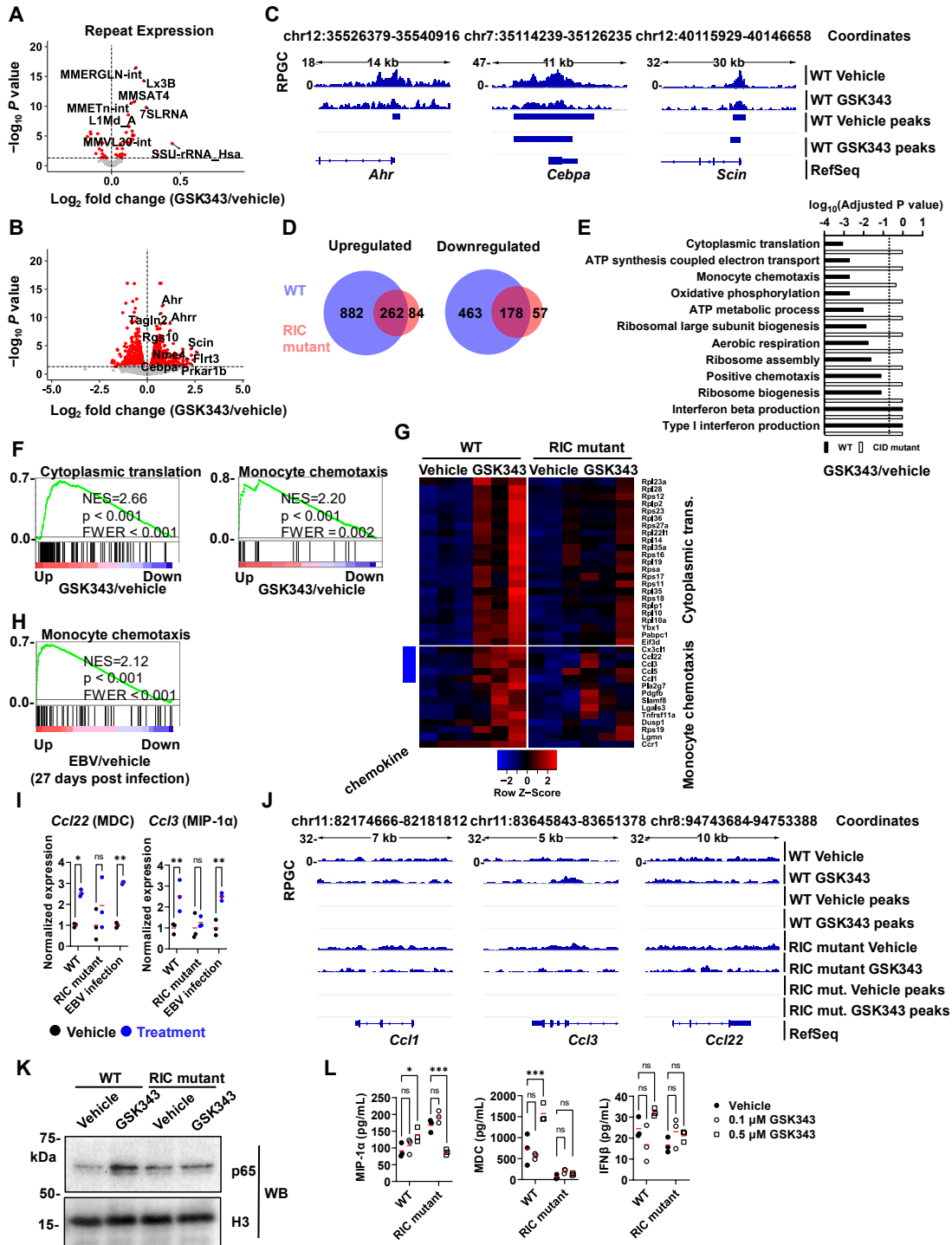


Figure 3.7: Cytosolic PRRs are required for GSK343 induced inflammatory signaling in B cells.

Figure 3.7: Cytosolic PRRs are required for GSK343 induced inflammatory signaling in B cells.

(A) Volcano plot depicting up- or downregulated repetitive elements in RIC mutant splenic B cells treated with DMSO or 0.5 μ M GSK343 for 48 h in culture. (B) Volcano plot depicting up- or downregulated genes in WT splenic B cells treated with DMSO or 0.5 μ M GSK343 for 48 h in culture. (C) Genome track view showing normalized coverage (RPGC) of merged H3K27me3 signal track at three genes that are differentially upregulated upon GSK343 treatment compared to DMSO in WT splenic B cells. Horizontal bars indicate peak calls. (D) Venn diagrams showing the number of up or downregulated genes upon GSK343 treatment between WT and RIC mutant splenic B cells. (E) Bar plot depicting adjusted P values (FWER) of GSEA of Gene Ontology (GO) biological processes. Vertical dotted line indicates P value cut-off at 0.2. (F) GSEA plots of GO pathways significantly enriched in GSK343 treated WT B cells compared to vehicle, but not enriched in GSK343 treated RIC mutant B cells. (G) Expression heatmap of genes annotated in indicated gene sets (cytoplasmic translation and monocyte chemotaxis) in WT and RIC mutant splenic B cells. Expression is shown as a Z-score of the mean of each row. (H) GSEA plots of GO pathways significantly enriched in EBV-infected human lymphoblastoid B cells compared to control. (I) Expression of chemokines that are significantly upregulated in GSK343 treated WT B cells (compared to vehicle) and EBV infected human lymphoblastoid B cells (compared to control), but not in GSK343 treated RIC mutant B cells. Horizontal red bars represent the mean. * $p < 0.05$, ** $p < 0.005$ by two-way ANOVA with Sidak's multiple test correction. (J) Genome track view showing normalized coverage (RPGC) of merged H3K27me3 signal tracks at genes encoding chemokines in "monocyte chemotaxis" GO pathway. (K) Western blot of NF κ B p65 in chromatin fractions from WT and RIC mutant splenic B cells treated with DMSO or 0.5 μ M GSK343 for 48 h in culture. Representative image of biological duplicate experiments. (F) Quantification of MIP-1 α (*Ccl3*), MDC (*Ccl22*) and IFN β from cell culture supernatant of WT and RIC mutant splenic B cells treated with DMSO, 0.1 or 0.5 μ M GSK343 for 48 h in culture. * $p < 0.05$, *** $p < 0.001$ by two-way ANOVA with Dunnett's multiple test correction.

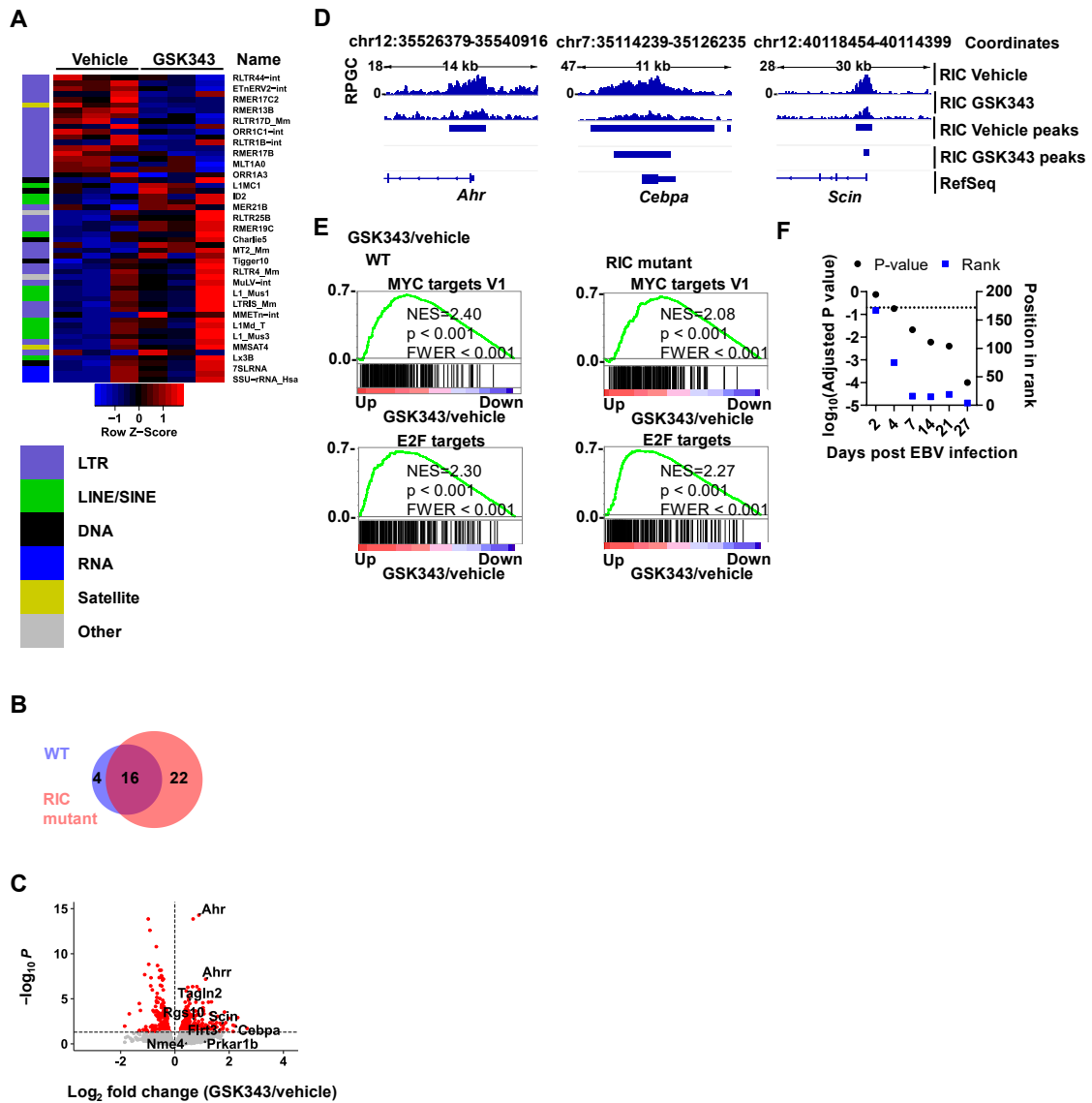


Figure 3.8: Changes in gene/repetitive element expression and H3K27me3 upon GSK343 treatment in RIC mutant splenic B cells.

Figure 3.8: Changes in gene/repetitive element expression and H3K27me3 upon GSK343 treatment in RIC mutant splenic B cells.

(A) Heatmap of differential repetitive element expression of three RIC mutant splenic B cells treated with either DMSO or 0.5 μ M GSK343 for 48 h. Expression is shown as a Z-score of the mean of each row. The leftmost column annotates each repeat into its repClass. (B) Venn diagrams showing the number of upregulated repetitive elements upon GSK343 treatment between WT and RIC mutant splenic B cells. (C) Volcano plot depicting up- or downregulated genes in RIC mutant splenic B cells treated with DMSO or 0.5 μ M GSK343 for 48 h in culture. (D) Genome track view showing normalized coverage (RPGC) of merged H3K27me3 signal track at three genes that are differentially upregulated upon GSK343 treatment compared to DMSO in RIC mutant B cells. Horizontal bars indicate peak calls. (E) GSEA plots of Hallmark pathways comparing GSK343 to DMSO in WT and RIC mutant B cells. (F) Adjusted P values (FWER) and position in ranked list (out of all tested gene sets) of “monocyte chemotaxis” GO biological process pathway at indicated days post EBV infection in human lymphoblastoid B cells. Horizontal dotted line indicates P value cut-off at 0.2.

In addition, most genes that were significantly upregulated or downregulated in GSK343 treated RIC mutant cells showed a similar change in WT (Figure 3.7B), although RIC mutants showed fewer genes with altered expression compared to WT. Furthermore, several gene sets were commonly upregulated in both WT and RIC mutants (Figure 3.8E). In both genotypes, ‘MYC targets’ and ‘E2F targets’ were among the top five upregulated Hallmark gene sets upon EZH2 inhibition. This confirms that EZH2-mediated repression of a common set of coding genes irrespective of PRR functional status, but some gene expression changes in WT were missing in RIC mutants.

Next, we sought to identify differences in gene expression between WT and RIC mutants due to the loss of the cytosolic PRRs through gene set enrichment analysis (GSEA). We found several pathways that were significantly enriched in WT, but not in RIC mutants (Figure 3.7E). Categories entitled ‘cytoplasmic translation’ and ‘monocyte chemotaxis’ pathways were enriched in GSK343 treated WT samples compared to GSK343 treated RIC mutants (Figure 3.7F). We note that interferon signaling pathways were not enriched in contrast to previous studies that described viral mimicry upon epigenetic inhibition (Chiappinelli et al., 2015; Liu et al., 2018; Morel et al., 2021; Roulois et al., 2015). Upregulation of genes in cytoplasmic translation and monocyte chemotaxis gene sets were more consistent and robust in WT compared to RIC mutants (Figure 3.7G). Notably, several of these genes were secreted chemokines with pro-inflammatory functions. Several genes in this pathway—*Ccl1*, *Ccl3*, and *Ccl22*—are known to be upregulated in human B cells infected with Epstein-Barr Virus (EBV), a dsDNA virus (Ehlin-Henriksson et al., 2009; Nakayama et al., 2004). To validate our data analysis and compare our system with a bona fide viral infection model, we performed the same GSEA on existing RNA-seq data of EBV infected human lymphoblastoid B cells at various time points (Wang et al., 2019). We found that monocyte chemotaxis gene set was significantly enriched in EBV infected cells compared to control at five out of six time points (Figure 3.7H, 3.8F). Furthermore, upregulation of *Ccl22* and *Ccl3* were comparable between GSK343 treated WT B cells and EBV infected human B cells, while GSK343 treated RIC mutant B cells did not significantly upregulate them (Figure 3.7I). Importantly, upregulation of these chemokines in WT, but not RIC mutant B cells,

was not associated with direct loss of H3K27me3 as evidenced by the absence of peaks at these genes (Figure 3.7J). This suggests that their upregulation is mediated by GSK343-induced repetitive element expression, activation of cytosolic PRRs and subsequent signaling, and not direct derepression of gene expression by GSK343 treatment.

Next, we tested if PRR dependent signaling leading to chemotactic gene expression was indeed blocked in the RIC mutants following GSK343 treatment. We stimulated WT and RIC mutant B cells with GSK343, isolated the chromatin fraction from these cells, and blotted for NF- κ B p65 (Figure 3.7K). This revealed that GSK343 induces chromatin association of this transcription factor while RIC mutant cells do not, indicating an interruption in signaling from PRRs to transcriptional targets. Similarly, detection of secreted cytokines by array analysis demonstrates specific upregulation of MIP-1 α (encoded by *Ccl3*) and MDC (encoded by *Ccl22*), but not IFN β upon GSK343 treatment (Figure 3.7L). This is consistent with our finding that chemokines, but not interferons, are activated by GSK343 treatment (Figure 3.7E). As expected, MIP-1 α /*Ccl3* and MDC/*Ccl22* were not upregulated in RIC mutant cells despite GSK343 treatment, which agrees with our gene expression and chromatin fraction data (Figure 3.7G, I, K).

In sum, these data indicate that the cytosolic PRRs are required to upregulate pro-inflammatory cytokine signalling and chemokine production upon EZH2 inhibition with GSK343 and this effect is blocked in RIC mutants. This observation is not attributable to lack of EZH2 inhibition in RIC mutants because upregulation of repetitive elements upon GSK343 treatment is retained. We suggest that in WT B cells, EZH2 inhibition activates PRRs that stimulates NF- κ B activation and expression of chemokines such as MIP-1 α /*Ccl3* and MDC/*Ccl22*.

3.4.5 Cytosolic PRRs mediate an inflammatory response upon EZH2 inhibition

Our data revealed that the cytosolic PRRs are required for pro-inflammatory gene expression in isolated splenic B cells upon EZH2 inhibition. We next determined if PRR loss blocks the cellular inflammatory response in the spleen. As before, we I.P. injected either vehicle or 100 mg/kg GSK343 daily for two days. We harvested the spleen and

stained erythrocyte-lysed splenocytes with a multicolour antibody panel to identify key cell populations based on cell surface markers (Figure 3.9A). CD19⁺ staining of CD45⁺ cells demonstrated that in WT spleens B cells were reduced nearly two-fold, but only modestly in the RIC mutants (Figure 3.10A). We also found that the proportion of CD3⁺ T cells was increased upon GSK343 treatment in WT mice. However, this effect was also blunted in RIC mutants. Notably, the proportion of CD8⁺ cytotoxic T cells amongst CD3⁺ cells was increased in WT, but not significantly changed in RIC mutants upon EZH2 inhibition (Figure 3.9B). This suggests that in the absence of inflammatory cytokine signaling from RIC mutant B cells, they not only survive, but fail to recruit T effector cell populations.

We also quantified the proportion of myeloid cells in the spleen and found that CD11b⁺ cells were significantly increased in WT spleens, but unchanged in RIC mutants (Figure 3.9C, left). More specifically, the increase in the proportion of Ly6C⁺ Ly6G⁺ neutrophils (out of CD11b⁺) was significantly limited in the mutants (Figure 3.9C). We also measured absolute counts of each cell population per unit volume using counting beads. These data largely corroborate the proportions of cells described here (Figure 3.10B). The significantly smaller proportions or absolute counts of CD3⁺CD8⁺ cytotoxic T cells, and CD11b⁺Ly6C⁺Ly6G⁺ neutrophils in GSK343-treated RIC mutant spleens compared to WT implies that the inflammatory response in the mutants is greatly reduced.

Importantly, given EZH2's role in B lineage development we tested if GSK343 treatment in our experiments affected hematopoiesis. Staining and flow cytometry of bone marrow cells indicates that overall levels of CD19 and CD43 are unchanged in the course of these two day experiments (Figure 3.9D). This suggests that GSK343 treatment does not alter CD43⁺ CD19⁻ progenitors to CD43⁻ CD19⁺ immature B cell progression. Nor does it increase Ly6C⁺ Ly6G⁺ neutrophils (out of CD11b⁺) in the bone marrow (Figure 3.9D). This further suggests that the decrease in B cells or increase in neutrophils in the spleen upon GSK343 treatment is not due to similar changes in their production in the bone marrow during hematopoiesis.

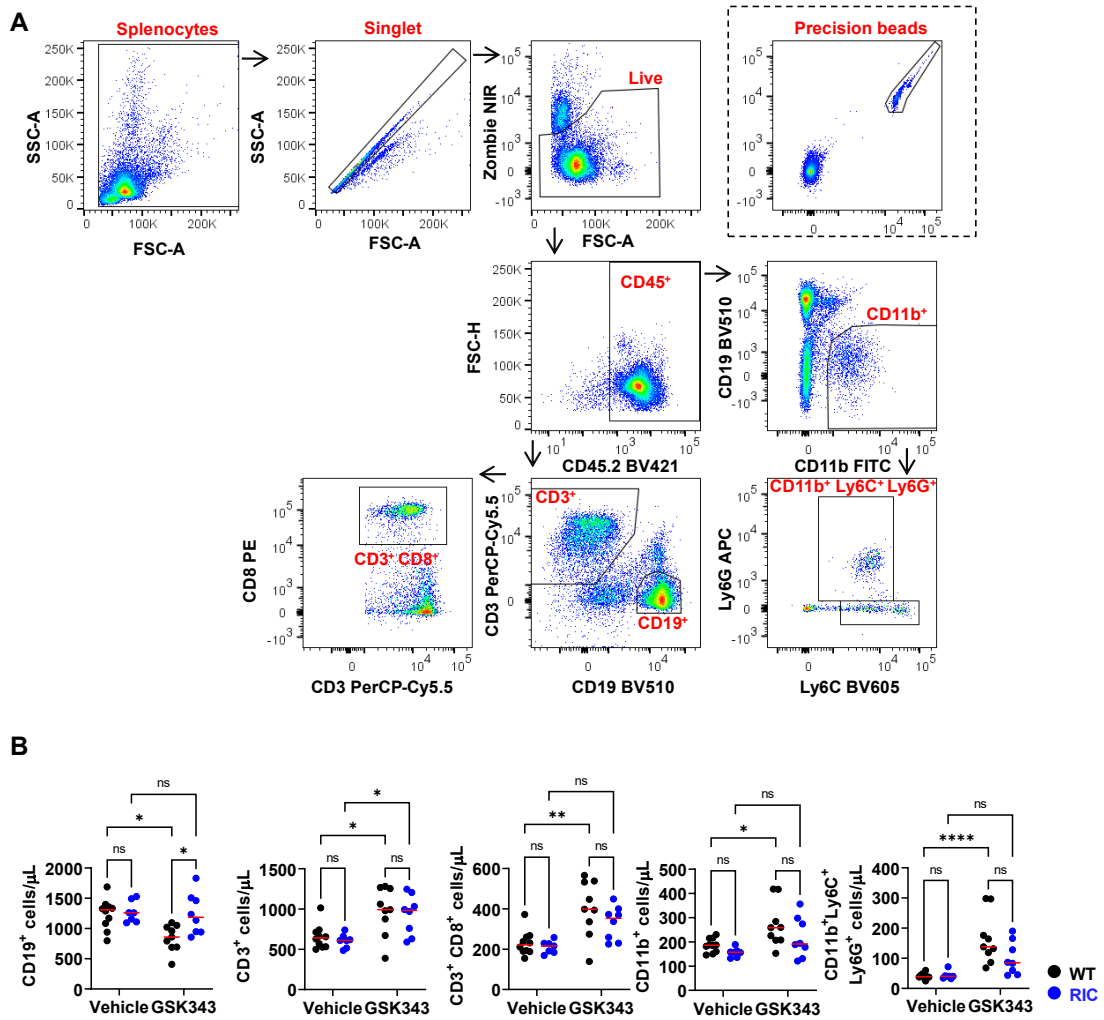


Figure 3.9: Gating strategy and absolute cell counts of splenic immune cells.

(A) Flow chart showing the gating strategy. Arrows indicate successive child gates. Gated populations are labeled in red. A gate for counting beads is shown in a box outlined by dotted lines. (B) Absolute counts (per microlitre) of indicated immune cells in the spleen were quantified by normalizing cell counts to bead counts.

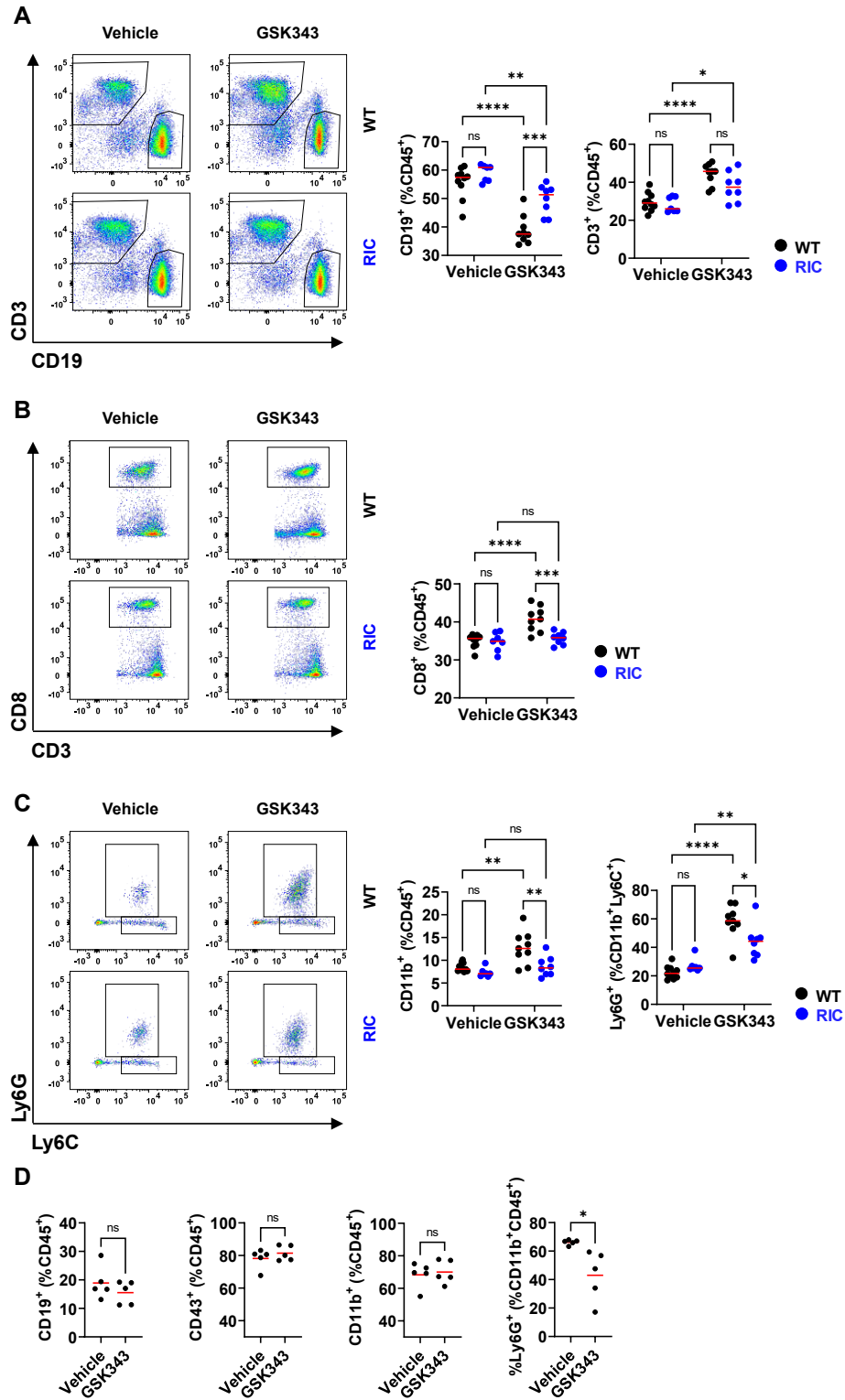


Figure 3.10: Cytosolic PRRs mediate GSK343 induced inflammation *in vivo*.

Figure 3.10: Cytosolic PRRs mediate GSK343 induced inflammation *in vivo*.

(A-C) WT and RIC mutant mice were I.P. injected with either vehicle or 100 mg/kg/day GSK343 for two days. Spleens were harvested and erythrocyte-lysed splenic lymphocytes were subjected to flow cytometry to quantify different immune cell populations. In each panel, a representative dot plot is shown for indicated cell populations under each treatment for WT and RIC mutant mice. Graphs on the right summarizes the proportions of each immune cell type as indicated (n=7-10). Horizontal red bars represent the mean. (D) WT mice were I.P. injected with either vehicle or 100 mg/kg/day GSK343 for two days. Erythrocyte-lysed bone marrow cells were subjected to flow cytometry to quantify different immune cell populations, and analyzed as above (n=5). Horizontal red bars represent the mean. * $p < 0.05$, ** $p < 0.01$, *** $p < 0.001$, **** $p < 0.0001$ by two-way ANOVA with Tukey's multiple test correction.

Overall, this flow cytometric analysis of splenic cells in WT and RIC mutant mice following GSK343 treatment support the conclusion that cytosolic PRRs mediate an inflammatory response upon EZH2 inhibition. Our data suggests EZH2 inhibited B cells misexpress repeat elements, activate PRRs, and secrete chemokines such as MDC and others. This attracts T cells and neutrophils ultimately leading to B cell death.

3.5 Discussion

Our work demonstrates a central role for PRRs in responding to EZH2 inhibition *in vivo*. Through ChIP-seq of H3K27me3, we confirmed that GSK343 inhibition of EZH2 decreased heterochromatin at numerous genomic locations and of most relevance, repetitive elements. Repeat misexpression is detected in WT and RIC mutant B cells treated with GSK343, indicating that the functional loss of the PRRs does not compromise the initial, on-target effects of EZH2 inhibition. In contrast, the RIC mutant B cells failed to activate NF- κ B and upregulate expression of pro-inflammatory cytokines as evidenced by lower gene expression and cytokine production in GSK343 treated cultures. In mice, systemic delivery of GSK343 leads to an inflammatory response in the spleen and the elimination of follicular B cells. In the absence of PRRs, B cells are preserved and cytotoxic CD8⁺ T cells or Ly6C⁺ Ly6G⁺ neutrophils are greatly reduced in the spleen. Based on these findings, we propose the signaling model in Figure 3.11 that highlights a key aspect of EZH2 chemical inhibition as the induction of a viral mimicry response, self-recognition of B cells by the immune system, and their destruction. The identification of viral mimicry as an unappreciated response to EZH2 inhibitors in normal cells, in the absence of any underlying pathology has important implications for their use and suggests new applications for this class of therapeutic.

Our data cannot exclude the possibility that GSK343 treatment impacts cell types other than B cells, or that RIC mutations compromise pathogen detection mechanisms in other cell types. However, we note that EZH2 function in B lineage development (Su et al., 2003), and in germinal centre formation (Béguelin et al., 2017) have established a unique role for EZH2 and H3K27me3 in B cell biology. The prevalence of activating mutations in EZH2 in B lymphomas further highlights the unique connection between this gene and cell type (Souroullas et al., 2016; Yap et al., 2011). These observations support our focus on B cells in the response to GSK343 and the fact that B cells are specifically targeted for death by GSK343 without affecting bone marrow development emphasizes it is the central target of EZH2 inhibition. Lastly, a targeted *Rbl* mutant mouse strain that fails to recruit EZH2 to repeats, and possesses this defect in all cells is

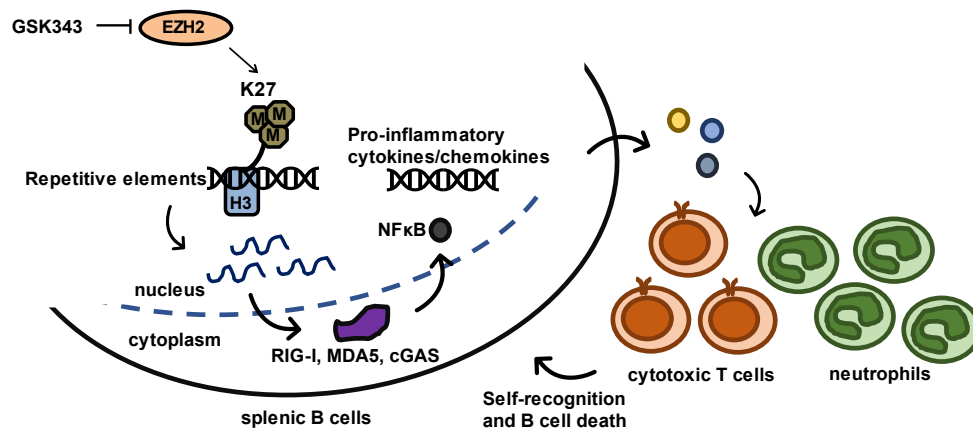


Figure 3.11: Model of EZH2 inhibition and activation of inflammation.

GSK343 inhibits EZH2 leading to loss of H3K27me3. Subsequent misexpression of repetitive elements stimulates pattern recognition receptors that activate NF- κ B, inflammatory cytokines, and the recruitment of neutrophils and T cells.

characterized by inflammation in the spleen and frequent development of lymphomas (Ishak et al., 2016). From a number of perspectives, EZH2 inhibition is uniquely impactful on resting B cells in the spleen.

EZH2-mediated repression of gene expression has been studied extensively, and this has led to the development of potent and selective EZH2 inhibitors like GSK343 (McCabe et al., 2012). Our H3K27me3 ChIP-seq data reveals a striking preference for GSK343 causing decreased H3K27me3 in intronic and intergenic regions in comparison with proximal promoters. Furthermore, our work reveals that there is extensive overlap of H3K27me3 intersecting with repetitive elements and GSK343 can induce their expression. One interpretation of these findings is that B cell derived inflammatory signals following GSK343 are a chemical biology phenomenon that doesn't reflect the activation of a physiological response. We note that Epstein-Barr Virus, a dsDNA virus, is known to activate expression of *Csfl*, *Ccl22* (MDC), *Ccl1*, *Ccl3*, and *Ccl5* upon infection of B cells (Ehlin-Henriksson et al., 2009; Nakayama et al., 2004), and these chemokines are all activated by GSK343 in a PRR dependent manner in our experiments. Therefore, the surprising induction of inflammation and immune self-recognition by GSK343 demonstrated in this report likely reflects the activation of an antiviral response intrinsic to B cells. Importantly, this connection emphasizes that our work reveals a true viral mimicry response to GSK343 in untransformed cells that is distinct from interferon activating paradigms described in cancer cells.

The rationale for generating EZH2 inhibitors is to counteract overactive H3K27me3 deposition that arises from overexpressed or mutationally activated EZH2. This study reveals the consequence of inhibition of endogenous, WT EZH2. Our findings suggest a number of important considerations and potential applications for EZH2 inhibitors in the future. Short term treatment with these inhibitors is capable of inducing inflammation and depleting B cells. Recent studies using other EZH2 inhibitors, DZNep or GSK126, to treat mouse models of systemic lupus erythematosus demonstrated phenotypic improvement in a number of measures of disease pathology (Rohraff et al., 2019; Wu et al., 2021). These studies rationalized use of EZH2 inhibitors based on high

level EZH2 expression in a number of different cell types including B cells. The effects of EZH2 inhibitors that activate viral mimicry in B cells after only brief treatment suggests an alternate explanation to reduced immune cells in these models. The specificity of viral mimicry related stimulation of the immune system in cancer treatment is based on the concept that in transformed cells repeat silencing is precarious because of epigenetic alterations, such that inhibitors of DNA methyltransferases will selectively cause repeat expression in cancer cells. Our work suggests that EZH2 inhibitors may be deployed based on a similar logic, without the need for EZH2 overexpression to suggest applicability. However, our findings also raise the question of whether the activation of inflammatory signaling upon EZH2 inhibition from prolonged treatment can lead to chronic inflammation that may render the therapy less effective. Overall, our work reveals a new effect of EZH2 inhibitors in immune function that is likely to have a significant impact on the use of these agents in clinical applications.

3.6 References

- Babaian, A., and Mager, D.L. (2016). Endogenous retroviral promoter exaptation in human cancer. *Mob. DNA* 7. .
- Béguelin, W., Rivas, M.A., Calvo Fernández, M.T., Teater, M., Purwada, A., Redmond, D., Shen, H., Challman, M.F., Elemento, O., Singh, A., et al. (2017). EZH2 enables germinal centre formation through epigenetic silencing of CDKN1A and an Rb-E2F1 feedback loop. *Nature Communications* 8, 877. <https://doi.org/10.1038/s41467-017-01029-x>.
- Béguelin, W., Teater, M., Meydan, C., Hoehn, K.B., Phillip, J.M., Soshnev, A.A., Venturutti, L., Rivas, M.A., Calvo-Fernández, M.T., Gutierrez, J., et al. (2020). Mutant EZH2 Induces a Pre-malignant Lymphoma Niche by Reprogramming the Immune Response. *Cancer Cell* 37, 655-673.e11. <https://doi.org/10.1016/j.ccell.2020.04.004>.
- Bulut-Karslioglu, A., De La Rosa-Velázquez, I.A., Ramirez, F., Barenboim, M., Onishi-Seebacher, M., Arand, J., Galán, C., Winter, G.E., Engist, B., Gerle, B., et al. (2014). Suv39h-Dependent H3K9me3 Marks Intact Retrotransposons and Silences LINE Elements in Mouse Embryonic Stem Cells. *Molecular Cell* 55, 277–290. <https://doi.org/10.1016/j.molcel.2014.05.029>.
- Cao, R., Wang, L., Wang, H., Xia, L., Erdjument-Bromage, H., Tempst, P., Jones, R.S., and Zhang, Y. (2002). Role of Histone H3 Lysine 27 Methylation in Polycomb-Group Silencing. *Science* 298, 1039–1043. <https://doi.org/10.1126/science.1076997>.

Chen, R., Ishak, C.A., and De Carvalho, D.D. (2021). Endogenous Retroelements and the Viral Mimicry Response in Cancer Therapy and Cellular Homeostasis. *Cancer Discovery* *11*, 2707–2725. <https://doi.org/10.1158/2159-8290.CD-21-0506>.

Chiappinelli, K.B., Strissel, P.L., Desrichard, A., Li, H., Henke, C., Akman, B., Hein, A., Rote, N.S., Cope, L.M., Snyder, A., et al. (2015). Inhibiting DNA Methylation Causes an Interferon Response in Cancer via dsRNA Including Endogenous Retroviruses. *Cell* *162*, 974–986. [10.1016/j.cell.2015.07.011](https://doi.org/10.1016/j.cell.2015.07.011).

Collinson, A., Collier, A.J., Morgan, N.P., Sienerth, A.R., Chandra, T., Andrews, S., and Rugg-Gunn, P.J. (2016). Deletion of the Polycomb-Group Protein EZH2 Leads to Compromised Self-Renewal and Differentiation Defects in Human Embryonic Stem Cells. *Cell Reports* *17*, 2700–2714. <https://doi.org/10.1016/j.celrep.2016.11.032>.

Cradick, T.J., Qiu, P., Lee, C.M., Fine, E.J., and Bao, G. (2014). COSMID: A Web-based Tool for Identifying and Validating CRISPR/Cas Off-target Sites. *Molecular Therapy - Nucleic Acids* *3*, e214. <https://doi.org/10.1038/mtna.2014.64>.

Criscione, S.W., Zhang, Y., Thompson, W., Sedivy, J.M., and Neretti, N. (2014). Transcriptional landscape of repetitive elements in normal and cancer human cells. *BMC Genomics* *15*, 583. <https://doi.org/10.1186/1471-2164-15-583>.

Day, D.S., Luquette, L.J., Park, P.J., and Kharchenko, P.V. (2010). Estimating enrichment of repetitive elements from high-throughput sequence data. *Genome Biology* *11*, R69. <https://doi.org/10.1186/gb-2010-11-6-r69>.

Dellino, G.I., Schwartz, Y.B., Farkas, G., McCabe, D., Elgin, S.C.R., and Pirrotta, V. (2004). Polycomb silencing blocks transcription initiation. *Molecular Cell* *13*, 887–893. [https://doi.org/10.1016/s1097-2765\(04\)00128-5](https://doi.org/10.1016/s1097-2765(04)00128-5).

Desai, N., Sajed, D., Arora, K.S., Solovyov, A., Rajurkar, M., Bledsoe, J.R., Sil, S., Amri, R., Tai, E., MacKenzie, O.C., et al. (2017). Diverse repetitive element RNA expression defines epigenetic and immunologic features of colon cancer. *JCI Insight* *2*, e91078. <https://doi.org/10.1172/jci.insight.91078>.

Doucet-O’Hare, T.T., Rodić, N., Sharma, R., Darbari, I., Abril, G., Choi, J.A., Ahn, J.Y., Cheng, Y., Anders, R.A., Burns, K.H., et al. (2015). LINE-1 expression and retrotransposition in Barrett’s esophagus and esophageal carcinoma. *Proceedings of the National Academy of Sciences* *112*, E4894–E4900. <https://doi.org/10.1073/pnas.1502474112>.

Ehlin-Henriksson, B., Liang, W., Cagigi, A., Mowafi, F., Klein, G., and Nilsson, A. (2009). Changes in chemokines and chemokine receptor expression on tonsillar B cells upon Epstein-Barr virus infection. *Immunology* *127*, 549–557. <https://doi.org/10.1111/j.1365-2567.2008.03029.x>.

Eskeland, R., Leeb, M., Grimes, G.R., Kress, C., Boyle, S., Sproul, D., Gilbert, N., Fan, Y., Skoultchi, A.I., Wutz, A., et al. (2010). Ring1B Compacts Chromatin Structure and

Represses Gene Expression Independent of Histone Ubiquitination. *Molecular Cell* 38, 452–464. <https://doi.org/10.1016/j.molcel.2010.02.032>.

Ewing, A.D., Gacita, A., Wood, L.D., Ma, F., Xing, D., Kim, M.-S., Manda, S.S., Abril, G., Pereira, G., Makohon-Moore, A., et al. (2015). Widespread somatic L1 retrotransposition occurs early during gastrointestinal cancer evolution. *Genome Res* 25, 1536–1545. [10.1101/gr.196238.115](https://doi.org/10.1101/gr.196238.115).

Francis, N.J., Kingston, R.E., and Woodcock, C.L. (2004). Chromatin compaction by a polycomb group protein complex. *Science (New York, N.Y.)* 306, 1574–1577. <https://doi.org/10.1126/science.1100576>.

Goubau, D., Deddouche, S., Reis, and Sousa, C. (2013). Cytosolic Sensing of Viruses. *Immunity* 38, 855–869. .

Hansen, K., Prabakaran, T., Laustsen, A., Jørgensen, S.E., Rahbæk, S.H., Jensen, S.B., Nielsen, R., Leber, J.H., Decker, T., Horan, K.A., et al. (2014). *Listeria monocytogenes* induces IFN β expression through an IFI16-, cGAS- and STING-dependent pathway. *The EMBO Journal* 33, 1654–1666. <https://doi.org/10.15252/embj.201488029>.

Howard, G., Eiges, R., Gaudet, F., Jaenisch, R., and Eden, A. (2008). Activation and transposition of endogenous retroviral elements in hypomethylation induced tumors in mice. *Oncogene* 27, 404–408. <https://doi.org/10.1038/sj.onc.1210631>.

Ishak, C.A., and De Carvalho, D.D. (2020). Reactivation of Endogenous Retroelements in Cancer Development and Therapy. *Annual Review of Cancer Biology* 4, 159–176. <https://doi.org/10.1146/annurev-cancerbio-030419-033525>.

Ishak, C.A., Marshall, A.E., Passos, D.T., White, C.R., Kim, S.J., Cecchini, M.J., Ferwati, S., MacDonald, W.A., Howlett, C.J., Welch, I.D., et al. (2016). An RB-EZH2 Complex Mediates Silencing of Repetitive DNA Sequences. *Molecular Cell* 64, 1074–1087. <https://doi.org/10.1016/j.molcel.2016.10.021>.

Karimi, M.M., Goyal, P., Maksakova, I.A., Bilenky, M., Leung, D., Tang, J.X., Shinkai, Y., Mager, D.L., Jones, S., Hirst, M., et al. (2011). DNA Methylation and SETDB1/H3K9me3 Regulate Predominantly Distinct Sets of Genes, Retroelements, and Chimeric Transcripts in mESCs. *Cell Stem Cell* 8, 676–687. <https://doi.org/10.1016/j.stem.2011.04.004>.

Karolchik, D., Hinrichs, A.S., Furey, T.S., Roskin, K.M., Sugnet, C.W., Haussler, D., and Kent, W.J. (2004). The UCSC Table Browser data retrieval tool. *Nucleic Acids Research* 32, D493–D496. <https://doi.org/10.1093/nar/gkh103>.

Kent, W.J., Zweig, A.S., Barber, G., Hinrichs, A.S., and Karolchik, D. (2010). BigWig and BigBed: enabling browsing of large distributed datasets. *Bioinformatics* 26, 2204–2207. <https://doi.org/10.1093/bioinformatics/btq351>.

Kleer, C.G., Cao, Q., Varambally, S., Shen, R., Ota, I., Tomlins, S.A., Ghosh, D., Sewalt, R.G.A.B., Otte, A.P., Hayes, D.F., et al. (2003). EZH2 is a marker of aggressive breast cancer and promotes neoplastic transformation of breast epithelial cells. *Proceedings of the National Academy of Sciences of the United States of America* *100*, 11606–11611. <https://doi.org/10.1073/pnas.1933744100>.

Kondo, Y., and Issa, J.-P.J. (2003). Enrichment for Histone H3 Lysine 9 Methylation at Alu Repeats in Human Cells. *J. Biol. Chem* *278*, 27658–27662. .

Koning, A.P.J. de, Gu, W., Castoe, T.A., Batzer, M.A., and Pollock, D.D. (2011). Repetitive Elements May Comprise Over Two-Thirds of the Human Genome. *PLOS Genet* *7*, 1002384. .

Ku, M., Koche, R.P., Rheinbay, E., Mendenhall, E.M., Endoh, M., Mikkelsen, T.S., Presser, A., Nusbaum, C., Xie, X., Chi, A.S., et al. (2008). Genomewide Analysis of PRC1 and PRC2 Occupancy Identifies Two Classes of Bivalent Domains. *PLOS Genetics* *4*, e1000242. <https://doi.org/10.1371/journal.pgen.1000242>.

Kuzmichev, A., Nishioka, K., Erdjument-Bromage, H., Tempst, P., and Reinberg, D. (2002). Histone methyltransferase activity associated with a human multiprotein complex containing the Enhancer of Zeste protein. *Genes & Development* *16*, 2893–2905. <https://doi.org/10.1101/gad.1035902>.

Lamprecht, B., Walter, K., Kreher, S., Kumar, R., Hummel, M., Lenze, D., Köchert, K., Bouhrel, M.A., Richter, J., Soler, E., et al. (2010). Derepression of an endogenous long terminal repeat activates the CSF1R proto-oncogene in human lymphoma. *Nature Medicine* *16*, 571–579. <https://doi.org/10.1038/nm.2129>.

Leeb, M., Pasini, D., Novatchkova, M., Jaritz, M., Helin, K., and Wutz, A. (2010). Polycomb complexes act redundantly to repress genomic repeats and genes. *Genes & Development* *24*, 265–276. <https://doi.org/10.1101/gad.544410>.

Levin, H.L., and Moran, J.V. (2011). Dynamic interactions between transposable elements and their hosts. *Nat. Rev. Genet* *12*, 615–627. .

Liao, Y., Smyth, G.K., and Shi, W. (2014). featureCounts: an efficient general purpose program for assigning sequence reads to genomic features. *Bioinformatics* *30*, 923–930. <https://doi.org/10.1093/bioinformatics/btt656>.

Liu, M., Thomas, S.L., DeWitt, A.K., Zhou, W., Madaj, Z.B., Ohtani, H., Baylin, S.B., Liang, G., and Jones, P.A. (2018). Dual Inhibition of DNA and Histone Methyltransferases Increases Viral Mimicry in Ovarian Cancer Cells. *Cancer Research* *78*, 5754–5766. <https://doi.org/10.1158/0008-5472.CAN-17-3953>.

Liu, S., Brind'Amour, J., Karimi, M.M., Shirane, K., Bogutz, A., Lefebvre, L., Sasaki, H., Shinkai, Y., and Lorincz, M.C. (2014). Setdb1 is required for germline development and silencing of H3K9me3-marked endogenous retroviruses in primordial germ cells. *Genes & Development* *28*, 2041–2055. <https://doi.org/10.1101/gad.244848.114>.

- Lock, F.E., Rebollo, R., Miceli-Royer, K., Gagnier, L., Kuah, S., Babaian, A., Sistiaga-Poveda, M., Lai, C.B., Nemirovsky, O., Serrano, I., et al. (2014). Distinct isoform of FABP7 revealed by screening for retroelement-activated genes in diffuse large B-cell lymphoma. *Proc Natl Acad Sci U S A* *111*, E3534-3543. [10.1073/pnas.1405507111](https://doi.org/10.1073/pnas.1405507111).
- Margueron, R., Li, G., Sarma, K., Blais, A., Zavadil, J., Woodcock, C.L., Dynlacht, B.D., and Reinberg, D. (2008). Ezh1 and Ezh2 Maintain Repressive Chromatin through Different Mechanisms. *Molecular Cell* *32*, 503–518. <https://doi.org/10.1016/j.molcel.2008.11.004>.
- Martens, J.H.A., O’Sullivan, R.J., Braunschweig, U., Opravil, S., Radolf, M., Steinlein, P., and Jenuwein, T. (2005). The profile of repeat-associated histone lysine methylation states in the mouse epigenome. *EMBO J* *24*, 800–812. [10.1038/sj.emboj.7600545](https://doi.org/10.1038/sj.emboj.7600545).
- McCabe, M.T., Ott, H.M., Ganji, G., Korenchuk, S., Thompson, C., Van Aller, G.S., Liu, Y., Graves, A.P., Iii, A.D.P., Diaz, E., et al. (2012). EZH2 inhibition as a therapeutic strategy for lymphoma with EZH2-activating mutations. *Nature* *492*, 108–112. [10.1038/nature11606](https://doi.org/10.1038/nature11606).
- Morel, K.L., Sheahan, A.V., Burkhart, D.L., Baca, S.C., Boufaied, N., Liu, Y., Qiu, X., Cañadas, I., Roehle, K., Heckler, M., et al. (2021). EZH2 inhibition activates a dsRNA-STING-interferon stress axis that potentiates response to PD-1 checkpoint blockade in prostate cancer. *Nature Cancer* *2*, 444–456. <https://doi.org/10.1038/s43018-021-00185-w>.
- Morschhauser, F., Tilly, H., Chaidos, A., McKay, P., Phillips, T., Assouline, S., Batlevi, C.L., Campbell, P., Ribrag, V., Damaj, G.L., et al. (2020). Tazemetostat for patients with relapsed or refractory follicular lymphoma: an open-label, single-arm, multicentre, phase 2 trial. *The Lancet Oncology* *21*, 1433–1442. [https://doi.org/10.1016/S1470-2045\(20\)30441-1](https://doi.org/10.1016/S1470-2045(20)30441-1).
- Müller, J., Hart, C.M., Francis, N.J., Vargas, M.L., Sengupta, A., Wild, B., Miller, E.L., O’Connor, M.B., Kingston, R.E., and Simon, J.A. (2002). Histone methyltransferase activity of a Drosophila Polycomb group repressor complex. *Cell* *111*, 197–208. [https://doi.org/10.1016/s0092-8674\(02\)00976-5](https://doi.org/10.1016/s0092-8674(02)00976-5).
- Nakayama, T., Hieshima, K., Nagakubo, D., Sato, E., Nakayama, M., Kawa, K., and Yoshie, O. (2004). Selective induction of Th2-attracting chemokines CCL17 and CCL22 in human B cells by latent membrane protein 1 of Epstein-Barr virus. *Journal of Virology* *78*, 1665–1674. <https://doi.org/10.1128/jvi.78.4.1665-1674.2004>.
- Rodriguez-Martin, B., Alvarez, E.G., Baez-Ortega, A., Zamora, J., Supek, F., Demeulemeester, J., Santamarina, M., Ju, Y.S., Temes, J., Garcia-Souto, D., et al. (2020). Pan-cancer analysis of whole genomes identifies driver rearrangements promoted by LINE-1 retrotransposition. *Nature Genetics* *52*, 306–319. [10.1038/s41588-019-0562-0](https://doi.org/10.1038/s41588-019-0562-0).
- Rohruff, D.M., He, Y., Farkash, E.A., Schonfeld, M., Tsou, P.-S., and Sawalha, A.H. (2019). Inhibition of EZH2 Ameliorates Lupus-Like Disease in MRL/lpr Mice. *Arthritis & Rheumatology (Hoboken, N.J.)* *71*, 1681–1690. <https://doi.org/10.1002/art.40931>.

- Roulois, D., Loo Yau, H., Singhania, R., Wang, Y., Danesh, A., Shen, S.Y., Han, H., Liang, G., Jones, P.A., Pugh, T.J., et al. (2015). DNA-Demethylating Agents Target Colorectal Cancer Cells by Inducing Viral Mimicry by Endogenous Transcripts. *Cell* 162, 961–973. [10.1016/j.cell.2015.07.056](https://doi.org/10.1016/j.cell.2015.07.056).
- Schmidt, A., Rothenfusser, S., and Hopfner, K.-P. (2012). Sensing of viral nucleic acids by RIG-I: From translocation to translation. *Eur. J. Cell Biol* 91, 78–85. .
- Schuettengruber, B., Chourrout, D., Vervoort, M., Leblanc, B., and Cavalli, G. (2007). Genome Regulation by Polycomb and Trithorax Proteins. *Cell* 128, 735–745. <https://doi.org/10.1016/j.cell.2007.02.009>. 1.
- Sheng, W., LaFleur, M.W., Nguyen, T.H., Chen, S., Chakravarthy, A., Conway, J.R., Li, Y., Chen, H., Yang, H., Hsu, P.-H., et al. (2018). LSD1 Ablation Stimulates Anti-tumor Immunity and Enables Checkpoint Blockade. *Cell* 174, 549–563.e19. [10.1016/j.cell.2018.05.052](https://doi.org/10.1016/j.cell.2018.05.052).
- Souroullas, G.P., Jeck, W.R., Parker, J.S., Simon, J.M., Liu, J.-Y., Paulk, J., Xiong, J., Clark, K.S., Fedorow, Y., Qi, J., et al. (2016). An oncogenic Ezh2 mutation induces tumors through global redistribution of histone 3 lysine 27 trimethylation. *Nature Medicine* 22, 632–640. <https://doi.org/10.1038/nm.4092>.
- Su, I.-hsin, Basavaraj, A., Krutchinsky, A.N., Hobert, O., Ullrich, A., Chait, B.T., and Tarakhovskiy, A. (2003). Ezh2 controls B cell development through histone H3 methylation and Igh rearrangement. *Nature Immunology* 4, 124–131. <https://doi.org/10.1038/ni876>.
- Tamburri, S., Lavarone, E., Fernández-Pérez, D., Conway, E., Zanotti, M., Manganaro, D., and Pasini, D. (2020). Histone H2AK119 Mono-Ubiquitination Is Essential for Polycomb-Mediated Transcriptional Repression. *Molecular Cell* 77, 840–856.e5. <https://doi.org/10.1016/j.molcel.2019.11.021>.
- Teissandier, A., Servant, N., Barillot, E., and Bourc'his, D. (2019). Tools and best practices for retrotransposon analysis using high-throughput sequencing data. *Mobile DNA* 10, 52. <https://doi.org/10.1186/s13100-019-0192-1>.
- Varambally, S., Dhanasekaran, S.M., Zhou, M., Barrette, T.R., Kumar-Sinha, C., Sanda, M.G., Ghosh, D., Pienta, K.J., Sewalt, R.G.A.B., Otte, A.P., et al. (2002). The polycomb group protein EZH2 is involved in progression of prostate cancer. *Nature* 419, 624–629. <https://doi.org/10.1038/nature01075>.
- Velichutina, I., Shaknovich, R., Geng, H., Johnson, N.A., Gascoyne, R.D., Melnick, A.M., and Elemento, O. (2010). EZH2-mediated epigenetic silencing in germinal center B cells contributes to proliferation and lymphomagenesis. *Blood* 116, 5247–5255. <https://doi.org/10.1182/blood-2010-04-280149>.
- Wang, C., Li, D., Zhang, L., Jiang, S., Liang, J., Narita, Y., Hou, I., Zhong, Q., Zheng, Z., Xiao, H., et al. (2019). RNA Sequencing Analyses of Gene Expression during Epstein-

Barr Virus Infection of Primary B Lymphocytes. *Journal of Virology* 93, e00226-19. <https://doi.org/10.1128/JVI.00226-19>.

Wang, H., Wang, L., Erdjument-Bromage, H., Vidal, M., Tempst, P., Jones, R.S., and Zhang, Y. (2004). Role of histone H2A ubiquitination in Polycomb silencing. *Nature* 431, 873–878. <https://doi.org/10.1038/nature02985>.

Wang, H., Yang, H., Shivalila, C.S., Dawlaty, M.M., Cheng, A.W., Zhang, F., and Jaenisch, R. (2013). One-Step Generation of Mice Carrying Mutations in Multiple Genes by CRISPR/Cas-Mediated Genome Engineering. *Cell* 153, 910–918. <https://doi.org/10.1016/j.cell.2013.04.025>.

Wassef, M., Rodilla, V., Teissandier, A., Zeitouni, B., Gruel, N., Sadacca, B., Irondelle, M., Charruel, M., Ducos, B., Michaud, A., et al. (2015). Impaired PRC2 activity promotes transcriptional instability and favors breast tumorigenesis. *Genes & Development* 29, 2547–2562. <https://doi.org/10.1101/gad.269522.115>.

Wu, L., Jiang, X., Qi, C., Zhang, C., Qu, B., and Shen, N. (2021). EZH2 Inhibition Interferes With the Activation of Type I Interferon Signaling Pathway and Ameliorates Lupus Nephritis in NZB/NZW F1 Mice. *Frontiers in Immunology* 12, 653989. <https://doi.org/10.3389/fimmu.2021.653989>.

Yap, D.B., Chu, J., Berg, T., Schapira, M., Cheng, S.-W.G., Moradian, A., Morin, R.D., Mungall, A.J., Meissner, B., Boyle, M., et al. (2011). Somatic mutations at EZH2 Y641 act dominantly through a mechanism of selectively altered PRC2 catalytic activity, to increase H3K27 trimethylation. *Blood* 117, 2451–2459. <https://doi.org/10.1182/blood-2010-11-321208>.

Yin, J., Leavenworth, J.W., Li, Y., Luo, Q., Xie, H., Liu, X., Huang, S., Yan, H., Fu, Z., Zhang, L.Y., et al. (2015). Ezh2 regulates differentiation and function of natural killer cells through histone methyltransferase activity. *Proceedings of the National Academy of Sciences* 112, 15988–15993. <https://doi.org/10.1073/pnas.1521740112>.

Zhang, Y., Ma, Z., Wang, Y., Boyer, J., Ni, G., Cheng, L., Su, S., Zhang, Z., Zhu, Z., Qian, J., et al. (2020). Streptavidin Promotes DNA Binding and Activation of cGAS to Enhance Innate Immunity. *IScience* 23, 101463. <https://doi.org/10.1016/j.isci.2020.101463>.

Zhao, Y., Ding, L., Wang, D., Ye, Z., He, Y., Ma, L., Zhu, R., Pan, Y., Wu, Q., Pang, K., et al. (2019). EZH2 cooperates with gain-of-function p53 mutants to promote cancer growth and metastasis. *The EMBO Journal* 38, e99599. <https://doi.org/10.15252/embj.201899599>.

Chapter 4

4 Both RIG-I and cGAS are required to upregulate interferon signaling upon EZH2 inhibition in B16 melanoma cells

4.1 Introduction

Immune checkpoint blockade (ICB) therapy harnesses the power of intrinsic host immunity to target and eliminate cancer cells (Topalian et al., 2015). While the immune system is theoretically able to mount an anti-tumour response, this is inhibited by the same molecular processes that maintain self-tolerance, and limit autoimmunity and collateral tissue damage in an immune response. One of these processes is a regulatory negative feedback loop that suppresses cytotoxic T cell activity. T cell activation requires two cell surface receptor interactions: the main T cell receptor (TCR) with cognate peptide-major histocompatibility complex I (MHC I), and costimulation of CD28 with its ligands, CD80 and CD86 (Lenschow et al., 1996). Upon activation, checkpoint receptor cytotoxic T lymphocyte antigen 4 (CTLA-4) is mobilized to the cell surface, which competes with CD28 to engage with CD80 and CD86 (Alegre et al., 2001). This blocks the requisite costimulatory signal for T cell activation. Similarly, programmed death 1 (PD1) expressed on activated T cells can interact with its ligands, PD-L1 and 2, which inhibit cytotoxic effector functions (Sharpe and Pauken, 2018).

Cancer cells often hijack this mechanism to evade the immune system, thus gaining a key selective advantage. Genetic alterations and deregulated signaling pathways can enable constitutive expression of PD-L1 (Topalian et al., 2015). Furthermore, tumour cells can upregulate PD-L1 in an adaptive response to interferon (IFN)- γ , a pro-inflammatory cytokine secreted by certain activated, anti-tumour immune cells.

These observations led to the development of anti-CTLA-4 and anti-PD-1 antibodies (ipilimumab and nivolumab, respectively) and eventually their use to treat various cancers (Brahmer et al., 2012; Herbst et al., 2014; Larkin et al., 2019; Motzer et al., 2015; Wolchok et al., 2017). Improved clinical outcome with the use of both

antibodies compared to one alone suggests that further immune modulation will result in better anti-tumour activity. One of the emerging avenues for this goal is the use of pharmacological inhibitors targeting epigenetic writers, DNA methyltransferase I (DNMT1) and enhancer of zeste homolog 2 (EZH2) (Chiappinelli et al., 2015; Liu et al., 2018; Morel et al., 2021; Roulois et al., 2015). In various cancer models, their inhibition has been shown to activate an anti-viral immune response that stimulates anti-tumour activity in culture and *in vivo*. Mechanistically, this is mediated through cytosolic pattern recognition receptors (PRRs), which are sensors that directly detect nucleic acids derived from viruses or DNA damage (Goubau et al., 2013). Inhibition of DNMT1 or EZH2 derepresses endogenous repetitive DNA elements that are normally silenced by them through DNA methylation or histone 3 lysine 27 trimethylation (H3K27me3), respectively. These repetitive elements activate the PRRs to upregulate anti-viral signaling, which blocks tumour proliferation and enhances anti-tumour immune response in colorectal and prostate cancer cells (Morel et al., 2021; Roulois et al., 2015). This mechanism, however, has not yet been tested in cancer models that are refractory to ICB therapy. This raises the question whether immune modulation through epigenetic inhibition and subsequent anti-viral signaling can improve ICB efficacy.

In this chapter, we present evidence that pharmacological inhibition of EZH2 induces IFN and innate immune gene expression pathways in B16-F10 mouse melanoma cells. This is mechanistically dependent on both retinoic acid inducible gene 1 (RIG-I) and cyclic AMP-GMP synthetase (cGAS) where deletion of either PRRs abolishes the immune activation. This work reveals a new pathway that can be leveraged to target melanoma through EZH2 inhibition.

4.2 Materials and Methods

4.2.1 Cell culture and lentiviral transduction

B16-F10 melanoma cells were a gift from Dr. Charles Ishak. The cells were grown in DMEM (Wisent) supplemented with 10% (v/v) FBS, 2 mM L-glutamine, penicillin, and streptomycin at 37 °C in 5% CO₂. For lentiviral transduction, HEK293T cells at 70% confluency on 6-well plates were transfected with 12 µg pLentiCRISPRv2 (targeting cGAS, RIG-I or β-gal/luciferase), 9 µg pMD2.G (#12259) and 3 µg psPAX2 (#12260) using Lipofectamine 3000 (Life Technologies, #L3000001) following manufacturer's recommendations. After 48 hours, the culture media were harvested and passed through a 0.45 µm filter. B16-F10 cells were transduced with the appropriate filtrate containing 8 µg/mL polybrene. To select for transduced cells, B16-F10 cells were maintained in media containing 1 µg/mL puromycin. To isolate cGAS/RIG-I single, or double KO cells, puromycin-selected cells were seeded on 96-well plates at low density, and subpopulations were tested for protein expression by Western blotting. Those with confirmed loss of cGAS/RIG-I expression were pooled together for subsequent experiments.

For GSK343 treatment, B16-F10 cells (3×10^5) were seeded on 6-well plates. Next day, DMSO or 2 µM GSK343 were added, and the cells were treated for four days. Culture media were replaced daily.

4.2.2 RNA extraction and Quantitative real-time qPCR

Following treatment, RNA was harvested using Monarch Total RNA miniprep kit (NEB, #T2010) and residual genomic DNA was digested by treating 1 µg RNA with 1 U DNaseI (ThermoFisher, #18068015) for 15 min at RT. DNaseI was then inactivated by adding EDTA and incubating at 65 °C for 10 min. For qRT-PCR, RNA was then reverse-transcribed into cDNA with iScript Supermix (Biorad, #1708840) and diluted five-fold with H₂O. PCR was performed with iQ SYBR Green Supermix (Biorad, #1708882) on a CFX96 (Biorad). For sequencing, DNaseI-treated RNA was purified with Monarch RNA cleanup kit (NEB, #T2040). rRNA depletion and library preparation were performed with VAHTS total RNA-seq library prep kit (GeneBio, #NR603-01) at the London Regional

Genomics Center. Libraries were pooled and sequenced on NextSeq 500 at the London Regional Genomics Center with a high output 75 cycle kit to yield single-end 75-bp reads.

4.2.3 RNA-seq analysis

Demultiplexed FASTQ files were downloaded from BaseSpace. Reads were mapped to mm10 genome with STAR/2.7.8a and resulting sam files were converted to sorted, indexed bam files with samtools/1.12. HTSeq/0.11.0 was used to assign mapped reads to GENCODE mouse M22 comprehensive gene annotation.

To identify differentially expressed genes, edgeR/3.28.1 was used. Heatmaps were generated with heatmap.2. GSEA was performed as recommended (Subramanian et al., 2005).

4.2.4 Protein extraction, SDS-PAGE and Western blotting

B16-F10 cells were lysed in RIPA buffer (50 mM Tris pH 7.4, 150 mM NaCl, 1% NP-40, 0.5% sodium deoxycholate, 0.1% SDS, supplemented with protease inhibitors as above) on ice for 10 min. Debris was cleared by centrifugation at 16 000 x g for 30 min at 4 °C. Bradford assays were used to quantify protein concentration. RIPA extracts were denatured by adding Laemmli buffer to 1x and boiling at 95 °C for 5 min. SDS-PAGE was performed following standard procedures. Samples were transferred to PVDF membrane using TransBlot Turbo (Biorad) and blocked in 5% skim milk in TBST for 1 h at RT. Membranes were incubated overnight at 4 °C with gentle shaking with the following primary antibodies: α - tubulin (CST, #2125, 1:5000), cGAS (CST, #31659, 1:1000), RIG-I (Santa Cruz, #376845, 1:1000). The next day, membranes were washed five times with TBST and incubated with AffiniPure goat anti-rabbit IgG-HRP (JIR, #111-035-144, 1:5000-10000). After five washes with TBST, membranes were incubated in SuperSignal WestDura (ThermoFisher, #34075) and visualized on a ChemiDoc (Biorad).

4.3 Results

4.3.1 Generation of RIG-I KO, cGAS KO and RIG-I/cGAS double KO (DKO) cell lines

We sought to test whether RIG-I and cGAS are both required to induce viral mimicry in B16-F10 melanoma cells upon GSK343 treatment. To this end, we transduced parental B16-F10 cells with lentiviruses expressing Cas9 and gRNAs targeting β -gal and luciferase as a negative control, RIG-I or cGAS (Figure 4.1A). To delete both RIG-I and cGAS, cells were transduced with pooled lentiviruses. Next, we isolated a number of subclones for each cell line (control, RIG-I knock-out (KO), cGAS KO, and RIG-I/cGAS double KO (DKO)) by seeding at limiting dilution to find those with no detectable protein expression of the target genes. As B16-F10 cells are known to be a heterogeneous mixture of spindle-shaped and epithelial-like cells, we pooled the subclones with loss of RIG-I/cGAS protein expression, confirmed by Western blotting (Figure 4.1B-D), to avoid any clonal effect. Figure 4.2E depicts Western blot images of the four derived cell lines with deletion of RIG-I or cGAS, or their co-deletion that were used for subsequent experiments.

4.3.2 Both RIG-I and cGAS are indispensable to activate ISGs upon GSK343 treatment.

These cell lines were then treated with vehicle or 2 μ M GSK343 for four days in culture. We extracted total RNA and performed qRT-PCR for three IFN-stimulated genes (ISGs), *Ifih1*, *Isg15*, and *Ifitm3*, to elucidate the role of RIG-I and cGAS in immune signaling upon GSK343 treatment. Whereas the control cells significantly upregulated all three ISGs, none of the three KO lines upregulated their expression (Figure 4.1F). Strikingly, the upregulation of the ISGs was completely abrogated in single KO lines, comparably to DKO. This suggests that both RIG-I and cGAS are required to signal upregulation of ISGs upon GSK343 in a non-redundant manner.

Next, we performed RNA-seq to ask if upregulation of a broader IFN signaling is abrogated in the KO cell lines transcriptome-wide. To annotate changes in gene expression with functional meaning, we performed GSEA. In the control cells, GSK343

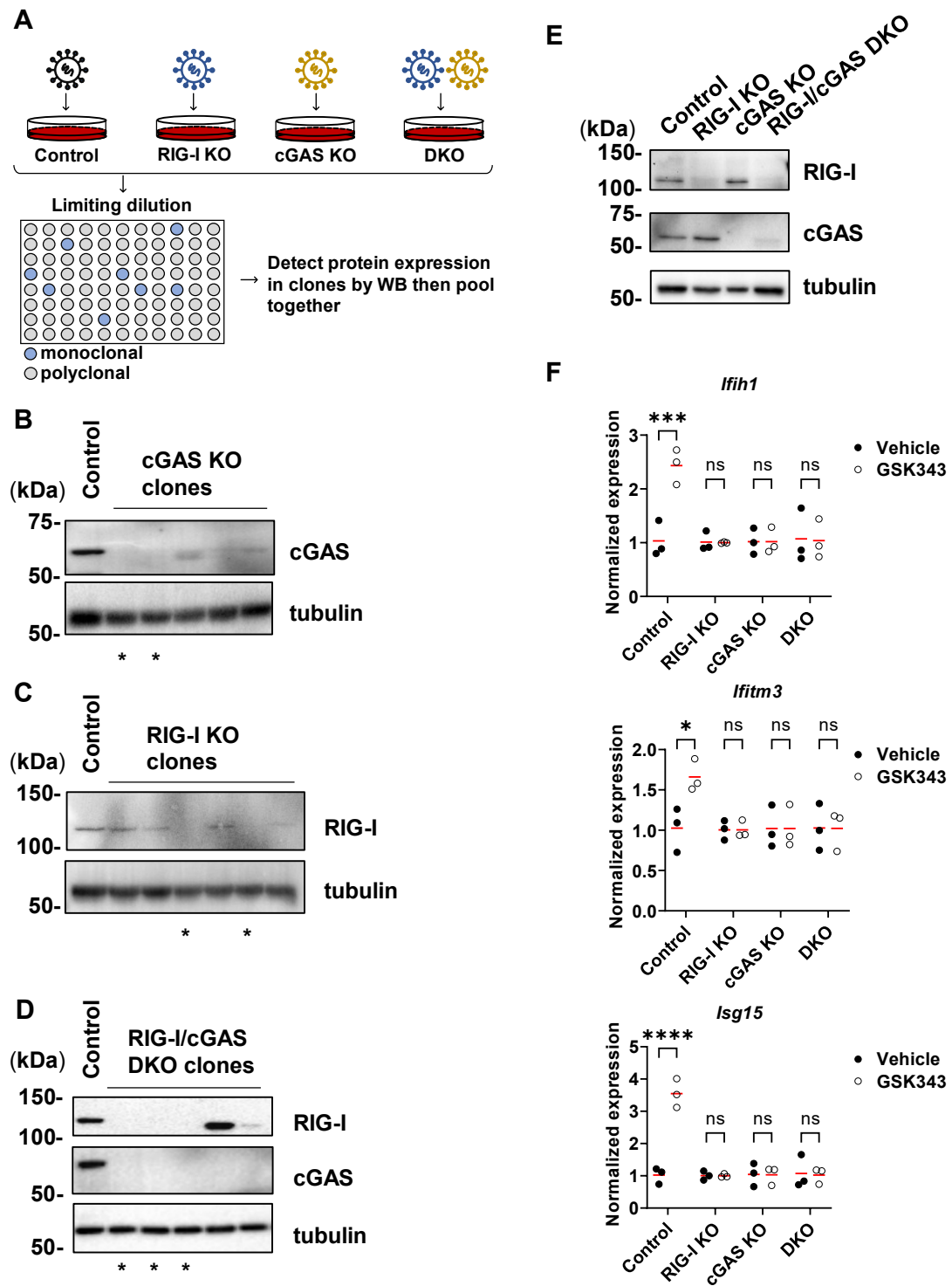


Figure 4.1: Generation of RIG-I/cGAS single or double KO B16-F10 melanoma cells and induction of ISGs upon GSK343 treatment.

Figure 4.1: Generation of RIG-I/cGAS single or double KO B16-F10 melanoma cells and induction of ISGs upon GSK343 treatment.

(A) Schematic describing lentiviral transduction and subcloning to isolate cells that are RIG-I/cGAS deficient. (B-D) Western blots of control vs. KO clones confirming lack of cGAS and/or RIG-I expression in samples denoted by *. (E) Western blots of control or pooled KO cells from (B-D). (F) qRT-PCR quantification of three indicated ISGs upon GSK343 treatment compared to vehicle. B16-F10 cells were treated with DMSO or 2 μ M GSK343 for four days. Expression was normalized to the average of DMSO treatment within each genotype.

treatment significantly upregulated pathways related to sterol metabolism and IFN activation, as seen by P values below the cut-off and top rank among thousands of gene sets tested (Figure 4.2A-B). While the sterol metabolic pathways were also upregulated (Figure 4.3C), IFN response pathways were not significantly upregulated despite GSK343 treatment in the KO cell lines. This is consistent with earlier results based on qRT-PCR. Furthermore, Figure 4.2C depicts a heatmap of the top 200 differentially expressed genes for each of the four cell lines upon GSK343 treatment compared to vehicle. We found that genes with a role in innate immune and IFN responses were among the most significantly upregulated genes in the control, as seen by dense vertical “barcodes” on the left of the heatmap that indicate the position of genes that belong in each gene set. In contrast, all the KO cell lines failed to upregulate such breadth of genes as seen by the sparse barcodes. Importantly, a number of repetitive elements were comparably induced in all four cell lines upon GSK343 treatment (Figure 4.2C). This confirms that deletion of RIG-I or cGAS (individually or in combination) did not affect EZH2 inhibition with GSK343 and subsequent derepression of repetitive elements. These findings suggest that activation of innate immune and interferon response genes is a key consequence of GSK343 treatment, and that both RIG-I and cGAS play a critical role in mediating such response.

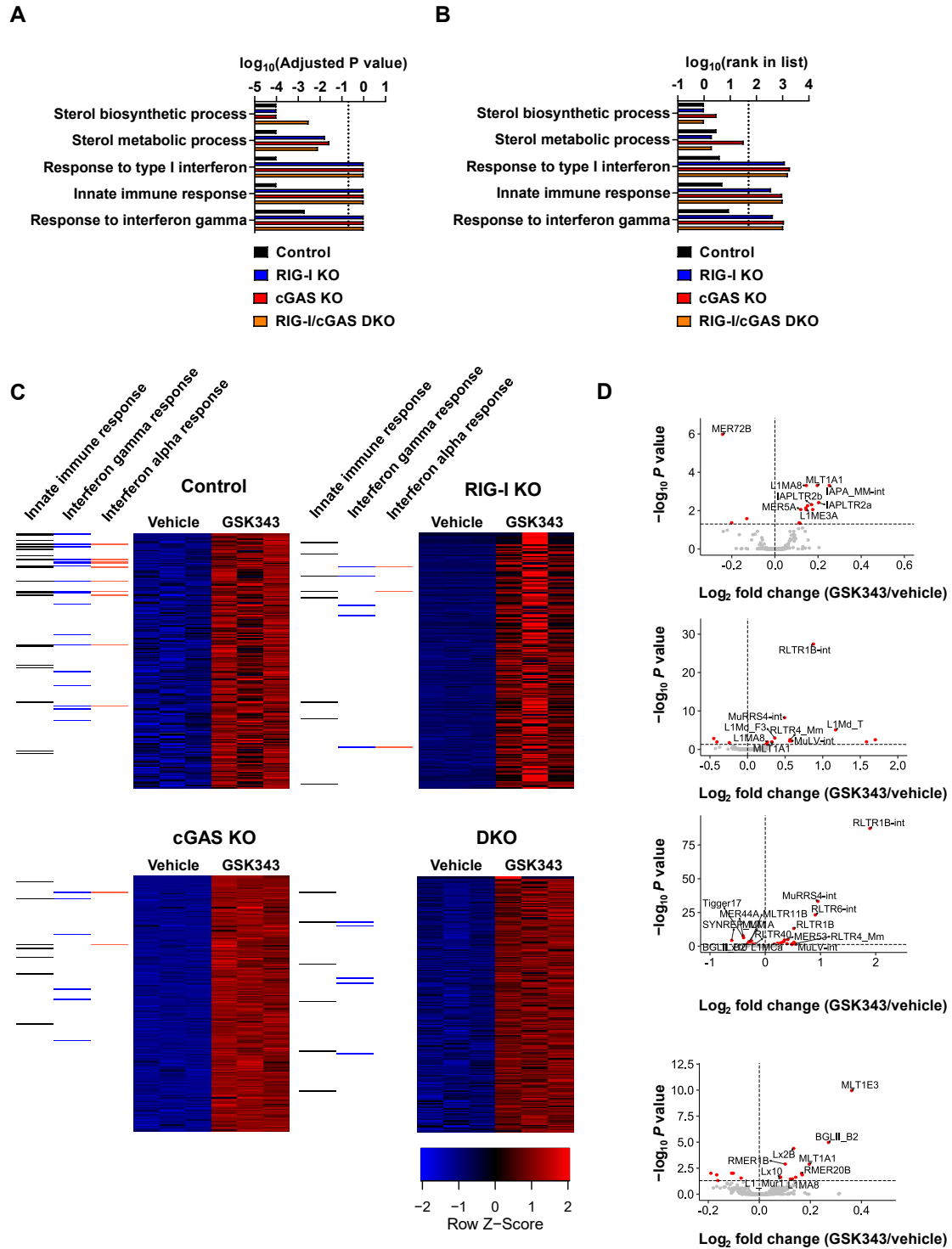


Figure 4.2: RIG-I and/or cGAS deletion blocks B16-F10 cells from significantly upregulating IFN and innate immune genes and pathways upon GSK343 treatment.

Figure 4.2: RIG-I and/or cGAS deletion blocks B16-F10 cells from significantly upregulating IFN and innate immune genes and pathways upon GSK343 treatment.

(A) Adjusted P values of indicated GO gene sets for each cell line. Vertical dotted line indicates cut-off at 0.2. (B) Position in ordered rank list of indicated GO gene sets for each cell line. Vertical dotted line indicates the 50th rank. (C) Vertical barcodes on the left of each heatmap indicates the position of genes that are annotated in the labelled gene sets. Each row represents a gene and the top 200 differentially upregulated genes are shown in order from top to bottom. Expression is shown as a Z-score of the mean of each row. (D) Volcano plots depicting significantly up- or downregulated (red) repetitive elements upon GSK343 treatment.

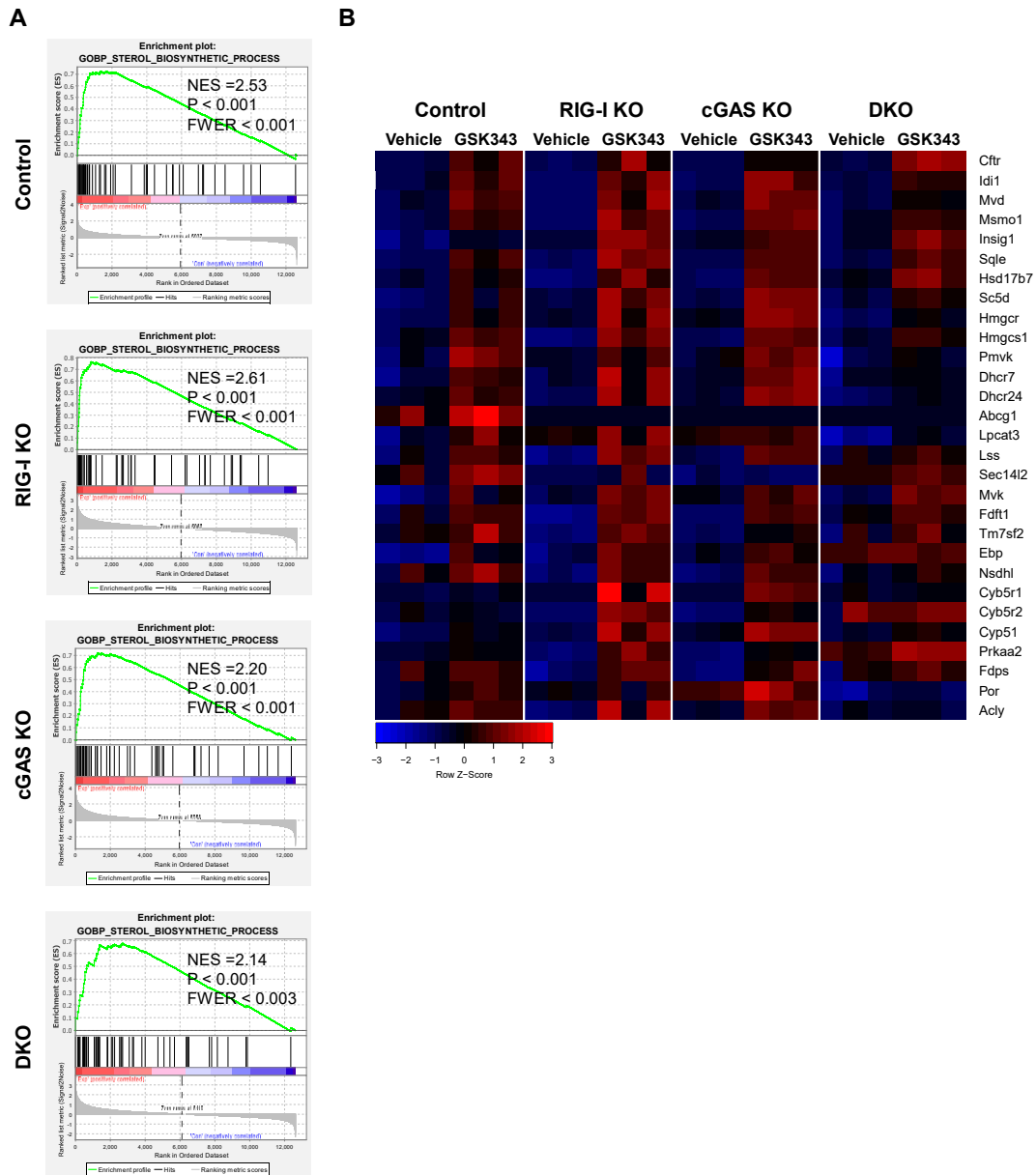


Figure 4.3: Sterol biosynthetic process gene set is commonly upregulated upon GSK343 treatment regardless of RIG-I/cGAS expression.

(A) GSEA plots showing significant, positive enrichment of sterol biosynthetic process pathway upon GSK343 treatment (GO biological process). (B) Expression heatmap of genes annotated in sterol biosynthetic process pathway. Expression is shown as a Z-score of the mean of each row.

4.4 Discussion

Through RNA-seq and gene expression profiling, we conclude that both RIG-I and cGAS are cytosolic PRRs that mediate IFN and innate immune signaling in B16-F10 melanoma cells upon EZH2 inhibition with GSK343 in culture. This finding is consistent with existing literature and complements other known functions of EZH2 in murine models of ICB therapy.

First, loss of FBXW7-mediated RIG-I stabilization has been shown to abrogate anti-tumour response to anti-PD-1 therapy against D4M3A murine melanoma cells *in vivo* (Gstalter et al., 2020). Although the mechanism of RIG-I stabilization is not clear, deletion of FBXW7 results in loss of RIG-I expression, reduced type I/II IFN signaling and tumour infiltrating cytotoxic T cells. Conversely, inducing MAVS aggregation, the downstream effect of RIG-I signaling, was sufficient to rescue the anti-tumour response through anti-PD-1 therapy. Furthermore, abrogated activity of cytosolic PRRs as a resistance mechanism may be relevant in human melanoma as FBXW7 loss of function was initially discovered in a metastatic melanoma patient who displayed resistance to anti-PD-1 in a single tumour site despite response in other disease sites.

Upregulation of sterol biosynthetic and metabolic gene sets, regardless of RIG-I or cGAS expression, serves as a positive control for EZH2 inhibition as it is a known consequence of EZH2 inhibition in various models. Treatment of B16-F10 melanoma cells with GSK126, an analog of GSK343, similarly upregulated these gene sets in an independent study (Zhang et al., 2022). It also showed loss of H3K27me3 at the promoters of a subset of genes in these gene sets. Similarly, upregulation of genes involved in cholesterol synthesis and corresponding loss of H3K27me3 at their promoters were observed upon EZH2 inhibition in hepatocellular carcinoma cell lines (Xu et al., 2021). Intriguingly, this paper also found that type I IFN signaling was one of the top upregulated gene sets. This reinforces the notion that cytosolic PRR-mediated detection of repetitive elements may be a general consequence of EZH2 inhibition. Lastly, silencing biosynthetic and metabolic genes may be a conserved function of EZH2 as its

pharmacological inhibition has been shown to induce lipid accumulation in zebrafish embryos (den Broeder et al., 2020).

To further investigate the role of the cytosolic PRRs, IFN and innate immune signaling in anti-tumour response *in vivo*, EZH2 function outside of silencing repetitive elements should be considered together. For example, in various mouse melanoma models, both tumour-infiltrating cytotoxic T cells and tumour cells upregulate PRC2 subunits and H3K27me3 upon IL-2 or anti-CTLA4 immunotherapy (Zingg et al., 2017). EZH2 inactivation (by drug inhibition or deletion) reduces aberrant histone methylation at genes coding antigen processing/presentation and chemokines in tumour cells. Ultimately, EZH2 inactivation synergizes with IL-2 or anti-CTLA4 immunotherapy to delay tumour growth and improve tumour-free survival. Furthermore, EZH2 inhibition has been shown to suppress regulatory T cell activity, which in turn promotes anti-tumour cytotoxic and helper T cell functions (DuPage et al., 2015; Wang et al., 2018; Yang et al., 2015). Elucidating the impact of EZH2-mediated silencing of non-coding, repetitive elements on response to immunotherapy may be confounded by the diversity of EZH2 function in immune cells, but may also reveal an unappreciated facet of EZH2 that can be leveraged to improve existing ICB therapies.

4.5 References

- Alegre, M.-L., Frauwirth, K.A., and Thompson, C.B. (2001). T-cell regulation by CD28 and CTLA-4. *Nat Rev Immunol* 1, 220–228. <https://doi.org/10.1038/35105024>.
- Brahmer, J.R., Tykodi, S.S., Chow, L.Q.M., Hwu, W.-J., Topalian, S.L., Hwu, P., Drake, C.G., Camacho, L.H., Kauh, J., Odunsi, K., et al. (2012). Safety and activity of anti-PD-L1 antibody in patients with advanced cancer. *N Engl J Med* 366, 2455–2465. <https://doi.org/10.1056/NEJMoa1200694>.
- den Broeder, M.J., Ballangby, J., Kamminga, L.M., Aleström, P., Legler, J., Lindeman, L.C., and Kamstra, J.H. (2020). Inhibition of methyltransferase activity of enhancer of zeste 2 leads to enhanced lipid accumulation and altered chromatin status in zebrafish. *Epigenetics & Chromatin* 13, 5. <https://doi.org/10.1186/s13072-020-0329-y>.
- Chiappinelli, K.B., Strissel, P.L., Desrichard, A., Li, H., Henke, C., Akman, B., Hein, A., Rote, N.S., Cope, L.M., Snyder, A., et al. (2015). Inhibiting DNA Methylation Causes an Interferon Response in Cancer via dsRNA Including Endogenous Retroviruses. *Cell* 162, 974–986. <https://doi.org/10.1016/j.cell.2015.07.011>.

- DuPage, M., Chopra, G., Quiros, J., Rosenthal, W.L., Morar, M.M., Holohan, D., Zhang, R., Turka, L., Marson, A., and Bluestone, J.A. (2015). The Chromatin-Modifying Enzyme Ezh2 Is Critical for the Maintenance of Regulatory T Cell Identity after Activation. *Immunity* 42, 227–238. <https://doi.org/10.1016/j.immuni.2015.01.007>.
- Goubau, D., Deddouche, S., and Reis e Sousa, C. (2013). Cytosolic sensing of viruses. *Immunity* 38, 855–869. <https://doi.org/10.1016/j.immuni.2013.05.007>.
- Gstalter, C., Liu, D., Miao, D., Lutterbach, B., DeVine, A.L., Lin, C., Shettigar, M., Pancholi, P., Buchbinder, E.I., Carter, S.L., et al. (2020). Inactivation of Fbxw7 Impairs dsRNA Sensing and Confers Resistance to PD-1 Blockade. *Cancer Discovery* 10, 1296–1311. <https://doi.org/10.1158/2159-8290.CD-19-1416>.
- Herbst, R.S., Soria, J.-C., Kowanetz, M., Fine, G.D., Hamid, O., Gordon, M.S., Sosman, J.A., McDermott, D.F., Powderly, J.D., Gettinger, S.N., et al. (2014). Predictive correlates of response to the anti-PD-L1 antibody MPDL3280A in cancer patients. *Nature* 515, 563–567. <https://doi.org/10.1038/nature14011>.
- Larkin, J., Chiarion-Sileni, V., Gonzalez, R., Grob, J.-J., Rutkowski, P., Lao, C.D., Cowey, C.L., Schadendorf, D., Wagstaff, J., Dummer, R., et al. (2019). Five-Year Survival with Combined Nivolumab and Ipilimumab in Advanced Melanoma. *New England Journal of Medicine* 381, 1535–1546. <https://doi.org/10.1056/NEJMoa1910836>.
- Lenschow, D.J., Walunas, T.L., and Bluestone, J.A. (1996). CD28/B7 system of T cell costimulation. *Annu Rev Immunol* 14, 233–258. <https://doi.org/10.1146/annurev.immunol.14.1.233>.
- Liu, M., Thomas, S.L., DeWitt, A.K., Zhou, W., Madaj, Z.B., Ohtani, H., Baylin, S.B., Liang, G., and Jones, P.A. (2018). Dual Inhibition of DNA and Histone Methyltransferases Increases Viral Mimicry in Ovarian Cancer Cells. *Cancer Res* 78, 5754–5766. <https://doi.org/10.1158/0008-5472.CAN-17-3953>.
- Morel, K.L., Sheahan, A.V., Burkhart, D.L., Baca, S.C., Boufaied, N., Liu, Y., Qiu, X., Cañadas, I., Roehle, K., Heckler, M., et al. (2021). EZH2 inhibition activates a dsRNA-STING-interferon stress axis that potentiates response to PD-1 checkpoint blockade in prostate cancer. *Nat Cancer* 2, 444–456. <https://doi.org/10.1038/s43018-021-00185-w>.
- Motzer, R.J., Rini, B.I., McDermott, D.F., Redman, B.G., Kuzel, T.M., Harrison, M.R., Vaishampayan, U.N., Drabkin, H.A., George, S., Logan, T.F., et al. (2015). Nivolumab for Metastatic Renal Cell Carcinoma: Results of a Randomized Phase II Trial. *J Clin Oncol* 33, 1430–1437. <https://doi.org/10.1200/JCO.2014.59.0703>.
- Roulois, D., Loo Yau, H., Singhania, R., Wang, Y., Danesh, A., Shen, S.Y., Han, H., Liang, G., Jones, P.A., Pugh, T.J., et al. (2015). DNA-Demethylating Agents Target Colorectal Cancer Cells by Inducing Viral Mimicry by Endogenous Transcripts. *Cell* 162, 961–973. <https://doi.org/10.1016/j.cell.2015.07.056>.

Sharpe, A.H., and Pauken, K.E. (2018). The diverse functions of the PD1 inhibitory pathway. *Nat Rev Immunol* 18, 153–167. <https://doi.org/10.1038/nri.2017.108>.

Subramanian, A., Tamayo, P., Mootha, V.K., Mukherjee, S., Ebert, B.L., Gillette, M.A., Paulovich, A., Pomeroy, S.L., Golub, T.R., Lander, E.S., et al. (2005). Gene set enrichment analysis: A knowledge-based approach for interpreting genome-wide expression profiles. *PNAS* 102, 15545–15550. <https://doi.org/10.1073/pnas.0506580102>.

Topalian, S.L., Drake, C.G., and Pardoll, D.M. (2015). Immune checkpoint blockade: a common denominator approach to cancer therapy. *Cancer Cell* 27, 450–461. <https://doi.org/10.1016/j.ccell.2015.03.001>.

Wang, D., Quiros, J., Mahuron, K., Pai, C.-C., Ranzani, V., Young, A., Silveria, S., Harwin, T., Abnousian, A., Pagani, M., et al. (2018). Targeting EZH2 Reprograms Intratumoral Regulatory T Cells to Enhance Cancer Immunity. *Cell Reports* 23, 3262–3274. <https://doi.org/10.1016/j.celrep.2018.05.050>.

Wolchok, J.D., Chiarion-Sileni, V., Gonzalez, R., Rutkowski, P., Grob, J.-J., Cowey, C.L., Lao, C.D., Wagstaff, J., Schadendorf, D., Ferrucci, P.F., et al. (2017). Overall Survival with Combined Nivolumab and Ipilimumab in Advanced Melanoma. *N Engl J Med* 377, 1345–1356. <https://doi.org/10.1056/NEJMoa1709684>.

Xu, X., Chen, J., Li, Y., Yang, X., Wang, Q., Wen, Y., Yan, M., Zhang, J., Xu, Q., Wei, Y., et al. (2021). Targeting epigenetic modulation of cholesterol synthesis as a therapeutic strategy for head and neck squamous cell carcinoma. *Cell Death Dis* 12, 1–15. <https://doi.org/10.1038/s41419-021-03760-2>.

Yang, X.-P., Jiang, K., Hirahara, K., Vahedi, G., Afzali, B., Sciume, G., Bonelli, M., Sun, H.-W., Jankovic, D., Kanno, Y., et al. (2015). EZH2 is crucial for both differentiation of regulatory T cells and T effector cell expansion. *Sci Rep* 5, 10643. <https://doi.org/10.1038/srep10643>.

Zhang, T., Guo, Z., Huo, X., Gong, Y., Li, C., Huang, J., Wang, Y., Feng, H., Ma, X., Jiang, C., et al. (2022). Dysregulated lipid metabolism blunts the sensitivity of cancer cells to EZH2 inhibitor. *EBioMedicine* 77. <https://doi.org/10.1016/j.ebiom.2022.103872>.

Zingg, D., Arenas-Ramirez, N., Sahin, D., Rosalia, R.A., Antunes, A.T., Haeusel, J., Sommer, L., and Boyman, O. (2017). The Histone Methyltransferase Ezh2 Controls Mechanisms of Adaptive Resistance to Tumor Immunotherapy. *Cell Reports* 20, 854–867. <https://doi.org/10.1016/j.celrep.2017.07.007>.

Chapter 5

5 Discussion

5.1 Summary of findings

This thesis investigates the mechanisms that either control or act downstream of chromatin regulatory complexes recruited by the RB-E2F1 complex. My work suggests that non-CDK phosphorylation of RB regulates its interaction with condensin II and subsequent chromosome condensation. In addition, I have shown that cytosolic pattern recognition receptors (PRRs) mediate downstream viral mimicry response in splenic B cells upon EZH2 inhibition. Overall, this thesis elucidates previously unappreciated facets of chromatin regulatory complexes recruited by RB.

Chapter 2 identifies S838/T841 as non-CDK phosphorylation sites in the RB C-terminus (RBC) that are regulated by T cell receptor (TCR) signaling. p38 MAPK is activated by TCR signaling and can directly phosphorylate RB at these sites. Chromatin recruitment of RB, E2F1 and condensin II is regulated by RB S838/T841 phosphorylation. In line with known functions of condensin II, its dissociation from chromatin results in chromatin decondensation upon TCR signaling and RB phosphorylation.

In chapter 3, the effect of EZH2 inhibition and its mechanism are investigated. EZH2 inhibition with a pharmacological inhibitor upregulates expression of repetitive elements in splenic B cells and eliminates them *in vivo*. Mutant mice with abrogated cytosolic PRR function are partly protected from such B cell death. While EZH2 inhibition reduces target histone methylation levels at repetitive elements in both WT and mutant B cells, the mutants fail to upregulate chemokines that attract T cells and neutrophils. Indeed, infiltration of cytotoxic T cells and neutrophils is diminished, and B cell survival is higher in the mutants compared to WT upon EZH2 administration *in vivo*.

Chapter 4 investigates the dependence of viral mimicry upon EZH2 inhibition on cytosolic PRRs in B16-F10 melanoma cells. The parental melanoma cells robustly upregulate innate and interferon (IFN) responses upon EZH2 inhibition. In contrast,

ablation of either RIG-I or cGAS inactivates such gene expression despite comparable misexpression of repetitive elements in all cell lines.

5.2 Diverse RB functions are regulated by phosphorylation

The classic model of RB regulation by phosphorylation is that cyclin-CDK complexes hyperphosphorylate RB, which disrupts its repression of E2F transcription factors (Burke et al., 2010; Chellappan et al., 1991; Lundberg and Weinberg, 1998; Mittnacht, 1998). However, recent literature suggests that RB phosphorylation regulates RB in other ways. For example, p38 MAPK phosphorylates RB at S249/T252 in response to chemical stress, which promotes RB-E2F interaction and blocks proliferation (Gubern et al., 2016). Biochemically, S249/T252 phosphorylation is predicted to create an alternate interaction site between RB and E2F even in the presence of high cyclin-CDK activity and RB hyperphosphorylation. Overexpression of an RB construct with S249E/T252E phosphomimetic substitutions has also been shown to reduce cancer cell proliferation. This demonstrates how non-CDK phosphorylation of RB can balance CDK phosphorylation-induced cell cycle progression upon chemical stress. However, this is not to say that CDK phosphorylation of RB merely regulates its cell cycle control. Various mono-phosphorylated (mP) RB species at its CDK sites have distinct interactions and functions (Sanidas et al., 2019). For example, S811 mP RB binds to various components of the nucleosome remodeling and deacetylase (NuRD) complex, in contrast to hypophosphorylated or T373, S780, T826 mP-RB. Functionally, RB-NuRD interaction represses transcription of DNA damage response genes. In addition, S811, T821 or T826 mP-RB promotes expression of genes involved in oxidative phosphorylation, and cells expressing these mP-RB species show higher rate of cellular respiration. Lastly, RB S249/T252 phosphorylation by cyclin-CDKs enables its repression of a NF- κ B family protein, p65 (Jin et al., 2019). This phosphorylation promotes RB-p65 interaction and sequesters p65 from activating its target genes. Notably, p65 repression by RB downregulates immune checkpoint genes such as *PD-L1* in prostate cancer cells that aids tumour immune evasion. Therefore, this is yet another facet of RB's tumour suppressive role mediated through a separate mechanism from its repression of E2F transcription factors. In line with these examples, the discovery of RB S838/T841 phosphorylation by

p38 MAPK as a regulatory mechanism of chromosome decondensation is an insightful addition to the growing diversity of RB function.

5.3 p38 MAPK-mediated RB phosphorylation in early development

Existing phosphoproteomic data provided a rationale for investigating poorly characterized RB phosphorylation in Jurkat leukemia T cells upon TCR signaling (Mayya et al., 2009). Defective thymocyte development in mice carrying the *nessy* allele of CAP-H2, one of the subunits of condensin II, further hinted that chromatin condensation is a key process in T cells (Gosling et al., 2007; Rawlings et al., 2011). However, given the general paucity of detailed molecular evidence for phosphorylation of the RB C-terminus (RBC), it may be that RB S838/T841 phosphorylation is highly specific to cell types or stimuli (Hornbeck et al., 2012). For example, Gubern *et al.* reported that p38 MAPK only phosphorylated S249/T252 in the RB N-terminus in MEFs upon chemical stress (Gubern et al., 2016). This presents a discrepancy with the data presented in chapter 2, but substantial differences in cell type and stimulation may be the cause (Figure 2.3B). On the other hand, this also raises the question whether p38-mediated RB phosphorylation plays a role in different contexts.

Similarities between embryonic lethality of RB and p38 α MAPK suggest that p38-mediated RB phosphorylation may be required during early development. Both *Rbl*^{-/-} and *p38 α* ^{-/-} fetuses fail to develop past E16 with the earliest sign of growth retardation evident at E10.5-11.5 (Clarke et al., 1992; Lee et al., 1992; Mudgett et al., 2000; Tamura et al., 2000). Between E12.5-13.5, the number of hepatocytes is reduced and the size of fetal livers of the mutants are smaller compared to WT. This is associated with abnormal erythropoiesis of erythrocytes that occurs mostly in the liver starting at midgestation. Around E15, nucleated erythrocytes mature into enucleated erythrocytes in WT, but in *Rbl*^{-/-} and *p38 α* ^{-/-} fetal liver and peripheral blood, immature nucleated erythrocytes are dominant. In addition, conditional RB loss in the liver increases the susceptibility to carcinogen-induced liver tumourigenesis in adult mice (Mayhew et al., 2007). Similarly, low p38 MAPK activity has been associated with human hepatocellular carcinoma (Iyoda

et al., 2003). These studies suggest that an interplay between RB and p38 MAPK may be relevant in normal development and proliferative control of hepatocytes.

Furthermore, the mutants share placental defects where the thickness of the labyrinth layer is reduced, and lacks vascularization compared to WT (del Barco Barrantes et al., 2011; Mudgett et al., 2000; Wenzel et al., 2007). As demonstrated in chapter 2, p38 MAPK can directly phosphorylate RB and regulate its localization to chromatin and condensin II-mediated chromosome condensation. The observation that homozygous loss of *Rb1* and *p38α* results in very similar defects suggests that they function together in a common pathway that is crucial for embryonic development. Future investigation of p38-mediated RB phosphorylation in midgestational embryos may reveal novel RB functions.

5.4 Structural changes to the RB-E2F1 complex and its chromatin dissociation upon S838/T841 phosphorylation

A set of structural changes to the RB-E2F1 complex upon S838/T841 phosphorylation must underlie its dissociation from chromatin. Curiously, RB and E2F1 retained interaction with each other based on co-immunoprecipitation experiments (Figure 2.4C). Based on a crystal structure of the RBC-E2F1-DP1 complex, S838/T841 phosphorylation occurs in the loop region of a strand-loop-helix structure composed of 32 “core” residues in the RBC (Rubin et al., 2005). While the loop does not contribute significantly to intermolecular contacts, various side chains of the strand and the helix form hydrogen bonds and van der Waals interactions with the marked box domains (MBDs) of E2F1 and DP1. Therefore, electrostatic forces of S838/T841 phosphorylation at the loop likely disrupts these interactions. Despite this, RB and E2F1 must still be able to retain interaction through the pocket-transactivation domain (TAD). Such alternate RB-E2F1 complex appears to be incompatible with its own and condensin II chromatin localization (Figure 2.5A).

This is reminiscent of post-translation modifications that dictate RB-E2F1 interaction upon etoposide-induced DNA damage response in U2OS cells (Carnevale et al., 2012). Various serine phosphorylation and lysine methylation of E2F1 contribute to

forming free E2F1, while RB S364 phosphorylation is found exclusively in RB-E2F1 complexes. Importantly, both free and RB-bound E2F1 are required to fully upregulate apoptotic genes and induce cell death, which suggests that distinct structures perform non-redundant functions in this context.

Chromatin sonication as a read-out for chromatin compaction has been reported previously (Rawlings et al., 2011). Importantly, availability of sonication-resistant chromatin through gel electrophoresis negatively correlates with molecular accessibility of anti-histone tail antibodies *in situ*. A higher resolution characterization of chromosome decondensation upon RB S838/T841 phosphorylation and condensin II dissociation would be possible through assay for transposase-accessible chromatin (ATAC) with high throughput sequencing. A bacterial transposase, Tn5, can be integrated more readily into accessible regions over highly compact ones (Li et al., 2020). Adaptor ligation, which occurs simultaneously with Tn5 integration, subsequent sequencing and read mapping will reveal precise loci that are preferentially decondensed. Furthermore, changes in the three-dimensional organization of DNA upon RB phosphorylation and condensin II dissociation can be quantified by Hi-C (van Berkum et al., 2010). In this assay, high throughput sequencing of ligated, chimeric DNA captures linear and non-linear DNA interactions genome wide. As the RB-E2F1-condensin II complex has been shown to regulate long range chromosome interactions in MEFs, loss of such interactions may also underlie the overall chromosome decondensation described in chapter 2 (Marshall et al., 2020).

5.5 The RIC mutant mouse model

The RIC mutant mice described in chapter 3 are an indispensable model required to gain the mechanistic insight into the role of upregulated repetitive elements and its consequences upon EZH2 inhibition. In particular, it would have been impossible to determine without these mice that the cytosolic pattern recognition receptors (PRRs) mediate a viral mimicry response that results in infiltration of cytotoxic T cells and neutrophils, accompanied by B cell death in the spleen. This model has not only served as an important tool for this thesis, but it also represents a realization of technical application of CRISPR-Cas9 *in vivo*. Although the methodology to generate compound

mutant mice through CRISPR-Cas9 has been described a few years ago, its real-life application to test biological questions is scarce in the literature (Wang et al., 2013).

In addition to their utility in this thesis, the functional deficiency of the RIC mutant mice makes them an attractive model to further study non-canonical functions of RB. For example, *Rb1^{ΔS}* splenocytes misexpress repetitive elements and the mice eventually succumb to splenic lymphoma (Ishak et al., 2016). This is in line with known tumourigenic potential of derepressed repetitive elements. Considering how the cytosolic PRRs are required to induce splenic B cell death upon EZH2 inhibition and subsequent misexpression of repetitive elements, functional PRRs in *Rb1^{ΔS}* splenocytes may initially trigger an immune elimination of repeat-misexpressing cells, and block tumourigenesis. One may hypothesize that the immune system becomes desensitized to PRR signaling over time, allowing the tumourigenic potential of depressed repetitive elements to be realized in aged mice. Indeed, cytotoxic T cell exhaustion was initially described in chronic viral infection in mice (Gallimore et al., 1998; Zajac et al., 1998). The late onset of splenic lymphomas in *Rb1^{ΔS}* mice is also consistent with the fact that T cell exhaustion entails progressive and hierarchical loss of functions such as decreased proliferation and production of IL-2, TNF- α and IFN- γ (Ishak et al., 2016; Wherry, 2011). *Rb1^{ΔS}*/RIC compound mutant mice would lack the initially tumour suppressive function of the cytosolic PRRs compared to *Rb1^{ΔS}* mice, allowing this question to be tackled mechanistically.

Furthermore, functional deficiency of cGAS in the RIC mutants can be used to further explore the genome instability phenotype in the *Rb1^{ΔL}* model. Although genome instability is a characteristic of many cancers, the *Rb1^{ΔL}* mice do not spontaneously develop tumours (Isaac et al., 2006; Negrini et al., 2010). However, the *Rb1^{ΔL}* allele significantly decreases the time of onset of thymic lymphoma in *Trp53^{-/-}* background, which underscores the tumourigenic potential of genome instability (Coschi et al., 2014). This suggests that a protective mechanism may be detecting and eliminating aneuploid cells before they become neoplastic. Intriguingly, cGAS detect dsDNA of micronuclei, created from lagging chromosomes or DNA damage, and activates an innate immune signaling specifically in cells containing micronuclei (Mackenzie et al., 2017). Therefore,

combining cGAS deficiency with *Rbl^{4L}* mutation may create an interesting model to study tumour susceptibility due to genome instability *in vivo*.

5.6 Diverse consequences of pharmacological EZH2 inhibition

The original pharmacological EZH2 inhibitor was designed to target somatic heterozygous mutations in the catalytic domain of EZH2 that occur frequently in diffuse large B cell lymphoma (DLBCL) and follicular lymphoma (FL) (McCabe et al., 2012a; Verma et al., 2012). Mutant EZH2 gain altered substrate preference that leads to increased H3K27me₃, thus the rationale was to counteract such deregulated activity as a means of therapy (McCabe et al., 2012b; Yap et al., 2011). Indeed, treating DLBCL cell lines with GSK126 inhibited growth of EZH2 mutant lymphoma cell lines both in culture and *in vivo*. More importantly, patients with relapsed or refractory, EZH2 mutant FL have shown durable response to GSK126 monotherapy, which is now approved by the FDA (Morschhauser et al., 2020).

Since then, pharmacological EZH2 inhibition has been tested in various experimental models, and its consequences are diverse. For instance, this thesis demonstrates that EZH2 inhibition activates anti-viral immune signaling through cytosolic PRRs in resting splenic B cells and mouse melanoma cells. Indeed, such viral mimicry response has been described in cancer models upon inhibition of epigenetic silencers as discussed earlier (Chiappinelli et al., 2015; Liu et al., 2018; Morel et al., 2021; Roulois et al., 2015). Furthermore, EZH2 inhibition in small cell lung cancer (SCLC) cells has been shown to upregulate ERV expression, IFN signaling, and promote lineage plasticity into non-neuroendocrine cells (Mahadevan et al., 2021). It also synergizes with cGAS-STING activation to reduce tumour burden in syngeneic mice. Indeed, STING agonists alone can activate T and natural killer cells to eliminate glioblastoma and malignant pleural mesothelioma cells, respectively (Berger et al., 2022; Knelson et al., 2022). Importantly, tumour-immune infiltration is strongly associated with expression of dsRNA transcribed from ERVs in patient tumour samples in The Cancer Genome Atlas (TCGA) database across various tissues (Cañadas et al., 2018). While these studies are examples that support the central model of this thesis, that

pharmacological EZH2 inhibition and subsequent derepressed repetitive elements activate an immune response through PRRs, the next section briefly considers the effect of EZH2 inhibition in different contexts.

Systemic administration of EZH2 inhibitors has been shown relieve intestinal inflammation, or colitis, and colitis-associated cancer (CAC) in mouse models (Zhou et al., 2019). Chronic, relapsing gastrointestinal inflammation is the defining characteristic of inflammatory bowel disease (IBD), which is a key risk factor for developing colorectal cancer (Ullman and Itzkowitz, 2011). Administering dextran sodium sulphate (DSS) in drinking water is the gold standard for studying colitis and CAC in mice as their pathology resembles human IBD closely (Wirtz et al., 2017). Intravenous injection of EZH2 inhibitors, GSK126 or GSK343, was shown to both prophylactically and therapeutically improve the disease burden of DSS-induced colitis based on intestinal histology, weight loss and survival. Mechanistically, this effect is dependent on infiltration of CD11b⁺ Gr-1⁺ myeloid-derived suppressor cells (MDSCs) as their depletion negated any anti-inflammatory effect of EZH2 inhibition *in vivo*.

Importantly, resistance to DSS-induced colitis is specific to acute EZH2 inhibition as its constitutive loss has been shown to paradoxically promote DSS-induced colitis (Liu et al., 2017). This earlier study found that EZH2 was downregulated in intestinal epithelial cells (IECs) in IBD patients compared to healthy controls. In addition, genetic EZH2 ablation in IECs exacerbated DSS-induced colitis, and promoted expression of TNF- α , IL-6 and IFN- γ , which are pro-inflammatory cytokines. Conversely, overexpression of EZH2 in IECs reduced morbidity and pro-inflammatory cytokines in the colon upon DSS-induced colitis compared to controls expressing baseline EZH2. Mechanistically, EZH2 was required in IECs to modulate NF- κ B signaling upon its activation by TNF- α . Taken together, these studies demonstrate the disparity in outcome between pharmacological EZH2 inhibition and its complete ablation even in the same disease model.

Disrupted development and activation are the most well-known consequences of EZH2 loss-of-function in B cells. Conditional loss of EZH2 has been shown to decrease

precursor B cells in the bone marrow (Su et al., 2003). Mechanistically, EZH2 is required for immunoglobulin heavy chain recombination during progenitor to precursor B cell transition, as expression of a heavy chain transgene rescues this defect. More recent work has shown that EZH2-mediated gene silencing is required for germinal center (GC) formation. T cell mediated, antigen-dependent activation of naive B cells occurs in the interfollicular zone in lymph nodes (De Silva and Klein, 2015). GC B cells become highly proliferative and undergo processes such as somatic hypermutation and affinity maturation that ultimately select for clones that produce high affinity antibodies against the initial antigen. Mice with selective EZH2 deficiency in GC B cells were unable to form GCs upon immune stimulation with sheep red blood cells or nitrophenyl-keyhole limpet hemocyanin, well-established agents that activate the humoral immune system (Béguelin et al., 2013; Ladics et al., 1995, 1998). Pharmacological inhibition of EZH2 by intraperitoneal injections after immunization similarly abrogated GC formation and high affinity antibody production in WT mice. Conversely, mice expressing mutant EZH2 in GC B cells displayed hyperplastic GCs associated with global increase in H3K27me3 compared to control (Béguelin et al., 2013). This is consistent with the fact that GC B cells give rise to a large portion of DLBCL based on gene expression profiling and that EZH2 mutation is found frequently in such GC B cell-derived DLBCL (Alizadeh et al., 2000; Morin et al., 2010). siRNA or shRNA-mediated depletion of mutant EZH2 abrogated their proliferation. The role of mutant EZH2 as the oncogenic driver is specific to GC B cell-derived DLBCL as EZH2 inhibition (by genetic ablation or pharmacological inhibitors) was shown to be ineffective against activated B cell DLBCL subtype (Béguelin et al., 2013).

Overall, these studies outline the function of EZH2 in B cell development and differentiation into GC B cells, and the consequences following its inhibition. Therefore, this thesis provides valuable insight into a new facet of EZH2 function of repressing repetitive elements in resting splenic B cells.

5.7 Implications for the use of EZH2 inhibitors in the clinic

Viral mimicry upon EZH2 inhibition in splenic B cells may represent an unappreciated therapeutic vulnerability for FL and DLBCL. EZH2 inhibition was initially a therapeutic strategy for lymphoma with EZH2 activating mutations in its catalytic SET domain. Indeed, DLBCL lines harbouring EZH2 mutations were the most sensitive to GSK126 compared to EZH2 WT counterparts (McCabe et al., 2012a). This was mirrored in the clinic that showed that the objective response rate to tazemetostat was nearly double in EZH2 mutant versus EZH2 WT FL patients (Morschhauser et al., 2020).

However, the therapeutic benefit and the mechanism of action of tazemetostat in SMARCB1 (also called SNF5, INI1 and BAF47)-deficient cancers have revealed its utility against EZH2 WT cancers (Italiano, 2020; Stacchiotti et al., 2019). SMARCB1 is one of the subunits of the SWI/SNF chromatin remodeling complex (Kadoch and Crabtree, 2015). The antagonistic relationship between the SWI/SNF complex and PRC2 complex was first discovered in *Drosophila* (Kadoch et al., 2016). Genes coding the trithorax group proteins, some of which are homologs of the mammalian SWI/SNF complex, promote homeotic (*Hox*) gene expression, whereas the polycomb group genes (PcGs) repress them (Kennison, 1995; Kennison and Tamkun, 1988; Lewis, 1978). The SWI/SNF complex depends on ATP hydrolysis to facilitate nucleosome sliding, destabilization and ejection from chromatin, thus activating gene transcription (Clapier and Cairns, 2009; Kwon et al., 1994; Narlikar et al., 2013).

Clinical data has shown that SMARCB1 is often mutated or deleted in atypical teratoid/rhabdoid tumours (ATRT), malignant rhabdoid tumours (MRTs) and epithelioid sarcomas (ES) (Alimova et al., 2013; Biegel et al., 1999, 2002; Hornick et al., 2009; Sullivan et al., 2013; Versteeg et al., 1998). Given the relationship between the SWI/SNF complex and PRC2, it was postulated that SMARCB1 loss of function would confer oncogenic dependency on PRC2 activity in these cancers. Indeed, preclinical studies showed that pharmacological EZH2 inhibitor treatment suppresses ATRT and MRT proliferation and promotes apoptosis (Alimova et al., 2013; Knutson et al., 2013). Although these findings were not translated to the clinic for rhabdoid tumours, a subset of

advanced or metastatic ES patients showed partial or durable response to tazemetostat treatment (Italiano et al., 2018; Schoffski et al., 2017; Stacchiotti et al., 2019).

Taken together, these studies provide proof-of-principle evidence that pharmacological EZH2 inhibition can induce synthetic lethality to target human cancer even in the absence of direct EZH2 mutations. This thesis shows that chemokine expression by splenic B cells upon GSK343 treatment promotes infiltration of cytotoxic T cells into the spleen. Gene expression profile of these B cells closely resemble that of EBV infected B cells, and EBV-specific T cell response has been documented during symptomatic and asymptomatic EBV primary infections (Long et al., 2019). Thus, one may reasonably hypothesize that EZH2 WT DLBCL or FL can be targeted by combining EZH2 inhibitor treatment with immunotherapy to elicit cell-extrinsic mechanisms that can eliminate cancer cells. For example, monoclonal antibodies such as ipilimumab, nivolumab and pembrolizumab inactivate immune checkpoints in cytotoxic T cells that block and attenuate their activity to reduce collateral damage and to maintain immune tolerance (Ribas and Wolchok, 2018). Sustained chemokine expression by malignant B cells treated with EZH2 inhibitors and matching cytotoxic T cell activity through immune checkpoint blockade appear to be plausible based on the literature and the findings presented in this thesis.

5.8 Final summary

This thesis elucidates the mechanisms that either control or act downstream of chromatin regulatory complexes recruited by the RB-E2F1 complex. First, non-CDK phosphorylation of RB at S838/T841 by p38 MAPK is inducible upon TCR signaling. This leads to dissociation of RB, E2F1 and condensin II from chromatin, which results in chromatin decondensation. Importantly, RB S838/T841 phosphorylation is crucial in these effects. Second, EZH2, recruited by the RB-E2F1 complex to various repetitive elements, suppresses their expression in splenic B cells. Upon its pharmacological inhibition *in vivo*, derepressed repetitive elements stimulate cytosolic PRRs, which in turn activate immune signaling and chemokine expression that attract inflammatory immune cells and eliminate splenic B cells. The cytosolic PRRs also mediate IFN signaling in cancer cells upon EZH2 inhibition.

Overall, this thesis expands our understanding of chromatin regulatory complexes recruited by RB. Phosphorylation as a regulatory mechanism for RB-E2F1-condensin II interaction on chromatin and chromatin condensation suggests that it may have similar roles in different contexts. Induction of viral mimicry upon EZH2 inhibition in resting splenic B cells reveals a pathway previously unappreciated in these cells that may be leveraged to target B cell lymphoma in novel ways.

5.9 References

- Alimova, I., Birks, D.K., Harris, P.S., Knipstein, J.A., Venkataraman, S., Marquez, V.E., Foreman, Nicholas K., and Vibhakar, R. (2013). Inhibition of EZH2 suppresses self-renewal and induces radiation sensitivity in atypical rhabdoid teratoid tumor cells. *Neuro-Oncology* *15*, 149–160. <https://doi.org/10.1093/neuonc/nos285>.
- Alizadeh, A.A., Eisen, M.B., Davis, R.E., Ma, C., Lossos, I.S., Rosenwald, A., Boldrick, J.C., Sabet, H., Tran, T., Yu, X., et al. (2000). Distinct types of diffuse large B-cell lymphoma identified by gene expression profiling. *Nature* *403*, 503–511. <https://doi.org/10.1038/35000501>.
- del Barco Barrantes, I., Coya, J.M., Maina, F., Arthur, J.S.C., and Nebreda, A.R. (2011). Genetic analysis of specific and redundant roles for p38 α and p38 β MAPKs during mouse development. *Proc. Natl. Acad. Sci. U.S.A.* *108*, 12764–12769. <https://doi.org/10.1073/pnas.1015013108>.
- Béguelin, W., Popovic, R., Teater, M., Jiang, Y., Bunting, K.L., Rosen, M., Shen, H., Yang, S.N., Wang, L., Ezponda, T., et al. (2013). EZH2 is required for germinal center formation and somatic EZH2 mutations promote lymphoid transformation. *Cancer Cell* *23*, 677–692. <https://doi.org/10.1016/j.ccr.2013.04.011>.
- Berger, G., Knelson, E.H., Jimenez-Macias, J.L., Nowicki, M.O., Han, S., Panagioti, E., Lizotte, P.H., Adu-Berchie, K., Stafford, A., Dimitrakakis, N., et al. (2022). STING activation promotes robust immune response and NK cell-mediated tumor regression in glioblastoma models. *Proceedings of the National Academy of Sciences* *119*, e2111003119. <https://doi.org/10.1073/pnas.2111003119>.
- van Berkum, N.L., Lieberman-Aiden, E., Williams, L., Imakaev, M., Gnirke, A., Mirny, L.A., Dekker, J., and Lander, E.S. (2010). Hi-C: a method to study the three-dimensional architecture of genomes. *J Vis Exp* 1869. <https://doi.org/10.3791/1869>.
- Biegel, J.A., Zhou, J.Y., Rorke, L.B., Stenstrom, C., Wainwright, L.M., and Fogelgren, B. (1999). Germ-line and acquired mutations of INI1 in atypical teratoid and rhabdoid tumors. *Cancer Res* *59*, 74–79. .

- Biegel, J.A., Tan, L., Zhang, F., Wainwright, L., Russo, P., and Rorke, L.B. (2002). Alterations of the hSNF5/INI1 gene in central nervous system atypical teratoid/rhabdoid tumors and renal and extrarenal rhabdoid tumors. *Clin Cancer Res* 8, 3461–3467. .
- Burke, J.R., Deshong, A.J., Pelton, J.G., and Rubin, S.M. (2010). Phosphorylation-induced conformational changes in the retinoblastoma protein inhibit E2F transactivation domain binding. *J Biol Chem* 285, 16286–16293. <https://doi.org/10.1074/jbc.M110.108167>.
- Cañadas, I., Thummalapalli, R., Kim, J.W., Kitajima, S., Jenkins, R.W., Christensen, C.L., Campisi, M., Kuang, Y., Zhang, Y., Gjini, E., et al. (2018). Tumor innate immunity primed by specific interferon-stimulated endogenous retroviruses. *Nat Med* 24, 1143–1150. <https://doi.org/10.1038/s41591-018-0116-5>.
- Carnevale, J., Palander, O., Seifried, L.A., and Dick, F.A. (2012). DNA Damage Signals through Differentially Modified E2F1 Molecules To Induce Apoptosis. *Molecular and Cellular Biology* 32, 900–912. <https://doi.org/10.1128/MCB.06286-11>.
- Chellappan, S.P., Hiebert, S., Mudryj, M., Horowitz, J.M., and Nevins, J.R. (1991). The E2F transcription factor is a cellular target for the RB protein. *Cell* 65, 1053–1061. .
- Chiappinelli, K.B., Strissel, P.L., Desrichard, A., Li, H., Henke, C., Akman, B., Hein, A., Rote, N.S., Cope, L.M., Snyder, A., et al. (2015). Inhibiting DNA Methylation Causes an Interferon Response in Cancer via dsRNA Including Endogenous Retroviruses. *Cell* 162, 974–986. <https://doi.org/10.1016/j.cell.2015.07.011>.
- Clapier, C.R., and Cairns, B.R. (2009). The biology of chromatin remodeling complexes. *Annu Rev Biochem* 78, 273–304. <https://doi.org/10.1146/annurev.biochem.77.062706.153223>.
- Clarke, A.R., Maandag, E.R., van Roon, M., van der Lugt, N.M.T., van der Valk, M., Hooper, M.L., Berns, A., and te Rielef, H. (1992). Requirement for a functional Rb-1 gene in murine development. *Nature* 359, 328–330. <https://doi.org/10.1038/359328a0>.
- Coschi, C.H., Ishak, C.A., Gallo, D., Marshall, A., Talluri, S., Wang, J., Cecchini, M.J., Martens, A.L., Percy, V., Welch, I., et al. (2014). Haploinsufficiency of an RB-E2F1-Condensin II Complex Leads to Aberrant Replication and Aneuploidy. *Cancer Discovery* 4, 840–853. <https://doi.org/10.1158/2159-8290.CD-14-0215>.
- De Silva, N.S., and Klein, U. (2015). Dynamics of B cells in germinal centres. *Nat Rev Immunol* 15, 137–148. <https://doi.org/10.1038/nri3804>.
- Gallimore, A., Glithero, A., Godkin, A., Tissot, A.C., Plückthun, A., Elliott, T., Hengartner, H., and Zinkernagel, R. (1998). Induction and exhaustion of lymphocytic choriomeningitis virus-specific cytotoxic T lymphocytes visualized using soluble tetrameric major histocompatibility complex class I-peptide complexes. *J Exp Med* 187, 1383–1393. <https://doi.org/10.1084/jem.187.9.1383>.

Gosling, K.M., Makaroff, L.E., Theodoratos, A., Kim, Y.-H., Whittle, B., Rui, L., Wu, H., Hong, N.A., Kennedy, G.C., Fritz, J.-A., et al. (2007). A mutation in a chromosome condensin II subunit, kleisin beta, specifically disrupts T cell development. *Proceedings of the National Academy of Sciences* *104*, 12445–12450. <https://doi.org/10.1073/pnas.0704870104>.

Gubern, A., Joaquin, M., Marquès, M., Maseres, P., Garcia-Garcia, J., Amat, R., González-Nuñez, D., Oliva, B., Real, F.X., de Nadal, E., et al. (2016). The N-Terminal Phosphorylation of RB by p38 Bypasses Its Inactivation by CDKs and Prevents Proliferation in Cancer Cells. *Molecular Cell* *64*, 25–36. <https://doi.org/10.1016/j.molcel.2016.08.015>.

Hornbeck, P.V., Kornhauser, J.M., Tkachev, S., Zhang, B., Skrzypek, E., Murray, B., Latham, V., and Sullivan, M. (2012). PhosphoSitePlus: a comprehensive resource for investigating the structure and function of experimentally determined post-translational modifications in man and mouse. *Nucleic Acids Res.* *40*, D261-270. <https://doi.org/10.1093/nar/gkr1122>.

Hornick, J.L., Dal Cin, P., and Fletcher, C.D.M. (2009). Loss of INI1 expression is characteristic of both conventional and proximal-type epithelioid sarcoma. *Am J Surg Pathol* *33*, 542–550. <https://doi.org/10.1097/PAS.0b013e31818882c54>.

Isaac, C.E., Francis, S.M., Martens, A.L., Julian, L.M., Seifried, L.A., Erdmann, N., Binné, U.K., Harrington, L., Sicinski, P., Bérubé, N.G., et al. (2006). The Retinoblastoma Protein Regulates Pericentric Heterochromatin. *Mol Cell Biol* *26*, 3659–3671. <https://doi.org/10.1128/MCB.26.9.3659-3671.2006>.

Ishak, C.A., Marshall, A.E., Passos, D.T., White, C.R., Kim, S.J., Cecchini, M.J., Ferwati, S., MacDonald, W.A., Howlett, C.J., Welch, I.D., et al. (2016). An RB-EZH2 Complex Mediates Silencing of Repetitive DNA Sequences. *Mol Cell* *64*, 1074–1087. <https://doi.org/10.1016/j.molcel.2016.10.021>.

Italiano, A. (2020). Targeting epigenetics in sarcomas through EZH2 inhibition. *J Hematol Oncol* *13*, 33. <https://doi.org/10.1186/s13045-020-00868-4>.

Italiano, A., Soria, J.-C., Toulmonde, M., Michot, J.-M., Lucchesi, C., Varga, A., Coindre, J.-M., Blakemore, S.J., Clawson, A., Suttle, B., et al. (2018). Tazemetostat, an EZH2 inhibitor, in relapsed or refractory B-cell non-Hodgkin lymphoma and advanced solid tumours: a first-in-human, open-label, phase 1 study. *Lancet Oncol* *19*, 649–659. [https://doi.org/10.1016/S1470-2045\(18\)30145-1](https://doi.org/10.1016/S1470-2045(18)30145-1).

Iyoda, K., Sasaki, Y., Horimoto, M., Toyama, T., Yakushijin, T., Sakakibara, M., Takehara, T., Fujimoto, J., Hori, M., Wands, J.R., et al. (2003). Involvement of the p38 mitogen-activated protein kinase cascade in hepatocellular carcinoma. *Cancer* *97*, 3017–3026. <https://doi.org/10.1002/cncr.11425>.

Jin, X., Ding, D., Yan, Y., Li, H., Wang, B., Ma, L., Ye, Z., Ma, T., Wu, Q., Rodrigues, D.N., et al. (2019). Phosphorylated RB Promotes Cancer Immunity by Inhibiting NF-κB

Activation and PD-L1 Expression. *Molecular Cell* 73, 22-35.e6.
<https://doi.org/10.1016/j.molcel.2018.10.034>.

Kadoch, C., and Crabtree, G.R. (2015). Mammalian SWI/SNF chromatin remodeling complexes and cancer: Mechanistic insights gained from human genomics. *Science Advances* 1, e1500447. <https://doi.org/10.1126/sciadv.1500447>.

Kadoch, C., Copeland, R.A., and Keilhack, H. (2016). PRC2 and SWI/SNF Chromatin Remodeling Complexes in Health and Disease. *Biochemistry* 55, 1600–1614.
<https://doi.org/10.1021/acs.biochem.5b01191>.

Kennison, J.A. (1995). THE POLYCOMB AND TRITHORAX GROUP PROTEINS OF DROSOPHILA: Trans-Regulators of Homeotic Gene Function. *Annual Review of Genetics* 29, 289–303. <https://doi.org/10.1146/annurev.ge.29.120195.001445>.

Kennison, J.A., and Tamkun, J.W. (1988). Dosage-dependent modifiers of polycomb and antennapedia mutations in *Drosophila*. *Proc. Natl. Acad. Sci. U.S.A.* 85, 8136–8140.
<https://doi.org/10.1073/pnas.85.21.8136>.

Knelson, E.H., Ivanova, E.V., Tarannum, M., Campisi, M., Lizotte, P.H., Booker, M.A., Ozgenc, I., Nouredine, M., Meisenheimer, B., Chen, M., et al. (2022). Activation of Tumor-Cell STING Primes NK-Cell Therapy. *Cancer Immunology Research* 10, 947–961. <https://doi.org/10.1158/2326-6066.CIR-22-0017>.

Knutson, S.K., Warholic, N.M., Wigle, T.J., Klaus, C.R., Allain, C.J., Raimondi, A., Porter Scott, M., Chesworth, R., Moyer, M.P., Copeland, R.A., et al. (2013). Durable tumor regression in genetically altered malignant rhabdoid tumors by inhibition of methyltransferase EZH2. *Proceedings of the National Academy of Sciences* 110, 7922–7927. <https://doi.org/10.1073/pnas.1303800110>.

Kwon, H., Imbalzano, A.N., Khavari, P.A., Kingston, R.E., and Green, M.R. (1994). Nucleosome disruption and enhancement of activator binding by a human SW1/SNF complex. *Nature* 370, 477–481. <https://doi.org/10.1038/370477a0>.

Ladies, G.S., Smith, C., Heaps, K., Elliott, G.S., Slone, T.W., and Loveless, S.E. (1995). Possible incorporation of an immunotoxicological functional assay for assessing humoral immunity for hazard identification purposes in rats on standard toxicology study. *Toxicology* 96, 225–238. [https://doi.org/10.1016/0300-483X\(94\)02967-Y](https://doi.org/10.1016/0300-483X(94)02967-Y).

Ladies, G.S., Smith, C., Elliott, G.S., Slone, T.W., and Loveless, S.E. (1998). Further evaluation of the incorporation of an immunotoxicological functional assay for assessing humoral immunity for hazard identification purposes in rats in a standard toxicology study. *Toxicology* 126, 137–152. [https://doi.org/10.1016/S0300-483X\(97\)00179-0](https://doi.org/10.1016/S0300-483X(97)00179-0).

Lee, E.Y.-H.P., Chang, C.-Y., Hu, N., Wang, Y.-C.J., Lai, C.-C., Herrup, K., Lee, W.-H., and Bradley, A. (1992). Mice deficient for Rb are nonviable and show defects in neurogenesis and haematopoiesis. *Nature* 359, 288–294.
<https://doi.org/10.1038/359288a0>.

Lewis, E.B. (1978). A gene complex controlling segmentation in *Drosophila*. *Nature* 276, 565–570. <https://doi.org/10.1038/276565a0>.

Li, N., Jin, K., Bai, Y., Fu, H., Liu, L., and Liu, B. (2020). Tn5 Transposase Applied in Genomics Research. *Int J Mol Sci* 21, 8329. <https://doi.org/10.3390/ijms21218329>.

Liu, M., Thomas, S.L., DeWitt, A.K., Zhou, W., Madaj, Z.B., Ohtani, H., Baylin, S.B., Liang, G., and Jones, P.A. (2018). Dual Inhibition of DNA and Histone Methyltransferases Increases Viral Mimicry in Ovarian Cancer Cells. *Cancer Res* 78, 5754–5766. <https://doi.org/10.1158/0008-5472.CAN-17-3953>.

Liu, Y., Peng, J., Sun, T., Li, N., Zhang, L., Ren, J., Yuan, H., Kan, S., Pan, Q., Li, X., et al. (2017). Epithelial EZH2 serves as an epigenetic determinant in experimental colitis by inhibiting TNF α -mediated inflammation and apoptosis. *Proceedings of the National Academy of Sciences* 114, E3796–E3805. <https://doi.org/10.1073/pnas.1700909114>.

Long, H.M., Meckiff, B.J., and Taylor, G.S. (2019). The T-cell Response to Epstein-Barr Virus—New Tricks From an Old Dog. *Frontiers in Immunology* 10. .

Lundberg, A.S., and Weinberg, R.A. (1998). Functional inactivation of the retinoblastoma protein requires sequential modification by at least two distinct cyclin-cdk complexes. *Mol. Cell. Biol.* 18, 753–761. <https://doi.org/10.1128/mcb.18.2.753>.

Mackenzie, K.J., Carroll, P., Martin, C.-A., Murina, O., Fluteau, A., Simpson, D.J., Olova, N., Sutcliffe, H., Rainger, J.K., Leitch, A., et al. (2017). cGAS surveillance of micronuclei links genome instability to innate immunity. *Nature* 548, 461–465. <https://doi.org/10.1038/nature23449>.

Mahadevan, N.R., Knelson, E.H., Wolff, J.O., Vajdi, A., Saigí, M., Campisi, M., Hong, D., Thai, T.C., Piel, B., Han, S., et al. (2021). Intrinsic Immunogenicity of Small Cell Lung Carcinoma Revealed by Its Cellular Plasticity. *Cancer Discovery* 11, 1952–1969. <https://doi.org/10.1158/2159-8290.CD-20-0913>.

Marshall, A.E., Ishak, C.A., and Dick, F.A. (2020). An RB-Condensin II Complex Mediates Long-Range Chromosome Interactions and Influences Expression at Divergently Paired Genes. *Mol Cell Biol* 40, e00452-19. <https://doi.org/10.1128/MCB.00452-19>.

Mayhew, C.N., Carter, S.L., Fox, S.R., Sexton, C.R., Reed, C.A., Srinivasan, S.V., Liu, X., Wikenheiser-Brokamp, K., Boivin, G.P., Lee, J., et al. (2007). RB Loss Abrogates Cell Cycle Control and Genome Integrity to Promote Liver Tumorigenesis. *Gastroenterology* 133, 976–984. <https://doi.org/10.1053/j.gastro.2007.06.025>.

Mayya, V., Lundgren, D.H., Hwang, S.-I., Rezaul, K., Wu, L., Eng, J.K., Rodionov, V., and Han, D.K. (2009). Quantitative Phosphoproteomic Analysis of T Cell Receptor Signaling Reveals System-Wide Modulation of Protein-Protein Interactions. *Science Signaling* 2, ra46–ra46. <https://doi.org/10.1126/scisignal.2000007>.

- McCabe, M.T., Ott, H.M., Ganji, G., Korenchuk, S., Thompson, C., Van Aller, G.S., Liu, Y., Graves, A.P., Iii, A.D.P., Diaz, E., et al. (2012a). EZH2 inhibition as a therapeutic strategy for lymphoma with EZH2-activating mutations. *Nature* *492*, 108–112. <https://doi.org/10.1038/nature11606>.
- McCabe, M.T., Graves, A.P., Ganji, G., Diaz, E., Halsey, W.S., Jiang, Y., Smitheman, K.N., Ott, H.M., Pappalardi, M.B., Allen, K.E., et al. (2012b). Mutation of A677 in histone methyltransferase EZH2 in human B-cell lymphoma promotes hypertrimethylation of histone H3 on lysine 27 (H3K27). *PNAS* *109*, 2989–2994. <https://doi.org/10.1073/pnas.1116418109>.
- Mittnacht, S. (1998). Control of pRB phosphorylation. *Curr Opin Genet Dev* *8*, 21–27. [https://doi.org/10.1016/s0959-437x\(98\)80057-9](https://doi.org/10.1016/s0959-437x(98)80057-9).
- Morel, K.L., Sheahan, A.V., Burkhart, D.L., Baca, S.C., Boufaied, N., Liu, Y., Qiu, X., Cañadas, I., Roehle, K., Heckler, M., et al. (2021). EZH2 inhibition activates a dsRNA-STING-interferon stress axis that potentiates response to PD-1 checkpoint blockade in prostate cancer. *Nat Cancer* *2*, 444–456. <https://doi.org/10.1038/s43018-021-00185-w>.
- Morin, R.D., Johnson, N.A., Severson, T.M., Mungall, A.J., An, J., Goya, R., Paul, J.E., Boyle, M., Woolcock, B.W., Kuchenbauer, F., et al. (2010). Somatic mutations altering EZH2 (Tyr641) in follicular and diffuse large B-cell lymphomas of germinal-center origin. *Nat Genet* *42*, 181–185. <https://doi.org/10.1038/ng.518>.
- Morschhauser, F., Tilly, H., Chaidos, A., McKay, P., Phillips, T., Assouline, S., Batlevi, C.L., Campbell, P., Ribrag, V., Damaj, G.L., et al. (2020). Tazemetostat for patients with relapsed or refractory follicular lymphoma: an open-label, single-arm, multicentre, phase 2 trial. *The Lancet Oncology* *21*, 1433–1442. [https://doi.org/10.1016/S1470-2045\(20\)30441-1](https://doi.org/10.1016/S1470-2045(20)30441-1).
- Mudgett, J.S., Ding, J., Guh-Siesel, L., Chartrain, N.A., Yang, L., Gopal, S., and Shen, M.M. (2000). Essential role for p38 α mitogen-activated protein kinase in placental angiogenesis. *Proc. Natl. Acad. Sci. U.S.A.* *97*, 10454–10459. <https://doi.org/10.1073/pnas.180316397>.
- Narlikar, G.J., Sundaramoorthy, R., and Owen-Hughes, T. (2013). Mechanisms and Functions of ATP-Dependent Chromatin-Remodeling Enzymes. *Cell* *154*, 490–503. <https://doi.org/10.1016/j.cell.2013.07.011>.
- Negrini, S., Gorgoulis, V.G., and Halazonetis, T.D. (2010). Genomic instability — an evolving hallmark of cancer. *Nat Rev Mol Cell Biol* *11*, 220–228. <https://doi.org/10.1038/nrm2858>.
- Rawlings, J.S., Gatzka, M., Thomas, P.G., and Ihle, J.N. (2011). Chromatin condensation via the condensin II complex is required for peripheral T-cell quiescence. *EMBO J.* *30*, 263–276. <https://doi.org/10.1038/emboj.2010.314>.

- Ribas, A., and Wolchok, J.D. (2018). Cancer Immunotherapy Using Checkpoint Blockade. *Science* 359, 1350–1355. <https://doi.org/10.1126/science.aar4060>.
- Roulois, D., Loo Yau, H., Singhanian, R., Wang, Y., Danesh, A., Shen, S.Y., Han, H., Liang, G., Jones, P.A., Pugh, T.J., et al. (2015). DNA-Demethylating Agents Target Colorectal Cancer Cells by Inducing Viral Mimicry by Endogenous Transcripts. *Cell* 162, 961–973. <https://doi.org/10.1016/j.cell.2015.07.056>.
- Rubin, S.M., Gall, A.-L., Zheng, N., and Pavletich, N.P. (2005). Structure of the Rb C-terminal domain bound to E2F1-DP1: a mechanism for phosphorylation-induced E2F release. *Cell* 123, 1093–1106. <https://doi.org/10.1016/j.cell.2005.09.044>.
- Sanidas, I., Morris, R., Fella, K.A., Rumde, P.H., Boukhali, M., Tai, E.C., Ting, D.T., Lawrence, M.S., Haas, W., and Dyson, N.J. (2019). A Code of Mono-phosphorylation Modulates the Function of RB. *Molecular Cell* 73, 985-1000.e6. <https://doi.org/10.1016/j.molcel.2019.01.004>.
- Schoffski, P., Agulnik, M., Stacchiotti, S., Davis, L.E., Villalobos, V.M., Italiano, A., George, S., Cote, G.M., Blakemore, S., Clawson, A., et al. (2017). Phase 2 multicenter study of the EZH2 inhibitor tazemetostat in adults with synovial sarcoma (NCT02601950). *JCO* 35, 11057–11057. https://doi.org/10.1200/JCO.2017.35.15_suppl.11057.
- Stacchiotti, S., Schoffski, P., Jones, R., Agulnik, M., Villalobos, V.M., Jahan, T.M., Chen, T.W.-W., Italiano, A., Demetri, G.D., Cote, G.M., et al. (2019). Safety and efficacy of tazemetostat, a first-in-class EZH2 inhibitor, in patients (pts) with epithelioid sarcoma (ES) (NCT02601950). *JCO* 37, 11003–11003. https://doi.org/10.1200/JCO.2019.37.15_suppl.11003.
- Su, I.-hsin, Basavaraj, A., Krutchinsky, A.N., Hobert, O., Ullrich, A., Chait, B.T., and Tarakhovskiy, A. (2003). Ezh2 controls B cell development through histone H3 methylation and Igh rearrangement. *Nat Immunol* 4, 124–131. <https://doi.org/10.1038/ni876>.
- Sullivan, L.M., Folpe, A.L., Pawel, B.R., Judkins, A.R., and Biegel, J.A. (2013). Epithelioid sarcoma is associated with a high percentage of SMARCB1 deletions. *Mod Pathol* 26, 385–392. <https://doi.org/10.1038/modpathol.2012.175>.
- Tamura, K., Sudo, T., Senftleben, U., Dadak, A.M., Johnson, R., and Karin, M. (2000). Requirement for p38 α in Erythropoietin Expression: A Role for Stress Kinases in Erythropoiesis. *Cell* 102, 221–231. [https://doi.org/10.1016/S0092-8674\(00\)00027-1](https://doi.org/10.1016/S0092-8674(00)00027-1).
- Ullman, T.A., and Itzkowitz, S.H. (2011). Intestinal Inflammation and Cancer. *Gastroenterology* 140, 1807-1816.e1. <https://doi.org/10.1053/j.gastro.2011.01.057>.
- Verma, S.K., Tian, X., LaFrance, L.V., Duquenne, C., Suarez, D.P., Newlander, K.A., Romeril, S.P., Burgess, J.L., Grant, S.W., Brackley, J.A., et al. (2012). Identification of

Potent, Selective, Cell-Active Inhibitors of the Histone Lysine Methyltransferase EZH2. *ACS Med. Chem. Lett.* *3*, 1091–1096. <https://doi.org/10.1021/ml3003346>.

Versteeg, I., Sévenet, N., Lange, J., Rousseau-Merck, M.F., Ambros, P., Handgretinger, R., Aurias, A., and Delattre, O. (1998). Truncating mutations of hSNF5/INI1 in aggressive paediatric cancer. *Nature* *394*, 203–206. <https://doi.org/10.1038/28212>.

Wang, H., Yang, H., Shivalila, C.S., Dawlaty, M.M., Cheng, A.W., Zhang, F., and Jaenisch, R. (2013). One-Step Generation of Mice Carrying Mutations in Multiple Genes by CRISPR/Cas-Mediated Genome Engineering. *Cell* *153*, 910–918. <https://doi.org/10.1016/j.cell.2013.04.025>.

Wenzel, P.L., Wu, L., Bruin, A. de, Chong, J.-L., Chen, W.-Y., Dureska, G., Sites, E., Pan, T., Sharma, A., Huang, K., et al. (2007). Rb is critical in a mammalian tissue stem cell population. *Genes Dev.* *21*, 85–97. <https://doi.org/10.1101/gad.1485307>.

Wherry, E.J. (2011). T cell exhaustion. *Nat Immunol* *12*, 492–499. <https://doi.org/10.1038/ni.2035>.

Wirtz, S., Popp, V., Kindermann, M., Gerlach, K., Weigmann, B., Fichtner-Feigl, S., and Neurath, M.F. (2017). Chemically induced mouse models of acute and chronic intestinal inflammation. *Nat Protoc* *12*, 1295–1309. <https://doi.org/10.1038/nprot.2017.044>.

Yap, D.B., Chu, J., Berg, T., Schapira, M., Cheng, S.-W.G., Moradian, A., Morin, R.D., Mungall, A.J., Meissner, B., Boyle, M., et al. (2011). Somatic mutations at EZH2 Y641 act dominantly through a mechanism of selectively altered PRC2 catalytic activity, to increase H3K27 trimethylation. *Blood* *117*, 2451–2459. <https://doi.org/10.1182/blood-2010-11-321208>.

Zajac, A.J., Blattman, J.N., Murali-Krishna, K., Sourdive, D.J., Suresh, M., Altman, J.D., and Ahmed, R. (1998). Viral immune evasion due to persistence of activated T cells without effector function. *J Exp Med* *188*, 2205–2213. <https://doi.org/10.1084/jem.188.12.2205>.

Zhou, J., Huang, S., Wang, Z., Huang, J., Xu, L., Tang, X., Wan, Y.Y., Li, Q., Symonds, A.L.J., Long, H., et al. (2019). Targeting EZH2 histone methyltransferase activity alleviates experimental intestinal inflammation. *Nat Commun* *10*, 2427. <https://doi.org/10.1038/s41467-019-10176-2>.

Appendices

Appendix A: List of primers

Name	Sequence	Purpose	Chapter	Reference
RBC mutagenic F	TTAGTATCAATTGGTGAAGCATTC GGGGCTTCTGAGAAGTTCCAGAAA	Mutagenesis	2	This thesis
RBC mutagenic R	TTAGTATCAATTGGTGAAGCATTC GGGGCTTCTGAGAAGTTCCAGAAA	Mutagenesis	2	This thesis
LINE1 ORF1 For	actcaaagcgaggcaacactaga	RT-qPCR	3	Muotri et al. 2005
LINE1 ORF1 Rev	gttcagattcttcttaggttcc	RT-qPCR	3	Muotri et al. 2005
LINE1 ORF2 For	cctccattgttggtgggatt	RT-qPCR	3	Muotri et al. 2005
LINE1 ORF2 Rev	ggaaccgccagactgatttc	RT-qPCR	3	Muotri et al. 2005
Gapdh For	gagccagggactctctttt	RT-qPCR	3, 4	Cecchini et al. 2014
Gapdh Rev	ctgcacctgctacagtctc	RT-qPCR	3, 4	Cecchini et al. 2014
Cgas ex1-2 For	caccGGGCAGCTCCGGATCCAGGA	ligation	3, 4	This thesis
Cgas ex1-2 Rev	aaacTCCTGGATCCGGAGCTGCCC	ligation	3, 4	This thesis
Ifih1 ex5-4 For	caccGCAGGCATCTGAATCCGGGA	ligation	3	This thesis
Ifih1 ex5-4 Rev	aaacTCCCGGATTCAGATGCCTGC	ligation	3	This thesis
Rigi ex9-2 For	caccGTGGAGATGCTAAGACCGCGG	ligation	3,4	This thesis
Rigi ex9-2 Rev	aaacCCGCGGTCTTAGCATCTCCAC	ligation	3, 4	This thesis
T7-Cgas ex1-2	ttaatagactcactata GGCAGCTCCGGATCCAGGA	<i>in vitro</i> gRNA synthesis	3	This thesis
T7-Ifih1 ex5-4	ttaatagactcactatagg CAGGCATCTGAATCCGGGA	<i>in vitro</i> gRNA synthesis	3	This thesis
T7-Rigi ex9-2	ttaatagactcactatagg TGGAGATGCTAAGACCGCGG	<i>in vitro</i> gRNA synthesis	3	This thesis
T7-sgRNA-rev	AAAAGCACCGACTCGGTGCC	<i>in vitro</i> gRNA synthesis	3	This thesis

ISD45 prob For	biotin-TACAGATCTACTAGTGATCTA TGACTGATCTGTACATGATCTACA	Pull-down	3	Stetson and Medzhitov 2006
ISD45 prob Rev	TGTAGATCATGTACAGATCAGT CATAGATCACTAGTAGATCTGTA	Pull-down	3	Stetson and Medzhitov 2006
Cgas For	GCTCACCAAAGATGCACAGC	Genotyping	3	This thesis
Cgas Rev	CCTTACGACTTTCCGCGCCT	Genotyping	3	This thesis
Ifih1 For	AAAGAGTATCCCCCGAGCCA	Genotyping	3	This thesis
Ifih1 Rev	AGGGAGCACAGGAGCGTAT	Genotyping	3	This thesis
Rigi For	CTTACAGGTCGTTGGGCTGA	Genotyping	3	This thesis
Rigi Rev	GGTTACAAAGTCGCGAGGTG	Genotyping	3	This thesis
Cgas 1-2 For	GCTCACCAAAGATGCACAGC	cDNA-PCR	3	This thesis
Cgas 1-2 Rev	TTCATTAGGAGCAGAAATCTTCACA	cDNA-PCR	3	This thesis
Cgas 1-3 For	GCTCACCAAAGATGCACAGC	cDNA-PCR	3	This thesis
Cgas 1-3 Rev	TCCACACTGACATCTATATCTTTGA	cDNA-PCR	3	This thesis
Cgas 2-4 For	ACGAGGAAATCCGCTGAGTC	cDNA-PCR	3	This thesis
Cgas 2-4 Rev	TTTGCTCCGGAAGATTCACA	cDNA-PCR	3	This thesis
Ifitm3 For	CCGTGAAGTCTAGGGATCGG	RT-qPCR	4	This thesis
Ifitm3 Rev	ACAATGGTGATAACAACCATCAGG	RT-qPCR	4	This thesis
Isg15 For	AGCAATGGCCTGGGACCTAA	RT-qPCR	4	This thesis
Isg15 Rev	CACGGACACCAGGAAATCGT	RT-qPCR	4	This thesis
Ifih1 For	AACAGCGGGAATGAGTCAGG	RT-qPCR	4	This thesis
Ifih1 Rev	ACGAGTTAGCCAAGTCTGTGTT	RT-qPCR	4	This thesis

Appendix B: List of reagents

REAGENT or RESOURCE	SOURCE	IDENTIFIER	Chapter	Notes
<i>Antibodies</i>				
Rabbit RB pS838/pT841 antibody	This thesis		2	WB-1:1000
RB antibody (G3-245)	BD Biosciences	Cat#554136	2	WB-1:1000; IP-1:50
Rabbit MAPKAPK2 pT334 antibody	CST	Cat#3007	2	WB-1:1000
Rabbit ZAP70 pY319 antibody	CST	Cat#2701	2	WB-1:1000
Rabbit ZAP70 antibody	CST	Cat#3165	2	WB-1:1000
Rabbit p38 pT180/pY182 antibody	CST	Cat#9211	2	WB-1:1000
Rabbit p38 antibody	CST	Cat#9212	2	WB-1:1000; IP-1:50
Rabbit RB pS807/pS811 antibody	CST	Cat#9308	2	WB-1:1000
Rabbit E2F1 antibody (C-20)	Santa Cruz	Cat#193	2	WB-1:1000
Rabbit E2F2 antibody (CC11)	Santa Cruz	Cat#56663	2	WB-1:1000
Rabbit CD3 antibody (OKT3)	BioLegend	Cat#317301	2	TCR crosslinking- 5 µg/mL
Rabbit CD28 antibody (CD28.2)	BioLegend	Cat#302903	2	TCR crosslinking- 5 µg/mL
Rabbit CAPH2 antibody	Bethyl laboratories	Cat#A302-275A	2	WB-1:1000
Rabbit SMC1 antibody	Bethyl laboratories	Cat#A300-055A	2	WB-1:1000
Rat HA antibody	Millipore Sigma	Cat#12158167001	2	WB-1:1000
AffiniPure Goat Anti-mouse antibody (H+L)	JIR	Cat#115-005-003	2	TCR crosslinking- 30 µg/mL

Rat CD43 microbeads (Ly-48)	Miltenyi Biotec	Cat#130-049-801	3	MACS: 1:20
Rabbit H3K27me3 antibody	Millipore-Sigma	Cat#07-449	3	ChIP: 4 µg/30 µg chromatin
Mouse CD45.2 BV421 antibody (104)	BioLegend	Cat#109831	3	
Rat CD19 BV510 antibody (6D5)	BioLegend	Cat#115545	3	
Rat Ly6C BV605 antibody (HK1.4)	BioLegend	Cat#128035	3	
Rat CD11b FITC antibody (M1/70)	BioLegend	Cat#101206	3	
Armenian hamster CD3ε PerCP/Cy5.5 antibody (145-2C11)	BioLegend	Cat#100327	3	
Rat CD8α PE antibody (53-6.7)	BioLegend	Cat#100707	3	
Rat Ly6G APC antibody (1A8)	BioLegend	Cat#127613	3	
Rat CD43 PerCP/Cy5.5 antibody (S11)	BioLegend	Cat#143219	3	
Rat CD45R PE antibody (RA3-6B2)	BioLegend	Cat#103207	3	
Rabbit α-tubulin antibody (11H10)	CST	Cat#2125	2, 3, 4	WB-1:5000
Rabbit cGAS antibody (D3O8O)	CST	Cat#31659	3, 4	WB-1:1000
Rabbit MDA5 antibody (D74E4)	CST	Cat#5321	3	WB-1:1000
Mouse RIG-I antibody (D-12)	Santa Cruz	Cat#376845	3, 4	WB-1:1000
AffiniPure goat IgG-HRP	JIR	Cat#111-035-144	3	WB
Rabbit CD68 antibody	Abcam	Cat#125212	3	IHC-1:100

Goat anti-rabbit IgG biotinylated	VectorLabs	Cat#BA-1000-1.5	3	IHC-1:200
<i>Bacterial strains</i>				
<i>E. coli</i> DH5 α				
<i>Plasmids</i>				
pSicoR-Ef1a-mCh-puro	Addgene	Cat#31845	2	Lab stock #863
pSicoR-Ef1a-HA-RBLP	This thesis		2	Lab stock #853
pSicoR-Ef1a-HA-RBLP S838A/T841A	This thesis		2	Lab stock #854
GEX-GST-RBC			2	Lab stock #866
GEX-GST-RBC T841A	This thesis		2	Lab stock #867
GEX-GST RBC S838A	This thesis		2	Lab stock #868
GEX-GST RBC S838A/T841A	This thesis		2	Lab stock #869
pMD2.G	Addgene	Cat#12259	2, 4	
psPAX2	Addgene	Cat#12260	2, 4	
pSpCas9(BB)-2A-Puro (pX459)	Addgene	Cat#62988	3	Lab stock #865
pLentiCRISPR-v2 Rigi	This thesis		4	Lab stock #855
pLentiCRISPR-v2 Cgas	This thesis		4	Lab stock #856
pLentiCRISPR-v2 control	This thesis	Targets luciferase and β -gal. Made by James MacDonald	4	Lab stock #870
pLentiCRISPR-v2	Addgene	Cat#52961	4	Lab stock #862
<i>Chemicals, peptides and recombinant proteins</i>				
834-SIGESFGTSEKF-845	ThermoFisher		2	
834-SIGE(pS)FG(pT)SEKF-845	ThermoFisher		2	
GSK343	Tocris	Cat#6128	3, 4	
Captisol	Captisol	Cat#RC-0C7	3	
poly(I:C)	Millipore-Sigma	Cat#P1530	3	
IL-4	BioLegend	Cat#574302	3	
BAFF	BioLegend	Cat#591202	3	

m-IgG Gc BP-HRP	Santa Cruz	Cat#525409	3, 4	
<i>Commercial assays and kits</i>				
QuikChange II site-directed mutagenesis	Agilent	Cat#200523	2	
Monarch Total RNA miniprep kit	NEB	Cat#T2010	3, 4	
iScript Supermix	Biorad	Cat#1708840	3, 4	
iQ SYBR Green Supermix	Biorad	Cat#1708882	3, 4	
Monarch RNA cleanup kit	NEB	Cat#T2040	3, 4	
Monarch PCR/DNA cleanup kit	NEB	Cat#T1030	3, 4	
NEBNext Ultra II DNA library kit	NEB	Cat#E7645	3	
Multiplex Oligos	NEB	Cat#E7600	3	
Phire Animal Tissue Direct PCR kit	ThermoFisher	Cat#F140WH	3	
VAHTS total RNA-seq library kit	GeneBio	Cat#NR603-01	3	
<i>Deposited data</i>				
Raw and processed sequencing data	This thesis	GEO: GSE198232	3	
<i>Experimental models</i>				
HEK293T cells	ATCC	Cat#CRL-3216	2, 3, 4	
Jurkat T-cell leukemia cells E6-1	ATCC	Cat#TIB-152	2	
C57BL/6NCr1	Charles River	Cat#027	3	
CID mutant mice	This paper		3	
B16-F10 mouse melanoma cells	Dr. Charles Ishak	De Carvalho Lab, Toronto, ON	4	
<i>Software and algorithms</i>				
Repenrich2	(Criscione et al., 2014)	github.com/nerettilab/RepEnrich2	3, 4	RNA-seq
featureCounts	(Liao et al., 2014)	subread.sourceforge.net/	3	RNA-seq

bowtie2/2.4.2	(Langmead and Salzberg, 2012)	bowtie-bio.sourceforge.net/bowtie2/index.shtml	3	ChIP-seq
samtools/1.12	(Li et al., 2009)	htslib.org/	3, 4	ChIP-seq
STAR	(Dobin et al., 2013)	github.com/alexdobin/STAR	3, 4	RNA-seq
HTSeq/0.11.0	(Anders et al., 2015)	htseq.readthedocs.io/en/master/	3, 4	RNA-seq
edgeR/3.28.1	(Robinson et al., 2010)	bioconductor.org/packages/release/bioc/html/edgeR.html	3, 4	RNA-seq
VennDiagram	(Chen and Boutros, 2011)	cran.r-project.org/web/packages/VennDiagram/index.html	3	RNA-seq
GSEA	(Subramanian et al., 2005)	gsea-msigdb.org/gsea/index.jsp	3, 4	RNA-seq
MACS2/2.2.7.1	(Zhang et al., 2008)	github.com/macs3-project/MACS	3	ChIP-seq
deepTools/3.5.1	(Ramírez et al., 2016)	deeptools.readthedocs.io/en/develop/	3	ChIP-seq
bedtools/2.30.0	(Quinlan and Hall, 2010)	bedtools.readthedocs.io/en/latest/	3	ChIP-seq
ChIPseeker	(Yu et al., 2015)	guangchuangyu.github.io/software/ChIPseeker/	3	ChIP-seq
igv/2.11.1	(Robinson et al., 2011)	software.broadinstitute.org/software/igv/	3	ChIP-seq
EnhancedVolcano		github.com/kevinblighe/EnhancedVolcano	3, 4	RNA-seq
<i>Miscellaneous items</i>				
96-well magnetic PCR tube rack	Dr. Sam Asfaha lab		3	
Lipofectamine 3000	ThermoFisher	Cat#L3000001	2, 3, 4	
Glutathione Sepharose 4B	Millipore Sigma	Cat#GE17-0756-01	2	
LD column	Miltenyi Biotec	Cat#130-042-901	3	
VarioMACS separator	Miltenyi Biotec	Cat#130-090-282	3	
Bioruptor Pico	Diagenode	Cat#B01060010	2, 3	
Dynabeads Protein G	ThermoFisher	Cat#10004D	2, 3	
Ampure XP beads	Beckman Coulter	Cat#A63880	3	
Zombie NIR	BioLegend	Cat#423105	3	
Brilliant Stain Buffer	BD	Cat#563794	3	
TruStain monocyte blocker	BioLegend	Cat#426102	3	
TruStain FcX plus	BioLegend	Cat#156603	3	

Precision counting beads	BioLegend	Cat#424902	3	
AbC total antibody compensation beads	ThermoFisher	Cat#A10497	3	
ArC amine reactive compensation beads	ThermoFisher	Cat#A10628	3	
Dynabeads streptavidin	ThermoFisher	Cat#11205D	2, 3	
SuperSignal WestDura	ThermoFisher	Cat#34075	2, 3, 4	
Streptavidin-HRP RTU	VectorLabs	Cat#SA-5704-100	3	
ImmPact DAB substrate kit	VectorLabs	Cat#SK-4105	3	
GelCode Blue	ThermoFisher	Cat#24590	2, 3	

Appendix C: PCR mixes and reactions

QuikChange Mutagenesis

PCR mix

Material	Volume (μL)
10X buffer	5
pEF1α-HA-RBLP (10 ng/μL)	1
Forward primer (125 ng/μL)	1
Reverse primer (125 ng/μL)	1
dNTP mix	1
H ₂ O	41
<i>PfuUltra</i> HF DNA pol. (2.5U/μL)	1

RIC mutant genotyping

PCR mix

Material	Volume (μL)
2X Phire Master Mix	5
Forward primer (20 μM)	0.3
Reverse primer (20 μM)	0.3
Tail DNA	1
H ₂ O	3.4

cDNA synthesis

DNaseI digestion

Material	Volume (μL)
10X DNaseI buffer	1.44
RNA (500 ng)	varies
DNaseI (0.5U/μL)	1
H ₂ O	upto 14.4

cDNA synthesis mix

PCR reaction

Step	Temp (°C)	Time (m:s)
1	95	1:30
2	95	0:50
3	60	0:50
4	68	20:00
5	go to step 2 (x18)	
6	68	7:00
7	12	∞

PCR reaction

Step	Temp (°C)	Time (m:s)
1	98	5:00
2		0:05
3		0:05
4		0:20
5	go to step 2 (x34)	
6	72	1:00
7	12	∞

DNaseI digestion

Step	Temp (°C)	Time (m:s)
1	22	15:00
then digest at RT for 15 min		

cDNA synthesis reaction

Restriction digest mix

Material	Volume (μL)
10X CutSmart/Tango/R Buffer	2
PCR DNA	5
restriction enzyme	0.2
H ₂ O	2.8
then digest at 37 °C for 15 min	

DNaseI inactivation

Material	Volume (μL)
RNA mix	14.4
50 mM EDTA	1.6
then digest at 65 °C for 10 min	

Material	Volume (μ L)
5X iScript Master Mix	4
RNA mix	16

ChIP-seq library prep*PCR amplification*

Material	Volume (μ L)
Adaptor ligated DNA	15
Ultra II Q5 Master Mix	25
i5 primer	5
i7 primer	5

Step	Temp ($^{\circ}$ C)	Time (m:s)
1	25	5:00
2	46	20:00
3	95	1:00
4	4	∞

PCR reaction

Step	Temp ($^{\circ}$ C)	Time (m:s)
1	98	0:45
2	98	0:15
3	60	0:10
4	go to step 2 (x10 for ChIP, x15 for input)	
5	72	1:00
6	4	∞

Appendix D: RIC mutant alleles

Gene	Allele name	Genomic alteration
<i>Cgas</i>	<i>Cgas</i> ^{em1Fad} - d48a	chr9:del178350047-78350094
<i>Cgas</i>	<i>Cgas</i> ^{em2Fad} - d48b	chr9:del178350041-78350088
<i>Ifih1</i>	<i>Ifih1</i> ^{em1Fad} - d7	chr2:del62447626-62447632
<i>Ifih1</i>	<i>Ifih1</i> ^{em2Fad} - d13	chr2:del62447623-62447635
<i>Rigi</i>	<i>Rigi</i> ^{em1Fad} - d2	chr4:del40222150-40222151
<i>Rigi</i>	<i>Rigi</i> ^{em2Fad} - d18	chr4:del40222142-40222159

Appendix E: Off-target mutations in RIC mutant founder mice

Gene	Off-target coordinates	ID	Mutation	Notes
<i>Cgas</i>	chr2:174658835-174658856	N/A	N/A	N/A
<i>Cgas</i>	chr18:45302633-45302654	E604	chr18:del45302635	het.
<i>Ifih1</i>	chr7:125027663-125027684	N/A	N/A	N/A
<i>Ifih1</i>	chr9:86583251-86583272	N/A	N/A	N/A
<i>Rigi</i>	chr11:72267085-72267107	N/A	N/A	N/A
<i>Rigi</i>	chr14:105923043-105923065	E602	chr14:del105923066	het.

Appendix F: Permission for publication by Journal of Biological Chemistry

Data presented in chapter 2 is published in Journal of Biological Chemistry. This is an open access article distributed under the terms of the Creative Commons CC-BY license, which permits unrestricted use, distribution, and reproduction in any medium, provided the original work is properly cited.

Kim, S.J., MacDonald, J.I., and Dick, F.A. (2021). Phosphorylation of the RB C-terminus regulates condensin II release from chromatin. *Journal of Biological Chemistry* 296. <https://doi.org/10.1074/jbc.RA120.016511>.

Curriculum Vitae

Seung June Kim

Education

Western University-PhD Candidate 2016-2022
Supervisor: Dr. Fred Dick

Western University
Hon. BSc Biochemistry of Infection and Immunity 2012-16

Honours and Awards

Ontario Graduate Scholarship (\$15 000) May 2020 - 2021
Howard Hughes Medical Institute Stipend (\$1000) Sept 2018
Cancer Research and Technology Transfer Scholarship (\$17000) 2017-2018
Western Graduate Research Scholarship (\$4500) 2016-2022
Western Science Undergraduate Dean's Honour List 2012-16
Korean Canadian Scholarship Foundation Scholarship (\$2500) 2015

Publications

Kim, S. J., Kiser, P. K., DeKoter, R. P., and Dick, F. A. (2022) EZH2 inhibition stimulates viral mimicry causing immune destruction of splenic B cells. *Submitted*.

Kim, S. J., MacDonald, J. I., and Dick, F. A. (2021) Phosphorylation of the RB C-terminus regulates condensin II release from chromatin. *Journal of Biological Chemistry*. [10.1074/jbc.RA120.016511](https://doi.org/10.1074/jbc.RA120.016511)

Kim, S. J., Asfaha, S., and Dick, F. A. (2019) CDK4 inhibitors thwart immunity by inhibiting phospho-RB-NFkB complexes. *Mol Cell*. **73**, 1–2

Ishak, C. A., Marshall, A. E., Passos, D. T., White, C. R., **Kim, S. J.**, Cecchini, M. J., Ferwati, S., MacDonald, W. A., Howlett, C. J., Welch, I. D., Rubin, S. M., Mann, M. R. W., and Dick, F. A. (2016) An RB-EZH2 Complex Mediates Silencing of Repetitive DNA Sequences. *Mol Cell*. **64**, 1074–1087

Local Meetings

Kim, S. J., Kiser, P. K., DeKoter, R. P., and Dick, F. A. Elucidating the mechanism behind EZH2 inhibition and immune activation. Oncology Research & Education Day. London ON, Canada 2022
*poster award

Kim, S.J., and Dick, F.A. Elucidating the mechanism behind EZH2 inhibition and anti-viral immune signaling. Oncology Research & Education Day. London ON, Canada 2021
*Selected for oral presentation

Kim, S.J., Ishak, C.A., and Dick, F.A. Pharmacological inhibition of EZH2 activates anti-viral immunity. London Immuno-Oncology Symposium
London ON, Canada 2020
*Selected for oral presentation

Kim, S.J., Ishak, C.A., and Dick, F.A. Pharmacological inhibition of the pRB-E2F1-EZH2 complex to modulate the innate immune system. London Health Research Day.
London ON, Canada 2019
*Selected for oral presentation

Kim, S.J., Ishak, C.A., and Dick, F.A. Pharmacological inhibition of E1A-insensitive pRB-E2F1-EZH2 complex activates anti-viral immunity. Oncology Research and Education Day.
London ON, Canada 2019

Kim, S.J., Ishak, C.A., and Dick, F.A. Investigating the role of repetitive DNA expression in immune modulation. Oncology Research and Education Day.
London ON, Canada 2018
*poster award

International Meetings

Kim, S.J., Ishak, C.A., and Dick, F.A. Pharmacological inhibition of E1A-insensitive pRB-E2F1-EZH2 complex activates anti-viral immunity. ICGEB DNA Tumour Virus Meeting.
Trieste, Italy. 2019
*Selected for oral presentation

Leadership and Community Activity

London Research Information Outreach Team Sept 2020-2021
VON London volunteer Aug 2018-present
CaRTT Visiting Speaker Selection Committee Member 2017-2018
Let's Talk Cancer Workshop Volunteer/presenter 2017, 2020-2021
Department of Oncology Strategic Planning Trainee Focus Group
Undergraduate representative 2016

Academic Experience

Advanced Sequencing Technologies and Applications Course, Cold Spring Harbor Laboratory, NY, USA Nov 2018
Graduate Teaching Assistantship Sept 2018-Apr 2021